Molecular genetic investigations of renal cell carcinoma predisposition

Department of Medical Genetics

Submitted for the degree of Doctor of Philosophy by

Philip Simon Smith (USN: 303248033)

Darwin College

April 2019

Declaration

This dissertation is the result of my own work and includes nothing which is the outcome of work done in collaboration except as declared in the Preface and specified in the text. It is not substantially the same as any that I have submitted, or, is being concurrently submitted for a degree or diploma or other qualification at the University of Cambridge or any other University or similar institution except as declared in the Preface and specified in the text. I further state that no substantial part of my dissertation has already been submitted, or, is being concurrently submitted for any such degree, diploma or other qualification at the University of Cambridge or any other University or similar institution except as declared in the Preface and specified in the text. This thesis does not exceed the prescribed word limit for the relevant Degree Committee to which it is being submitted.

Abstract

Name: Philip Simon Smith

Title: Molecular genetic investigations of renal cell carcinoma predisposition

Renal Cell Carcinomas (RCC) are a diverse group of histologically and genetically distinct renal neoplasms accounting for 2.4% of all cancers worldwide. While a majority of RCC cases are sporadic in nature, a proportion are due to genetic predisposition caused by syndromic and non-syndromic conditions. Inherited renal cell carcinoma is associated with alterations in genes such as *VHL*, *MET*, *FH*, and *FLCN* and identification of these genes has been critical to understanding the molecular biology of both inherited and sporadic RCC, informing both clinical management and treatment. Despite the large number of known genes which are linked to RCC predisposition, most individuals with features of RCC predisposition do not harbour variants in known inherited RCC genes, suggesting additional unknown causes of heritability have yet to be uncovered. This study has utilised a range of genomic sequencing methodologies, scaling from single gene to whole genome sequencing, on individuals with features of renal cell carcinoma predisposition in order to identify novel causes of heritability associated with RCC. Multiple genomic sequencing approaches in these individuals has uncovered a range of potential genetic features that could be associated with predisposition to RCC, including genes not previously known to be associated with RCC, discovery of new molecular mechanisms of genetic inheritance for known RCC predisposition syndromes, and provided innovative methods for the identification and characterisation of molecular alterations in specific inherited RCC subtypes.

Table of Contents

Acknowledgements

The writing of this thesis has undoubtedly been the greatest labour of love I have undertaken in my scientific career and I have numerous people to thank who have supported, educated, guided, and most of all tolerated me over the last four years. After four years of dedicated work on human genetics, inherited cancer, and bioinformatics, I am elated to still feel the same passion and curiosity at the end of this journey that I felt when I began.

First and foremost, I wish to thank Professor Eamonn Maher for his mentorship, guidance, and patience, as well as graciously allowing me to pursue my PhD whilst maintaining my role as a research assistant. Professor Maher's support and discussions have vastly improved my approach to science, my understanding of human genetics, as well as continually challenged me to push myself and develop my knowledge in an area of biology I adore. Secondly, I am grateful to Dr Marc Tischkowitz, who as my second supervisor, provided me with productive discussions, insightful comments, critiques on my experimental plans and scientific thinking, and always provided a consistent and ever-present support system if I needed it.

I am exceptionally grateful and owe more thanks than I can possibly bestow to my friends and colleagues that I have had the privilege of working with over the last four years. The conversations, discussions, and collaborations I have made with all my colleagues have been invaluable for my development and growth as a scientist. There are several people who deserve special mention for supporting me in my academic endeavours and as such I would like to personally thank Dr Ruth Casey, Dr Graeme Clark, Dr France Docquier, Dr Eleanor Fewings, Dr Mae Goldgraben, Dr Benoit Lan-Leung, Dr Alexey Larionov, Dr Eguzkine Ochoa, Dr Hannah West, and Dr James Whitworth.

Finally, I would like to thank my family who have consistently supported my ambition of working in science and have been endlessly understanding of my absences at family engagements, putting up with my long explanations of what I am doing, and keeping me motivated. Without their support and guidance, I am certain that I would not have had the will, drive, or opportunity to submit this thesis.

1.0 Introduction

1.0.1 Table of contents

1.1 Medical genetics: From Mendel to gene therapy

1.1.1 Discovery of genetics

Mendelian inheritance, as first described by Gregor Mendel in 1865 in the Proceedings of the Natural History Society of Brünn (1), was the beginning of our understanding of how genetic traits and phenotypic features were passed from one generation to the next and is widely considered the birth of the field of genetics. Rapid developments in the understanding, models, and theories regarding genetics and genetic inheritance led to the identification of genetic alterations, which could confer detrimental or beneficial survival advantages, as explored by scientists such as Charles Darwin and Thomas Hunt Morgan, amongst many other 20th century geneticists. The application of genetic inheritance to human disease traits in the mid to late 20th century transformed our understanding of various diseases, demonstrating that diseases could be investigated as underlying inheritable traits and their genetic aetiology understood.

1.1.2 Models of inheritance

Genetic diseases, defined as a condition that manifests due to a genetic abnormality, occur at varying levels of pervasiveness within human populations and at varying clinical severities. While many genetic disorders follow Mendelian inheritance, multiple models of inheritance have now been defined and implicated in human disease, including but not limited to, X and Y-linked inheritance, co-dominant inheritance, mitochondrial inheritance, and polygenic or complex traits. Further complexity is added by way of incomplete or partial penetrance of phenotypes, as well as specific genotype-phenotype correlations. Penetrance, for example, is the probable likelihood for any given genotype to result in a phenotype, where a genotype is considered 100% penetrant when its associated phenotype is always present. Genotype-phenotype correlations describe the phenomenon of different alterations in one gene loci resulting in different phenotypic presentations, for example a lower risk of phaeochromocytomas in Von Hippel-Lindau disease if resulting from a truncating mutation in the tumour suppressor gene *VHL* compared to a missense substitution (2).

1.1.3 De novo variants and mosaicism

De novo genetic events, as a result of newly acquired alterations during zygote formation, can lead to disease phenotypes without being inherited from the parental genomes. In fact, all genetically inherited diseases will have stemmed from an initial *de novo* mutational event, with subsequent generations inheriting that disease-causing allele. *De novo* events often lead to increased disease prevalence within isolated human populations due to founder effects (e.g. Ellis–van Creveld syndrome in Amish populations (3)) as a consequence of increased endogamy and consanguinity or, in the case of autosomal recessive sickle cell disease, caused by variants in β-globin (*HBB*) gene, due to the selective advantage conferred in the heterozygous state to malaria infection (4). *De novo* events can also result in mosaic alterations, depending upon which cellular division in embryonic development that the alteration occurred in, resulting in two cell populations with differing genotypes within the same organism. Mosaicism is subdivided into somatic and germline mosaicism, based on the subset of cells affected, with somatic cells unaffected in germline mosaicism. Mosaicism is a prevalent mechanism for the occurrence of genetic disease and potential for unusual inheritance patterns in the case of germline mosaic variants, as reviewed by Forsberg and Gisselsson (2017)(5).

1.1.4 Landscape of genetic alterations

Genetic aberrations are heterogeneous in nature but include alterations such as chromosomal aneuploidy, chromosomal rearrangements (e.g. translocations and inversion), epigenetic and imprinting defects, copy number alterations, and single or small nucleotide base errors (e.g. nucleotide substitutions, insertions, and deletions). The human genome is highly variable with every individual harbouring thousands of inherited alterations and tens of *de novo* alterations (6), many of which confer no phenotype or no known effect. For non-neutral variants, the alterations vary greatly in how they mechanistically lead to disease phenotypes but they broadly lead to altered or absent protein products either via 1) haploinsufficiency, in which a single functional gene allele is insufficient to generate sufficient protein to perform its biological function, 2) recessive variant or bi-allelic inactivation of a gene leading to insufficient or inactive protein products, or 3) generation of a dominant negative effect in which the affected gene product interferes with wildtype protein functions, all of which cause aberrations in downstream molecular pathways resulting in abnormal phenotypic presentations.

1.1.5 Medical genetics in the present

Understanding genetic alterations and their role in genetic diseases has developed and transformed into the field of medical genetics. Medical genetics is now a broad, multi-disciplinary, scientific field focused on identifying, classifying, and diagnosing genetic disorders and seeking to provide clinical prognoses, counselling, and treatment options for affected individuals and related family members. Prognosis of any genetic disorder varies widely based on the disease, ranging from only a minor impact on quality of life to severe life-long medical intervention. Genetic disorders, in general, intrinsically do not have any known cures (i.e. methods to correct the causative genetic alteration) due to the causative alterations being ubiquitous to every cell, though some success has been seen in the treatment of genetic autoimmune diseases in bone marrow utilising gene therapy and marrow transplants (7).

Treatments for genetic disorders focus on methods to alleviate or remove disease symptoms, slow the advances of disorders which become progressively worse with time, and provide counselling for affected individuals and their families regarding screening and prophylactic options, transplantation of the affected organ, as well as family planning in regard to fertility and likely transmission rates for offspring. Currently, medical genetics is focused on the application of personalised medicine for clinical management and the development of gene therapies, in order to provide a curative option for patients afflicted with genetic diseases. Utilisation of genomic sequencing to inform pharmacological contraindications and responses (8), potential tolerances and responses to treatment plans are already being implemented and used in cancer genomics through analysis of tumour sequencing, allowing for targeted use of tumour-specific therapeutics (9).

Gene therapies are a recent form of therapeutic measures for genetic disorders that aim to directly alter the genetics of an affected individual. Gene therapy can be applied by two distinct approaches, either somatic or germline, where somatic is by far the most common. Somatic applications could be used to fix genetic alterations in specific tissues or organs, such as lung epithelial tissue in cystic fibrosis (10), where the effect is not permanent and based on the ability of delivery methods to reach the affected cells. Germline methods function identically but occur by altering the DNA of germline cells, meaning that alterations are heritable. Most recently, the application of CRISPR-Cas9 nucleotide base editing has been seen as potential milestone in gene therapy with the ability to permanently repair mutations in genes causing diseases, with the resulting change present in subsequent cell divisions, but there are a number of ethical and practical concerns, particularly regarding germline applications (11).

1.2 Cancer: A genetic disease

Cancer is multi-systemic group of diseases resulting from abnormal and uncontrolled cellular growth in any organ within the human body leading to tumour formation. Cancers, in contrast to benign tumours, have malignant properties and can invade and metastasise to other tissues, leading to organ failure and ultimately death.

1.2.1 Genetic origin of cancer

Cancers are, at the most fundamental level, a genomic disease and the occurrence and accumulation of genetic alterations or alterations in epigenetic regulation. These alterations lead to a cellular environment in which uncontrolled replication can occur, which in turn leads to growth of tumour cells in the affected organ. In all cells, mutations and damage to DNA are acquired over time through both endogenous and exogenous mechanisms but they are generally either successfully repaired (12), detected by cell cycle check points (13), or the alterations are functionally neutral or result in no change to fitness (14).

Genetic alterations in genes leading to cancer development are defined by altering either one of two core types of genes, tumour suppressor genes (TSGs) or oncogenes, which function in opposing roles in the prevention and promotion of cellular proliferation and survival. TSGs are classically associated with the transcription of proteins, which act to negatively regulate pathways involved in cell cycle progression, replication, and positive regulation of pathways inducing apoptosis or cellular senescence. Tumour suppressor genes are consistently inactivated by genetic alterations in cancer cells, resulting in a loss of these functions. Conversely, proto-oncogenes (termed oncogenes after a causal genetic alteration has occurred) serve to negatively regulate apoptotic pathways and are positive drivers of cell cycle progression and division. Alterations in oncogenes, in contrast to TSGs, are not inactivating and act to either increase the function of the transcribed protein, cause constitutional protein activity, or elevate transcription rates, leading to further upregulation of their target molecular pathways.

The identification of both TSGs and oncogenes led to the development of hypothesises on how an acquired genetic alteration can specifically result in carcinogenic transformation. Knudson's two-hit hypothesis is regarded as one of the pivotal discoveries in cancer biology stating that loss or inactivation of a single TSG allele is insufficient to result in cancer and a secondary 'hit' to inactivate the remaining wild type allele is needed for cancer to develop (15). As with any rule there are exceptions, such as TSGs expressing dominant negative effects or haploinsufficiency (16), but most TSGs conform to this theory with secondary hits via additional inactivating variants or chromosomal deletions (which result in loss of heterozygosity (LOH)) of the remaining wild type allele.

Proto-oncogenes typically do not follow the same two-hit hypothesis and most are dominant in nature, with a single activating event sufficient to initiate oncogenic processes. In many cases, the loss of TSGs and activation of proto-oncogenes act in concert to drive tumour initiation, which consequently results in increased clonal expansion and genetic alterations to drive tumour evolution through acquired driver mutations. The process of clonal expansion and tumour evolution is not dissimilar to evolution that occurs at a species level, with acquired mutations conferring or reducing survival advantages for sub-clones of the initiating tumour cell (17). These features of tumour development resulted in the emergence of cancer cell traits termed the "hallmarks of cancer", a series of biological processes by which cancers can expand, survive, and resist detection and death (18).

Lastly, temporal distribution over which the first initiating event and the progression towards oncogenic potential occur, has been recently highlighted by the assessment of mutational profiles in normal tissues. Evidence for the occurrence of cancer driver mutations found clonally in normal tissues, such as skin and oesophageal, have demonstrated that driver mutations in both proto-oncogenes and tumour suppressors have been found in a large proportion of normal cells, increasing with age and exposure to exogenous mechanisms of DNA damage. These mutations were observed to have occurred as early as infancy, indicating that initiating event occur and persist over large temporal spans but cells harbouring these driver variants lacked additional oncogenic features such as higher mutational burden and chromosomal instability seen in cancer cells of the respective tissues (19–21). Furthermore, assessment of the timing of mutational events seen in clear cell RCC in the TRACERx renal study demonstrated that initial clonal expansion consists of only a few hundred cells harbouring a 3p loss initiating event, occurring upwards of 20 years prior to inactivation of *VHL* (considered to be the second hit). Following the inactivation of *VHL,* diagnosis of clear cell RCC was not found until between 10-30 years after numerous additional driver events had occurred (22). The importance of the temporal distribution of driver events is that cancer cells, relative to cancer at a patient-level, have extremely low penetrance and rarely result in a tumour.

1.2.2 Hallmarks of cancer

The hallmarks of cancer, as reviewed by Hanahan & Weinberg (2011)(18), are a set of biological features that are intrinsically linked to tumour initiation and development, acting to drive tumour proliferation or hinder pathways and external mechanisms that would act moderate, attenuate, or prevent tumour growth. Different cancers utilise different constituents of the hallmarks, manipulating both intracellular pathways and the external surrounding tissues and making use of different molecular networks and mechanisms to sustain cellular proliferation, the consequences of which drive the diversity in both cancer types, histologies, and prognoses. The hallmarks of cancer are not a definitive list of factors that drive cancer but a robust framework that acts to categorise the broadest number of molecular features that can drive tumour progression (see 1.2 Figure 1).

Loss of control of biological processes such as proliferative signalling, induction of replicative immortality by activation of telomerases, and the promotion metabolically favourable intracellular conditions act to increase cellular growth and replication. In tandem, disruption of cellular mechanisms functioning as growth suppressors through cell cycle checkpoints and negative feedback loops, resisting cell death via inhibition or inactivation of apoptotic signalling pathways, and the avoidance of immune destruction through dysregulation of cell surface markers and extracellular signalling, act to reduce cancer cell death by either internal molecular routes or external immune detection. Finally, tumours utilise the surrounding stromal tissue to establish a supportive environment for growth and development by inducing angiogenesis via activation of angiogenic pathways and prompting local inflammatory responses, which aid in tumour development, the consequence of which leads to the formation of a tumour microenvironment in which cellular growth, clonal expansion and evolution, and tissue invasion can flourish. The ability to be invasive and cause metastases is a distinct property of cancers, making this hallmark potentially the most significant in terms of disease mortality. While many benign tumours utilise the hallmarks of cancer sustain and promote their growth, local and distal invasion through increased motility and large-scale changes to underlying cellular subtype, as such the epithelial-mesenchymal transition (EMT), are properties only exploited by cancers. These two traits are the greatest contributors to the lethality of cancers with almost all cancers showing significant decreases in survival metrics once metastatic disease has occurred (23).

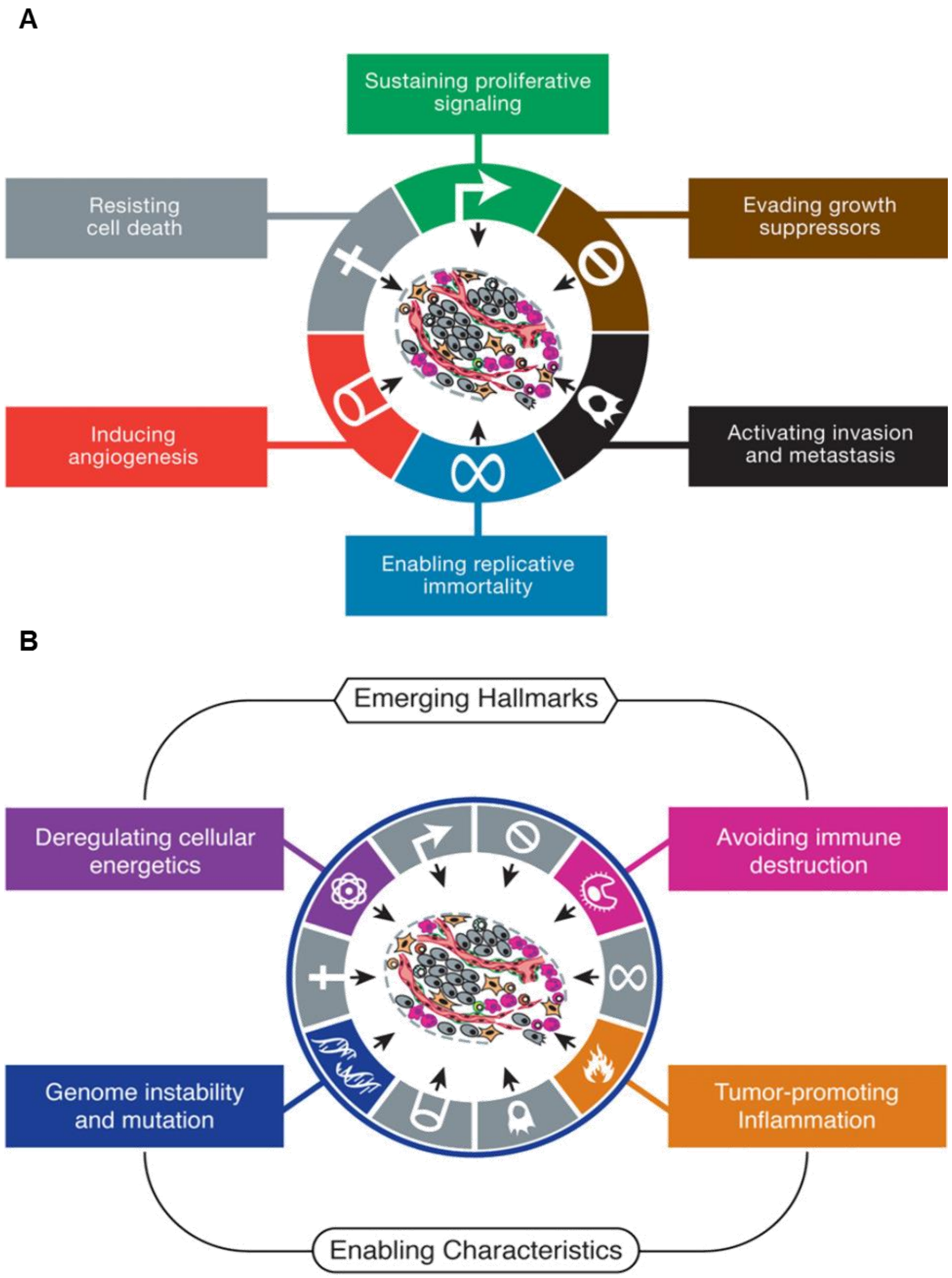
A
Sustaining proliferative signaling
Resisting cell death
Evading growth suppressors
Inducing angiogenesis
Activating invasion and metastasis
Enabling replicative immortality
B
Emerging Hallmarks
Deregulating cellular energetics
Avoiding immune destruction
Genome instability and mutation
Tumor-promoting Inflammation
Enabling Characteristics

1.2 Figure 1

Hallmarks of cancer – 1A Diagram depicting the features that comprise the hallmarks of cancer. Biological mechanisms tumours used to promote growth and survival. 1B Diagram demonstrating the newly discovered hallmarks of cancer regarding immune evasion and metabolic dysregulation, and non-hallmark characteristics which support tumour growth and development. Figure adapted from (18).

1.2.3 Genetic inheritance of cancer

While cancers most frequently occur sporadically, with incidence rates increasing proportionally to age in line with random acquisition of genetic variation and exposure to environmental factors, familial inheritance of cancers and susceptibility to cancers is well documented. A predisposition to cancer is most commonly identified by a strong family history of one or several cancer types within a pedigree but is also signified by a reduction in the average age of onset in the presenting individuals, or the presentation of multifocal or bilateral tumours. In many cases, these features present concurrently, with family histories containing individuals presenting with earlier onset and multiple tumours on presentation.

The mechanism for cancer development in an inherited disease is essentially identical to that of sporadic cases in regard to the genetic mechanisms and subsequent biological changes which result in oncogenesis, although the age of onset and cancer-specific presentations can differ, for example inheritance of a null TP53 allele results in Li-Fraumeni syndrome (24), a syndrome characterised by predisposition of a number of rare cancer types. Conversely, sporadic occurrences of TP53 mutations results in more common cancer types such as small cell lung, oesophageal, and ovarian cancers (25). Inheritable cases of cancer arise due to the inheritance, or in some cases *de novo* acquisition, of a constitutional variant in a TSG or proto-oncogene. The stable presence of a non-wild type TSG allele in all cells has a significant impact on the probability of tumour development; for TSGs, the barrier for complete allelic loss (as proposed in Knudson's two-hit hypothesis) is halved as only one somatic inactivating variant is required in the remaining wild type allele, rather than two as required in sporadic cases (15). For proto-oncogenes the process is similar; constitutional variants in proto-oncogenes overcome the requirements for somatic activation by already being constitutionally active and only requiring the loss of additional TSGs or the correct cellular environments to allow for tumour progression. Many syndromes associated with cancer risk phenotypically display an array of non-cancer pathologies as a result of a non-wild type allele in genes with multiple biological functions (26). Conversely, several cancer predisposition phenotypes only manifest as a predisposition to cancer development, despite most associated genes having functions outside of the remit of a TSG or oncogene, such as *BRCA1 DNA repair associated* and *BRCA2 DNA repair associated* (*BRCA1* and *BRCA2*) in Hereditary breast–ovarian cancer syndrome (27).

1.3 Renal cell carcinoma

1.3.1 Incidence

Renal cell carcinoma (RCC) is the most frequent form of kidney cancer accounting for more than 90% of diagnosed cases, the remaining of which includes cancers of the renal medulla and transitional cell carcinomas of the renal pelvis. Kidney cancers account for approximately 2% of new cancer diagnoses and 1.5% of cancer deaths per year, globally (28). RCC occurs on average at 64 years of age (29), with age of onset being significantly lowered in individuals presenting with RCC predisposition syndromes (30). Life time risk for individuals in the United Kingdom are estimated at 3% for males and 2% for females (31), with approximately 34% of cases being defined as preventable (attributed to lifestyle and environmental factors) (32).

The primary lifestyle factors attributable to RCC risk are increased body mass index (BMI; kg/m^2) and tobacco usage. Increased BMI results in combined relative risk increases for both sexes of 28% and 77% for overweight and obese individuals, respectively. BMI-linked RCC risk is biased towards females with increased risk at 38% compared to 22% in overweight individuals and 95% compared to 63% in obese individuals (33). Tobacco usage has also been showed to provide increased risk for RCC development with a relative risk increase of 16-36% for tobacco users compared to never-smokers (34). Other lifestyle and environmental factors for RCC risk include hypertension (35), acquired cystic kidney disease (36), diabetes (37,38), non-prescription analgesic usage (39), poor dietary choices (40,41), and exposure to specific chemical compounds (42,43).

Kidney cancer has seen the greatest increase in age-standardised incidence rate (ASIR) among all cancers, having seen a 23% increase in incidence between 1990 and 2013. Furthermore, kidney cancer occurs more readily in developed countries but has seen a similar increases of 34% and 36% in incidence rates between both developing and developed countries, respectively (28). Increases in ASIRs for kidney cancer may be attributable to increased rates of obesity (44), particularly in developed countries, which is directly linked to poor dietary choices (45), as well as compounding other risk factors such as hypertension (46) and diabetes (47). Moreover, kidney cancers have been historically difficult to detect due to being relatively asymptomatic until late in tumour progression (48), meaning technological advances such as use of abdominal ultrasound imaging, improved screening, and increased life expectance may lead to a greater proportion of kidney cancers being reported.

1.3.2 Major histological subtypes

Though RCC is broadly discussed as a singular disease, it is more accurately defined as collection of renal neoplasms with distinct morphologies, molecular mechanisms, and genetic backgrounds. According to the International Society of Urological Pathology (ISUP) more than 15 histological subtypes of RCC can be defined but a majority of cases are categorised into three primary groups; clear cell RCC, papillary RCC, and chromophobe RCC, which accounts for a vast majority of all RCC cases (49) (1.3 Figure 2).

Clear cell RCC is the most commonly diagnosed histological subtype of RCC with an occurrence rate of 63-83% of all RCC cases (50,51). Clear cell RCC occurs more predominantly in males than females (1.5-3:1 male to female ratio) and has its highest incidence between 60 and 70 years of age. Clear cell RCC is thought to originate from epithelial cells of proximal convoluted tubule and is defined by large clear cytosolic cell body due to lipid accumulation (52,53). In term of gross morphology, clear cell RCCs are solid, yellow tumours with a high degree of vascularisation (54). Clear cell RCC has the worst clinical prognosis compared to both papillary RCC and chromophobe RCC, with cancer-specific 5 years survival rates being 68.9%, 87.4%, and 86.7%, respectively (55). The most frequent tumour stage at diagnosis in clear cell RCC is stage I but some studies reported inconsistently, with stage III in two European studies (54,56) but stage I in a Japanese cohort (57).

Papillary RCC is the second most common histological subtype of RCC reported, split into two further subtypes type 1 and type 2, accounting for 11-18.5% of all RCC (50,51). As discussed in relation to clear cell RCC, type 1 papillary RCC have better prognoses and are clinically less aggressive (55), where type 2 papillary RCC are similar in clinical presentation. In similarity to clear cell RCC, patients most frequently report at stage I and at a median age of 65 (55). The two subtypes are designated as basophilic (type 1), due to the presence of small hyperchromatic basophiles with minimal cytoplasm, and eosinophilic (type 2) resulting from the presence of tumour cells with abundant eosinophilic cytoplasm (58). Morphologically, papillary tumours are solid, well-demarcated with minimal vascularity, particularly compared to clear cell RCC, and are slow growing (59). Differences between type 1 and type 2 papillary RCC, while they present at similar frequencies, are that type 2 papillary RCC more frequently present at higher grades and has markedly worse survival outcomes compared to type 1 (50).

Chromophobe RCC occurs in 5-6% of reported RCC tumours (50,51) and is considered the least aggressive subtype of the three major subtypes (55), with 5-year survival rates as high as 94% (51), and metastasis only seen in a small proportion of cases (58). Histologically, chromophobe RCC consists of large cells with webbed cytoplasm and haloed nuclei. Conversely to clear cell and papillary RCC, chromophobe RCC appears to occur more frequently or equally in females and occurs most frequently at lower stages, rarely being diagnosed at stage III or IV (50,55).

Additional histological subtypes of RCC do occur but most are rare relative to the frequency of the three primary types already discussed. These subtypes include, but are not limited to, clear cell tubulopapillary RCC, a histological subtype with characteristics similar to that of both clear cell RCC and papillary RCC (60). MiT-family translocation RCC, a subtype driven by recurrent somatic translocations of *Transcription Factor Binding To IGHM Enhancer 3* (*TFE3*) on Xp11.2 and t(6;11)(p21;q12) translocations involving *Transcription Factor EB* (*TFEB*), as well as *Melanocyte Inducing Transcription Factor* (*MITF*) and *Transcription Factor EC* (*TFEC*) (61). Mucinous tubular and spindle cell carcinoma, subtype with strong similarities to papillary RCC but recently described as a distinct histological subtype, reviewed by Zhao *et al.* (2015)(62). Lastly, succinate dehydrogenase (SDH)-deficient RCC tumours, caused by loss of the SDH complex components, are a recently classified histological subtype of RCC defined by distinctive eosinophilic inclusions corresponding to giant mitochondria (49).

A histological feature that appears independently of histological subtype but has a substantial effect on prognosis is presence or absence of sarcoma-like histology. Approximately 1-5% of RCC tumours consist of a sarcoma-like or sarcomatoid histology which is strongly associated with a much poorer prognosis compared to other histologies alone (63). While not consistently attributable to a single primary histological subtype, sarcomatoid RCC is more frequent in chromophobe RCC histologies though comprehensive data is limited (64,65). Sarcomatoid RCC is linked to a shift from an epithelial to mesenchymal phenotype (EMT) (66) and EMT is linked with metastatic potential and increases in mobility and invasiveness (67), explaining the increase in aggressiveness of RCC tumours with any sarcomatoid histology present.

1.3 Figure 2

Histological appearances of the three main tumour types of RCC: 2A Histological presentation of clear cell RCC. 2B Histological presentation of type 1 papillary RCC. 2C Histological presentation of type 2 papillary RCC. 2D Histological presentation of chromophobe RCC. Images adapted from Muglia *et al.* (2015)(58).

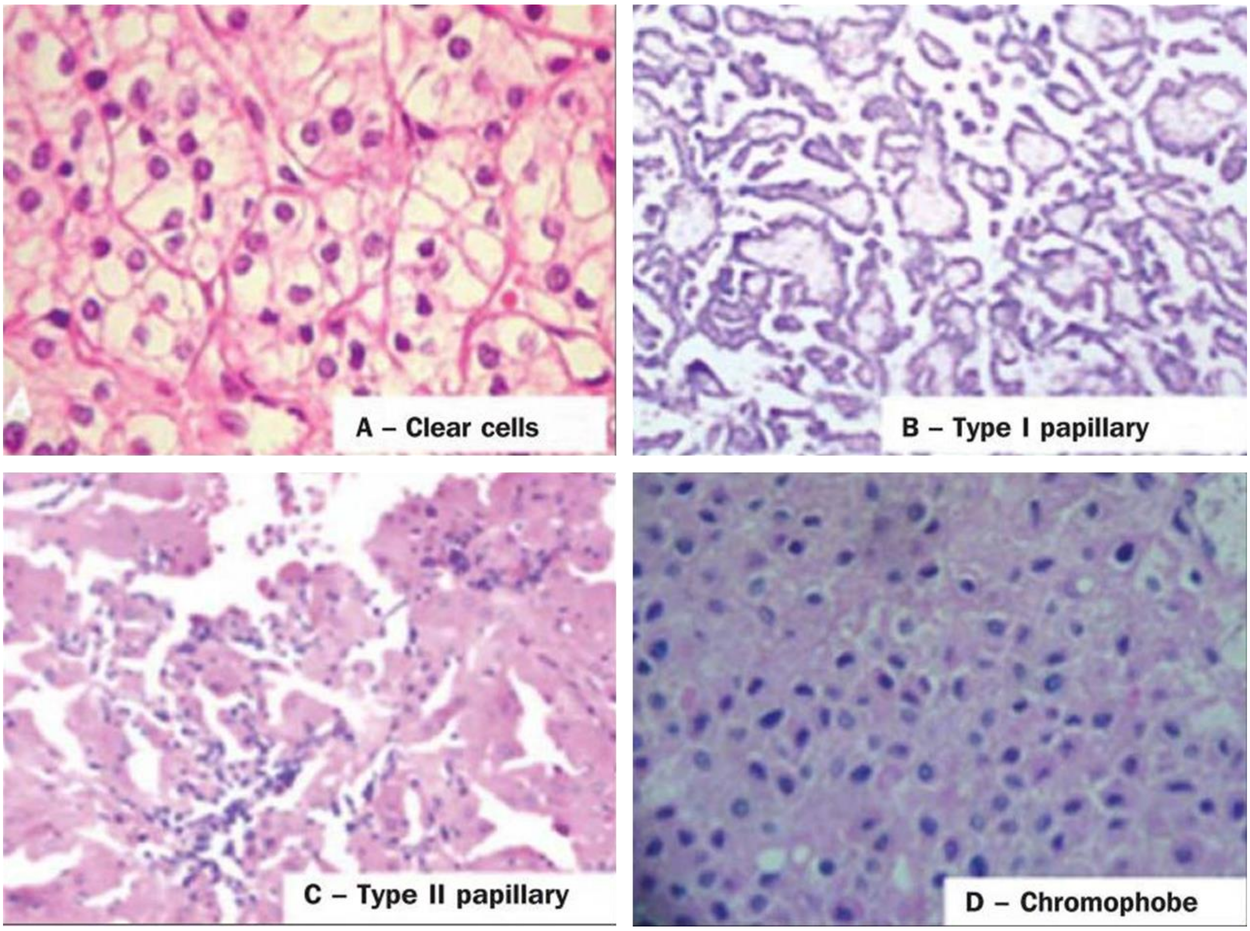

1.3.3 Tumour staging

Typically RCC is staged according to the degree of tumour spread throughout the body, where tumour size and invasiveness are taken into account (68). RCC stage is characterised and designated by classifications laid out by the American Joint Committee on Cancer as a combinatorial function of tumour size (T0-4), lymph node metastasis (NX, N0, or N1), and distant metastasis (M0 or M1) (69). 1.3 Table 1 describes the TNM system and its associated staging.

1.3.4 Tumour grade

The prognostic value of RCC tumour grades has long been recognised and widely utilised as a metric for outcome prediction and tumour progression rates (70). Tumour grading based on microscopic cellular morphology and differentiation of tumours acts as a surrogate for numerous underlying molecular and biochemical processes that influence the prior factors. Classically, RCC tumours have been widely graded by the Fuhrman grading system (71) but more recent studies have demonstrated that Fuhrman grading inadequately models tumour differentiation and that grading based on individual histological subtype is more representative of predicted disease progression (49).

Current grading of RCC tumours was proposed jointly by the world health organisation (WHO) and ISUP in 2012, with clear cell and papillary RCC being graded independently using nucleolar prominence and tumour necrosis for clear cell and nucleolar prominence only for papillary (72). Due to poor correlation with grading parameters (73) it was suggested that chromophobe grading should not be performed (49). With all other histological subtypes, application of ISUP grading guidelines is considered challenging due to lack of large enough cohorts to perform stratified analysis to inform survival predictions.

1.3 Table 1

Features and classification for staging of RCC tumours

Stage	TNM classification	Description
Stage I	T1, N0, M0	Tumour limited to kidney, less than 7 centimetres in size with no lymph node or distant metastasis.
Stage II	T2, N0, M0	Tumour limited to kidney, greater than 7 centimetres in size with no lymph node or distant metastasis
Stage III	T3, N0, M0	Tumour expanded to invade large proportion of kidney including major veins but with no lymph node or distant metastasis **or** tumour is any size and does not extend to the renal vein but lymph node metastasis
	T3, N0, M0	
	T2, N1, M0	
Stage IV	T4, N0, M0	Tumour extends beyond the kidney tissues into external tissues **or** any kidney tumour with distant metastasis.
	T4, N1, M0	
	T1-4, N0-1, M1	

1.3.5 Survival

Overall survival rates for kidney cancer are approximately 72.4%, 56.2%, and 49.5% for 1-year, 5-year, and 10-year survival, respectively. Survival rates for kidney cancers are strongly dependent on tumour stage, grade, and histological subtype, as discussed previously. Survival declines sharply if diagnosed at stage III or IV, with 5-year survival of 92.6% at stage I compared to 68.7% at stage III and only 11.6% at stage IV (29). 5-year survival is also impacted by age of diagnosis where individuals diagnosed before 45 years of age have a net survival rate of 87.8% compared to only 67.5% for those over 65 years of age (29).

1.3.6 Generalised treatment

While discussing all potential therapeutic routes and methods currently available for RCC is beyond the scope of this thesis, this section covers the general patterns and principles guiding RCC treatments as summarised from clinical guidelines (74).Treatment for RCC cases is generally directed by tumour stage at presentation, with surgical intervention being the most effective current treatment option. Surgical resection by partial, simple, or radical nephrectomy to remove tumour tissue with increasing amount of the surrounding normal kidney based on tumour spread, is the first line treatment for RCC where a lymphadenectomy is typically performed in stage III cases to remove affected regional lymph node tissues (74). In stage IV tumours use of radical nephrectomy is still widely used though is usually palliative due to tumour metastasis or tumour embolisms into the circulatory system, and where resection of distance metastases is also performed where applicable (74).

Across all stages, targeted therapeutic agents are deployed as both first- and second line treatments for RCC. Anti-angiogenic agents, such as sunitinib and pazopanib, which target vascular endothelial growth factor receptor (VEGFR), are commonly used in RCC due to known upregulations in angiogenic pathways driven by VEGFR and other kinases in RCC tumours (75,76). Most targeted therapeutic agents of this type are multi-kinase inhibitors and target VEGFR and its various isoforms, as well as epidermal growth factor receptor (EGFR), Platelet-derived growth factor receptor (PDGFR), mast/stem cell growth factor receptor (KIT), and hepatocyte growth factor receptor (MET) tyrosine kinases (77–79).

Further targeted pharmaceutical agents, such as temsirolimus and everolimus, have been design to target and inhibit mammalian target of rapamycin (mTOR) (80,81) due to its function in cell growth, proliferation, and cell motility via the PI3K-AKT-mTOR pathway which includes proteins coded by RCC-associated genes (82). Most recently, the development of Hypoxia inducible factor 2 alpha (HIF2-α) antagonists has shown potential in down regulation of angiogenic pathways in metastatic RCC with substantial pre-treatment with other agents (83). Phase I clinical trials utilising these compounds have demonstrated their tolerability as well as some moderate evidence for disease progression attenuation (84).

Immune therapy utilising monoclonal antibodies have been used as second line treatments for individuals with RCC (74). Use of antibodies, such as ipilimumab and nivolumab show increased overall survival and act to impair immune checkpoint mechanisms by inhibiting proteins Programmed death-ligand 1 (PD-1) and cytotoxic T-lymphocyte-associated protein 4 (CTLA-4), resulting in reduced cancer immune evasion (85,86). Additional treatments such as bevacizumab have also been used to target VEGFR, therefore blocking angiogenic pathways in a manner similar to that of sunitinib and pazopanib (87). Cytokine-based therapies have also been used for the treatment of RCC to augment immune response to cancer cells. Cytokines such as interferon-α and interleukin-2 have been widely given as conjunctive first line therapies with targeted therapeutic agents, though overall efficacy is modest (74).

Though therapeutic routes for many RCC patients are relatively effective, particularly in early stage diagnosis with high disease free and overall survival, therapeutic resistance is a well-documented outcome in metastatic RCC treatment in both clear cell (88) and non-clear cell subtypes (89). Resistance to tyrosine kinase inhibitors, such as sorafenib and sunitinib, which antagonise cell surface receptors VEGFR and PDGFR to supress angiogenic response, occurs frequently in metastatic RCC after 6-12 months (90), leading to disease progression despite continued treatment. While the mechanism of resistance is not fully elucidated, there are several proposed routes by which advanced RCC develop therapeutic resistance including drug resistance through reduced uptake or lysosomal sequestration (91,92), activation of alternative angiogenic pathways (93), and upregulation of pro-angiogenic cytokine Interleukin-8 (94). The effects of the tumour microenvironment has also been implicated in resistance through external expression of VEGF via pericytes supporting angiogenic growth in surviving endothelial cancer cells (95) and the recruitment of pro-angiogenic inflammatory cells to the tumour site (96). More recently, EMT and its associated transcriptional and morphological changes have been implicated as a mechanism of tyrosine kinase inhibitor resistance, with suppression of EMT-related gene expression resulting in attenuated therapeutic resistance in cell models (97).

1.4 Genetics of renal cell carcinoma

A number of Mendelian causes of RCC have been described and there is also evidence for the involvement low penetrance susceptibility alleles in RCC predisposition. In this section I will first describe Mendelian disorders associated with susceptibility to RCC and the results of GWAS studies for susceptibility alleles.

1.4.1 Inherited renal cancer

Though a majority of RCC cases are sporadic in origin, an estimated 2-4% of RCC cases are due to an inherited disorder (98). This minority of cases has been highly informative in sporadic cases for the determination of involved molecular and genetic pathways that are affected in RCC (99), as well as potential therapeutic targets for curative or palliative treatment (76,81,100). A summary of the different syndromic and non-syndromic RCC predisposing conditions is provided in 1.4 Table 2 and are discussed in further detail below.

1.4.2 Additional genetic risks factors in RCC predisposition

Family history of RCC is a significant risk factor with a relative risk of RCC incidence being at least 2.2 fold greater in individuals with a family history of kidney cancer (101). Regardless of familial history, early presentation of RCC is a strong indication of predisposition, with early onset being predictive of a positive detection of a pathogenic variant in a RCC predisposition gene (102). Lastly, presentation of RCC with multiple foci or bilateral occurrence is also a common indication of genetic predisposition of RCC with a significantly increased occurrence in comparison to sporadic cases (103). In an assessment of heritability of RCC in Icelandic populations, 58% of RCC cases were found in families with 2 or more affected family members, with increased relative risk for siblings and parents, particularly if incidence was prior to 65 years of age (104). Nordic twin studies have also validated the genetic component of RCC within families with a reported heritability of 38% (95% CI, 21%-55%), with no significant contribution from a shared environment (105).

In addition to the rare Mendelian causes of RCC predisposition described above, several studies have attempted to identify risk loci through genome wide association studies (GWAS) of RCC patients but, in contrast to the large number of susceptibility alleles identified for breast and colorectal cancers, there have been a limited number of loci identified as predisposing to RCC. Two SNPs (rs11894252 and rs7579899) found at 2p21 were shown to be associated with RCC risk and were present within intron 1 of *Endothelial PAS Domain Protein 1* (*EPAS1*; *HIF2-α*) with an odds ratio (OR) = 1.18, a gene with inherent links to carcinogenic mechanisms in RCC (106,107), as well as an additional locus at 11q13.3 (rs7105934) associated with reduced risk (108). Fine mapping of the region surrounding 2p21 and detailed single nucleotide polymorphism (SNP) imputation, three further SNPs (rs4953346, rs12617313 and rs9679290) which were not correlated with the SNPs reported previously (108), were associated with RCC risk and suggest a complex haplotype surrounding *EPAS1* (109).

A follow-up study, which included meta-analysis of both studies (108,110), confirmed both previously described loci as risk loci in RCC on 2p21 and 11q13.3, and suggested two additional SNPs in linkage disequilibrium on 12p11.23 (rs718314 and rs1049380) located proximally to the gene *Inositol 1,4,5-Trisphosphate Receptor Type 2* (*ITPR2*) (110). Analysis of clinical features of individuals carrying rs7105934 on 11q13.3 and rs1049380 on 12p11.23 demonstrated increased and reduced age of onset in RCC patients, respectively (111). A GWAS study in Icelandic participants further elucidated risk loci for RCC, identifying a dinucleotide SNP (rs35252396) on 8q24.1, in the vicinity of *MYC proto-oncogene, BHLH transcription factor* (*MYC*)*,* conferring an OR = 1.27 which had already been associated with other cancer types (112). Several additional studies then identified risk loci on 2q22.3, associated with rs12105918 in intron 2 of *Zinc Finger E-Box Binding Homeobox 2* (*ZEB2*), and on 1q24.1, associated with rs3845536 within intron 4 of *Aldehyde Dehydrogenase 9 Family Member A1* (*ALDH9A1*) (113,114). Association studies have also identified that risk loci on 11q13.3 are able to modify the binding of HIF to the transcriptional enhancer of *cyclin* D1 (*CCND1*) (115) and that SNPs rs1944129 and rs7177 found within *CCND1* may contribute towards RCC risk in Chinese populations (116). Most recently, association studied have demonstrated an association between cumulative SNPs linked to increased leukocyte telomere lengths and risk of RCC, implicating several additional loci with RCC risk (117).

The calculated population statistics and the limited risk conferred by common SNPs suggests that 2-4% of RCC cases linked to predisposition is likely an underestimate and there remains a relatively large unexplained proportion of heritability. Underestimation of heritability is supported by recent assessments of patients meeting genetic referral, where consensus referral criteria provided by the American College of Medical Genetics (ACMG) across two independent RCC cohorts resulted in 24-33.7% individuals in which their clinical features and histological findings would make them eligible for genetic testing (118), suggesting that many individuals with heritability may not be referred for genetic analysis in the first instance.

1.4.3 Von Hippel-Lindau disease

Von Hippel-Lindau disease (VHL; OMIM: 193300) is an inherited, autosomal dominant syndrome associated with predisposition to multiple benign and malignant tumour types. Individuals with VHL disease are subject to a range of clinical features including haemangioblastomas of the nervous system and retina, renal cysts, clear cell RCC, phaeochromocytomas (PCCs), cystadenomas, pancreatic neuroendocrine tumours, and endolymphatic sac tumours (119,120). VHL disease is a rare condition, at a prevalence of 1:39,000-91,000 and a birth incidence of 1:22,000-42,987 (121,122). Though VHL disease predisposes to various clinical features and multiple tumour types, clear cell RCC has a cumulative lifetime risk of ~70%, at a mean age of 44 years (123,124).

VHL disease was first described by Treacher Collins in 1894 who described two siblings with retinal haemangioblastomas (125). Studies in 1904 by Eugen von Hippel and further characterisation by Arvid Lindau in 1927 solidified the clinical features of VHL disease but the genetic cause was not uncovered until a century after the initial description. Comparisons made between the age of onsets in sporadic RCC cases and VHL disease cases suggested that the genetic component responsible for VHL was a tumour suppressor following Knudson's two-hit hypothesis (30), and loss of 3p in RCC was suggestive that this region contained the causal gene (126). Subsequent gene mapping, determination of the gene loci from collections of co-segregating disease-specific loci, led to the discovery of the gene *von Hippel-Lindau* (*VHL*) on the short arm of chromosome 3 at 3p25.3 (127). Investigations into mutational patterns in VHL disease patients and sporadic RCC cases revealed frequent inactivation of *VHL* and LOH in tumours, confirming it as a primary cause for RCC in both VHL disease and sporadic RCC cases (128,129).

A majority of individuals with VHL disease present with a family history of VHL with dominant inheritance of the affected *VHL* allele, though *de novo* variants and mosaicism is estimated to occur in 23% of cases (130,131). Interestingly, pathogenic alterations in *VHL* are also associated with familial erythrocytosis type 2 (ECYT2; OMIM: 263400), an autosomal recessive condition caused by homozygous or compound heterozygous specific missense variants in both *VHL* alleles (132) with little to no overlap of the clinical features with those of VHL disease (133).

Pathogenic variants in *VHL* are remarkably penetrant at the patient-level (contrary to cellular penetrance described earlier) with individuals developing at least one VHL-related cancer before 65 years of age in approximately 80-90% of cases (122,123). VHL disease is broadly categorised into four subtypes, corresponding to differential phenotypic presentations concentrated on presence and risk of RCC and phaeochromocytomas. The subtypes are defined as follows: Type 1 – RCC present with no phaeochromocytomas, which is further subdivided into high and low RCC risk dependent on the absence or occurrence of *BRK1* deletions in concert with *VHL* deletions (134), designated as Type 1A and 1B. Type 2A – Phaeochromocytomas with low RCC risk, Type 2B – both Phaeochromocytomas and RCC, and Type 2C – Phaeochromocytomas with no RCC (135). Though *VHL* is a well conserved gene, amino acids 1-53 show low evolutionary conservation and non-truncating variants in these amino acids do not appear to cause VHL disease (136). Variant types that lead to inactivation of *VHL* cover the full spectrum of molecular alterations including nonsense, frameshifting insertions and deletions, missense, partial or complete loci deletions (136), and most recently synonymous and intronic splice site affecting variants (137).

The *VHL* gene codes for the von Hippel-Lindau protein (pVHL) which functions in the regulation of cellular response to hypoxia. Under normoxic conditions Egl-9 Family Hypoxia Inducible Factor 1, 2 and 3 (EGLN1, EGLN2 and EGLN3; prolyl hydroxylases; PHDs) act to hydroxylate specific proline residues of HIF-α proteins, after which pVHL acts to bind hydroxylated HIF-α as a component of an pVHL E3 ubiquitin ligase complex (VCB), resulting in ubiquitin-directed proteolysis (138). During hypoxia, the oxygen-dependent hydroxylation of HIF-α proteins by PHDs does not occur, therefore the VCB complex does not bind and ubiquitinate HIF-α proteins, leading to an accumulation of hypoxia inducible factors (107,139). The translocation to the nucleus and cellular abundance of HIF-α allow for hetero-dimer formation with HIF1-β subunits which then bind hypoxia response element (HRE) motifs upstream of genes associated with hypoxic response (140). This leads to an upregulation of transcription of genes associated with growth, angiogenesis, metabolism and stem cell like phenotypes, reviewed by Keith *et al.* (2012)(141).

Loss of pVHL results in pseudo-hypoxic cellular environment, in which HIF1-α and HIF2-α substrates are not targeted for degradation regardless of hydroxylation status, which leads to upregulation of hypoxic response genes under normoxic conditions (141), consequentially driving tumour initiation. It is worth noting that although both HIF1-α and HIF2-α function in response to hypoxia, they have diverging functions and some reports suggest HIF1-α may act in opposition to HIF2-α as a tumour suppressor gene (142,143) and loss of HIF1-α is rarely reported somatically (144).

While pVHL primarily functions in the regulation of hypoxia, pVHL also functions in the regulation of cell cycle control, via p27 (145), microtubule organisation and spindle assembly (146), and regulation of p53 (147). While these alternative functions are well defined and have functions related to preventing tumourigenesis and progression, they are less rigorously studied, and the primary route of pathogenesis is presumed to be loss of HIF regulation. Animal modelling of *VHL* loss have provided some evidence to support the current theory regarding *VHL*-driven tumourigenesis.

Though homozygous *VHL* knockout mice models are embryonic lethal, heterozygous knockouts develop haemangioblastoma-like liver growths and VHL disease-like renal cysts (148,149) but studies were unable to show RCC development with *VHL* loss alone and suggest that tumour development is not dependent on constitutional activation of HIF pathways (150). This in turn is supported by the lack of cancer phenotype in bi-allelic inactivation of *VHL* seen in erythrocytosis type 2, where hypomorphic *VHL* alleles are present in every cell (133), the frequent loss of 3p as a second hit somatically (151), and by mouse models which recapitulated human clear cell RCC development in kidney-specific deletions of *VHL* and *Polybromo 1* (*PBRM1*) together but not alone (152).

1.4.4 Hereditary leiomyomatosis and renal cell carcinoma

Hereditary leiomyomatosis and renal cell carcinoma (HLRCC; OMIM: 150800) is an autosomal dominant disease resulting in a predisposition to tumours including RCC as well as cutaneous and uterine leiomyomas (153,154). The population prevalence of HLRCC syndrome is currently estimated to be 1 in 200,000 and relative risk for features of HLRCC have been estimated. HLRCC is highly penetrant for non-RCC phenotypes with most affected individuals presenting with leiomyomas, but risk for RCC appears to be reduced with occurrence between 15.6-31% (154,155). Median age of presentation of RCC in HLRCC cases is 37 years of age (range 10-77) (156), which matches to the age of onset described for other RCC predisposition syndromes and cases usually present with a limited or single tumour, though multifocal cases have been reported. Most tumours tend to be histologically classified as type 2 papillary RCC but also present with features of other histological subtypes (157). HLRCC RCC tumours tend to be highly aggressive (grade III or IV) (155), in contrast to most papillary RCC tumours which tend to be more latent (158).

HLRCC is associated with pathogenic variants in the *Fumarate Hydratase* (*FH*) gene (155,159,160). Most of the reported pathogenic variants within *FH* are missense mutations (68.2%), the remaining being small insertions or deletions, truncating mutations and splice altering variants (155,161). Pathogenic *FH* variants are not found in between 10-15% of HLRCC, suggesting there may be an unknown proportion of heritability that may be associated with undiscovered variants in *FH* (non-coding variation or copy number alterations) or associated with alterations in genes other than *FH* (155,160). As with *VHL*, *FH* is suggested to function as a tumour suppressor gene with bi-allelic loss of *FH* resulting in complete ablation of FH enzyme function (154,159). The *FH* gene is located at 1q43 at chr1:241,497,557-241,519,785 and consists of 10 exons which encodes the protein Fumarate hydratase, a core enzyme in the tricarboxylic acid (TCA) cycle (162).

FH catalyses the reversible hydration of fumarate to malate as part of the TCA cycle (163), driving generation of substrates such as purine triphosphates (adenosine/guanine triphosphates; ATP/GTP) and nicotinamide adenine dinucleotide (NADH) which are utilised by the electron transport chain for oxidative phosphorylation. Loss of FH results in perturbation of the TCA cycle, leading to a loss of oxidative phosphorylation and a metabolic switch to aerobic glycolysis to generate energy (164,165), in line with the metabolic shift described by the Warburg effect (164) in tumours. PHD enzymes function to hydroxylate proline residues of HIF2-α proteins, depending on cellular oxygen levels, and regulate hypoxic response (see above). Under normoxic conditions these post-translational modifications are added to HIF-α allowing pVHL complex binding and ubiquitination, leading to proteolysis of HIF-α (107,138,166). In cells with bi-allelic inactivation of FH, cellular fumarate accumulates and act as competitive inhibitors of PHDs which in turn results in the constitutive activation of HIF-α, establishment of pseudo-hypoxia, and transcription of genes associated with angiogenesis, cell growth, and metabolism (167–169).

Moreover, loss of FH can increase the number of reactive oxygen species (ROS) present which again acts to stabilise HIF2-α via inactivation of PHD proteins by reducing the availability of non-ROS oxygen molecules (170). Fumarate is able to post-translationally modify Kelch-like ECH Associated Protein 1 (KEAP1), a protein associated with a E3 ubiquitin ligase complex which regulates the stabilisation of nuclear factor erythroid 2-related factor 2 (NFE2L2) (171). NFE2L2 transcriptionally regulates genes associated with antioxidant response, upregulating genes which encode proteins which function in antioxidant response element (ARE) controlled genes (172). Specifically, ARE-controlled genes such as *aldo-keto reductase family 1 member B10* (*AKR1B10*) is suggested to be upregulated in both sporadic type 2 papillary RCC and HLRCC type 2 papillary RCC, allowing for improved response to oxidative stress and confer a survival advantage, particularly given the increased oxidative stress of a Warburg-like or glycolysis driven metabolism (172).

This is contrary to previous studies suggesting ROS actively inhibit PHD enzymes. It is likely that the increase of intracellular ROS is a genuine consequence of FH loss, as loss of oxidative phosphorylation leads to increase oxidative stress (173), but that fumarate both competitively inhibits PHD enzymes and modifies KEAP1 directly while ROS themselves confer relatively little to the stabilisation of HIF-α proteins. Lastly, accumulation of intracellular fumarate results in the inhibition of α-ketoglutarate-dependent diooxygenases involved in histone and epigenetic demethylation, such as ten-eleven translocation enzymes (TET) and lysine-specific demethylase (KDM) family enzymes (174). Dysregulation of epigenetic modifications by the inhibition of these enzymes, particularly TET, were then demonstrated to result in the indirect upregulation of HIF-α via loss of epigenetic inhibition of HIF target transcripts (175).

In similarity to *VHL*, homozygous or compound heterozygous variants in *FH* result in a differential autosomal recessive disease with limited phenotypic overlap. Bi-allelic inactivation of *FH* causes Fumarase deficiency (FMRD; OMIM: 606812) which manifests as progressive neurological dysfunctions including seizures, cerebral atrophy, and metabolic irregularities including lactic, pyruvic, and fumaric aciduria (176,177). Phenotypic presentation appears to be variable in severity but no FMRD case has presented with features associated with HLRCC, however parents of a FMRD case did present with HLRCC (159). Currently, it is suggested that differences in phenotype presentation between HLRCC and FMRD is due to gene dosage differences and that a majority of FMRD cases have a high rate of mortality before an age at which HLRCC features typically develop.

1.4.5 Birt-Hogg-Dubé syndrome

Birt-Hogg-Dubé syndrome (BHD) is an autosomal dominant syndrome associated with fibrofolliculomas, pulmonary cysts, pneumothorax, and renal cancers. BHD is driven by genetic aberrations in the *folliculin* (*FLCN*) gene. BHD predisposes to renal neoplasms, with between 12-27% of BHD patients developing renal cancer, often presenting as hybrid chromophobe RCC, typically chromophobe/oncocytomas (178–180). In contrast to some other inherited RCC disorders, renal cancers in BHD are histologically diverse; though one study reported a majority of BHD-related tumours as hybrid chromophobe/oncocytoma or solely chromophobe (84%), with a minority of cases being clear cell, oncocytoma, or papillary RCC (9%, 5%, and 2% respectively), other studies have reported a majority of tumours were of clear cell subtypes (179). Additionally, there is some isolated evidence that tumour histology in BHD cases is determined by the underlying driver variants within early tumour clones, with tumours harbouring somatic mutations correlating to the presenting histological subtype (i.e. oncocytoma with a secondary *FLCN* variants, oncocytic papillary RCC carrying a *MET Proto-Oncogene* (*MET*) variant, and a clear cell RCC tumour harbouring a *VHL* variant) (181).

Multifocal and bilateral occurrences in BHD-resultant renal cancers have a prevalence of 60% and 77%, respectively (182), with more recent studies reconfirming that a majority of individuals (83%) present with either bilateral or multifocal RCC (183). While the primary clinical manifestation of BHD syndrome is fibrofolliculomas, pulmonary cysts, pneumothorax, and RCC, BHD has also been shown to be related to several other cancers. BHD has been linked to the development of thyroid tumours, parotid tumours, adrenal carcinomas, melanoma, and the development of colorectal cancer (CRC) and/or colorectal polyps which have also been suggested to be clinical features of BHD (184–188), though further evidence to substantiate the associations is needed.

FLCN is a candidate tumour suppressor gene first identified by genome linkage analysis of BHD families to 17p11.2 (189). Subsequently, genetic analysis mapped *FLCN* to chr17:17,206,924-17,237,188 coding for a single full-length transcript of 14 exons, the first three of which are non-coding. *FLCN* is a highly conserved gene with many pathogenic variants being truncating variants, or variants within heavily conserved protein domains and these variants have been demonstrated to generate unstable protein products and to be under purifying selection (190). Additionally, *FLCN* contains a mutational "hotspot" at exon 11 due to the high frequency in which BHD patients present with truncating variants within this loci (191,192), though frequent deletions of exons 1-3 and exons 9-14 have also been reported (193,194).

BHD patients harbouring a single inactivating variant in *FLCN* are frequently found to have acquired a secondary somatic variant in, or LOH of, the wild-type allele of *FLCN* in RCC tumours (195). Conversely, it has been suggested fibrofolliculomas do not appear to display LOH and the pathogenesis of fibrofoliculomas seem to be driven by haploinsufficiency (196). Several animal models have corroborated this hypothesis; Rat models harbouring a heterozygous germline variant in the rat orthologue of *FLCN* were shown to present with renal tumours, of which 91% presented with LOH of the wild type allele and the remaining LOH-negative tumour had deleterious frameshift variant within the wild type allele.

The FLCN protein acts within several cellular pathways to regulate functions related to cellular growth, metabolism, and apoptosis. Through interactions with Folliculin interacting protein 1 and 2 (FNIP1 and FNIP2), FLCN acts to regulate 5' AMP-activated protein kinase (AMPK), which functions in the upregulation of hamartin and tuberin in the PI3K-AKT-mTOR pathway, resulting in attenuated signalling (197–199). *FLCN* knockout models have also established increased mTOR activity where loss of the wild type allele occurs, demonstrating a mechanism for tumour development in BHD patients (200). Furthermore, FLCN and its complex proteins FNIP1 and FNIP2 have been shown to inhibit the function of the MITF-TFE3-TFEB complex by reducing nuclear localisation (201), where MITF has been shown to regulate both mTOR and HIFα.

1.4.6 Hereditary papillary renal cell carcinoma

Hereditary papillary renal cell carcinoma (HPRCC; OMIM: 605074) is an autosomal dominant condition conferring a predisposition to the development of multifocal and bilateral papillary RCC tumours (202). HPRCC is associated with type 1 papillary RCC, generally being low grade, well differentiated, and is highly penetrant (156,203). The median age of onset for HPRCC tumour is 41 years of age and HPRCC cases are frequently bilateral or multi focal, but conversely to sporadic and other germline causes of RCC, sex appears to be uniformly affected (156,204,205). HPRCC tumours, in contrast to many other RCC syndromes, rarely co-occur with renal cysts but microscopic lesions do occur proximally to the primary tumours (204,205) and much like sporadic type 1 papillary RCC, HPRCC with type 1 papillary RCC are usually indolent in nature (206).

HPRCC is known to be caused by activating variants in *MET* and all activating variants have been nonsynonymous changes with the MET tyrosine kinase domain (207,208). The *MET* gene is located at 7q31.2 at chromosome co-ordinates chr7:116,672,390-116,798,386 and encodes a 21-exon transcript for the C-MET tyrosine kinase receptor (MET). MET functions as a cell surface receptor for hepatocyte growth factor (HGF) as it’s only known ligand (209). Binding of HGF to MET allows for the transduction of a signal cascade through the PI3K-AKT-MTOR pathway and RAS-ERK pathways, leading to upregulation of genes associated with cell survival, proliferation, and motility (210), as well as increased HIF1-α and HIF2-α activity through mTOR activation (211). Nonsynonymous variants in the tyrosine kinase domain of MET result in a protein with constitutive MET auto-phosphorylation without the presence of HGF, resulting in a constant upregulation of the pathways, such as PI3K-AKT-mTOR pathway, leading to tumour initiation (208).

1.4.7 Succinate dehydrogenase renal cell carcinoma

Succinate dehydrogenase renal cell carcinoma (SDH-RCC) is a subtype of RCC driven by loss of function of the succinate dehydrogenase complex (SDH; electron transport chain complex II). Only recently recognised as a distinct subtype of RCC (49), germline pathogenic variants in genes encoding components of the succinate dehydrogenase complex leads to a predisposition to RCC in an autosomal dominant manner. Inactivation of Succinate dehydrogenase complex, subunits A-D via pathogenic variants in *SDHA*, *SDHB*, *SDHC*, and *SDHD* respectively, are frequently associated with paragangliomas (PGLs), PCCs, and gastrointestinal stromal tumours (GISTs) (212).

Variants in these same genes can lead to RCC predisposition with the most common cause being *SDHB* mutations (213–216), with *SDHA* mutations having only been demonstrated more recently (217,218). SDH-deficient PCC and PGL have also been linked to variants in *SDHAF2,* which codes for an SDH complex assembly factor but no germline variants have currently been described in relation to RCC predisposition (219), and evidence for this association is limited. SDH-RCC cases are rare compared to the other RCC predisposing syndromes with an incidence rate estimated at 0.05-0.2% of all RCC cases (220). In similarity to other RCC-predisposition syndromes, age of onset is earlier than in sporadic RCC cases with a median of 40-43 years of age and moderately more predominant in males compared to females (M:F=1.7-2.3:1) (220,221). Generally SDH-RCC tumours are low grade but are frequently observed to be multifocal or bilateral in 26% and harbour metastatic potential, with a reported 11-33% of cases developing metastatic disease (220,222).

While SDH-RCC usually occurs without other malignancies, studies suggest approximately 15% of cases will additionally present with PGL and/or wild type GISTs (220). Histologically, SDH-deficient tumours do not resemble the classical subtypes seen in other inherited conditions, having a strong resemblance to oncocytomas, with cytoplasmic inclusions containing excessive numbers of abnormal mitochondria, and features of other histological characteristics also seen (221). The difficulties resulting from similarities to other tumour subtypes, particularly non-cancer tumours such as renal oncocytomas, is that misdiagnosis of potentially malignant tumours as benign may impact clinical treatment. Additionally, SDH-RCC tumours may appear to resemble hybrid oncocytic/chromophobe RCC tumours seen in BHD as such confirmation of *SDH* gene or *FLCN* inactivating variants is critical to inform diagnostics.

While estimates for disease penetrance is challenging when assessing SDH-RCC cases, *SDHB* mutation carriers are more frequent than others and lifetime risk for RCC in *SDHB* variant carriers is reported to be up to 14% at 70 years of age (215). However, recent studies employing Bayesian estimates of penetrance of pathogenic variants in *SDH* genes compared to ExAC controls, as well as case studies, have provided lower estimates for penetrance rates for *SDH* genes in PCC/PGL at 22% for SDHB, 8.3% for SDHC, and 1.7% for SDHA (*SDHD* was not assessed) (223) and an additional study stating a penetrance of between 0.1%–4.9% for *SDHA* (224). Further assessment of RCC risk has been investigated for *SDHB* and suggested lifetime risk for *SDHB* mutation carriers to be 4.7% by 60 years (225), supporting the limited penetrance of variants in *SDH* genes, particularly given the occurrence of Renal and Phaeochromocytoma/Paraganglioma Tumour Association Syndrome (RAPTAS) cases and the strong correlation between PCC, PGL, and RCC (226).

Loss of any one of the components of the succinate dehydrogenase complex is enough to result in destabilisation of the entire complex (227). In a similar manner to HLRCC and inactivation of FH, loss of succinate oxidation by SDH into fumarate as part of both the TCA cycle and the electron transport chain leads to an accumulation of intracellular succinate (168) as well as a reduction in oxidative phosphorylation (228). The accumulated succinate acts identically to fumarate to act as a competitive inhibitor of various biological processes related to RCC tumourigenesis. Succinate both acts to inhibit the function of PHD proteins, which drive HIF-α destabilisation via pVHL and inhibits α-ketoglutarate-dependent demethylases known to result in up-regulation of HIF proteins (175,229). Though exceptionally rare, homozygous (or compound heterozygous) alterations to SDH complex are profoundly detrimental, resulting in severe metabolic disorder, loss of cardiac function, and infant mortality in one case report (230). This is supported by null knock out mouse models in which *SDHB*, *SDHC*, and *SDHD* resulted in embryonic lethality (231).

1.4.8 Tubular sclerosis complex

Tubular sclerosis complex (TSC; OMIM: 191100) is an autosomal dominant multi-cancer predisposition syndrome which can confer a risk to RCC caused by inactivating variants in *TSC Complex Subunit 1* (*TSC1*) or *TSC Complex Subunit 2* (*TSC2*) (232). Patients diagnosed with TSC classically present with neurodevelopmental delay and epilepsy (and intracranial hamartomas), with cutaneous features such as angiofibromas, cardiac rhabdomyomas, and renal manifestations. The most frequent renal manifestations are angiomyolipomas and renal cystics (233). Renal angiomyolipomas as an entity are not classed as an RCC subtype as they are benign in nature, but both renal cysts and angiomyolipomas are linked to (234,235) and difficult to distinguish from RCC (233), respectively.

In comparison to other RCC-predisposing syndromes, RCC risk is lower in TSC with a prevalence estimated at 2-3% in the general population (233). This rate is more significant given that the incidence rate of TSC is much higher than many of the other RCC-predisposing syndromes at 1:6,760–1:13,520 (236), thus increasing the number of individuals going on to develop RCC of the total diagnosed with TSC. While the incidence of RCC is low in TSC, an important aspect is the molecular biology of the disease and its overlaps with other RCC-predisposing syndromes in genetic causes and phenotypic presentation.

RCC presenting in TSC are observed at a mean age of between 30-42 years of age and, conversely to other RCC syndromes, occurs at an inverse sex ratio (1:2.0-2.6: male to female ratio). In approximately 47-55% cases present with either multifocal or bilateral RCC, with as many as 20 individual tumours reported in one case. Metastatic disease is rarely documented in TSC RCC cases and prognosis is generally favourable, with most tumours occurring as oncocytic hybrid chromophobe-like RCC or papillary-like RCC histologies (232,237).

As mentioned previously, TSC is known to be associated with loss of function variants in *TSC1* and *TSC2* which encode the proteins hamartin and tuberin, respectively, mentioned previously in relation to BHD. Mutational assessment of genotype-phenotype correlations suggest that pathogenic variants in *TSC2* result in more severe phenotypes and is also more frequently inactivated than *TSC1* (238). An estimated 15% of cases are not identified to carry either a coding single nucleotide variant (SNV) or copy number variant (CNV) resulting in inactivation of either *TSC1* and *TSC2,* though a recent analysis suggested mosaic and intronic variants account for a large proportion of the pathogenic variation in TSC (238,239).

Hamartin and tuberin form a protein-complex, which functions as a tumour suppressor. The hamartin-tuberin heterodimer is regulated by RAC-alpha serine/threonine-protein kinase (AKT) (240) and is an inhibitor of GTP-binding protein Rheb (RHEB) (241), as components of the PI3K-AKT-mTOR pathway. RHEB functions upstream of mTOR and primarily acts to upregulate mTOR activity through direct interaction or induction of a conformational change in the mTOR complex, leading to an increase in mTOR phosphorylation (242). Increased activation of mTOR (and its associated complex mTORC1) leads to the same increase in cellular proliferation, motility, survival, and autophagy as described in HPRCC and BHD syndromes (82).

1.4.9 Cowden syndrome

Inactivating variants in the *Phosphatase and tensin homolog* (*PTEN*) gene are associated with Cowden syndrome (CS; OMIM: 158350), an autosomal dominant condition causing some neurodevelopmental disorders, as well as both benign and malignant tumours, including RCC. Cowden syndrome has an occurrence is estimated at 1 in 200,000 with a significant risk of breast, thyroid, endometrial cancers, and RCC. Life time risk of RCC for individuals with CS a reported 34%, though estimates are variable given a limited number studies, ranging between 2-34% at age 70 years, with an elevated risk in women (243–245). A majority cases of CS with RCC exhibited papillary RCC tumours, with the remaining presenting as chromophobe RCC, and a majority of the tumours showed complete loss of PTEN protein expression under examination by immunohistochemistry (246).

PTEN is a tumour suppressor gene located at chr10:87,863,113-87,971,930, codes for a 9-exon protein Phosphatidylinositol 3,4,5-trisphosphate 3-phosphatase and dual-specificity protein phosphatase (PTEN). PTEN functions in the regulation of the PI3K-AKT-mTOR pathway, via the inhibition of Phosphatidylinositol 4,5-bisphosphate 3-kinase catalytic subunit alpha (PIK3CA). PTEN acts to dephosphorylate phosphoinositide molecules, a lipid substrate utilised in Phosphatidylinositol by PIK3CA, downstream of cell surface tyrosine kinase receptors like VEGFR. This antagonistic response to Phosphatidylinositol signalling attenuates PI3K-AKT-mTOR signalling, reducing expression of genes associated with cell growth, proliferation, and angiogenic processes (82).

Further forms of CS or CS-like syndromes, driven by epigenetic inactivation of *Killin, P53 Regulated DNA Replication Inhibitor* (*KLLN*) and activating mutations in *AKT* and *PI3KCA*, have also been associated with RCC development in *PTEN* negative cases (247,248). The *KLLN* gene is present at the same loci as that of *PTEN* on 10q23.31, sharing the same transcription start site but transcribed in the opposite orientation. Analysis of 123 CS and CS-like cases without germline *PTEN* variants demonstrated hypermethylation of the shared promotor region, which did not impact *PTEN* expression but reduced *KLLN* expression 250-fold. Individuals with *KLLN* hypermethylation presented with RCC in twice as many cases as those with germline *PTEN* variants (247).

Further assessment of CS and CS-like individuals without *PTEN* or *KLLN* alterations by Orloff *et al.* (2013) identified alterations in components of the PI3K-ATK-mTOR pathway in *AKT* and *PI3KCA*. Of 91 cases sequenced, 11% harboured variants in either *AKT* or *PI3KCA* (2 and 8, respectively) and two individuals, one carrying an *AKT* variant and the other a *PI3KCA* variant, presented with RCC at 47 and 32, respectively (248).

1.4.10 CDC73-Related disorders

Inactivating variants in *cell division cycle 73* (*CDC73*; also known as *HRPT2)* are known to cause a series of autosomal dominant genetic disorders including Hyperparathyroidism jaw tumour syndrome (HPT-JT; OMIM: 145001) which predisposes affected individuals to a range of renal manifestations, including RCC. HPT-JT is characterised by synchronous or metachronous presentation of hyperthyroidism, ossifying fibroma of the jaw bones, renal tumours, and uterine tumours (249). Penetrance of HPT-JT is estimated to be 83% at age 70 years, with lower penetrance in females (250). Approximately 20% of individuals diagnosed with HPT-JT display renal lesions of some form, most frequently renal cysts or hamartomas with Wilms tumours, a form of paediatric kidney cancer, also occurring in a subset of cases. Though RCC manifestations are rare in HPT-JT, papillary RCC has been reported in conjunction with germline *CDC73* variants and somatic LOH of 1q31.2 (251) and the known links between renal cysts and malignant renal phenotypes (234).

CDC73 on 1q31.2 is a tumour suppressor gene encoding a 17 exon, 531 amino acid protein parafibromin, a component of the Polymerase-Associated Factor 1 (PAF1) complex, which has a cellular role as RNA polymerase II complex, and has been shown to interact with histone-modifying H3K4-methyltransferase proteins (252,253) and is known to function in the regulation of cell cycle progression via regulation of cyclin D1 expression (254). Parafibromin has also been shown to act to repress the transcription of myc proto-oncogene protein (MYC) via promotor suppression and demonstrates a capacity to cause G1 phase cell cycle arrest (255,256), cementing *CDC73* as a tumour suppressor gene. *CDC73* inactivation is also seen regularly in somatic renal tumours (including clear cell, papillary, and chromophobe RCC) and inactivation is typically via LOH (257), though some studies have demonstrated that hypermethylation and mutations within the 5' untranslated region (UTR) also result in allelic loss (258).

1.4.11 Non-syndromic renal cell carcinoma

In recent years, investigations into the molecular basis of inherited RCC have elucidated some of the molecular causes of non-syndromic inherited RCC. The earliest of these occurred prior to the identification of *VHL* with the identification of a large Italian American family with a history of clear cell RCC, a high incidence of bilateral presentation, and no age of onset greater than 60 years of age (259). This family was found to harbour a t(3;8)(p14.2;q24.2) translocation resulting in disruption of *Fragile Histidine Triad* (*FHIT*) and *Ring Finger Protein 139* (*RNF139*) at the break point sites, and formation of a fusion transcript (260). Further assessment and screening of individuals with RCC presenting with features of heritability uncovered a number of other families and individuals carrying constitutional translocations, most of which involved chromosome 3, and suggested specific constitutional translocations could confer a risk to RCC development (261). In depth review and analysis of RCC-associated translocation cases is performed in Chapter 6.

Several studies assessed germline RCC cohorts and families for the presence of genetic alterations in significantly mutated genes in RCC tumours. Studies of patients with co-occurrence of RCC and melanoma demonstrated a missense substitution in *MITF* are associated with higher risk of RCC compared to controls (262). Screening of unrelated probands with features of predisposition revealed that, although rare, germline variants in *BRCA1 Associated Protein 1* (*BAP1*) segregated with RCC phenotype and demonstrated LOH in several tumours as well as somatic VHL loss (263). In an assessment of 35 individuals with unexplained family histories of clear cell RCC, one case was shown to have a co-segregating frameshift variant in *PBRM1* supporting predisposition to RCC (264). It should also be noted that germline *FLCN* and *SDHB* mutations may also be detected in a subset of patients with apparent non-syndromic inherited predisposition to RCC (214,265).

Lastly, exome sequencing and targeted resequencing of patients with features of familial RCC uncovered candidate pathogenic missense variants in *Cyclin Dependent Kinase Inhibitor 2B* (*CDKN2B*) (266). While the occurrence of variants in *MITF*, *BAP1*, *PBRM1*, and *CDKN2B* are relatively rare, with only a small number of individuals per cohort being affected, they suggest the remaining proportion of heritability is likely to be split across many genes at a low percentage, rather than the discovery an unknown VHL-like gene, harbouring a large proportion of the remaining risk.

1.4 Table 2

Summary of major conditions predisposing to RCC including relative incidence rates, RCC risk per incidence and other clinical features (a - Estimated prevalence from pedigrees, not calculated based on population data) - * cumulative risk across all genes.

Condition	Heritance pattern	Gene(s)	Locus	Prevalence	Syndrome penetrance	RCC risk (%)	Major histology	Other features
Von Hippel-Lindau	Autosomal dominant	*VHL*	3p25.2	1:39,000 to 1:90,000	High	24-45	Clear cell	Haemangioblastomas Renal cysts Phaeochromocytomas Cystadenomas Neuroendocrine tumours Angiomatosis Endolymphatic sac tumours
Hereditary leiomyomatosis and renal cell carcinoma	Autosomal dominant	*FH*	1q43	Unknown	High	15-30	Papillary (type 2)	Cutaneous leiomyomas Uterine leiomyomas
Birt-Hogg-Dubé syndrome	Autosomal dominant	*FLCN*	17p11.2	1:200,000 (a)	High	12-27	Hybrid Chromophobe	Fibrofolliculomas Pulmonary cysts Pneumothorax
Hereditary papillary renal cell carcinoma	Autosomal dominant	*MET*	7q31.2	Unknown	High	Increased	Papillary (type 1)	Renal cysts
Succinate dehydrogenase RCC	Autosomal dominant	*SDHB* *SDHC* *SDHD* *SDHA*	1p36.13 1q23.3 11q23.1 5p15.33	Unknown	Low to moderate	14 *	Hybrid	Paragangliomas Phaeochromocytomas Gastrointestinal stromal tumours
Tuberous sclerosis complex	Autosomal dominant	*TSC1* *TSC2*	9q34 16p13.3	1:6,000	Variable	2-4	Hybrid Oncocytic	Fibromas Neurological disorders Neurodevelopmental disorders Rhabdomyomas Renal angiomyolipomas Renal cystic disease
Cowden syndrome	Autosomal dominant	*PTEN*	10q23	1:200,000	High	2-34	Papillary	Neurodevelopmental disorders Breast cancer Thyroid cancer Endometrial cancer
Chromosome 3 translocation associated	Autosomal dominant	Case dependent		Unknown	Variable	Increased	Clear cell	None

1.5 Somatic variation in renal cell carcinoma

Large scale sequencing studies of RCC tumours have been performed to investigate and elucidate the genetic causes of RCC and its histological subtypes. As discussed previously, in alignment with their histological disparities, the major histological subtypes are genetically heterogeneous and numerous genetic and molecular overlaps exist between somatic and germline alterations in RCC.

1.5.1 Clear cell renal cell carcinoma

Clear cell RCC, as the most common subtype of RCC, has been extensively characterised by tumour profiling studies utilising multi-omic approaches. Copy number variations in clear cell RCC are large scale losses or gains of entire chromosome arms, most frequently 3p which carries multiple inherited RCC genes as previously discussed, and very few focal events. Loss of 3p occurred in more than 90% of tumours assessed, with gains of 5q and loss of 14q seen in 67% and 45% of tumours, respectively. Whole exome sequencing of tumours revealed *VHL, PBRM1*, *SET Domain Containing 2* (*SETD2*), Lysine Demethylase 5C (*KDM5C*), *PTEN*, *BAP1*, *MTOR* and *Tumour Protein P53* (*TP53*) as the most significantly mutated genes. Of note, approximately 20% of tumours assessed had no alterations in any of the highly mutated genes, suggesting alternative drivers in combination with chromosomal copy number alterations in 3p and 5q. Epigenetic inactivation of *VHL* was demonstrated in 7% of tumours and was mutually exclusive with somatic *VHL* SNVs. Network analysis showed dysregulation pathways for pVHL and its interacting components and chromatin remodelling (including genes *PBRM1* and *AT-Rich Interaction Domain 1A* (*ARID1A*))(267). Systematic sequencing of clear cell RCC recapitulated the pivotal role of *VHL* and hypoxia in sporadic clear cell RCC, with 55% of cases harbouring *VHL* mutations, 82% having upregulation of hypoxia pathways, and 87% demonstrating loss of 3p. Further analysis resulted in the identification of multiple somatic truncating mutations in histone modifying genes, containing *SETD2* which was frequently seen in other studies, including *KDM5C*, *Lysine Demethylase 6A* (*KDM6A*), and *Lysine Methyltransferase 2D* (*KMT2D*) (268). Comprehensive integrative studies across more than 100 clear cell RCC tumours reiterated other findings but also identified driver mutations in *Elongin C* (*TCEB1*), *TET2*, *KEAP1*, *TP53*, and *MTOR*. Of note, mutations in *TCEB1* were mutually exclusive with *VHL* variants, which is significant given they both function as part of the VCB complex (269).

More recent spatial and temporal sequencing approaches to understand the somatic variation of clear cell RCC have uncovered the range and depth of differences because of tumour heterogeneity both within and between tumours. Analysis of multi-site & multi-tumour data from the TRACERx renal study uncovered that specific driver events or clusters of events are associated with different clonal evolution trajectories, branching potentials, and intra-tumour heterogeneity, each of which have different prognosis outcomes and responses to clinical treatments (270). These evolutionary trajectories of specific sub-clones mirrors and explains the differences seen at the clonal driver mutation resolution (such as *PBRM1* loss tumours having poorer survival) and why other tumours with different drivers respond differently in both progression and response to treatment.

1.5.2 Papillary renal cell carcinoma

Genetic characterisation of papillary tumours reiterated the distinctions found histologically and implicates a different subset of genetic loci in tumour development (158). Type 1 papillary RCC, harbour frequent copy number gains of chromosome 7 and 17 whereas Type 2 papillary RCC tumours are characterised by significantly less copy number losses but two distinct clusters of cases with or without a high degree of chromosomal instability and loss of 9p. Whole exome analysis revealed that across all papillary RCC cases the most significantly affected genes included *MET*, S*ETD2*, *Neurofibromin 2* (*NF2*), *KDM6A*, and *SWI/SNF Related, Matrix Associated Actin Dependent Regulator of Chromatin Subfamily B, Member 1* (*SMARCB1*). Additional restriction to genes already implicated in cancer demonstrated *BAP1, PBRM1*, and *TP53*, among others were associated with papillary RCC. Lastly, gene fusions of *TFE3* and *TFEB* with various genes occurred in a proportion of papillary RCC tumours (10.6%), including *HIF1A*.

In regards to specific papillary RCC subtypes, type 1 papillary RCC tumours more frequently harboured variants in *MET* (18.6%), which clustered with known germline predisposition variants found in HPRCC, and had increased levels of *MET* expression compared to type 2 papillary RCC. Collectively, given the amplification of *MET* in cases with chromosome 7 gains, 83% of type 1 papillary RCC tumours carried *MET* alterations. In type 2 papillary tumours, *Cyclin Dependent Kinase Inhibitor 2A* (*CDKN2A*) alterations were more frequent (25%) with focal losses of 9q21, mutations, or hypermethylation as the cause. Additionally, *SETD2*, *BAP1*, and *PBRM1* were frequently altered, but in contrast to clear cell RCC, loss of 3p was infrequent. Additionally, CpG island methylator phenotype (CIMP) associated tumours, were designated as a subset of type 2 papillary tumours driven by somatic mutations in *FH.* In tumours identified with hypermethylation profiles, 55.6% carried alterations in *FH* as well as decreased mRNA expression of *FH* and increased expression genes associated with glycolysis. This agrees with HLRCC caused by germline inactivation of *FH,* where type 2 papillary RCC is most common (155) seen as well as the inhibition of epigenetic factors by accumulated fumarate (174).

1.5.3 Chromophobe renal cell carcinoma

Characterisation of chromophobe RCC by Davis *et al.* (2014) demonstrated the unique genetic features of this RCC subtype. Chromophobe RCC carries a distinctive copy number alteration pattern with loss of chromosomes 1, 2, 6, 10, 13, and 17 in most cases (86%), with wide spread non-focal loss of multiple other chromosomes, including chromosome 3 and was shown to have a low mutational rate, even compared to other RCC subtypes (approximately 3-fold less than clear cell RCC; 0.4 mutations per Mb). *TP53* was reported as the most altered gene being mutated in 32% of cases assessed, with variants also being present in *PTEN* (9%), *MTOR* (3%), and *TSC1* or *TSC2* (6%). In general, chromophobe RCC has fewer hypermethylation events in comparison to clear cell RCC and demonstrated epigenetic silencing of *CDKN2A* in 6% of cases. In relation to gene expression patterns, upregulation of genes associated with the TCA cycle and electron transport chain were seen, counterintuitively to the shift away from oxidative phosphorylation that may be expected due to the Warburg effect. In addition to metabolic expression changes, increased expression of genes involved with cell cycle progression was also described. Lastly, analysis of structural variation demonstrated a significant portion of chromophobe RCC cases have chromosomal break points with the *telomerase reverse transcriptase* (*TERT*) promotor, associated with telomeric end repair, and expression was shown to be elevated in these cases (271).

Further assessment of RCC tumours as a collective revealed additional focal losses and amplifications of genes with associations to germline predisposition cases including loss of *SDHD* and *PTEN*, as well as amplifications of *PIK3CA* and *sequestosome 1* (*SQSTM1*) (272), of which *SQSTM1* is implicated as the driver gene in 5q amplifications (273). Complementary assessment of data from the cancer genome atlas (TCGA) cancer study by Ricketts *et al.* (2018) recapitulated much of the previous work with some additional findings. Both type 2 papillary RCC and its subset CIMP-RCC have increased copy number loss of chromosome 22, which carries the loci for *NF2* and *SMARCB1* and both chromophobe RCC and CIMP-RCC have loss of 13q, which harbours *retinoblastoma 1* (*RB1*) and *BRCA2*. Furthermore, collective assessment of RCC subtypes together revealed that *TP53* and *PTEN* were the only significantly mutated genes shared by all RCC tumour types as well as deletion or hypermethylation of *CDKN2A* (274).

1.5.4 Epigenetics of renal cell carcinomas

Epigenetic inactivation is a well-established mechanism of cancer evolution and development (275) and analysis of epigenetic alterations in RCC tumours has also been crucial to understanding the molecular mechanisms driving tumourigenesis in RCC and its links to predisposition. Discoveries of hypermethylation of several genes on 3p, including *VHL* and *Ras association domain Family Member 1* (*RASSF1A*) in sporadic RCC seen in 19% and 26% of cases, respectively (276,277), demonstrated the potential for epigenetic alterations to define somatic tumour development. Additional genes in the 3p region were demonstrated to be hypermethylated including *family with sequence similarity 107 member A* (*FAM107A*) (278) and *FHIT* (279), with further candidate tumour suppressors associated with RCC and other cancers also being identified, such as *CDKN2A* (280)*,* *cadherin 1* (*CDH1*) (281)*,* and *Ras association domain family member 5* (*RASSF5*) (282)*.* Various further studies have implicated additional genes as downregulated in RCC through hypermethylation such as *KLLN* which is associated with Cowden syndrome (283), *secreted frizzled related protein 1* (*SFRP1*) a gene related to the downregulation of the Wingless/Integrated (WNT) signalling pathway (284), and *mutS homolog 2* (*MSH2*) which is related to DNA repair (285), as well as further genes altered across multiple RCC subtypes are detailed in a review by Shenoy *et al.* (2015)(286).

Further comprehensive analysis of epigenetic inactivation in RCC tumours has identified a range of different genes associated with hypermethylation in RCC, including the characterisation of CIMP tumours described previously (287). Initial genome-wide approaches to discover frequently hypermethylated promotor regions in RCC identified 9 genes. Of those genes identified, 6 displayed reduction in functional expression and activity in *in vitro* experiments suggestive of cellular roles as tumour suppressors (288) and follow-up methylation array studies identified more than 200 hypermethylated loci compared to normal tissues, including genes *solute carrier family 34 member 2* (*SLC34A2*), *ovo like transcriptional repressor 1* (*OVOL1*), and somatostatin (*SST*) in 64%, 40%, and 31% of tumours respectively (289).

Hypermethylation, outside of promotor-specific methylation, has also been examined where RCC samples were characterised by hypermethylation profiles preferentially occurring within coding regions. The hypermethylation disproportionately affected both kidney-specific enhancer regions associated with histone methylation as well as genes associated with hypoxia, likely as a consequence of ongoing dysregulation of hypoxic pathways (290). Finally, use of methylation alterations in RCC has been utilised as a biomarker, both diagnostically and predictively in the development and progression of RCC tumours which can act to detect recurrent events or predict prognostic features in assessed patient, reviewed by Lasseigne *et al.* (2018)(291).

1.6 Inherited and somatic variants in renal cell carcinoma

In general, somatic alterations in different RCC subtypes are characteristic of that specific histology but clear overlaps at a chromosomal level (e.g. loss of 3p in clear cell RCC), but perhaps more importantly, at a gene level occur in which a distinct but interconnected pattern of molecular pathways is delineated. Genetic alterations in both germline and somatic analysis can be defined broadly to being associated with one of three networks; VHL pathway, PI3K-AKT-mTOR pathway, and histone modifying and chromatin remodelling network. In both sporadic and inherited cases of RCC, the affected entities appear to map to one of these pathways with common proteins and metabolic substrates linking them together.

HIF-α proteins are one of the primary endpoints of both the VHL-driven pathway and the PI3K-AKT-mTOR pathway. *VHL* is found to be both inactivated in VHL disease and frequently lost in sporadic RCC through inactivating mutations and loss of 3p in clear cell RCC, both acting to drive tumour initiation and progression via HIF upregulation and a pseudo hypoxic gene response. Variants found in *FH* in HLRCC and *SDHA, SDHB, SDHC,* and *SDHD* in SDH-RCC, while acting to disrupt cellular metabolic processes also converge on the VHL pathway indirectly. Accumulation of both succinate and fumarate results in pseudo-hypoxic conditions due to the inhibition of PHD proteins and loss of HIF1-α and HIF2-α hydroxylation, consequently reducing HIF protein degradation via VHL (168).

The PI3K-AKT-mTOR pathway drives HIF upregulation as well as mTOR activity, and multiple positive and negative regulators and components are implicated in RCC. Activating variants seen in *MET*, as seen in HPRCC and amplification of chromosome 7 in sporadic papillary RCC result in constitutional activation of the PI3K-AKT-mTOR pathway at its origin point on the cell surface, causing continuous upregulation of all the downstream components, including HIF2-α and VEGFR (292). Inactivation of *PTEN* which acts as an inhibitor of PI3K signal transduction are observed in both Cowden syndrome and somatically in both clear cell and chromophobe RCC subtypes, resulting in loss of regulated signal transduction through PI3K proteins.

Further components of the PI3K-AKT-mTOR pathway are altered including *TSC1* and *TSC2* inactivation, as described in TSC and chromophobe RCC, which act to inhibit RHEB directly upstream of mTOR. Indirectly, the pathway is perturbed by variation in *MITF* and *FLCN*. Inactivation of *FLCN* in BHD syndrome where loss of *FLCN* results in both the loss of MITF inhibition and AMPK-driven upregulation of TSC1 and TSC2, though interestingly *FLCN* variants do not appear to occur somatically. Oncogenic alterations in *MITF* found in a subset of non-syndromic heritable RCC cases, as well as in Xp11.2 and t(6;11) sporadic translocation cases via fusion transcripts, cause direct upregulation of HIF-α proteins and increased activity of mTOR.

Finally, the histone and chromatin remodelling pathways are routinely affected somatically with components of the SWI/SNF complex, including *PBRM1* which is seen in germline predisposition, driving RCC through altered transcript and epigenetic alterations. *BAP1* is also seen both somatically and in heritable cases, resulting in the dysregulation of histone modifications. This final pathway is not decoupled from the others entirely though, with accumulations of fumarate and succinate resulting in the inhibition of TET and KDM proteins, and subsequently dysregulation of chromatin remodelling an epigenetic functions (175,229). 1.6 Figure 3 provides a diagrammatic overview of these overarching pathways, components and links to RCC predisposition and tumour formation, though it should be noted that this is not fully inclusive of all the genetic components to be implicated in RCC pathogenesis, in germline or somatic cases.

1.6 Figure 3

A diagrammatic representation of the main cellular pathways affected in RCC (adapted from Ricketts *et al.* (2016)(293)). Green components are substrates and/or signalling molecules. Blue components represent proteins coded by genes affected somatically in RCC. Orange components represent proteins coded by genes affected in germline predisposition to RCC (No key is provided for genes affected in both). Pointed arrows demonstrate positive or upregulation of the target component whereas blunted or flat ended arrows demonstrate inhibitory or downregulation of the target component. HIF1α and HIF2α are labelled in yellow as the key convergence point of multiple RCC-related pathways.

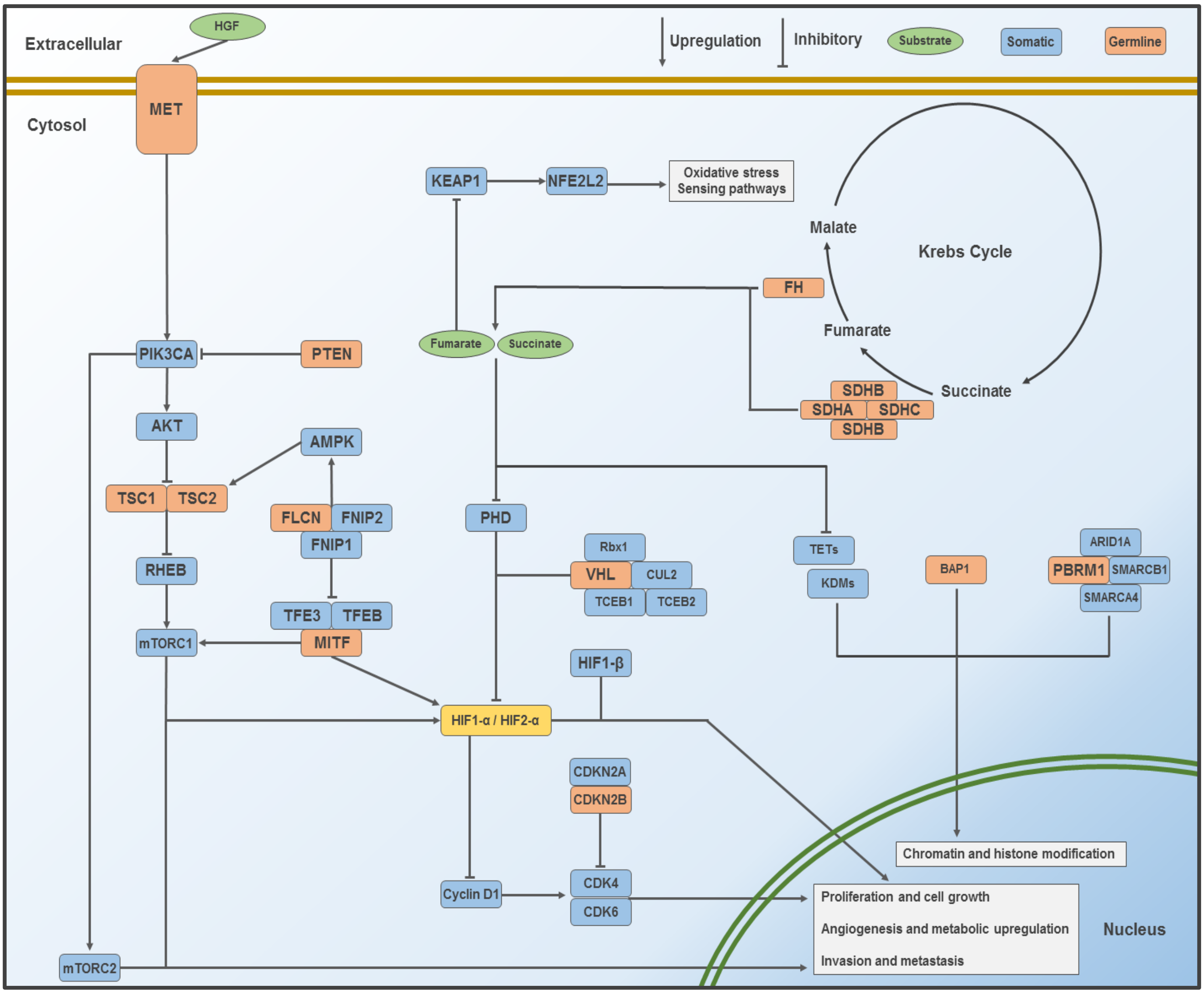

1.7 Sequencing in rare diseases

1.7.1 Sequencing technologies

The efficiency of identifying genetic alterations that result in disease phenotypes has progressed rapidly over the last two decades, with ever decreasing costs and ever-increasing breadth and depth of genetic information accurately interrogated by each technological iteration. A milestone in the advancement of DNA sequencing was the development of Sanger sequencing (294) and its application in automated capillary gel-electrophoresis (295), allowing for the sequencing of the complete human genome in 2001 (296).

Following this breakthrough, rapid development of technologies with greater throughput and lower economic and labour costs became the goal of genomic sequencing, culminating in the development of high-throughput platforms utilising technologies such as sequencing by synthesis (Illumina, 454, Ion Torrent) and sequencing by ligation (Complete Genomics, SOLiD). The widespread adoption of 2nd generation next generation sequencing (NGS) technologies, particularly Illumina-based platforms, resulted in large scale sequencing of thousands of rare disease and oncology cases. Additionally, development of sequencing adaptations such as RNA-seq (297), bisulphite sequencing (298), ChIP-seq (299), and many others have allowed for the generation of sequencing data in numerous “-omics”, leading to multi-dimensional analysis and providing greater biological insights. The ability to limit sequencing in 2nd generation NGS technologies to specific target regions (e.g. whole exome sequencing and targeted gene panels) has further improved efficacy, increasing the biological relevance of the sequenced regions and reducing overall cost compared to whole genome sequencing.

While 2nd generation NGS technologies have revolutionised genomic sequencing, 3rd generation sequencing technologies (Pacific Biosciences SMRT sequencing (PacBio SMRT), 10X Genomics and Oxford NanoPore Technologies (ONT)) are beginning to move into the spotlight, bringing with them unique advantages and disadvantages. Perhaps the greatest disadvantage for 2nd generation NGS technologies is the length of reads that are generated. The shorter read lengths limit coverage over complex genomic regions, result in difficulties resolving repetitive genomic loci, have poor resolution of structural variation, and an inability to perform accurate haplotype phasing.

The use of long read lengths overcomes many issues stemming from short reads. Use of long reads in all 3rd generation technologies has improved alignment to complex genomic regions and highly repetitive loci and has improved the calling and characterising of large structural variations. Specifically PacBio SMRT sequencing and 10X Genomics have seen vast improvements in haplotype phasing compared to short read sequencing (300,301). Furthermore, 3rd generation methods such as PacBio SMRT and ONT have demonstrated the ability to perform innate nucleotide base modification detection without the need for prior processing during library preparation (302,303), though it is currently restricted to CpG island methylation detection.

A clear shortcoming of 3rd generation technologies is a large increase in cost for similar sequencing throughput, particularly for ONT sequencing, but uptake by the scientific community will drive prices down with sufficient demand. A disadvantage to even PacBio and 10X genomic long read sequencing is the reliance of genomic centres with the financial and logistical means to provide sequencing, each having high costs, maintenance and large machinery requirements to run effectively. The development of ONT sequencing provided a reasonably high-throughput, portable sequencing option and demonstrated its efficacy in sequencing genomes in infectious disease outbreaks such as Ebola and Zika viruses (304,305). Furthermore, read lengths in ONT sequencing are only limited on the length of DNA provided to the sequencer after library preparation and physical constraints at the sequencing pore, allowing for exceptionally long reads of up to 2 Mb in length (306). This advantage has been critical in the use of ONT sequencing for the characterisation of structural variation larger than the read lengths of PacBio and 10X genomics (307), and where specific loci are known to carry structural variants but the precise nature is not known, including large deletions and tandem repeat expansions (308,309). Compared to both 2nd generation short read technologies and other 3rd generation methods, ONT has some significant disadvantages, including reduced throughput and increased per read error rates, particularly for repetitive regions, but far lower cost and ease of use make it highly versatile given the right context.

1.7.2 Sequencing technologies - The right tool for the job

While technologies have rapidly developed and evolved to generate vast quantities of data, no technology is without its niche, with Sanger sequencing still seeing ubiquitous use in both clinical and research environments for targeted sequencing projects, validation of NGS findings, and clinical diagnosis. In all, the selection of a specific sequencing technology relies upon the context in which it is being applied. The generation of whole genome sequencing via Sanger sequencing is now an absurd idea, resulting in substantially increased economic, labour, and time costs over newer 2nd and 3rd generation methods. Conversely, using long read PacBio sequencing for the identification of variants in a single exon of one gene is equally unreasoned, providing no practical benefits over simple polymerase chain reaction (PCR) amplification and Sanger sequencing. Important selection of the most appropriate sequencing method for the question being asked is vital to both maximise the biologically relevant data whilst minimising economic, labour, and computational costs. In 1.7 Table 3, a comparison is made for which sequencing approach is most appropriate to the study design being used if only utilising DNA sequencing.

1.7 Table 3

Summary of capabilities of various sequencing technologies for DNA only sequencing given with example of case use. Question marks suggest the application is possible but only under specific circumstances.

Sequencing technology	DNA only sequencing					Example
	SNVs	CNVs	SVs	Base modifications	Phasing	
Sanger sequencing	✓	✗	✗	✗	✗	Sequencing of a single exonic region or series of SNPs in 50 samples
Short read sequencing (Exome)	✓	?	✗	✗	✗	Sequencing of exonic regions of 100 genes in 100 samples
Short read sequencing (Genome)	✓	✓	?	✗	✗	Identify coding and non-coding SNVs and CNVs across the entire genome in any number of samples
Pacific Biosciences SMRT Sequencing	✓	✓	✓	✓	✓	Complete characterisation of genetic alterations in any number of samples
Oxford Nanopore Technologies	✓	✓	✓	✓	?	Targeted sequencing of SVs and complex regions or small genome sequencing - single or multiple samples
10X Genomics	✓	✓	✓	✗	✓	Complete characterisation of genetic alterations in any number of samples but without need for methylation

1.7.3 Variant detection in rare disease

The principal function of any sequencing technique is to identify the causal variant or variants associated with the disease phenotype being investigated. Given the vast number of variants some methods can uncover, filtering and identifying a causal variant can be a substantial challenge. In hereditary disease, there are three primary methods for variant identification which are familial segregation, trio analysis, and abundance in unrelated probands. Familial segregation is the effective presentation of a phenotype within a family pedigree where affected individuals carry the candidate genotype, where presentation is variable based on inheritance model and the penetrance of the phenotype. For example, in a fully penetrant autosomal dominant pedigree, any given carrier has a 50% probability of passing the causal variant to their offspring and all carriers are affected.

A major drawback of segregation analysis is the need for well documented family histories, accurate and meaningful phenotype data, as well as issues with identifying segregation in low penetrance or complex traits where inheritance patterns may be obfuscated. Use of trio analysis, classically in the form of mother-father-offspring trios, are a powerful method for variant detection and segregation. Trio analysis can be especially effective when attempting to identify *de novo* variation in an affected offspring, where both parents are unaffected, by removing the variants inherited from the paternal and maternal alleles. Trio analysis (or any variation of comparing multiple related individuals) is still viable for variants which aren't *de novo* provided that phenotypic penetrance is strong enough, as unaffected carriers will likely result in the filtering out of the causal variant.

Assessment of unrelated probands with the same disease can allow for the detection of single variants or genes that are associated with the phenotype of interest. By applying statistical methodology to allelic frequencies in cases compared to control sets, a calculation can be performed as to whether or not a given feature is overrepresented in the case set. This can apply to single loci, as is the case in genome-wide association studies (GWAS) studies or utilise more statistically complex analyses over fixed genomic regions such as genes, via methods such as variant collapsing or burden association tests (310).

Lastly, the assumption that any given cancer predisposition phenotype is likely to be autosomal dominant, with potentially variable penetrance, is well founded with many cases following this inheritance model. Conversely, there is increasing evidence for the role of complex or polygenic traits in cancer predisposition, with multiple low risk variants conferring additive cancer risk. In this instance, detection of low risk or polygenic traits is restricted to epidemiological studies with large enough sample sizes to detect small effect sizes and for rare cancer predisposition, such as those seen in RCC, the ability to detect these variants is juxtaposed to the sample size requirements.

1.8 Summary

RCC is complex set of renal neoplasm with distinct morphology, histology, and clinical courses and is a prominent cancer in both developing and developed countries, seeing an increased incidence globally. While clinical outcomes for stage I and low-grade tumours is favourable, tumours are often detected at later stages and as such have a much lower survival rate. Additionally, RCC tumours are treatment tolerant, with only moderate efficacies seen without targeted therapies and frequently become treatment resistant. Both the early detection, screening frequency and targeted therapies hinge on detection and understand the genetic components present both constitutionally and somatically.

Each subtype of RCC are genetically distinct entities with differing somatic and germline mutation patterns, as well clear genetic overlaps between causes of inherited RCC and somatic RCC driver mutations. While characterisation of somatic mutations across the differing histological subtypes has uncovered an array of genes involved in RCC tumourigenesis, understanding of RCC predisposition genes has been vital to understanding molecular mechanisms, cellular environments, and genetic circumstances which drive sporadic tumours.

While many genes associated with predisposition to RCC have been discovered, a large proportion of the remaining genetic component is currently unknown, with many cases which meet genetic screening criteria not carrying pathogenic variation in known RCC predisposition genes. By utilising multiple sequencing methodologies on individuals with features of inherited RCC (early onset, bilateral or multifocal tumours, and family history), potential candidate genes can be identified as associated with RCC predisposition and as such inform investigations in molecular mechanism, improve genetic testing and family screening, and provide potential targets for clinical management. It is worth noting that while this is a potential source of heritability which is currently not assessed, given the historical prior probability of an inherited cases of RCC (2-3%), the power to discover additional inherited cases within a cohort with suspected features of predisposition (24-33.7%) has low power without large sample numbers.

This posterior probability is a frequent challenge in the analysis of rare disease cohorts and significantly impacts a studies ability to elucidate new genetic features which are associated with RCC predisposition. In spite of this, rare disease studies do not have any robust alternative and a failure to perform a given study due to low probability of identifying novel outcomes is not a justification for ignoring the clinical and ethical needs of patients and families who present with rare diseases, including inherited RCC.

1.9 Aims

- To utilise multiple genomic targets and sequencing technologies to provide evidence to support the association of inherited RCC with previously reported genes.
- Use multiple genomic sequencing approaches and statistical case control analysis methods to identify novel genes which are associated with a predisposition to RCC.

2.0 Materials and methods

2.0.1 – Table of contents

2.0.2 Labour contributions

All methods described in this section were performed by the author with the exception of patient recruitment (performed by Professor Eamonn Maher), sample retrieval and extraction (section 2.1), and the contributions described in relation to DNA library preparations (section 2.6.5).

2.1 Sample preparation

2.1.1 Sample retrieval and extraction

Samples were received from various clinical genetic laboratories and DNA extraction methods will vary per recruitment site. Most recruited participants had DNA processed and extracted via either Cambridge University Hospital Addenbrookes East Anglian Medical Genetics Laboratory or Birmingham Women's Hospital West Midlands Regional Genetics Laboratory. Further subsets of samples were prepared at Melbourne, Exeter, Newcastle, King's College London and sent to Cambridge University Hospital Addenbrookes East Anglian Medical Genetics Laboratory for storage.

2.1.2 Sample source and storage

All but one sample used was blood serum-derived genomic DNA (one sample was buccal-derived DNA and was not found to be detrimental to experimental findings). All stock DNA extractions were stored in DNA Lo-bind microcentrifuge tubes (Eppendorf, Germany), sealed with Parafilm M (Bemis, United States) or tethered screw cap microtubes with rubber sealed lids (STARLAB, United Kingdom). Any samples received in containers not conforming to these storage requirements were transferred into the appropriate storage containers. DNA sample dilutions were prepared using Nuclease-free water (Qiagen, Germany) to required concentrations and quantified using either Qubit Broad Range or Qubit High Sensitivity DNA assay (Invitrogen, United States), depending on calculated target concentration (see section 2.2). All sample aliquots were stored at -20°C and dilutions were used where possible to reduce freeze-thaw cycling of stock DNA samples.

2.1.3 Patient cohort description

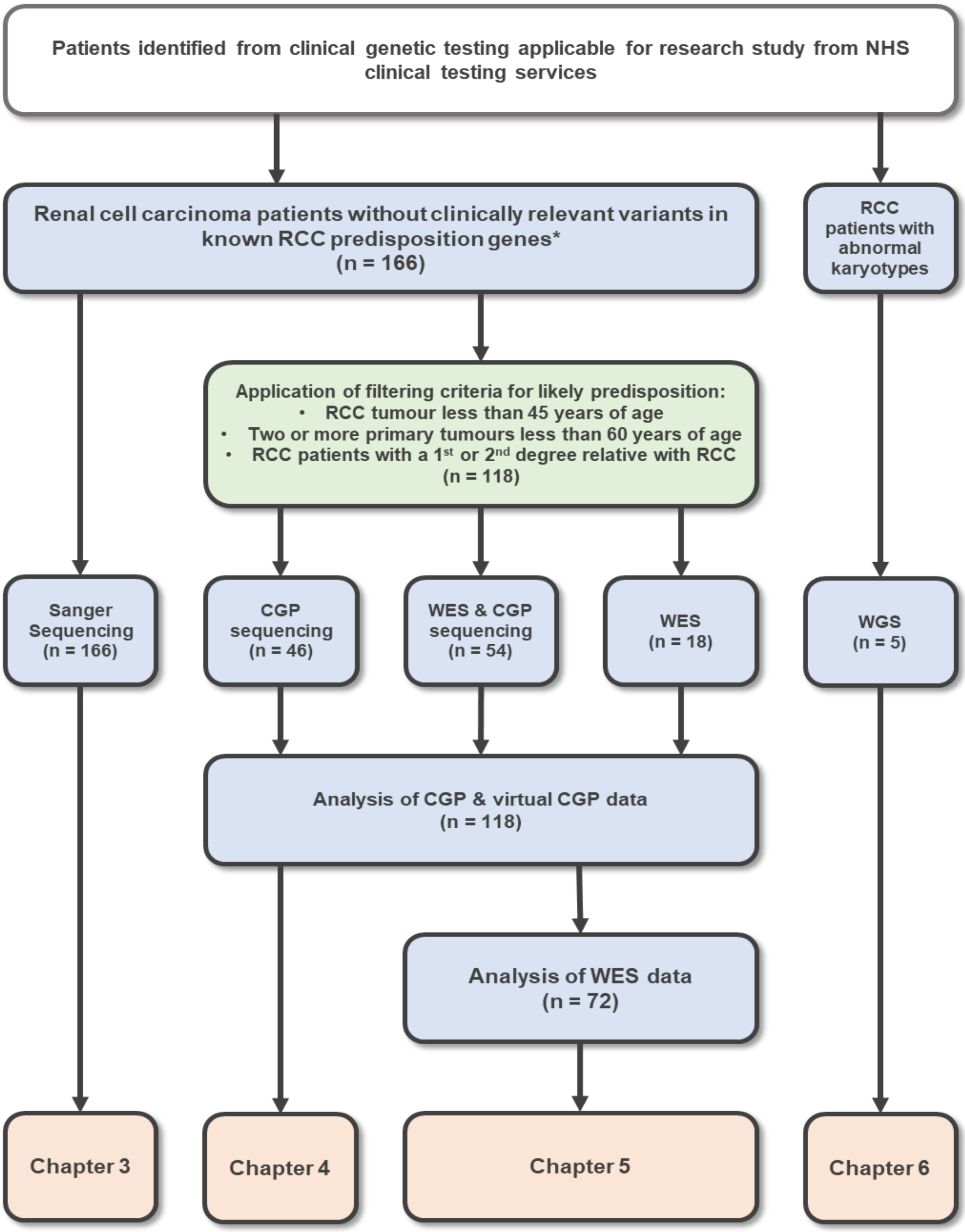
Patients identified from clinical genetic testing applicable for research study from NHS clinical testing services
Renal cell carcinoma patients without clinically relevant variants in known RCC predisposition genes* (n = 166)
RCC patients with abnormal karyotypes
Application of filtering criteria for likely predisposition:
• RCC tumour less than 45 years of age
• Two or more primary tumours less than 60 years of age
• RCC patients with a 1st or 2nd degree relative with RCC
(n = 118)
Sanger Sequencing (n = 166)
CGP sequencing (n = 46)
WES & CGP sequencing (n = 54)
WES (n = 18)
WGS (n = 5)
Analysis of CGP & virtual CGP data (n = 118)
Analysis of WES data (n = 72)
Chapter 3
Chapter 4
Chapter 5
Chapter 6

Flow chart depicting the patient selection procedure, patient filtering parameters, and sequencing methodologies used for each chapter described herein. Patient counts for each stage are denoted by [n = patient count]. Initialisms – national health service (NHS); renal cell carcinoma (RCC); cancer gene panel (CGP); whole exome sequencing (WES); whole genome sequencing (WGS).

2.2 Sample quality control and metrics

2.2.1 DNA quantification

DNA quantification was performed with Qubit Broad Range DNA assay (Invitrogen, United States) in most circumstances following the manufacturer’s protocol for 2 µl DNA input. In a limited number of cases where DNA quantity was low/insufficient or DNA quality was questionable or low concentration dilutions were required (e.g. DNA sequencing libraries) DNA aliquots were measured by Qubit High Sensitivity DNA assay (Invitrogen, United States) to determine concentration (following the manufacturer’s protocol for 2 µl DNA input) and NanoDrop 1000 Spectrophotometer (Thermofisher, United States) using 1 µl DNA input to determine sample purity from 260/230 nm and 280/260 nm absorption ratio (311).

2.2.2 Whole genome amplification of low quantity samples

In certain instances, low DNA yield samples limited available DNA for downstream experiments. In these cases, DNA was whole genome amplified using REPLI-g Mini kit (Qiagen, Germany) following manufacturers’ instructions provided for initial input of 5 µl. Whole genome amplified product concentrations were measured using the Invitrogen Qubit Broad Range DNA assay (see section 2.2.1). Whole genome amplified DNA was not used for high throughput sequencing methods due to described base replication errors and region-specific amplification (312).

2.3 Polymerase chain reaction (PCR) methods

2.3.1 Primer design

Target sequences for designed primers were retrieved using University of California, Santa Cruz (UCSC) Genome Browser (313) providing target co-ordinates from Human Genome build GRCh38/Hg38 (314). Primers were designed using the Primer3 (315). Primer sets were evaluated for non-specific binding and secondary structure formation using National Centre for Biotechnology Information's (NCBI) BLAST (Basic Local Alignment Search Tool) PrimerBLAST (316).

2.3.2 Short range PCR

PCR amplification was performed using AmpliTaq Gold DNA polymerase utilising GeneAmp10X PCR Buffer II with $MgCl_2$ (Applied Biosystems, United States). In most instances, PCR was performed as per the manufacture's protocol with a standard annealing temperature of 58°C and 30 cycles. In certain reactions, conditions required optimisation to produce a DNA product for downstream steps. The annealing temperature was adjusted with a temperature gradient (53-63°C) and the quantity of genomic DNA input required varied depending upon the quality of the DNA, increasing incrementally from 10ng/reaction up to a maximum of 50ng/reaction. TaqMan Control Genomic DNA (Applied Biosystems, United States) was used in place of patient genomic DNA, where appropriate, for optimisations and negative control reactions. Standard PCR protocol is given below in 2.3 Table 1.

2.3.2 Table 1

Thermocycler conditions and PCR master mix volumes for a standard short-range PCR reaction

PCR reaction cycle conditions	
95°C for 10 minutes	Initial denaturation
95°C for 15 seconds	x 25-35 cycles
55-65°C for 30 seconds (Reaction Dependent)	
72°C for 1 minute / Kb	
72°C for 10 minutes	Final extension / elongation
Hold at 4°C	End (Optional)

PCR reaction mixture (25µl)	
Template DNA	10-50 ng
AmpliTaq Gold polymerase (5U / µl)	0.125 µl
Forward primer (10 µm)	0.5 µl
Reverse primer (10 µm)	0.5 µl
dNTP mixture (10 mM)	0.5 µl
Buffer II with $MgCl_2$	2.5 µl
Nuclease-free H_2O	up to 25 µl

2.3.3 Nested PCR

For a subset of reactions, initial amplification of PCR targets was complicated by local DNA structures or sub-optimal primer designs. As such, expanded PCR amplicons were designed to span the original target with additional flanking DNA sequence between 500-2000 bp 5’ and 3’ of the initial PCR amplicon. Two PCR reactions as described in section 2.3.2 were performed, the first reaction utilising the expanded amplicon primers and the second reaction using the original amplicon primers but with the PCR product of former as the input DNA. For larger nested amplicons elongation times in the PCR cycling conditions were adjusted as necessary.

2.3.4 Long range PCR primer design

Long range PCR primers were designed in accordance with the details of section 2.3.1 with the alteration that primers should be purified via high performance liquid chromatography (HPLC) to ensure the removal of truncated primer sequences and impurities to reduce possible off target effects.

2.3.5 Long range PCR

Long range PCR amplicons were generated with the SequalPrep™ Long PCR Kit (Applied Biosystems, United States). Stringent optimisation was completed to improve amplicon generation via modification of the following conditions; Annealing temperature, concentration of enhancer, DMSO concentration & number of PCR cycles. TaqMan® Control Genomic DNA (Applied Biosystems, United States) was used for optimisation steps. Cycling conditions and reaction mixture set up is given in the 2.3 Table 2 below.

2.3.5 Table 2

Thermocycler conditions and PCR master mix volumes for a standard long range SequelPrep PCR

SequelPrep reaction cycle conditions	
94°C for 2 minutes	**Initial denaturation**
94°C for 10secs	**x 10 cycles**
55-65°C for 30 seconds (Reaction Dependent)	
68°C for 1 minute / Kb	
94°C for 10 minutes	**x 20-30 cycles**
55-65°C for 30 seconds (Reaction Dependent)	
68°C for 1 minute / Kb (+20 seconds / cycle)	
72°C for 5 minutes	**Final extension / elongation**
Hold at 4°C	**End (Optional)**

SequelPrep reaction mixture (20µl)	
Template DNA	**20-50 ng**
SequelPrep Long polymerase (5U / µl)	**0.125 µl**
Forward primer (10 µm)	**0.5 µl**
Reverse primer (10 µm)	**1 µl**
10X Enhancer (A or B)	**1-2 µl**
DMSO	**0.4 µl**
10X Reaction Buffer	**2 µl**
Nuclease-free H_2O	**up to 20 µl**

2.3.6 Gel electrophoresis

Gel electrophoresis was performed on a wide range of DNA products throughout the experiments described in this thesis. This describes a generalised protocol used for all instances in which gel concentrations, run times, and applied voltages differ between experiments. Prior to preparing a agarose gel, 50X Tris Acetate-EDTA (TAE) stock solution was made by dissolving 242 g Tris-base (Fisher Scientific, United States) in 500 ml of water (15 MΩ·cm), adding 37.2 g Ethylenediaminetetraacetic acid disodium salt dehydrate (EDTA; Sigma Aldrich, United States), 57.2 ml glacial acetic acid (Sigma Aldrich, United States), and making total volume up to 1 L, after which pH was adjusted to 8.5. This was diluted in 4.9 Litres of water (15 MΩ·cm) forming a 1X TAE buffer (40mM Tris, 20 mM acetic acid, 2 mM EDTA). Agarose gel was prepared by adding TAE solution to agarose (Sigma Aldrich, United States) to a final agarose gel mass concentration of between 5-30 mg/ml, depending on the weight of agarose and volume of 1X TAE.

Agarose gel solutions were cooled to approximately 10-15°C above solidifying temperature and 0.5X SYBR Safe DNA Gel Stain (10,000X in DMSO; Invitrogen, United States) was evenly mixed into solution. Gels were cast and left to set for 30 minutes, placed into a gel electrophoresis tank, and submerged in 1X TAE. Typically, 5 μl DNA product was mixed with 1 μl DNA Gel Loading Dye 6X (Thermo Scientific, United States) and loaded into each agarose gel well along with a ladder well containing either 2.5 μl GeneRuler 100 Bp Plus, FastRuler Low Range (Thermofisher, United States), or Quick-Load 1 kb DNA Ladder (New England Biolabs, United States) depending on estimated amplicon size.

Agarose gels were run for 40-80 minutes at 6-8 V/cm, depending on estimated product size and agarose concentration. Agarose gels were visualised using transient ultraviolet (UV) illumination on the Gel Doc XR+ Gel Documentation System (BioRad, United States) and gel images were saved as both BioRad proprietary 1SC format and standard JPEG format with minimal compression.

2.4 Sanger sequencing

2.4.1 PCR product clean-up

PCR products generated for Sanger sequencing were cleaned using ExoSAP to remove unwanted single-strand sequences and residual dNTPs from the PCR reaction. ExoSAP was prepared by mixing Exonuclease I (New England Biolabs, United States) and Shrimp Alkaline Phosphatase (SAP; Sigma Aldrich, United States) enzymes at a ratio of 1:2, respectively. Each PCR product had 1 µl of ExoSAP added directly to the PCR reaction mixture. ExoSAP-treated reaction mixtures were incubated for 60 minutes at 37°C, followed immediately by an inactivating incubation of 80°C for 15 minutes.

2.4.2 Sanger sequencing termination reaction

Sanger sequencing was performed using BigDye Terminator v3.1 Cycle Sequencing Kit (Applied Biosystems, United States). ExoSAP-purified PCR products were sequenced bi-directionally, sequencing both the forward and reverse strands, to improve alignment and sequencing quality where possible. Reaction mixtures consisted of 2 µl purified PCR product, 0.75 µl BigDye Terminator v3.1 Ready Reaction Mix, 1 µl primer (10 pmol; forward or reverse strand), 2µl 5X BigDye Sequencing buffer (Applied Biosystems, United States), and 4.25 µl nuclease-free water (Qiagen, United States). The reaction cycling conditions are given in 2.4.2 table 3.

2.4.2 Table 3

Thermocycler conditions for BigDye termination sequencing reaction

BigDye termination sequencing protocol	
96°C for 10 seconds	**X 25 cycles**
50°C for 5 seconds	
60°C for 3 minutes 30 seconds	
Hold at 4°C	**Prior to Isopropanol clean-up**

2.4.3 Isopropanol clean-up and DNA precipitation

Isopropanol clean-up was used as a sequence precipitation and clean-up method for removing unincorporated dyes and residual termination dNTPs left over from BigDye termination sequencing. To each Sanger sequencing reaction, 40µl of freshly prepared 75% v/v isopropanol (Sigma Aldrich, United States) was added and mixed gently by pipetting up and down twice. Reactions were then incubated at room temperature for 30 minutes and the subsequently centrifuged at 2092 relative centrifugal force (RCF) for 45 minutes. The reaction plate was then inverted onto absorbent paper and tapped to discard isopropanol, centrifuged for 30 seconds at 33 RCF, and left to air dry for 10 minutes until all isopropanol has evaporated. DNA pellets were re-suspended in 20 µl of Hi-Di Formamide (Applied Biosystems, United States).

2.4.4 Sequencing analysis

Sanger termination sequences were loaded onto either a 3730 DNA Analyzer or 3130xl DNA Analyzer (Applied Biosystems, United States) where dye terminator sequences were separated by capillary electrophoresis and dye florescence was recorded for analysis. Fluorescence chromatograms were analysed using Sequencher v5.3 (Gene Codes Corporation, United States), aligning sequences to a reference sequence of each targeted variant ±500 base pairs extracted from UCSC, as described in section 2.3.1.

2.5 Pooled amplicon clean-up

As part of chapter 3, normalisation of pooled long-range PCR amplicons of variable lengths was required prior to DNA library preparation for NGS sequencing. An efficient custom clean up method was developed in-house to remove unwanted DNA fragments and contaminants whilst retaining size-divergent pooled amplicons. Protocol is a hybridisation of the Agencourt AMPure XP PCR Purification Beads (Beckman Coulter, United States) and clean up protocol provided in Illumina TruSight Rapid Capture Sample Preparation Guide (Illumina, United States). Both systems mentioned above use the AMPure XP magnetic beads for the separation of DNA products (named "Sample Purification Beads" in the Illumina documentation).

A volume of each pooled sample amplicon was mixed well with a pipette and added to a deep-well storage plate (minimum volume used was 10 µl as lower volumes resulted in issues with sample manipulation whilst in contact with magnetic beads). Subsequently, 1.8 volumes of AMPure XP magnetic beads (at room temperature and well mixed) were added to each pooled sample amplicon well, sealed with an adhesive plate seal, shaken at 507 RCF for one minute, and left to incubate for 10 minutes at room temperature.

The deep-well storage plate was spun briefly to ensure no sample was lost and placed onto a magnetic stand for 2 minutes. Whilst remaining on the magnetic stand, supernatant was carefully removed without disturbing the pellet, to each well 200 µl of freshly prepared 80% v/v ethanol (Sigma Aldrich, United States) was added and incubated at room temperature for 30 seconds after which the supernatant was removed. This process was repeated twice for a total of two 80% v/v ethanol washes.

Any remaining ethanol was aspirated off using a 20 µl pipette and air dried at room temperature for a maximum of 5 minutes. The deep-well storage was removed from the magnetic stand and 40µl of nuclease-free water added to each pool sample amplicon well. Elution-bead mix was then shaken at 507 RCF for 1 minute. The deep-well storage plate was spun briefly to ensure no sample is lost and placed onto a magnetic stand for 2-10 minutes, with the eluate being subsequently transferred to a new labelled 96-well plate without disturbing the pellet.

Pooled sample concentrations were measured using the Invitrogen Qubit Broad Range DNA assay both before and after clean up to measure levels of DNA loss during the clean-up process (see section 2.2.1). Loss of DNA during clean-up is unavoidable using this method due to unbound DNA fragments. This protocol had to accommodate a broad range of DNA amplicon sizes – the rate loss that was seen typically 10-20% less than the original input (by total mass). Retention of all size ranges was confirmed by gel electrophoresis (5 mg/ml agarose gel at 6 V/cm for 60 minutes – See section 2.3.6).

2.6 DNA sequencing and library preparation

Full details of manufacturer's protocols are omitted for brevity but are available online (http://emea.support.illumina.com/array/protocols.html).

2.6.1 Illumina Nextera XT Library preparation and sequencing

Pooled amplicons underwent DNA library preparation using Illumina Nextera XT (Illumina, United States) following the manufacturer's protocol. All samples were diluted to 5ng/µl and processed according to the manufacturer's protocol. Pooled libraries were quantified by quantitative PCR and loaded onto an Illumina MiSeq Sequencer using Illumina MiSeq Reagent v.2 – 300 cycle Kit – paired end 150 bp (Illumina, United States).

2.6.2 Illumina TruSight Cancer library preparation and sequencing

Samples were prepared using the TruSight Cancer library prep kit (Illumina, United States) following the manufacturer's protocol. All samples were diluted to 5ng/µl and processed according to the manufacturer's protocol. Pooled libraries were quantified by quantitative PCR and loaded onto an Illumina MiSeq Sequencer using Illumina MiSeq Reagent v.2 – paired end 150 bp (Illumina, United States).

2.6.3 Illumina TruSeq rapid exome library preparation and sequencing

Samples were prepared using the TruSeq rapid exome library prep kit (Illumina, United States) following the manufacturer's protocol. All samples were diluted to 5ng/µl and processed according to the manufacturer's protocol. Pooled libraries were quantified by quantitative PCR and loaded onto an Illumina HiSeq 2500 Sequencer using Illumina HiSeq Reagent v.2 – paired end 150 bp (Illumina, United States).

2.6.4 Whole genome sequencing by Novogene

Whole genome sequencing (WGS) data was generated externally by a third-party company Novogene (Beijing, China) from submitted blood-extract DNA. DNA was quantified and quality checked as described in section 2.2 prior to submission to WGS. DNA underwent library preparation using Illumina Nextera DNA library prep kit and sequenced on the Illumina HiSeq X platform. Sequencing output was returned in trimmed and de-multiplexed FASTQ format on an external hard drive and transferred to departmental hard drives after MD5 checksums.

2.6.5 Library preparation labour contributions

Library preparations of various results chapters discussed within this body of work were not solely generated by the author and as such contributions are described as accurately as possible below.

Library preparation for section 2.6.1 were solely generated by the author and libraries were loaded into sequencing flow cells and onto the Illumina MiSeq platform by the stratified medicine core laboratory (SMCL) sequencing laboratory.

Library preparations for section 2.6.2 were performed by Dr Hannah West, Dr Andrea Luchetti, and the author divided approximately 40%, 20%, 40% of the total libraries, respectively, and libraries were loaded onto sequencing flow cells and onto both Illumina MiSeq and Illumina HiSeq 2500 platforms by the SMCL sequencing laboratory.

Library preparations for section 2.6.3, including the sequencing flow cell and Illumina HiSeq 2500 or Illumina HiSeq 4000 loading were solely performed by the SMCL sequencing laboratory.

2.7 Generalised sequencing pipeline

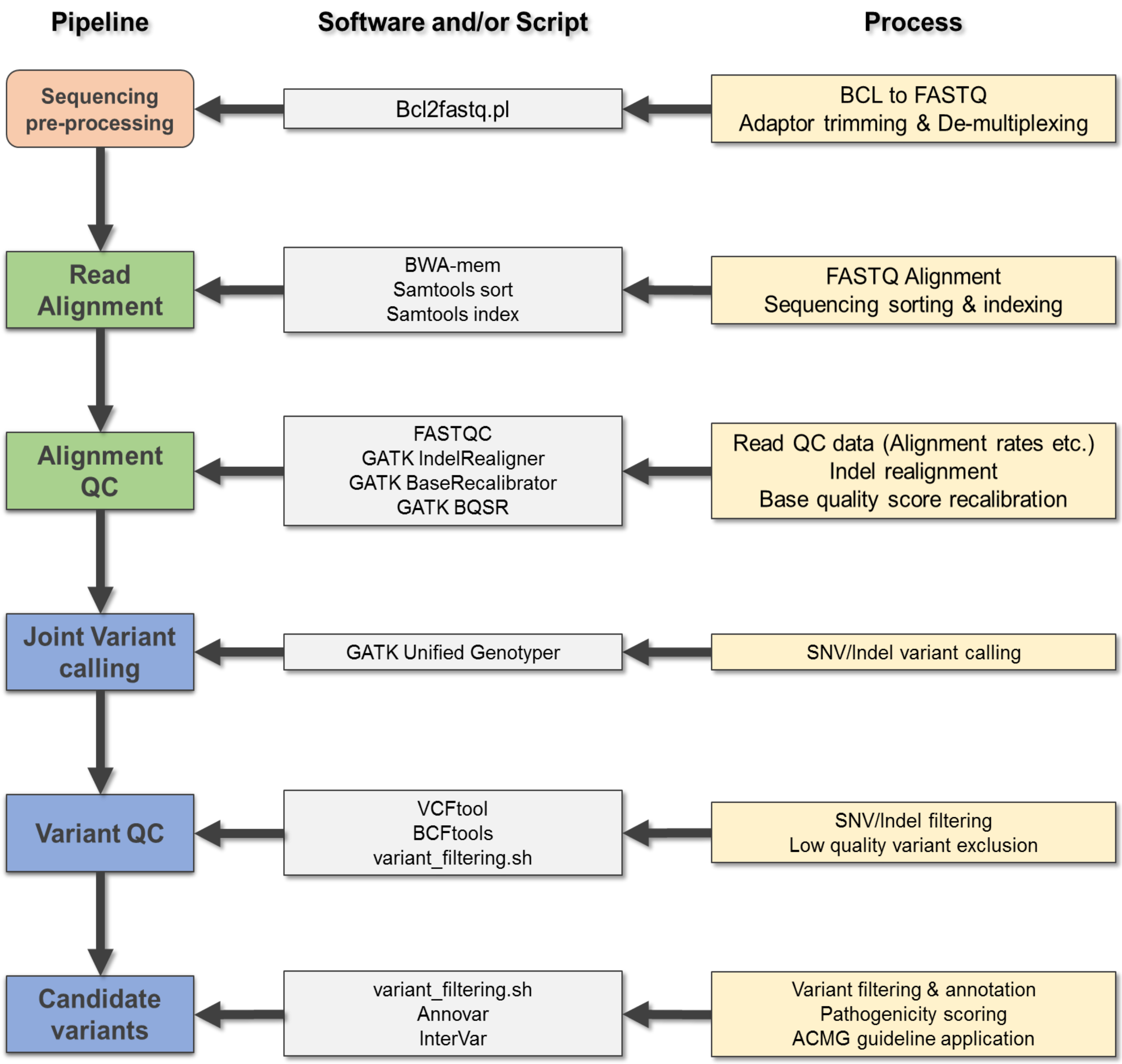

The diagram visualises the main steps and processes involved in the generation of candidate SNV variants. Full details of the sequencing pipeline scripts and runtime parameters are in appendix section 9.1.

2.8 Variant filtering and annotation

Variant filtering of NGS data for all chapters was performed using a variant filtering bash script (variant_filtering.sh) and an accompanying R script (variant_filtering.R) utilising VCFtools (317). An overview of the variant filtering steps are provided here and the full script is provided in appendix section 9.1.2.

Using VCFtools variant sites were filtered to the filter cut-offs described in the summary table below unless otherwise specified in the results chapters directly. Per site filters included minimum mean read depth across a site, maximum cohort minor allele frequency, site QUAL metric, and maximum missingness. Per genotype filters were minimum genotype quality. Minimum genotype quality filters were applied prior to maximum missingness as per genotype filters set failed genotypes to missing.

Minimum mean read depth	**Minimum genotype quality**	**Maximum minor allele frequency**	**Maximum missingness**	**Site QUAL**
> 10	> 30	< 0.05	< 0.2	> 100

Sites retained after the previously described filtering criteria were left aligned and normalised by GATK function ‘LeftAlignAndTrimVariants’ to split multi-allelic sites and present minimum representative calls for indels (318)(version 3.7-0-gcfedb67). Variants were annotated using Annovar (319) with the following databases; *refGene, 1000g2015aug_all, exac03, avsnp150, dbnsfp35a, clinvar_20180603, cosmic70, nci60, dbscsnv11*, and updated annotation databases were used when available.

The annotated variants were parsed by the variant_filtering.R script and were then filtered by genomic feature (restricted to “exonic”, “exonic;splicing”, or “splicing”) and removed variants classified as “synonymous” or intergenic, specified by “unknown”. Variants were filtered by global minor allele frequencies present in both the 1000 genomes project (320) and ExAC (321) cohorts. Variants were retained if present at less than 1% (0.01 allelic frequency) using an ‘AND’ selection, specifying variants should be present at less than 1% in both sets to pass filtering criteria. Variants occurring with heterozygous call rates greater than 15% of the total cohort were removed as they were considered to be either technical artefacts or undocumented common SNPs. Lastly, allelic depth information was extracted for each genotype and alternative allelic depth ratios were calculated. Sites in which no single non-reference genotype had an alternative allelic ratio (i.e. percentage of supporting reads) great than 0.3 were removed.

In silico predictive metrics where mentioned in the text refer to the use of Sift (322), PolyPhen (323), or CADD (324) applied either independently or collectively. Concordance for a variant being likely pathogenic between the software predictions was defined by a prediction of ‘likely pathogenic’ by Sift and PolyPhen and a CADD score greater than 25. Concordance for a variant being likely benign between the software predictions was defined by a prediction of ‘tolerated’ or ‘benign’ by Sift and PolyPhen and a CADD score lower than 10.

American College of Medical Genetics (ACMG) variant classification criteria (325) were automatically applied utilising the default parameters of InterVar (version 2.0.2 20180827)(326) and Annovar (as previously discussed). InterVar does not accept or output multi-sample VCF files so was provided a pseudo single sample VCF containing all variants present in a given multi-sample VCF with all genotypes set to heterozygous. Indels annotated by InterVar were right shifted so post-processing was used to reapply left shift and normalisation in InterVar results files.

2.9 Oxford Nanopore Technologies sequencing

2.9.1 Sample preparation and long-range PCR amplicon

The sample used in Nanopore long read sequencing was prepared and quality controlled as described in section 2.2. PCR products for the specific reactions described in the appropriate chapters were performed as described in section 2.3.2 and in accordance with any additional alterations specified in the chapter 6 materials and methods section referring to this portion of the materials and methods chapter (section 6.2.5).

2.9.2 Nanopore sequencing library preparation

PCR amplicons were quantified to between 1-1.5 μg of total DNA, as described in section 2.2 and libraries were generated using the manufacturer’s protocol (1D Amplicon by ligation SQK-LSK108), with adaptation for reduced input fragment size, and loaded onto a FLO-MIN106 flow cell and sequenced on a MinION sequencing platform utilising the MinION control software (version 18.12.9). Sequencing was run for 1 hour and data was output in FAST5 format.

2.9.3 Nanopore bioinformatics

FAST5 read data from Nanopore sequencing was base called using the ONT Albacore Sequencing Pipeline Software (version 2.3.3), generating both base called FAST5 output and FASTQ output files. FAST5 and FASTQ data was indexed using Nanopolish (version 0.10.2) (327). Sequencing quality was assessed by custom R script nano-qc.R, poretools (version 0.6.0) (328), and NanoStat (329). Long read FASTQ data was aligned to GRCh38 using Minmap2 (version 2.10-r761) (330) using ONT sequencing parameters. Full ONT Nanopore sequencing pipeline nano-pipe.sh is included in appendix section 9.1.3.

3.0 Sequencing of candidate genes by Sanger and targeted next generation sequencing approaches

3.0.1 - Table of contents

3.1 Introduction

Current clinical practice utilises targeted sequencing, either using next generation sequencing (NGS) panels such as cancer gene panels or ‘clinical’ exomes, or Sanger sequencing for specific genes that have been associated with known diseases. The primary benefits of using Sanger sequencing and genomic loci-limited NGS sequencing over more comprehensive NGS sequencing methods is both a decrease in financial burden, a reduction in the labour required to perform data generation and analysis, and an increase in the efficiency of accurate variant identification and assessment by reducing the scope of data generated. Genes that are frequently somatically altered in sporadic RCC tumours might be candidate targets for inherited disease. This is exemplified by the *VHL* TSG (99) and most recently by *PBRM1* and *BAP1* which have been implicated in familial and sporadic RCC (263,268,331). Assessment of these candidates allow for the selection of additional targets for sequencing that are related to the pathways known to be altered in RCC (98). Here, a subset of genes related to RCC predisposition or development were targeted by both Sanger and NGS techniques in order to identify potential variants of interest in genes associated with RCC.

3.1.1 – Candidate gene - CDKN2B

Cyclin-dependent kinase inhibitor 2B (*CDKN2B*) is a two-exon gene which encodes the protein p15^{INK4B} (i.e. Cyclin-dependent kinase 4 inhibitor B) with both a canonical 138 amino acid transcript (NM_004936) and a shorter 78 amino acid transcript (NM_078487). *CDKN2B* shares its genomic positions with *Cyclin-dependent kinase inhibitor 2B* (*CDKN2A*), which have overlapping loci on chromosome 9 (chr9:22002903-22009363 and chr9:21967752-21995301, respectively), along with a third associated protein, p14^{ARF}, which is encoded by *CDKN2A* utilising an alternative reading frame.

As its namesake suggests, p15^{INK4B} acts as an inhibitor of cyclin-dependent kinase 4 (CDK4), a protein associated with cell cycle progression and regulation of proliferation in a protein complex with cyclin-dependent kinase 6. CDK4 or CDK6 bind with Cyclin D1 (CD1) and function in the phosphorylation of retinoblastoma (RB) proteins which results in the upregulation of gene transcription via E2F proteins. Both p15^{INK4B} and p16^{INK4A} act to bind CDK4/CDK6-CD1 complexes and inhibit the phosphorylation of RB proteins, which acts to decrease the activity of E2F transcription factors (332,333). While the function of p15^{INK4B} and p16^{INK4A} have clear overlaps they are not functionally redundant and p15^{INK4B} has distinct functions as a tumour suppressor in the absence of p16^{INK4A} (334).

CDKN2A is reported to be frequently altered somatically across all RCC histological subtypes via either promotor hypermethylation or deletion of 9p, correlated with poorer survival (274) and TCGA data suggests copy number losses in RCC cases affect both *CDKN2A* and *CDKN2B* similarly (25). Though inactivating variants in *CDKN2B* are rare somatically, with only a single inactivating variant reported across all RCC samples in TCGA (25), hypermethylation of *CDKN2B* has been demonstrated in RCC and other cancers, including acute myeloid and lymphoid leukaemia (335), parathyroid adenomas (336), and colon cancer (337). Additionally, germline variants in *CDKN2B* (amongst other cyclin-dependent kinase inhibitors) were associated with predisposition to multiple endocrine neoplasia type 1 (MEN1), though the occurrence rate was low (338).

A previous study identified a truncating variant in an individual with familial clear cell RCC, and subsequent sequencing of a cohort of individuals with features of inherited RCC, without pathogenic variants in known RCC predisposition genes, resulted in candidate deleterious variants in *CDKN2B* in up to 5% of assessed samples (95% CI, 0.21%–9.43%) with a significant enrichment compared to dbSNP (0.2%) (266). Given the identification of *CDKN2B* as a candidate familial RCC cohort, replication of these findings in an independent RCC cohort would support the hypothesis that germline inactivation variants in *CDKN2B* is associated with RCC predisposition.

3.1.2 – Candidate gene - EPAS1

EPAS1 (also known as *HIF2-α*) is an enticing candidate gene for potential predisposition given its role in the HIF-driven hypoxia response (141) and direct targeting by VHL-dependent ubiquitination (107,138). *EPAS1* is a 16 exon coding gene at 2p21 which encodes the protein endothelial PAS domain-containing protein 1 (EPAS1). Under hypoxic conditions, EPAS1 together with HIF1A and HIF1B act to upregulate angiogenic pathways and increase angiogenesis and cellular growth through HRE-linked transcription (See 1.4.2 VHL disease).

Like many oncogenes, truncating or inactivating variants are not predicted to be pathogenic as they do not result in constitutional protein activation or increased transcriptional expression. Publications regarding *EPAS1* have demonstrated that missense mutations in exons 9 and 12 in PCC/PGL tumours are oncogenic (339,340), with *EPAS1* variant carrying tumours having significantly higher *EPAS1* expression. In a subset of these cases, the variants were also shown to be present in the germline indicating potential predisposition (339). These exons appear to be mutational hotspots, co-localising to the hydroxylation site and reducing pVHL binding affinity, respectively, resulting in constitutional activation of EPAS1 (341,342). GWAS studies in RCC have also demonstrated the presence of a complex risk locus surrounding *EPAS1*, suggesting potential linkage to functional variants in *EPAS1* which may increase an individual's risk for RCC (108,109).

Given the distinct genetic overlap between RCC and PCC/PGL through conditions such as VHL disease, SDH-deficient tumours, and *FH*-related predisposition, an *EPAS1* genotype association with PCC/PGL suggested *EPAS1* as a candidate for inherited RCC cases and as such exons 9 and 12 of *EPAS1* were selected as candidate sequencing regions in this series of patients with features of possible inherited RCC.

3.1.3 – Candidate genes - KMT2C and KMT2D

Somatic alterations frequently found in sporadic cases of RCC may indicate potential sources of undiscovered heritability. Large scale sequencing projects such as TCGA (25), amongst others, provide reliable data about which genes are frequently somatically altered in specific cancer types. Lysine methyltransferase 2C and 2D (*KMT2C* and *KMT2D*), are genes that are altered in sporadic RCC at frequencies of 5% and 3% respectively in TCGA renal cancer data set (25), with alteration rates in chromophobe RCC up to 15%. Investigations into frequently altered somatic genes may resolve the presence of germline alterations in those same genes, as is the case with genes such as *VHL*, *PBRM1, BAP1*, *PTEN,* and *MET*.

Both *KMT2C* and *KMT2D* are large coding genes situated at 7q36.1 and 12q13.12, respectively. *KMT2C* is a 59-exon gene encoding a 4,911 amino acid protein and *KMT2D* is a 54 exon gene encoding a 5,537 amino acid protein. Both genes encode Histone lysine-specific N-methyltransferase enzymes, which primarily act to catalyse the addition of methyl groups to lysine-4 residues of histone H3, aptly named KMT2C and KMT2D (343). Both *KMT2C* and *KMT2D* are frequently mutated in multiple cancers, demonstrating both an array of copy number gains, losses and SNVs (25). Originally, they were termed MLL2/4 and MLL3 (corresponding to KMT2D and KMT2C, correspondingly) due to being part of a family of proteins known as mixed-lineage leukaemia (MLL) associated with multiple cancers, including leukaemia (343). KMT2C and KMT2D form protein complexes with a series of common, and complex-specific proteins, including KDM6A, a lysine-specific demethylase dysregulated in clear cell RCC (344,345) and function in histone regulation through the addition of H3K4me1 groups to histones particularly in adipogenesis (346), though exactly how this promotes tumourigenesis has not been well established. Several studies have suggested H3K4me1 groups allow for open chromatin access to enhancer regions of oncogenic transcripts, whereas alternative hypothesises suggest H3K4me1 modifications block DNA methylation suggesting a loss of transcriptional repression via promotor methylation (347,348). KMT2C and KMT2D also appear to have tumour suppressor functions through co-activation of p53 in DNA repair via the ASCOM protein complex (349).

Given that *PBRM1* and *BAP1* are histone modifying and chromatin remodelling genes (350,351) frequently altered in somatic RCC (274) and have been recently associated with RCC predisposition (263,331), assessing other histone modifying or chromatin remodelling genes such as *KMT2C* or *KMT2D* may uncover new associations in individuals with predisposition to RCC. Finally, unpublished data from whole exome sequencing data identified a nonsense variant in *KMT2C* (NM170606.2: c.2263C>T: p.Gln755Ter: rs201234598) in a blood sample from a patent with familial RCC in the absence of any other variants in RCC predisposing genes, raising the possibility that germline variants in *KMT2C* or *KMT2D* might predispose to RCC.

Given these factors, sequencing of the full coding region of both *KMT2C* and *KMT2D* was performed to assess for the presence of pathogenic variants that may confer predisposition. Given the total size of the targeted regions standard Sanger sequencing was considered inappropriate and as such amplicon-based next generation short read sequencing was utilised to achieve complete coverage of the coding regions of both genes.

3.1.4 Aims

- To validate findings of pathogenic *CDKN2B* variants being associated with RCC predisposition in individuals with features of inherited RCC
- Assess hotspot regions of *EPAS1* to identify activating variants which may predispose individuals to RCC in a manner similar to that seen in PCC/PGL
- Evaluate the coding regions of *KMT2C* and *KMT2D* for pathogenic variants which may predispose individuals to RCC utilising long range PCR and NGS sequencing methods

3.2 Materials and methods

3.2.1 Samples

Samples selected were individuals with RCC who had been referred to research as having features of heritability, as described in section 2.1.3. A total of 166 individual germline whole blood DNA was utilised for targeted sequencing of *CDKN2B* and *EPAS1* exon 9 and exon 12. For NGS sequencing of *KMT2C* and *KMT2D*, a subset of 96 individuals were selected for sequencing from the primary cohort of 166 due to issues with sequencing relating to both capacity and economic constraints.

3.2.2 Sanger sequencing primer design and co-ordinates

Primers for both standard PCR reactions and long-range PCR reactions were designed as described in the main materials and methods (sections 2.3.1). PCR primers for all experiments in this chapter are reported in appendix section 9.2.1.

3.2.3 PCR reactions and Sanger sequencing

PCR reactions, bi-directional Sanger sequencing, and Sanger sequencing was performed as described in main material and methods section 2.3.2, section 2.4. Failed reactions were repeated with additional optimisation steps to improve PCR reaction parameters and sample DNA underwent quality control to assess potential issues as described in main material and methods (section 2.2). Reactions were repeated a maximum of 3 times.

3.2.4 Long range PCR

Long range PCR reactions were performed as described in section 2.3.5 of materials and methods as input amplicons for next generation sequencing. Long range PCR primers were optimised iteratively to a maximum of three iterations, after which regions were designated as poorly optimised and not included in long range PCRs downstream. Failed reactions were re-optimised and repeated an additional two times prior to being assigned ‘failed’ status.

3.2.5 Illumina Nextera XT library preparation for amplicon sequencing

DNA library preparation for *KMT2C*/*KMT2D* long range amplicons, including a custom developed amplicon normalisation method, was performed as described in the main materials and methods (section 2.5 and 2.6.1). Three individual libraries were prepared for 16 pooled samples for batch 1 and 2, and 21 samples for batch 3. Batches 1 and 2 were performed using a standard MiSeq flow cell whereas batch 3 utilised a MiSeq Nano flow cell. Library loading on to the Illumina MiSeq was performed by the SMCL sequencing service.

3.2.6 Primary bioinformatics

Primary bioinformatics from BCL to VCF was performed as described in the generalised pipeline in the material and methods (sections 2.7) from FASTQ to VCF, BCF to FASTQ and sample de-multiplexing was performed by the SMCL sequencing service.

3.2.7 Variant filtering, annotation, and classification

Variant quality filtering, feature annotation and classification was performed as described in the main materials and methods (sections 2.8).

3.2.8 Sequence identity comparison

Sequence identity comparison was performed using Emboss Matcher pair-wise sequence alignment algorithm to assess sequence similarities (352). FASTA sequences were downloads from NCBI (https://www.ncbi.nlm.nih.gov/gene/) and sequence identity compared. Conserved regions were generated using coordinate positions of matching sequence regions and converted to BED file format prior to plotting. Command line details are provided within the pair-wise sequence alignment results in appendix section 9.2.2.

3.2.9 Statistics

Fishers exact was performed using the fisher.test() function in stat package using R (version 3.5). Binomial proportions and confidence intervals were calculated using bionom.test() in the stats package using R (version 3.5).

3.3 Results

3.3.1 Targeted Sanger sequencing - PCR product generation

A cohort of 166 RCC cases were selected for targeted Sanger sequencing of the coding regions of *CDKN2B* and exons 9 and 12 of *EPAS1*. DNA was amplified to cover all targeted regions described prior, two amplicons were used to cover the two exons from *CDKN2B* and one amplicon for *EPAS1* exon 9 and 12 each (See 3.3 - Table 1). In total 1328 PCR reactions were performed and amplicons were successfully generated for 92.7% (154/166), 97.0% (161/166), 80.7% (134/166), and 97.6% (162/166) samples for amplicons *CDKN2B*-1, *CDKN2B*-2, *EPAS1*-exon9 and *EPAS1*-exon12*,* after PCR product generation was confirmed by agarose gel electrophoresis (3.3 - Figure 1 - Example gel). Sequencing was generated by Sanger sequencing for successful amplicons of samples. The mean success rate for uni-directional and bi-directional sequencing for all targets was 92.0% and 80.6%, respectively, where uni-directional sequencing was defined as the successful analysis of either the forward or reverse Sanger sequencing trace.

Overall, only 1.2% (2/166) samples failed to generate any usable PCR products for Sanger sequencing, 1.8% (3/166) of samples only generated uni-directional sequencing for *EPAS1* exon 12, 4.2% (7/166) of samples only generated usable sequencing for *CDKN2B-2* and *EPAS1* exon 12, 1.2% (2/166) of samples generated sequencing for all amplicons except for *EPAS1* exon 12, and a larger subset of 12.0% (20/166) failed to generate sequencing for *EPAS1* exon 9. In total, 79.5% (132/166) and 35.5% (59/166) of samples had uni-directional and bi-directional sequencing, respectively, for all amplicons for targets of *CDKN2B*, *EPAS1* exon 9, and *EPAS1* exon 12. A summary of Sanger sequencing product and trace generation is provided graphically in 3.3 - Figure 2.

3.3 - Table 1

Amplicons used in targeted Sanger sequencing analysis of *CDKN2B* and *EPAS1* exon 9 & 12

Amplicon	Target region	Amplicon size (bp)	Primer set name
CDKN2B-1	Exon 1	597	CDKN2B-1B-PS
CDKN2B-2	Exon 2	600	CDKN2B-2A-PS
EPAS1-exon9	Exon 9	565	ORF-EPAS1-Ex9-rep
EPAS1-exon12	Exon 12	829	ORF-EPAS1-Ex12-rep

3.3 - Figure 1

An example of an agarose gel used to confirm the generation of a PCR amplicon for each target prior to performing Sanger sequencing.

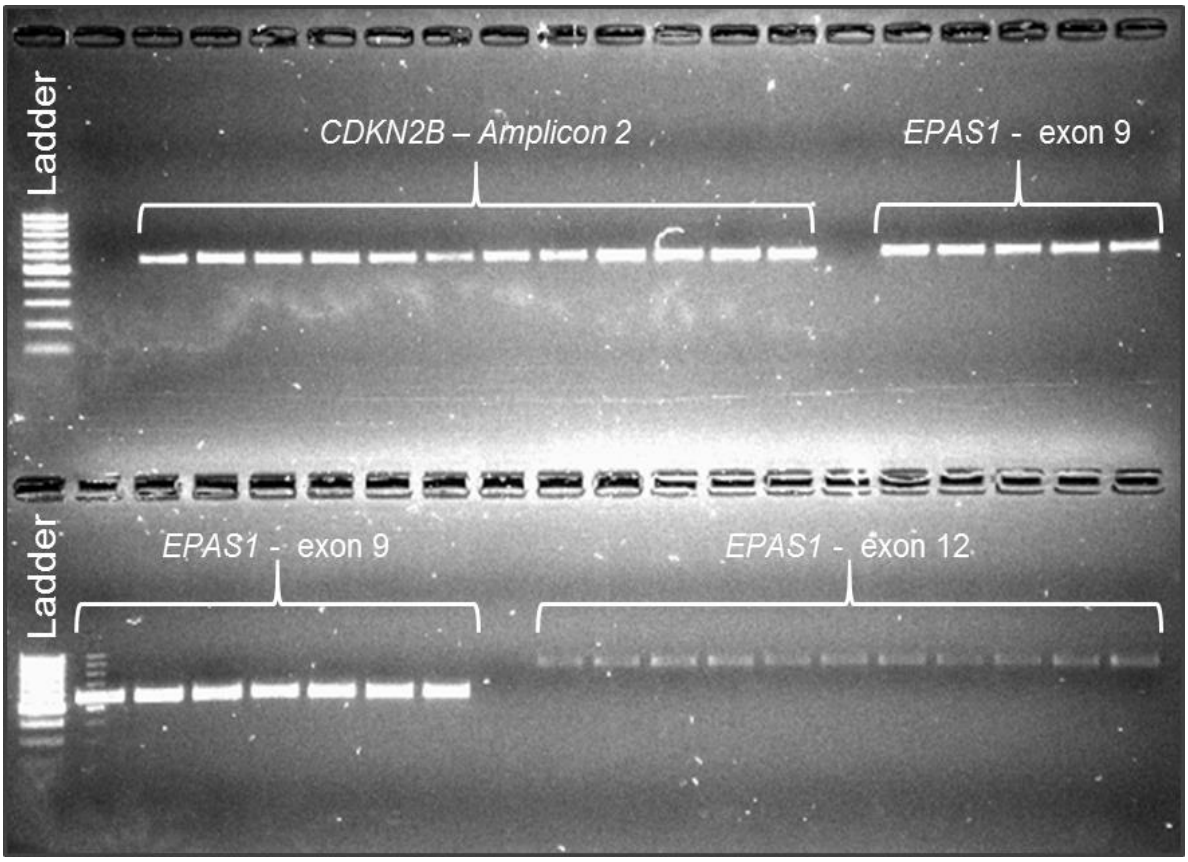

3.3 – Figure 2

Schematic heat map-style representation of amplicon sequencing visualising successfully analysed Sanger sequencing traces. Heat map is contiguous but split into three sections for clarity. X-axis is defined by both Amplicon and strand direction (Referred to by ‘F’ and ‘R’ columns). Green cell colouration indicates a trace was successfully analysed whereas red cell colouration indicates a trace failed to be analysed.

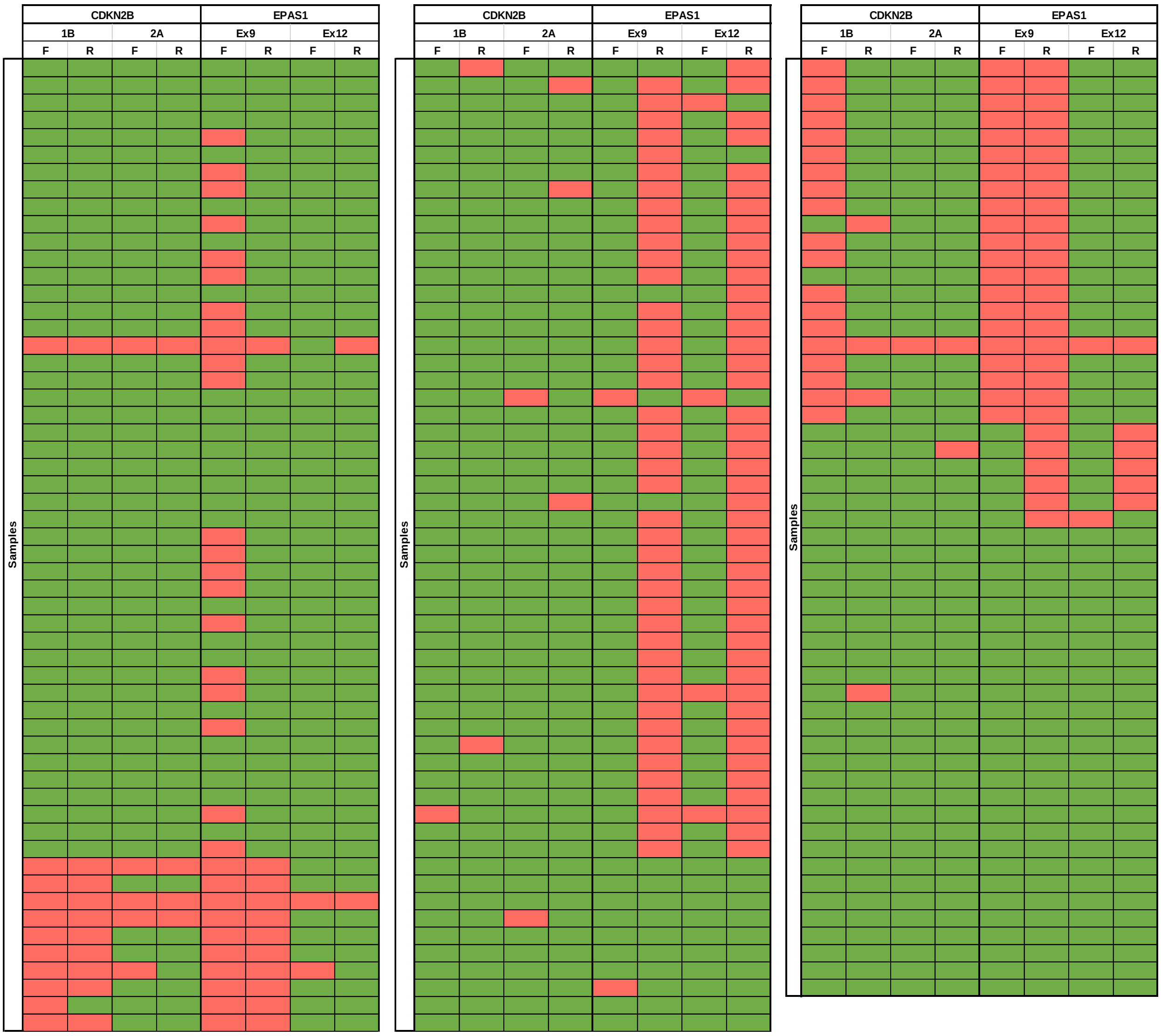

3.3.2 Targeted Sanger sequencing – Variant analysis

Sanger sequencing traces (bi-directional where available) were aligned to reference sequences for the corresponding genomic regions. Across the 164 samples assessed with viable Sanger data, variants were identified in 21 samples (12.7%), no sample carried more than a single variant, and variants were distributed across the targeted regions with a majority of samples carrying variants in *EPAS1* exon 12 (*CDKN2B* = 2, *EPAS1* exon 9 = 2, *EPAS1* exon 12 = 17)(Sanger traces shown in 3.3 - Figure 3). Most variants occurred more than once across the sample set, with only 5 unique sites altered, 1 in *CDKN2B*, 2 in *EPAS1* exon 9, and 2 in *EPAS1* exon 12 (See 3.3 - Table 2). Of the identified variants, 2 were classified as common SNPs, occurring in gnomAD (353) at an allele frequency of more than 1%. Remaining variants were assessed for pathogenicity based on manual annotation of criteria including functional consequence, clinical reporting, and *in silico* predictive metrics. Two individuals carried 1 variant in *CDKN2B* and two individuals carried variants in *EPAS1* exon 9. Filtered variants, including informative annotation, are described in 3.3 - Table 3.

EPAS1 exon 9 variants were present in 1.49% (2/134) individuals with available sequence information. The two variants present in *EPAS1* exon 9 (NM_001430:c.1104G>A: p.Met368Ile and NM_001430: c.1121T>A: p.Phe374Tyr) are flagged as likely benign according to ClinVar submissions, VUS and likely benign by ACMG interpretation, and *in-silico* tools SIFT, PolyPhen and CADD are in consensus that these missense alterations are unlikely to result in protein dysfunction. The remaining variant identified in exon 2 of *CDKN2B* in two individuals (NM_004936: c.256G>A: p.Asp86Asn) occurs at a minor allele frequency 1.22E-03 in the gnomAD dataset and falls within a functional domain and *in-silico* predictive metrics used suggest the variant is detrimental. The p.Asp86Asn variant is identical to that reported in the original report regarding RCC predisposition related to *CDKN2B* variants (266) which occurred at a rate of 1.19% (1/84; 95% CI 0.03-6.46%). Compared to this series, 1.24% (2/161; 95% CI 0.15-4.42%), the variant distributions are not statistically different (fishers exact; p = 1.00).

3.3 - Figure 3

Sanger traces of identified variants from targeted Sanger sequencing – Orange arrows indicate the position of the variant and each Sanger trace represents a single individual.

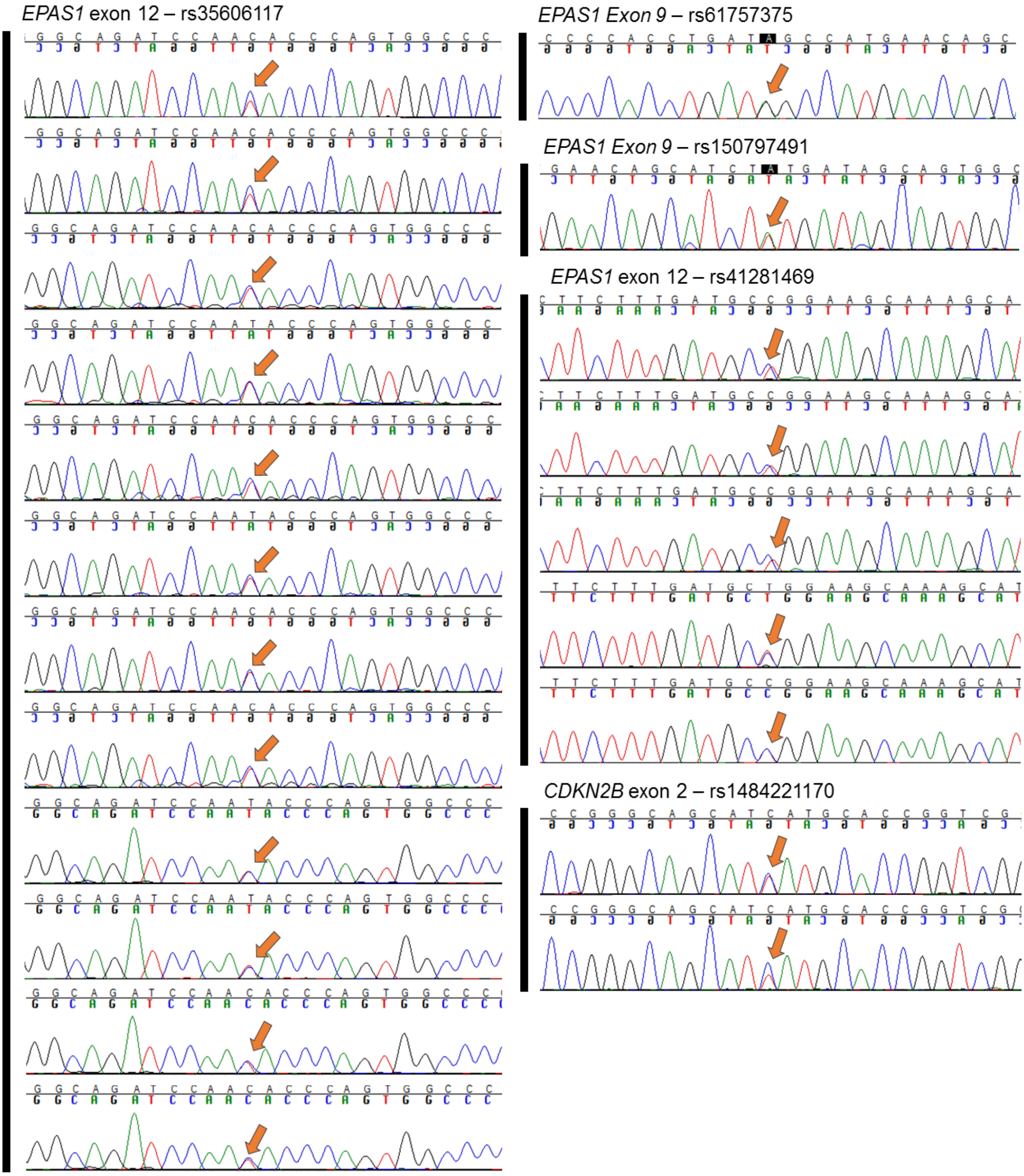

EPAS1 exon 12 – rs35606117

EPAS1 Exon 9 – rs61757375

EPAS1 Exon 9 – rs150797491

EPAS1 exon 12 – rs41281469

CDKN2B exon 2 – rs1484221170

3.3 - Table 2

Table of variants identified from Sanger sequencing data, predicted sequence alterations, global minor allele frequencies (gnomAD) and allele counts per variant across the series.

Chr	Pos	Ref	Alt	rsID	SYMBOL	Consequence	Transcript	EXON	CDS position	AA position	gnomAD AF	Allele Count
chr2	46376608	G	A	rs61757375	*EPAS1*	missense	NM_001430	exon 9	c.1104G>A	p.Met368Ile	0.0008081	1
chr2	46376625	T	A	rs150797491	*EPAS1*	missense	NM_001430	exon 9	c.1121T>A	p.Phe374Tyr	0.004008	1
chr2	46380505	C	T	rs41281469	*EPAS1*	synonymous	NM_001430	exon 12	c.1833C>T	p.Ala611Ala	0.01023	5
chr2	46380580	T	C	rs35606117	*EPAS1*	synonymous	NM_001430	exon 12	c.1908T>C	p.Asp636Asp	0.0236	12
chr9	22006148	C	T	rs148421170	*CDKN2B*	missense	NM_004936	exon 2	c.256G>A	p.Asp86Asn	0.00122	2

3.3 – Table 3

Table of variants identified in Sanger sequenced regions passing global minor allele frequency (gnomad) filtering (AF<0.01) with additional annotation information for affected protein domains and in-silico predictions.

Chr	Pos	Ref	Alt	rsID	SYMBOL	Conseq.	Transcript	EXON	CDS position	AA position	SIFT	PolyPhen	CADD phred	Interpro domain	gnomAD AF	ClinVar
chr2	46376608	G	A	rs61757375	*EPAS1*	missense	NM_001430	exon 9	c.1104G>A	p.Met368Ile	T (0.31)	B (0.02)	14.62	-	0.0008081	likely benign
chr2	46376625	T	A	rs150797491	*EPAS1*	missense	NM_001430	exon 9	c.1121T>A	p.Phe374Tyr	T (0.11)	B (0.06)	16.3	-	0.004008	likely benign
chr9	22006148	C	T	rs148421170	*CDKN2B*	missense	NM_004936	exon 2	c.256G>A	p.Asp86Asn	D (0.00)	Prob (0.99)	32	Ankyrin repeat	0.00122	uncertain significance

3.3.3 KMT2C & KMT2D targeted sequencing – Long range PCR product generation

For the targeted sequencing of *KMT2C* and *KMT2D*, long range HPLC-purified primer pairs were designed to cover the all exons and a proportion of intronic regions of both genes of both genes, encompassing exons 1-58 of *KMT2C* and 1-54 of *KMT2C* for a total targeted sequencing region size of 337 Kb. Amplicons were rejected if they failed to generate distinct or single amplicons and application of this filtering criteria resulted in no available coverage of 16/112 exons (14.2%) (See 3.3 - Table 4). Agarose gel containing all optimised long-range PCR amplicons is shown in 3.3 - Figure 4.

For the remaining optimised primer pairs, long range PCR amplification was carried out across 96 samples, totalling 1824 long range PCR reactions. After repeating long range PCRs, a total of 82.8% of reactions successfully generated suitable PCR products for library preparation. The number of successful amplicons was higher in *KMT2D* amplicons than *KMT2C* amplicons (87% compared to 81%), with the worst performing amplicon *KMT2C* exon 53-58 having 54.2% success rate and the best performing amplicon *KMT2D* exon 12-14 successfully generating long range amplicons in 94.8% of samples (See 3.3 - Figure 5).

Samples with complete sets of amplicons were batched into libraries for sequencing utilising Illumina NexteraXT kit as described in the methods (Section 3.2). Batch 1 and 2 consisted on amplicons for both *KMT2C* and *KMT2D* whereas batch 3 only contained amplicons for *KMT2D* due to complications discussed later in this chapter.

3.3 - Figure 4

Agarose gel on control genomic DNA for all 19 viable long range PCR amplicons

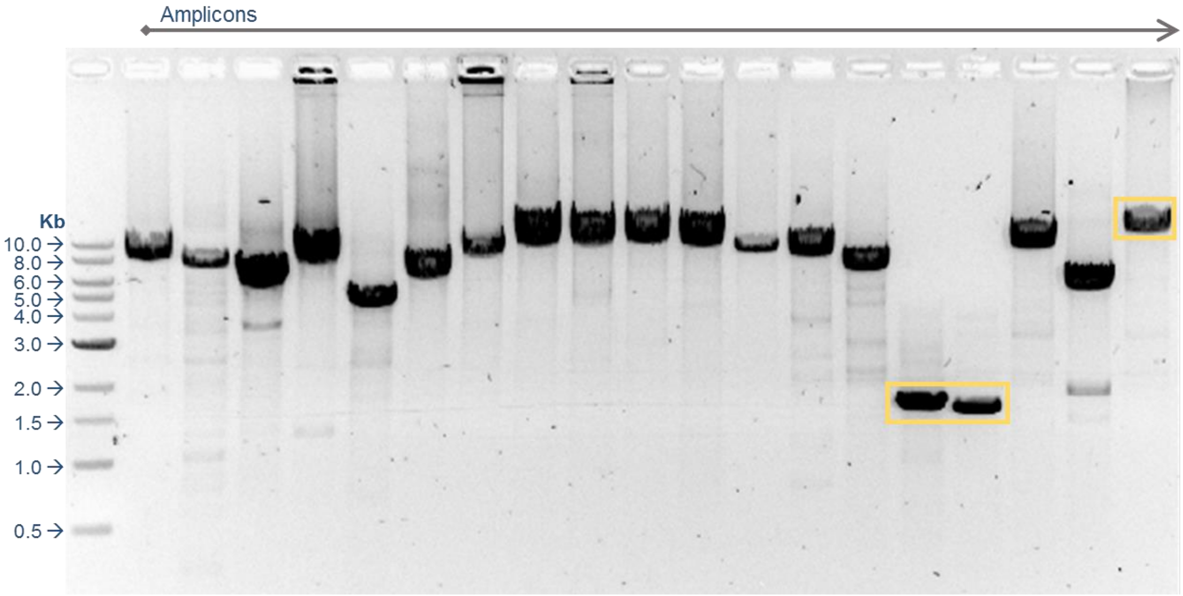

3.3 - Table 4

Details of primer optimisation process detailing reaction requirements for long range PCR and exclusion criteria

Gene	Exon Covered	Optimisation	Product Size (bp)	Annealing Temp. (°C)	DNA Conc. (ng/µl)	Notes
KMT2C	Exon 3	PASS	7854	61	10	
KMT2C	Exon 4 - 6	PASS	7457	60	10	
KMT2C	Exon 7	PASS	5668	61	10	
KMT2C	Exon 15 - 16	PASS	7243	61	10	
KMT2C	Exon 17 - 18	PASS	4806	59	10	
KMT2C	Exon 19-20	PASS	6219	60	10	
KMT2C	Exon 21 - 23	PASS	8008	60	10	
KMT2C	Exon 24 - 27	PASS	9375	59	10	
KMT2C	Exon 32 - 37	PASS	9205	59	10	
KMT2C	Exon 38 - 41	PASS	9776	58	10	
KMT2C	Exon 45 - 52	PASS	9169	58	10	
KMT2C	Exon 53 - 58	PASS	9896	62	10	
KMT2C	Exon 59	PASS	8076	59	10	
KMT2D	Exon 1 - 11	PASS	6579	59	10	
KMT2D	Exon 12 - 14	PASS	1623	59	10	
KMT2D	Exon 15 - 18	PASS	1518	57	10	
KMT2D	Exon 19 - 34	PASS	8433	59	10	
KMT2D	Exon 35 - 42	PASS	5064	62	10	
KMT2D	Exon 43 - 54	PASS	11,150	59	10	
KMT2C	Exon 1	FAIL	7909	NA	NA	Multiple Bands
KMT2C	Exon 8-9	FAIL	7826	NA	NA	Multiple Bands
KMT2C	Exon 10-14	FAIL	7986	59	10	Multiple Bands
KMT2C	Exon 42-44	FAIL	9047	58	10	Multiple Bands
KMT2C	Exon 2	FAIL	7950	60	10	Multiple Bands
KMT2C	Exon 28 - 31	FAIL	5512	58	10	Wrong Product size

3.3 - Figure 5

Schematic heat map representation of long-range PCR amplicon generation across 96 samples. Columns represent individual amplicons and rows correspond to samples. Numeric values on the x and y axis are completion percentages for each row/column/group. Green colouration indicates success and red indicates failure.

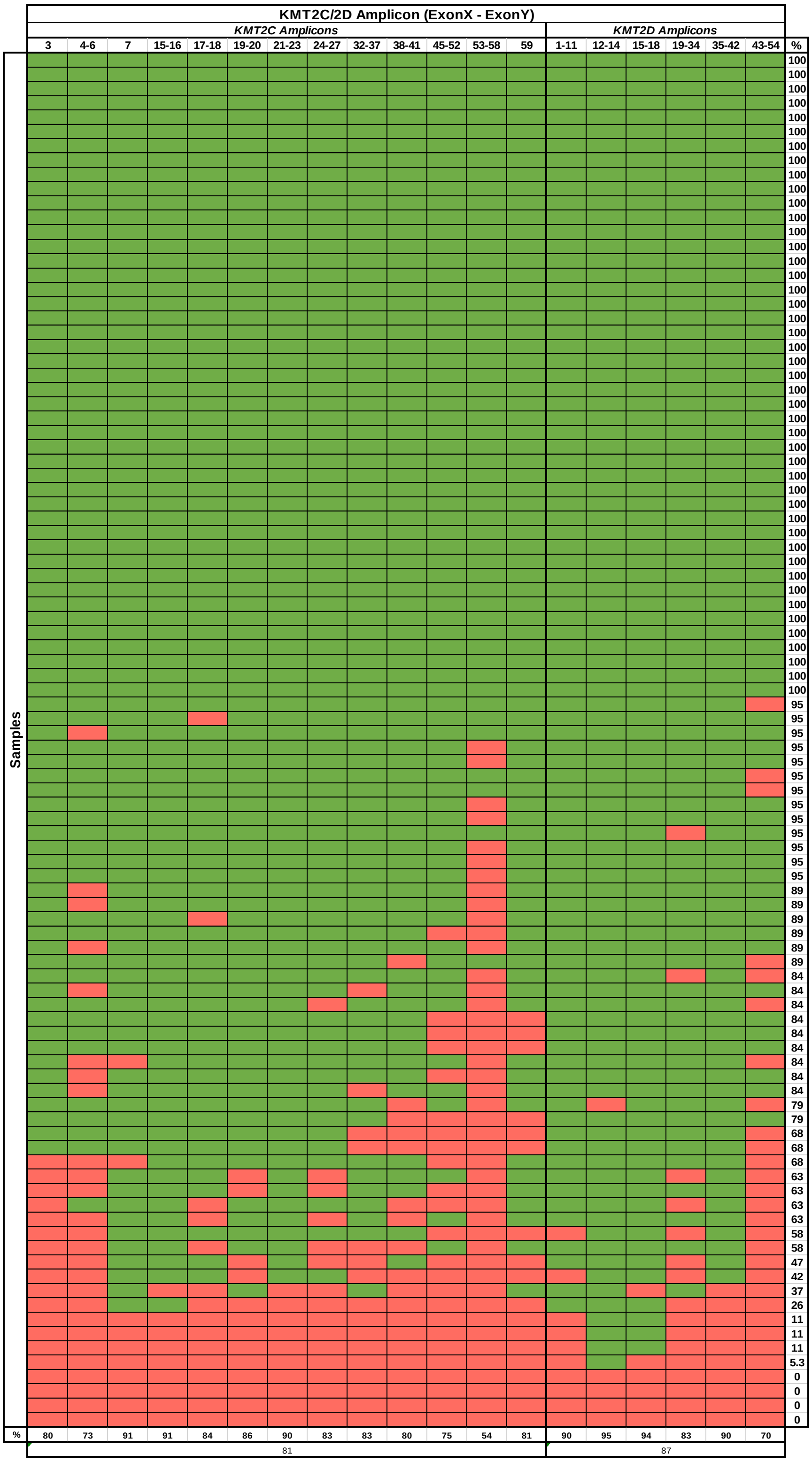

3.3.4 KMT2C & KMT2D targeted sequencing – Library preparation and quality control

Across each batch, the mean number of reads successfully aligned to human genome build GRCh38 was 99.87% (SD=0.06), 99.78% (SD=0.20), and 98.92% (SD=1.29) and estimates of PCR duplicates were calculated with a mean value of 14.3% (range 8.30-17.5; SD=2.52%), 20.7% (range 10.5-31.2%; SD=4.99), and 3.16% (range 1.5-5.3%; SD=1.06) for batches 1-3, respectively. Significant differences were found in PCR duplicate rates across batches (Kruskal-Wallis rank sum test; p=8.68E-10) but was solely related to input amplicons used across batches.

On-target sequencing rates were calculated based on the number of non-PCR duplicate reads intersecting within the genomic span of *KMT2C* and *KMT2D*. For batches 1-3, the on-target sequencing rates were 63.3% (SD=3.98), 60.3% (SD=5.11), and 89.1% (SD=3.81) of reads aligning to either the genomic regions of *KMT2C* or *KMT2D*, respectively. Significant differences in on-target alignment were seen between batches 1-2 and batch 3 (Kruskal-Wallis rank sum test; p=4.10E-09).

Mean coverage across targeted exonic regions was 353 (SD=63.2), 435 (SD=72.8), and 40.0 (SD=5.15) for batches 1-3, providing adequate coverage for variant calling. As mentioned previously, batch 3 was sequenced on a lower throughput sequencing flow cell and as such has lower mean coverage compared to batches 1 and 2. Overall sequencing metrics were deemed to be adequate for variant assessment given the sequence coverage levels. High levels of off-target sequence alignment were noted, particularly in batch 1 and 2. Sequence alignment and quality control metrics are shown in 3.3 - Figures 6-8 with additional sequencing statistics provided in appendix section 9.2.3.

3.3 – Figure 6

Mean read coverage counts across all targeted sequencing regions per sequencing batch. Batches are segregated by colouration.

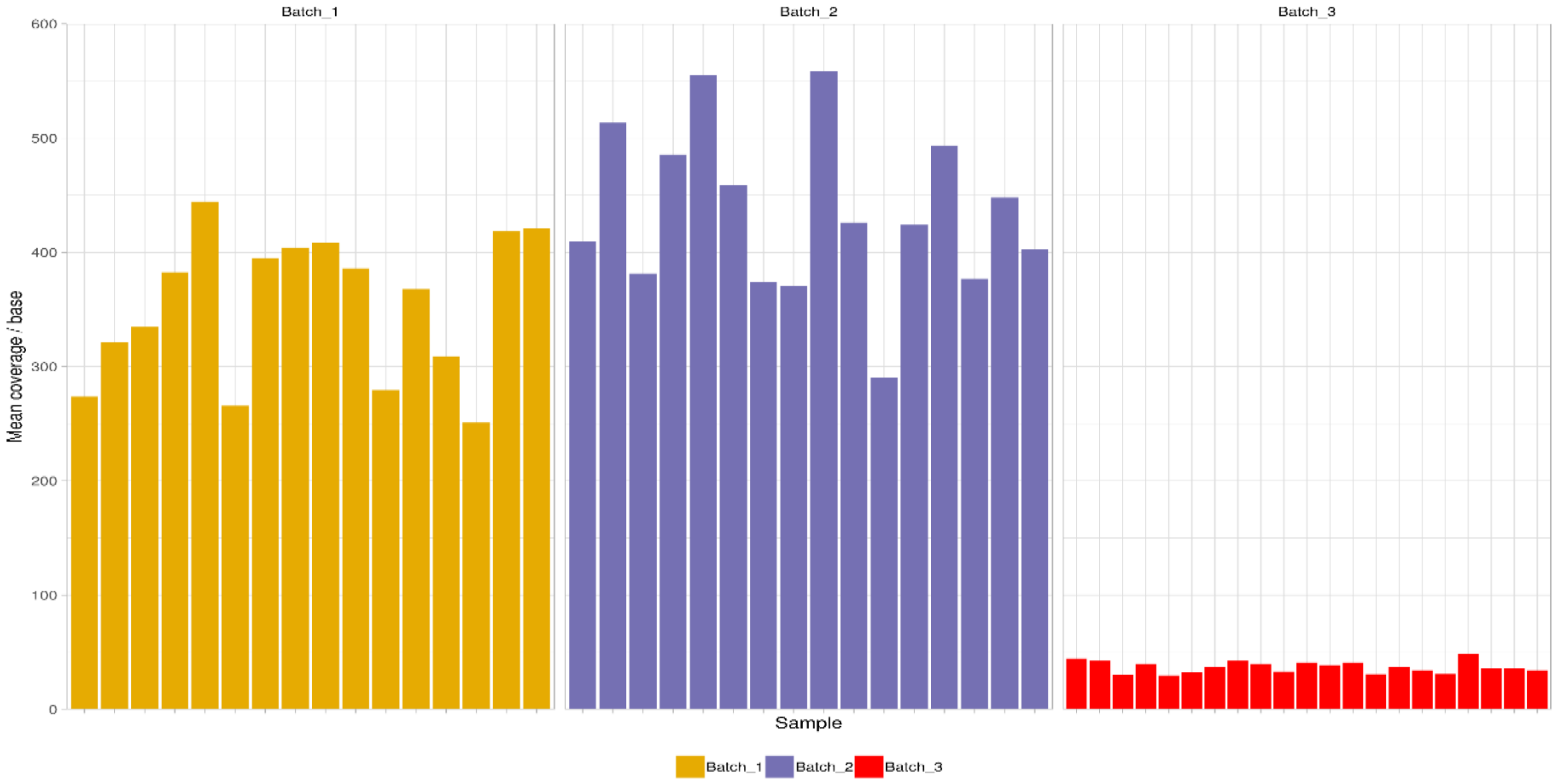

3.3 – Figure 7

Percentage of reads flagged as PCR duplicates across each sample, segregated by batch. Orange colouration indicates the duplicated proportion of reads per sample.

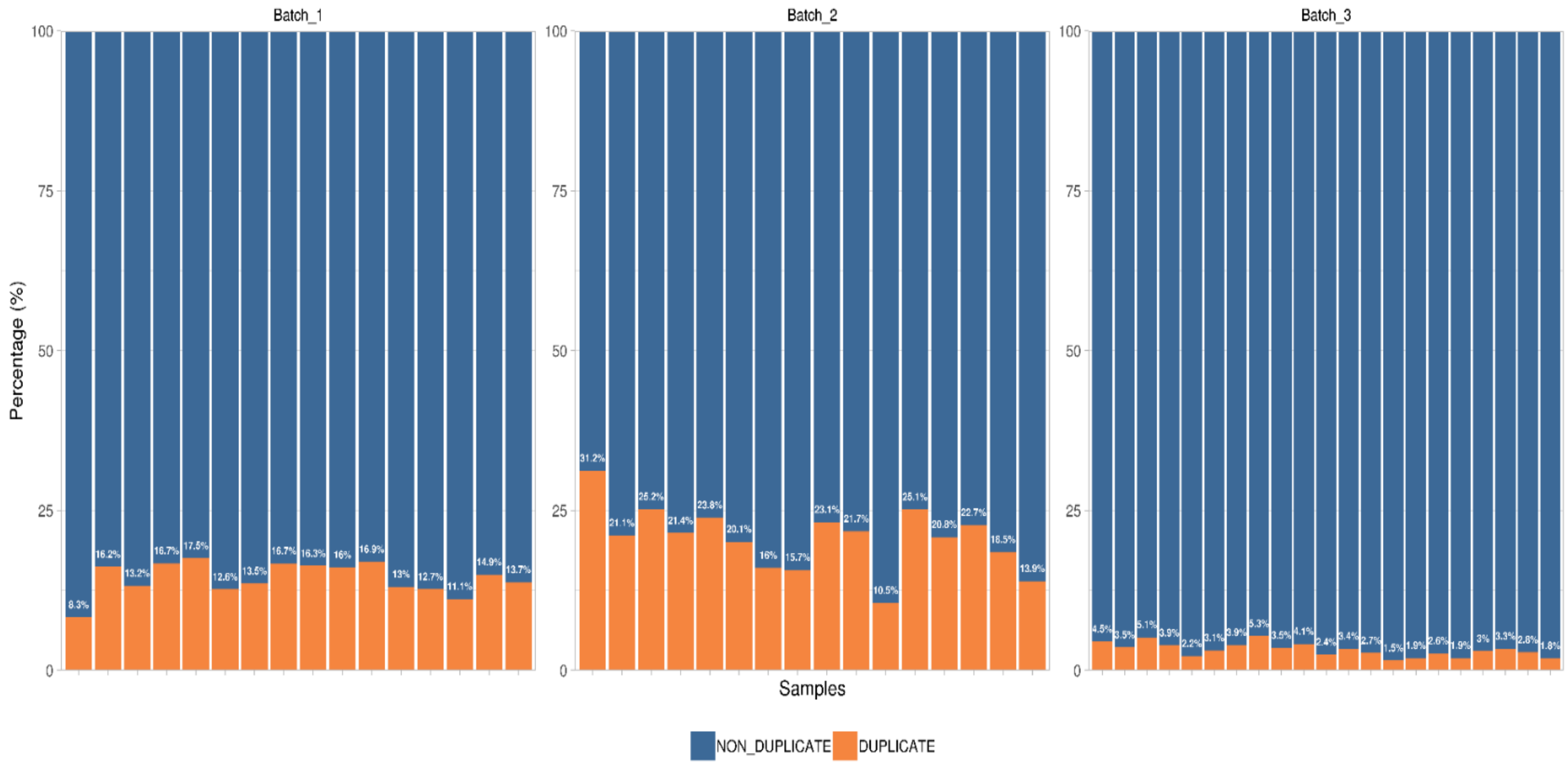

3.3 - Figure 8

Region depth of coverage plots displaying the mean read coverages across the *KMT2C* and *KMT2D* genomic regions. Line colourations indicate sequencing batch. The upper track displays mean coverage at each base and the lower track displays a representation of the exonic regions of the genes. 8A Coverage for batches 1-3 of *KMT2C.* 8B Coverage for batches 1-3 of *KMT2D.* 8C Coverage for batch of *KMT2D*.

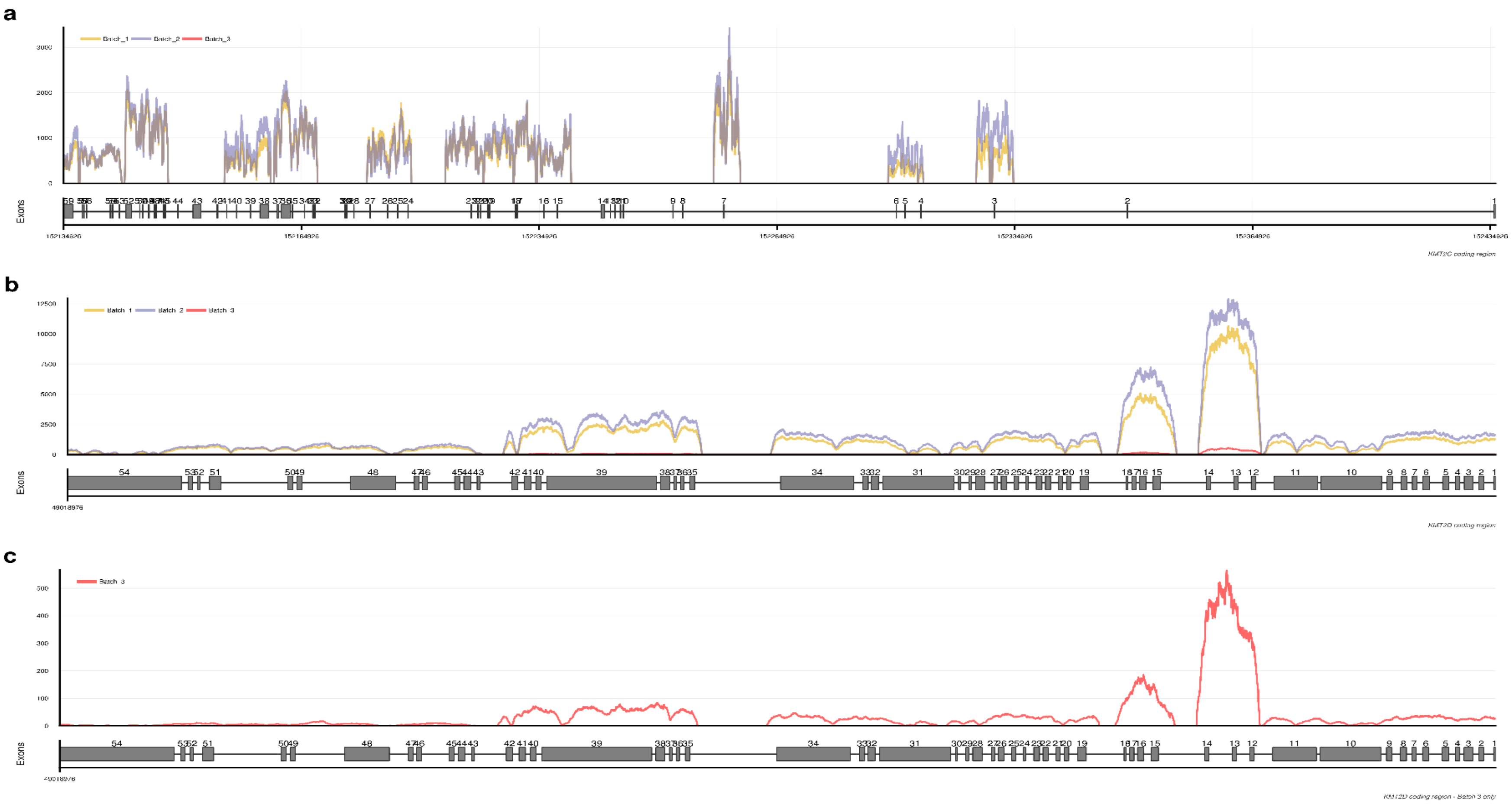

3.3.5 KMT2C & KMT2D targeted sequencing – Variant analysis

Variant calling was performed as described in material and methods section and called a total of 23,644 variants prior to filtering and quality control. After filtering called variants for depth, QUAL, and genotype quality a total of 1,773 variants were retained. Missingness filters were not applied due to no sequencing data being available for *KMT2C* in 39.6% of samples due to constraints applied to library batch 3.

Variants were annotated and further filtered as described in the methods and a total of 18 sites across 14 individuals were retained. After filtering for variants within the span of the coding region of *KMT2C* and *KMT2D*, 7 variants in 6 individuals were kept, with the remaining proportion being called in off-target regions. Variants were functionally annotated utilising Annovar and assessed for pathogenicity (See 3.3 Table 5). All variants identified were missense variants, 1 in *KMT2C* and 6 in *KMT2D*. Of the 7 variants identified in the coding regions of *KMT2C* or *KMT2D*, 3 variants were classified as variants of unknown significance (VUS) and 4 were classified as likely benign by ACMG criteria (325). No variants identified were classed as known pathogenic variants and only missense variant p.Gly1425Ser in *KMT2C* (NM_170606: c.4273G>A: p.Gly1425Ser) in exon 27 had consensus pathogenic or damaging *in silico* predictive metrics.

3.3 - Table 5

Variants occurring within the genomic regions of *KMT2C* and *KMT2D* passing all filtering criteria with additional *in silico* prediction, ACMG, and ClinVar annotations.

Chr	POS	rsID	REF	ALT	GENE	Transcript	Exon	cDNA	AA	CONSEQ.	X1000G	EXAC	CADD	SIFT	POLY PHEN	ACMG	CLINVAR
chr7	152199279	rs746270757	C	T	*KMT2C*	NM_170606	27	c.G4273A	p.G1425S	Missense	0.00E+00	8.35E-06	26.2	D	D	VUS	N/a
chr12	49040100	rs189888707	G	A	*KMT2D*	NM_003482	31	c.C7670T	p.P2557L	Missense	8.59E-03	8.50E-03	23.4	D	B	LB	Benign Likely benign
chr12	49038591	rs757791539	C	T	*KMT2D*	NM_003482	34	c.G8765A	p.R2922Q	Missense	0.00E+00	8.46E-06	24.3	T	B	VUS	N/a
chr12	49051743	rs200088180	G	T	*KMT2D*	NM_003482	10	c.C1940A	p.P647Q	Missense	0.00E+00	4.00E-04	4.622	T	B	LB	Conflicting interpretations of pathogenicity
chr12	49042232	rs754420100	G	A	*KMT2D*	NM_003482	28	c.C5966T	p.T1989M	Missense	0.00E+00	0.00E+00	23.9	T	D	VUS	N/a
chr12	49051554	rs758912919	G	C	*KMT2D*	NM_003482	10	c.C2129G	p.P710R	Missense	0.00E+00	5.18E-05	0.073	T	B	LB	N/a
chr12	49051609	rs202076833	G	T	*KMT2D*	NM_003482	10	c.C2074A	p.P692T	Missense	1.40E-03	4.20E-03	9.233	D	B	LB	Benign Likely benign

3.3.6 KMT2C & KMT2D Targeted sequencing – Off-target regions and read mapping

The initial number of called variants (23,644) compared to final filtered numbers resulted in investigations in variant calling metrics and quality control and analysis was performed to assess the number of total intragenic (within gene region) variants called across the cohort. As variant calling was performed genome-wide, a minor fraction would be expected to be present across off-target sites due to both mismapping reads, genomic contaminants, and variant calling errors. As expected, low levels (< 10 variants) intragenic variants were identified in 46 genes, the majority of which occurred within non-coding space but an apparent enrichment of variants was identified in BAGE Family Member 2 *(BAGE2*)(See 3.3 Figure 9).

Given that called variants are present due to mapped reads supporting a specific allele, analysis of read mapping was performed across the *BAGE2* coding regions to identify the total proportion of reads aligning to the region. Mean percentage of reads aligning within *BAGE2* in batches 1 and 2 was 8.35% (SD=1.16) and 7.67% (SD=1.26), respectively, while batch 3 did not contain any reads mapping to *BAGE2*. The mapping results suggest that alignment of reads with *BAGE2*, and as such variant calling, is due to the presence of *KMT2C* amplicons given that batch 3 consisted only of amplicons for *KMT2D*. Read alignment rates for *BAGE2, KMT2C, KMT2D, KMT2C/D* are shown in appendix section 9.2.3.

3.3 Figure 9

Variant counts for intragenic regions detected in targeted sequencing data of *KMT2C/D* prior to stringent rarity and consequence filters.

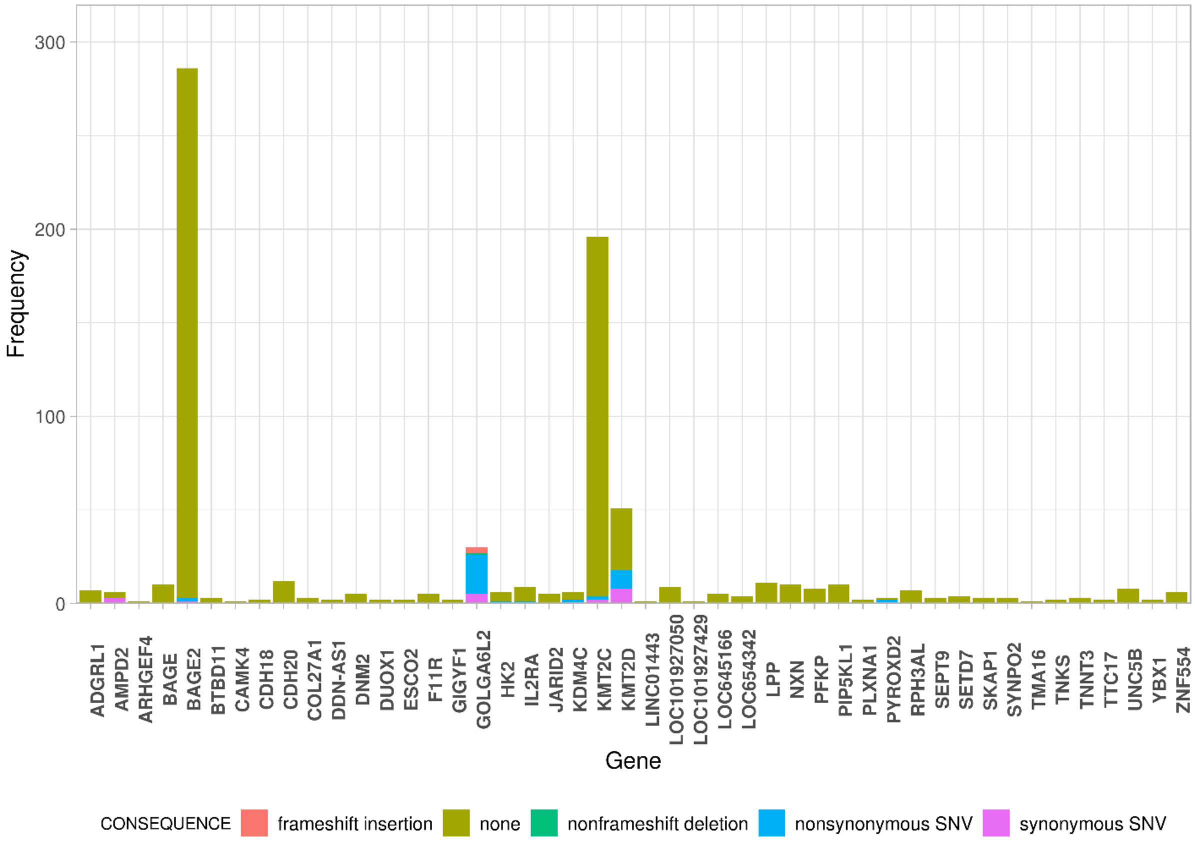

3.3.7 KMT2C & KMT2D Targeted sequencing – BAGE2 gene sequence comparison

The *BAGE* family of genes consisting of members *BAGE1-5*, of which only *BAGE2* and *BAGE5* have genomic positions designated in genome build GRCh38, where all others are unmapped and designated in chr21p11.1, in proximity to *BAGE2* (See Appendix 9.2.4). Since *BAGE2* read alignments only occur in samples containing *KMT2C* amplicons, it is likely sequence similarities exist between regions of *KMT2C* and *BAGE2*, resulting in off-target alignment. Using Emboss matcher, the coding sequences of *KMT2C* (ENSG00000055609) and *BAGE2* (ENSG00000187172) resulted in a pair-wise alignment sequence similarity of 86.6% and gap presence of 9%. Inverse pair-wise alignments resulted in similar levels of sequence identity between *KMT2C* and *BAGE2* (78.7%). Pair-wise sequence of mRNA sequences for *KMT2C* (NM_170606) and *BAGE2* (NM_182482) also demonstrated significant sequence similarity (73%) but a much greater introduction of sequence alignment gaps (25.4%), demonstrating lower identity within coding regions. Comparison of conserved sequence regions in *BAGE2* plotted across *KMT2C* demonstrated gene-wide conservation (See Appendix 9.2 for sequence comparisons, read alignment rates, and conservation plots).

3.3.8 Validation of KMT2C nonsense variant

Given the issues regarding *KMT2C* and multiple mapping of reads to *BAGE2* and others, DNA for the initial index case harbouring the *KMT2C* nonsense variant (NM170606.2: c.2263C>T: p.Gln755Ter: rs201234598) was acquired and Sanger sequencing was used to amplify the region containing the *KMT2C* variant. Sanger sequencing trace resolved a partial mosaic variant at the affected site, with a reduced allelic depth estimated at 0.2-0.3 (See 3.3 Figure 10).

Additional variant data was extracted from ExAC and gnomAD aggregated datasets to assess variant statistics related to the nonsense variant site. Both datasets employ a stringent series of filter criteria on variants detected within the cohorts and though rs201234598 is reported, it failed random forest filtering in both sets, suggesting the variant is artefactual. In addition to failing random forest filtering metrics, the variant is present in a large proportion of genomes reported in gnomAD with allele frequency reported in gnomAD greater than that in ExAC by an order of magnitude, 2.17E-03 compared to 4.1E-02.

3.3 - Figure 10

Sanger sequencing trace from affected individual alleged to carry the *KMT2C* nonsense variant (NM170606.2: c.2263C>T: p.Gln755Ter: rs201234598).

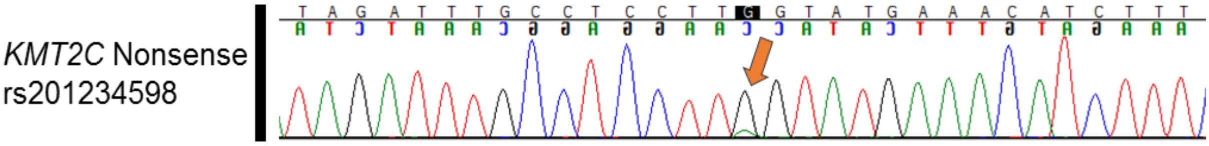

3.4 Discussion

Targeted Sanger sequencing of *EPAS1* exon 9 and 12 and *CDKN2B* revealed several potential variants of interest, though none were classified as pathogenic or likely pathogenic. Analysis of rare variants in *EPAS1* exon 9 and 12 identified two missense variants (NM_001430: c.1104G>A: p.Met368Ile and NM_001430: c.1121T>A: p.Phe374Tyr) in exon 9 which have previously been assessed in relation to polycythaemia and paragangliomas (342). While ClinVar and ACMG criteria regard these variants as likely benign or VUS variants, functional studies have demonstrated that *EPAS1* p.Phe374Tyr results in a gain-of-function, demonstrating increased stability over wildtype EPAS1, and protein interaction simulations suggested p.Phe374Tyr-EPAS1 protein disrupted pVHL binding to its complex components (342). The second *EPAS1* p.Met368Ile variant does not have supporting functional data but occurs at a lower allele frequency in reference datasets and in close proximity to the p.Phe374Tyr variant, suggesting that the p.Met368Ile variant may alter EPAS1 in a similar manner, though functional confirmation would be required. Germline predisposing variants in *EPAS1* in RCC would be particularly interesting if proven to be a true association given recent clinical trials of EPAS1 inhibitors as a treatment for RCC tumours (84), given the potential to attenuate EPAS1 function somatically and improve clinical outcome.

The remaining variant identified in the targeted Sanger sequencing experiment was in exon 2 of *CDKN2B* in two individuals (NM_004936: c.256G>A: p.Asp86Asn) and occurs at a minor allele frequency 1.22E-03 and falls within a Ankyrin repeat domain. All *in-silico* predictive metrics used suggest the variant is detrimental and previous publications determined that the variant resulted in diminished function by disrupting the interaction between p15^{INK4B} and CDK4 (354). The *CDKN2B* p.Asp86Asn variant, as well as being seen in parathyroid adenomas (355), is identical to the variant found in heritable RCC cases profiled previously (266) and supports the hypothesis that rare functionally damaging variants in *CDKN2B* can confer a risk to RCC. However, given the allele frequency in control non-cancer populations, high or complete penetrance is unlikely and variants in *CDKN2B* may act similarly to variants in *SDHB* genes conferring only a low risk of RCC (221), though further association data is required.

The issue regarding sequence identity between *KMT2C* and *BAGE2* is the primary issue with the outcome of the targeted sequencing of *KMT2C* and *KMT2D*. The first *BAGE* gene was originally identified due to encoding an antigen present in melanoma (356), after which further *BAGE* genes, including *BAGE2*, were identified mapping to both chromosome 9, 13, and 21 in juxtacentromeric regions and have reported regions of sequence identity between 92-99% in similarity (357). Evolutionary analysis of *BAGE2* sequence origin revealed that *BAGE2* and its related genes are formed due to a reshuffling and duplication of regions of *KMT2C* on chromosome 7, followed by further duplications across the chromosomes mentioned previously resulting in multiple *BAGE* sequences across the genome (358). This, in part, demonstrates why many reads generated by targeted sequencing of *KMT2C* produced off-target mapping to *BAGE2*.

The failure of amplicon generation of exons 1, 2, 8, 9, 10-14, 28-31, and 42-44 of *KMT2C* was unexpected during primer optimisation, but no primers failed due to an absence of products. Given the information regarding *BAGE2* and that all primers failing optimisation did so due to either incorrect or multiple primary products would suggest that long range primers are annealing to off target sites in *BAGE2* and its related genes despite rigorous primer design to minimise those factors. It cannot be stated that all amplicon primer sets that failed are as a result of *BAGE2* sequence similarity though, since primers generating multiple products could also be producing PCR amplicons outside of *BAGE2*. Loss of these amplicons resulted in a restriction in the available coding exons of *KMT2C* available for analysis, which included exon 14 in which the nonsense variant (NM170606.2: c.2263C>T: p.Gln755Ter: rs201234598) from the index case occurred.

For the amplicons that successfully passed optimisation, failure to generate products were either due to multiple products (as discussed above) or due to an absence of PCR product. In this instance, failure to generate products after iterative optimisation steps is likely due to DNA quality and degree of fragmentation which are decreased and increased, respectively, during long-term storage and freeze-thaw cycles. While a proportion of reads generated by NGS library preparation will map incorrectly to *BAGE2* due to sequence similarities, it is probable primer design resulted in the direct amplification and sequencing of *BAGE2* and *KMT2C* concurrently, with product sizes being indistinguishable on standard gel electrophoresis. This is supported by the primer design process which selected intronic regions for primer annealing, which are also highly conserved between the two genes.

The presence of mismapped reads and resulting variant calls is an important consideration when discussing variant calling due to the potential for false positive variant calls and is a documented pitfall of short read sequencing (359). If reads are misaligned from *KMT2C* to *BAGE2*, logically it suggests that reads are being conversely misaligned from *BAGE2* to *KMT2C*. For identical regions, this results in no detectable variation but if any read contained a sequence variation and aligned incorrectly it would suggest an alternative allele at the misaligned loci. Repeated occurrence of this process at the same site would provide enough supporting alternative reads to result in false positive variant calling. Presence of false positive calls introduced by low mapping quality reads in simulated data demonstrated that increase MAPQ filtering nullifies this concern generally (360) but MAPQ filtering in this study was already greater than the suggested threshold to eliminate this issue.

In the case of exome data and the nonsense variant described previously, it is plausible a false positive variant call occurred, given the difference in allelic frequencies between exome and genome sequencing data sets and the reduced alternative allelic fraction seen in the Sanger sequencing. Taken together, this provides informative data to suggest that the nonsense variant initially identified results as a consequence of sequence conformity between *KMT2C* and *BAGE2*, where PCR amplification from both regions results in the inclusion of sequence regions where differences in sequence are limited to only a single base. The increased allelic frequency in gnomAD genomes compared to exomes is likely due to the removal of biases introduced by exome target probe hybridisation. Moreover, this introduces doubt over the reliability of all variant calling within the *KMT2C* coding regions which share sequence identity with *BAGE2*, and as such caution should be taken when assessing variants in this gene. A vast majority of current sequencing projects, particularly somatic, utilise WES or capture-based sequencing to generate somatic variant calls. Given that somatic calls are typically made at lower allelic fractions than germline calls, mismapping in somatic cases could inadvertently result in an enrichment of false positive calls in genes identified to be significantly mutated in tumour datasets.

While *KMT2C* sequencing harboured major issues regarding off-target effects and data misalignment, *KMT2D* did not display these features and performed well by comparison, with no amplicons failing to generate sequencing data and on-target sequencing rates above 80% in all samples (See appendix section 9.2.3). One identified issue with sequencing of *KMT2D* was the overrepresentation of amplicons *KMT2D* Exon 12 – 14 and Exon 15 – 18 which sequenced at far greater depth than other targets (mean coverage > 20,000 for both) due to the size discrepancy between other amplicons. Both *KMT2D* Exon 12 – 14 and Exon 15 – 18 are less than 2 Kb in length (See 3.3 Figure 4 and Table 4), and as such pmol input of each amplicon, even after normalisation, resulted in several fold increases in fragment retention prior to library preparation compared to larger amplicons. Though this did not impact results generated in this study due to surplus sequence coverage, replication in studies with narrower margins of error for targeted coverage may result in disproportionate sequencing of these smaller amplicons, resulting in reduced or inadequate coverage of other amplicons.

Targeted NGS of *KMT2C* and *KMT2D* identified several rare missense substitution variants in both genes, but a majority occurred within *KMT2D* for the reasons specified previously. The single variant in *KMT2C* (NM_170606: c.G4273A: p.G1425S) was predicted to be pathogenic by SIFT, PolyPhen and CADD and reported with an allele frequency of 8.35E-06. The amino acid change glycine to serine is non-conservative, therefore more likely to be damaging to protein structure but the variant does not appear to affect any known regulatory or functional protein domain. Both variants *KMT2D* p.P2557L (NM_003482: c.C7670T: p.P2557L) and *KMT2D* p.P692T (NM_003482: c.C2074A: p.P692T) had no evidence to support pathogenicity and occurred at allele frequencies in ExAC at marginally lower than 1%, suggesting they are unlikely to be disease-causing. One variant in *KMT2D* (NM_003482: c.C1940A: p.P647Q) was predicted to be benign by *in silico* tools and had conflicting interpretation in ClinVar but on review was reported as causal in an individual affected with Kabuki syndrome but no case report was provided and multiple additional reports presented conflicting evidence (361,362). The remaining *KMT2D* variants (NM_003482: c.G8765A: p.R2922Q, NM_003482: c.C5966T p.T1989M, and NM_003482: c.C2129G: p.P710R) had contradictory or unsupportive *in silico* metrics but occurred at allele frequencies consistent with the potential to be disease causing, though none had any additional evidence to suggest pathogenicity.

KMT2C and *KMT2D* are associated with known autosomal dominant genetic disorders Kleefstra syndrome 2 and Kabuki syndrome, respectively, and are associated with heterozygous loss-of-function variants. Kleefstra syndrome 2 is a recently defined syndromic condition resulting in delayed psychomotor development, and dysmorphic anatomical features associated with frameshift, truncating and deletions of *KMT2C* (363). Kabuki syndrome is a well characterised syndrome causing cognitive impairment, growth restriction, facial dysmorphisms and cardiac and renal anomalies as a result of inactivating or truncating variants in *KMT2D* (364).

In this series no known pathogenic or loss of function variants were identified to substantiate the hypothesis that pathogenic inactivating variants in in *KMT2C* or *KMT2D* might be associated with RCC predisposition. For variants in *KMT2C,* presentation of kleefstra syndrome is typically seen with sub-telomeric loss of 9q, including loss of *EHMT1* or inactivation of *KMT2C* on chromosome 7 (365). In tumours, inactivating mutations or deletions of *KMT2C*, alterations have been demonstrated to downregulate DNA repair pathways (366), as well as mediate responses to oestrogen in breast cancers (367). A potential genotype-phenotype could be hypothesised in which variants in *KMT2C* under which loss of *KMT2C* can results in epigenetic reprogramming that corresponds with the phenotype seen in kleefstra syndrome whilst in the context of cancer, impedance of DNA repair and alternative epigenetic alterations could drive oncogenesis and cancer predisposition. While the exact mechanism and correlation of such a genotype-phenotype correlation is not known it may currently be the most likely hypothesis, particularly given functional links between *KMT2C*, *SMARCB1*, and the SWI/SNF complex of which several genes are already associated with predisposition to RCC (264) and the frequency at which *KMT2C* is altered somatically (25).

Moreover, *KMT2D* has conflicting evidence regarding its function as a tumour suppressor, being shown to upregulate p53 and supress tumour development (349,368) but also functions in an oncogenic capacity in maintaining tumour cell proliferation (369). Given that *KMT2D* has the potential to act as either a TSG or an oncogene in a tumour-specific manner it could be hypothesised that missense variants in *KMT2D* might predispose to renal cancer in the absence of Kabuki syndrome (if the former were activating mutations and the latter resulted from inactivating mutations). Additionally, single cell transcriptome and RNA sequencing data on patient-derived Kabuki syndrome cell lines carrying a *KMT2D* nonsense variant displayed reduced cell cycle progression, increased cell death, and most intriguingly demonstrated downregulated genes included an overrepresentation of genes containing HRE motifs (370), most commonly activated by HIF complex binding as discussed in relation to *VHL* regulation of hypoxia (138,140), proposing that activating mutations in *KMT2D* could cause constitutional upregulation of HRE-containing genes in a manner similar to HIF proteins. Only missense variants were identified in this series and no large deletions are observed somatically in *KMT2D* but significant further analysis and functional assessment of both the function of *KMT2D* in RCC and the identified variants are required before any conclusion could be made regarding either the pathogenicity of the identified variants or the role of *KMT2D* in RCC tumourigenesis.

However, an alternative hypothesis would be that missense variants with a partial loss of function effect could cause an attenuated (and unrecognised) form of Kabuki syndrome and predispose to renal cancer. Interestingly there are some case reports of tumour development in patients with Kabuki syndrome, though there is no evidence of clear increased risk of neoplasia (371–373). Furthermore, prostate tumour studies identified loss-of-function alterations in *KMT2D* in 60% of assessed patients and demonstrated attenuation of cell proliferation, invasion and migration in *KMT2D* knockout cell lines (374).

3.5 Conclusion

Targeted sequencing, both via Sanger sequencing and NGS techniques, can provide a robust and relatively simple way to adequately genotype a small set of genomic regions but it is clear that issues regarding pseudo-genes, DNA amplification rates, and DNA quality can give rise to difficulties in experimental design and interpretation of sequencing data. Regardless of the pitfalls encountered by the investigations present here, potential predisposition variants in both *CDKN2B* and *EPAS1* could be of interest but cautious interpretation should be applied before drawing causal relationships and a lack of an appropriate control group and technical issues regarding experimental design confound drawing any firm conclusions. Clear weaknesses of sequencing a limited number of genomic targets across a reduced a pre-screened cohort of samples is a reduction in power to detect associations, but alternative methodologies are either more financially demanding or requires a more complex analysis. Alterations in *KMT2C* and *KMT2D*, though occurring frequently in somatic RCC cases are difficult to assess accurately, given the issues that were encountered in this study, but several rare and potentially damaging variants were identified. No variants in *KMT2C* or *KMT2D* had evidence to suggest pathogenicity but without additional genetic or molecular data further conclusions cannot be made. In all cases, additional confirmation by co-segregation, validation sequencing, or tumour sequencing to assess secondary mutations are required to support that variants in *KMT2D, CDKN2B* or *EPAS1* exon 9 are associated with germline predisposition to RCC.

4.0 Cancer gene sequencing of individuals with features of inherited RCC

4.0.1 Table of contents

4.1 Introduction

Of all diagnosed RCC cases, approximately 3% are familial in nature (98). Molecular genetic studies have identified multiple genetic causes for RCC predisposition. As discussed previously, the best recognised cause of familial RCC is the dominantly inherited familial cancer syndrome von Hippel-Lindau (VHL) disease caused by germline mutations in the *VHL* tumour suppressor gene (99,127). Additionally, inactivating mutations in tumour suppressor genes (TSGs) *BAP1, FH, FLCN, SDHB, SDHD, SDHC, SDHA, PBRM1,* and *CDKN2B,* as well as activating mutations in the *MET* proto-oncogene have been implicated in predisposition to renal cancers (98). A majority of RCC with suspected predisposition do not carry pathogenic variants in known RCC predisposition genes and recent studies suggest between 24-33% of individuals presenting with RCC meet referral criteria for genetic testing (118). Taken together, there is an unidentified genetic component to non-syndromic RCC cases with features of predisposition.

As the previous chapter demonstrated, the rate of variant detection in single gene or exon sequencing is low and as such high throughput sequencing of high priority targets would enable the analyse of multiple genes of interest with reduced labour, at the expense of increased cost, computational, and bioinformatic requirements. While initially cancer-associated genes were described in relation to a single cancer phenotype, a greater number of genes are being associated with several or even a spectrum of cancer predispositions, in both syndromic and non-syndromic cases, such as *BRCA1* in breast, ovarian, and prostate cancers (27,375). Recently, studies in a number of human cancer types have identified pathogenic variants in a wide range of cancer predisposition genes than have been traditionally associated with the cancer of interest, as exemplified by Whitworth *et al* (2018) (376). A hypothesis can be proposed that adopting a wider testing strategy to a cohort of patients with features that might indicate a cancer predisposition gene mutation might improve knowledge of the molecular architecture of inherited RCC.

In order to identify new genetic components associated with renal cancer predisposition, 118 probands presenting with features of non-syndromic inherited RCC with no known pathogenic or likely pathogenic variants in *VHL, MET, FLCN, SDHB, CDKN2B* and *BAP1* were investigated and targeted sequencing was performed using the Illumina TruSight cancer sequencing panel or virtual TruSight cancer sequencing panel on available whole exome sequencing data. The sequencing technology applied in each instance was only because of a shift from targeted panel sequencing to whole exome sequencing as a laboratory standard operating procedure, not a specific experimental design choice.

4.1.1 Aims

- Confirm the lack of pathogenic or likely pathogenic variants in known RCC predisposition genes.
- Identify pathogenic or likely pathogenic variants in genes associated with RCC or other cancers through targeted cancer gene and SNP sequencing.

4.2 Methods

4.2.1 Patients

Patients diagnosed with RCC were assessed for eligibility based on the presence of clinical features associated with inherited RCC, as described in section 2.1.3. Patients were recruited if they matched one of the following criteria 1) Patient had at least one first or second degree relative with RCC 2) Presented with no family history but two or more separate primary RCC before age 60 years, or 3) Presenting with RCC at age 45 years or less (age of diagnosis corresponding to less than 10% of total cases as defined by SEER(377)). Patients with confirmed or likely mutations in *BAP1, FH, FLCN, MET, SDHB* and *VHL* were excluded from the study.

4.2.2 DNA extraction and quantification

DNA extraction from whole blood lymphocytes, quantification and quality control was performed as described in material and methods (section 2.1).

4.2.3 Library preparations and sequencing

Cancer gene panel library preparations were performed as described in materials and methods (section 2.6.2). WES library preparations were performed as described in materials and methods (section 2.6.3) performed by the SMCL sequencing service.

4.2.4 Sequencing bioinformatics

Primary bioinformatics (BCL to VCF) was performed as described in materials and methods (section 2.7) by the SMCL sequencing service. Variants from targeted sequencing panel and exome datasets were called independently and a 'virtual' panel applied to the exome variants via VCFtools, restricting the reported variants to the Cancer gene panel target bed intervals (with an additional 3bp padding)

4.2.5 Variant filtering and prioritisation

Variant filtering, annotation, and prioritisation was performed as described in the materials and methods (section 2.8) including Intervar variant interpretation using ACMG guidelines (325). Targets included in the cancer gene panel are given in appendix section 9.3.1 and were used to filter a virtual variant panel in the WES sequencing samples.

4.2.6 Statistical Analysis

Proportion confidence intervals were calculated using R base function binom.test() at CI 95%, using R (version 3.5). Two-tailed Fishers exact tests and odds ratios were calculated using the ‘oddsratio.fisher()’ function in epitools package (version 0.5-10), using R (version 3.5). Confidence interval for odds ratio calculation was set to 95%.

4.2.7 Sanger sequencing

Primer design and PCR amplicon generation for Sanger sequencing was performed as described in the main materials and methods (section 2.3). Sanger sequencing of variants was performed as described in the main materials and methods (section 2.4). *BRIP1* primer sequences are given in the appendix (section 9.3.2).

4.3 Results

4.3.1 Clinical features

The 118 unrelated individuals with RCC eligible for inclusion were subdivided into three clinical subsets: 44 cases with a positive family history and 74 sporadic cases comprising 30 cases with multifocal or bilateral disease and 44 cases with early onset RCC only). Median age of onset across all cases was 42 years (range 10-74) and 52 years (range 29-74) in the familial cases, 48 years (range 31-72) in multifocal/bilateral cases and 33 years (range 10-46) in early onset cases). Histological subtype was available for 70 of 118 cases (59.3 %) and comprised 68.6% clear cell RCC, 27.1% papillary RCC, and 4.29% chromophobe RCC). Summary of the distribution of clinical features are given in 4.3 Table 1.

4.3 Table 1

Summary of clinical features of individuals with suspected inherited RCC where available

Clinical feature		Value
Sex, Num. (%)		
	Male	71 (60.2)
	Female	47 (39.8)
Age, median (range)		
	All	43 (10-74)
	Familial	52 (29-74)
	Early onset	33 (10-45)
	Bi/Multi	48 (31-74)
Case type, Num. (%)		
	Familial	44 (37.2)
	Early onset	44 (37.2)
	Bi/Multi	30 (25.4)
Family history, Num. (%)		
	1st degree	27 (61.4)
	2nd degree	8 (18.2)
	Unspecified	9 (20.5)
Family history, Num. (%)		
	clear cell RCC	48 (68.6)
	papillary RCC	19 (27.1)
	chromophobe RCC	3 (4.29)
	non-specified RCC	48

4.3.2 Quality control and variant filtering

Quality control checks were performed to assess alignment rates, and depth of coverage and PCR duplicate rates for both cancer gene panel sequenced samples and WES sequenced samples. Read alignment rates a mean of 99.6% (range 92.3 - 99.8%) across all samples, with a mean coverage of 327X (range 226 - 719) (4.3 Figure 1). Quality control metrics for WES samples match those described in chapter 5 section 5.3.2.

A total of 3,817 variants were called in the targeted sequencing set of 100 samples (3,458 SNVs and 359 Indels) and 405 variants were called in region-filtered whole exome data of 18 samples (395 SNVs and 10 Indels). A total of 1,955 and 237 variants passed quality control filtering requirements for depth, QUAL, genotype quality, missingness and internal minor allele frequency for targeted panel and exome derived data, respectively. After filtering for variants occurring within coding regions or splice site consensus sequences, removing synonymous and common variants in 1000 genomes and ExAC datasets (>1%), and additional filters, a total of 264 and 38 variants were retained from the targeted sequencing and virtual panel sets, respectively. For downstream analysis, variants occurring in both sets were merged, consisting of 14 variant genotypes.

Analysis of the variants identified in this set were divided into three subpanels based on the inheritance patterns of the affected genes. 1) Group A genes with a known association with RCC predisposition 2) Group B genes in which heterozygous pathogenic variants are known to be associated with predisposition to multiple non-RCC tumours and 3) Group C genes which are associated with cancer predisposition when there are biallelic pathogenic variants or those which have been associated with a single non-RCC tumour phenotype. In broad terms, the three groups correspond to differing levels of prior probabilities for detecting an association with RCC (lowest in the latter group because non-syndromic RCC is usually inherited in an autosomal dominant manner).

4.3 Figure 1

Quality metrics from cancer gene panel sequencing batches. 1A Read alignment rates across cancer gene panel samples given as percentage of total reads generated per sample. Orange colouration indicates unmapped read proportion. 1B Mean read depth coverage across all cancer gene panel target intervals per sample. Dashed line indicates mean read depth across entire sample set.

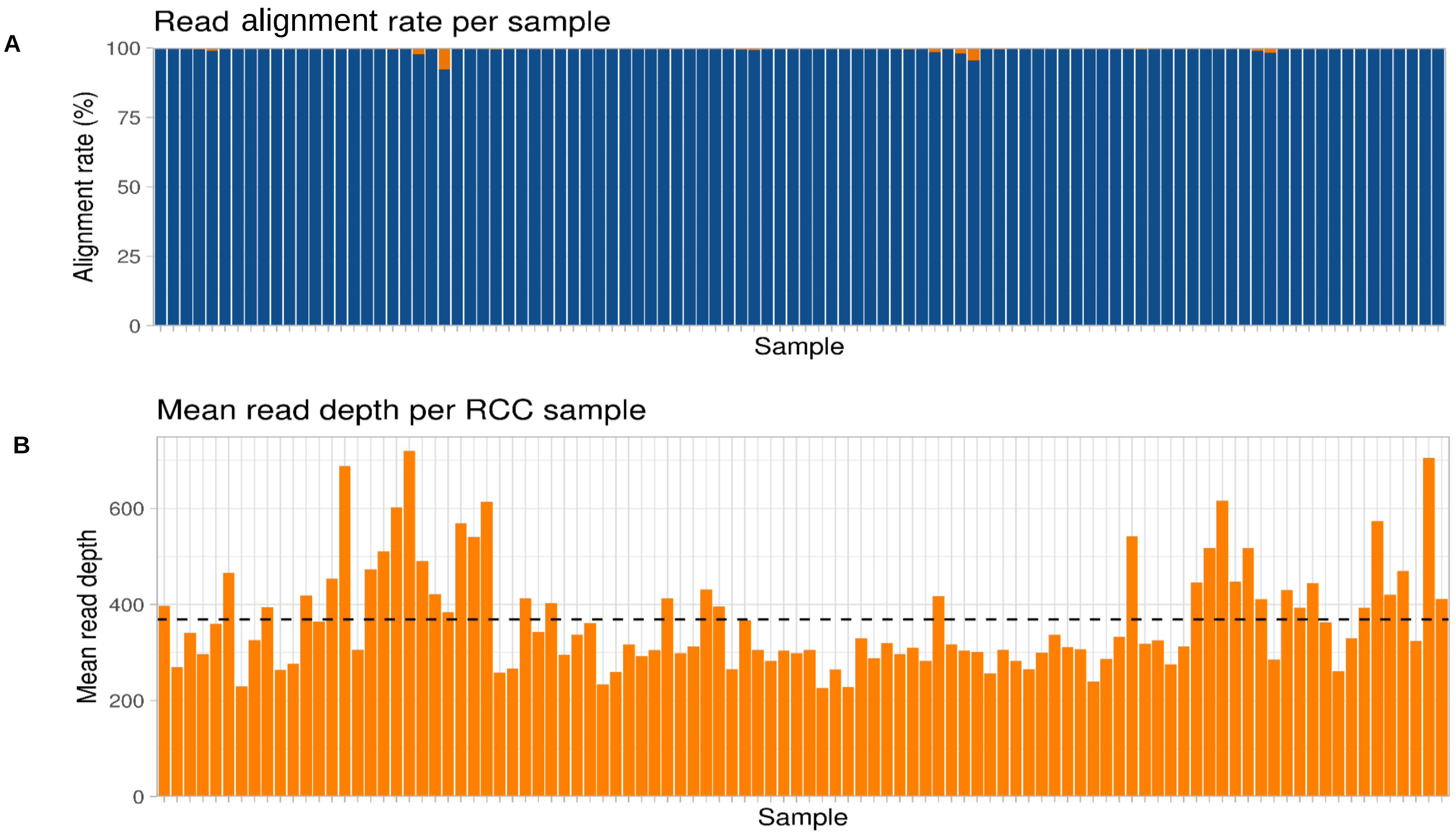

Variants passing filtering and meeting selection criteria were then assessed for pathogenicity using the InterVar tool (326) for automatic generation of ACMG variant classifications. Of the 288 variants assessed, a total of 19 were classified as pathogenic or likely pathogenic (P-LP) variants (5 pathogenic, 14 likely pathogenic), corresponding to 5 nonsense variants, 3 frameshift deletions, 2 frameshift insertions, 8 missense substitutions, and 1 splice site variant. The 19 variants were observed in a total of 21 individuals, giving an identification rate 21/118 (17.8%; 95% CI: 11.4-25.9) across all assessed cases. Pathogenic variants were equally distributed by count across the inherited subtypes (8 variants in familial, 6 variants in early onset, and 7 variants in bilateral/multifocal). All 19 pathogenic/likely pathogenic variants are described in 4.3 Table 2.

4.3.3 Detection variants in Group A cancer predisposition genes

As expected, no P/LP variants were detected in genes that had previously been analysed before inclusion in this study (*VHL, MET, FLCN, SDHB, CDKN2B* or *BAP1) and* only a single gene identified as harbouring a P/LP variant has been previously linked to RCC, either in germline or somatic sequencing. A *MITF* missense variant in (NM_000248: c.952G>A: p.E318K) was identified in an individual who presented with clear cell RCC at age 74 years and whose son was reported to have presented with clear cell RCC at age 53 years. Sequencing in the individual's unaffected brother did not carry the variant and though this variant had been previously associated with predisposition to RCC and melanoma (262), there was no family history of this tumour.

Three variants in *MET* (NM_000245: c.T2543C: p.V848A, NM_000245: c.G1406C: p.R469P, and NM_000245: c.A1336G: p.I446V) were present at allelic frequencies lower than 8.5E-05, with in silico predictions being variable, but none of the variants fall within the tyrosine kinase domain associated with constitutional activation of c-MET (204,208), and none had been reported as somatic events in sporadic RCC based on data from the catalogue of somatic mutations in cancer (COSMIC)(378).

Six missense variants were identified in *TSC2*, associated with tuberous sclerosis complex (MIM: 613254) which predisposes individuals to renal angiomyolipomas and cysts, as well as hybrid or oncocytic RCC in between 2-4% of cases (232,237). Histological information was not available for these individuals to assess if they presented with histologies consistent with loss of *TSC2*. The predicted pathogenicity of these missense variants, as well as the allele rarity, is variable but two variants (NM_000548 c.G4657T: p.G1553C & NM_000548: c.G5117A: p.R1706H) occur within the Rap GTPase activating protein domain implicated in RHEB inhibition (241) and one variant (NM_000548: c.C2476A: p.L826M) arises in a Tuberin-type domain, though its direct function is not known. None of the 6 variants identified in *TSC2* had been reported as somatic events in sporadic RCC in COSMIC.

4.3.4 Detection of variants in Group B cancer predisposition genes

A total of 6 P/LP variants were detected in the 3 genes in which heterozygous pathogenic variants are known to be associated with predisposition to multiple non-RCC tumour types. Two Group B genes, *BRIP1* and *CHEK2*, harboured germline P/LP variants in more than one proband. Three BRIP1 truncating variants (NM_032043: c.1161dupA: p.Gln388Thrfs*7, NM_032043: c.1871C>A: p.Ser624*, and NM_032043: c.2392C>T: p.Arg798*) were identified across four individuals, two of which carried a *BRIP1* p.Ser624* nonsense variant. The four probands consisted of 2 familial cases and 2 multifocal/bilateral cases. Age at diagnosis of RCC was 54, 64, 46, and 39 years and presented with papillary, two non-specified, and clear cell RCC, respectively (see 4.3 Table 3). Affected family members were available for one individual carrying the NM_032043: c.2698G>A: p.Arg798* and an affected second degree relative (clear cell RCC at age 57 years) and also found to harbour the NM_032043: c.2698G>A: p.Arg798* nonsense variant. In total, truncating variants in *BRIP1* were detected in 3.39% (4/118) of sequenced individuals. To compare frequencies to a comparable control set the ICR1000UK control set was aligned identically and was analysed for number of truncating variants. The ICR1000UK control cohort harboured truncating variants in 0.4% (4/999) corresponding to an enrichment of truncating variants in our cases (p=5.92E-03, OR 8.70, 95% CI: 1.60 – 47.4).

Evaluation of rare truncating variants in *BRIP1* compared to gnomAD revealed an estimated at 0.24% (123/51,300 (353); carriers were estimated using median allele number where alternative alleles were presumed to be mutually exclusive) which results in a significant enrichment in the case set (p=2.19E-04, OR 14.6, 95% CI: 3.85 – 39.35). Finally, statistical comparison to data published by Easton *et al* (2016)(379) also demonstrated a statistical enrichment in this series (p=1.21E-04, OR 18.2, 95% CI: 4.55 – 53.1) when compared to truncating variants in *BRIP1* in breast cancer, found at a rate of 0.19% (28/14,526). The *BRIP1* truncating variants were confirmed by Sanger sequencing (4.3 Figure 2).

4.3 Figure 2

Sanger sequencing traces for the *BRIP1* truncating variants identified as P/LP in this series including negative control traces. 2A Bidirectional sequencing of *BRIP1* frameshift insertion p.Gln388Thrfs*7. 2B Unidirectional traces for both individuals with *BRIP1* p.Ser624* nonsense variant. 2C Unidirectional traces for both the proband and affected 2nd degree relative carrying *BRIP1* p.Arg798* nonsense variant.

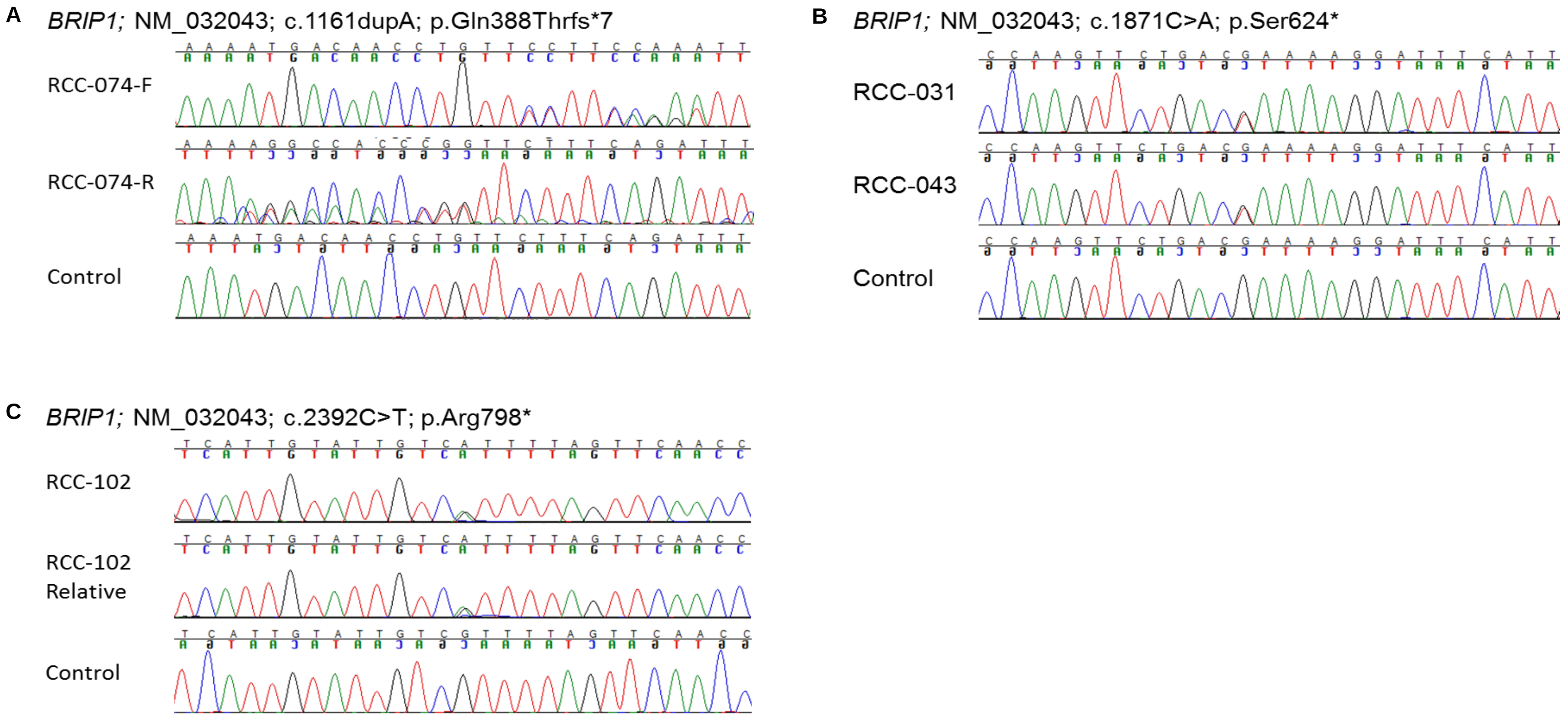

A *BRIP1;* NM_032043; c.1161dupA; p.Gln388Thrfs*7

B *BRIP1;* NM_032043; c.1871C>A; p.Ser624*

C *BRIP1;* NM_032043; c.2392C>T; p.Arg798*

A frameshift deletion in *CHEK2* (NM_007194: c.1263delT: p.Ser422Valfs*15) was identified in two individuals, both of whom presented with multifocal RCC at age 56 years, though the histology was not specified. The frameshift deletion is considered to be pathogenic and has previously been detected in both germline sequencing of breast (380) and prostate cancer (381,382). An additional *CHEK2* missense variant (NM_007194: c.1427C>T: p.Thr476Met) was also identified in one individual classified as likely pathogenic by InterVar (though there have been conflicting reports on ClinVar (VUS=7, LP=10). The variant falls within the protein kinase domain of CHEK2 and in vitro studies demonstrated a loss of kinase activity and loss of DNA repair function (383,384).

Finally, an individual carried a *BRCA1* frameshift deletion in exon15 (NM_007300: c.4563delA: p.Lys1521Asnfs*5) which was novel in ExAC and 1000 genomes, as well as not present in the non-cancer gnomAD data set. The individual presented with early onset papillary RCC at age 40 years.

4.3.5 Detection of variants in Group C cancer predisposition genes

A *PMS2* nonsense variant was identified in three individuals, purported to occur within the 4th amino acid (PMS2: c.11C>G: p.Ser4*) but on review was found only to affect non-canonical isoform 14 (NM_001322015), resulting in an intronic substitution within the canonical isoforms of *PMS2*. A P-LP missense variant in one individual was identified in *PMS2*, occurring within the canonical transcript (NM_000535: c.2066C>T: p.Thr689Ile). The *PMS2* missense substitution occurs within exon 12 resulting in a Threonine to Isoleucine substitution in a c-terminal dimerization domain. The variant occurs as a singleton in the gnomAD data set (353) and is considered to be highly deleterious by multiple in silico predictive tools.

A patient presenting with early onset clear cell RCC at age 39 years harboured a nonsense variant in *FANCE* (NM_021922: c.265C>T: p.Arg89*) within exon 2. The variant was seen only once in the gnomAD data set and due to occurring early in the amino acid sequence presumably leads to loss of the entire protein product but no further functional evidence was available.

Multiple P-LP variants were identified in genes associated with nucleotide excision repair pathways, including *ERCC2*, *XPA*, and *XPC*. Three missense variants were identified in *ERCC2* (NM_000400: c.2084G>A: p.Arg695His, NM_000400: c.1802G>A: p.Arg601Gln, and NM_000400: c.772C>T: p.Arg258Trp). Two of these missense variants were only present as singletons within the non-cancer gnomAD data set (353) (NM_000400: c.2084G>A: p.Arg695His*; AF = 4.22E-06* & NM_000400: c.772C>T: p.Arg258Trp; AF = 4.23E-06), with the remaining variant *ERCC2* (NM_000400: c.1802G>A: p.Arg601Gln) occurring at minor allele frequency of 1.68E-04. All three variants are within conserved functional protein domains, occurring within an ATP-dependent helicase C-terminal domain, P-loop containing nucleoside triphosphate hydrolase & ATP-dependent helicase C-terminal domain, and a DEAD2-type helicase ATP-binding domain, respectively. A nonsense variant in exon 4 of *XPA* (NM_000380: c.464delT: p.Leu155*) and a frameshift deletion in exon 2 of *XPC* (NM_004628: c.219delG: p.Val75Trpfs*4) were also found. Both truncating variants occur early in the reading frames of both genes and are novel variants not seen in the non-cancer Gnomad data set (353).

Genetic overlaps have been demonstrated between RCC and Pheochromocytomas (PCC) and paragangliomas (PGL), with variants in genes such as *VHL*, *SDHB/C/D*, and *FH* predisposing to both tumour types (124,155,215,385). Therefore, analysis of genes associated with PCC/PGLs may uncover new associations. One variant was present in *SDHAF2* and two in *RET* which are associated with predisposition to Phaeochromocytoma (386,387). The *SDHAF2* variant (NM_017841: p.R18G) is within exon 2, is present at a minor allele frequency of 2.8E-05 in gnomAD, and predictive in silico tools suggested it occurred in a conserved amino acid and therefore likely damaging. Two *RET* variants (NM_020975: c.C166A: p.L56M and NM_020975: c.G973A: p.A325T) occurred in one individual each with the first being repeatedly flagged as benign by Clinvar. The latter has conflicting interpretations of pathogenicity on Clinvar but SIFT, PolyPhen and CADD all suggest the variant is not pathogenic in nature, particularly given that RET activating variants are typically clustered in the tyrosine kinase domain (388).

4.3.6 Analysis of variants of uncertain significance

Of the 288 variants passing all quality control and filtering parameters, 134 variants were categorised as variants of uncertain significance (VUS) by ACMG guidelines applied by InterVar. Of these variants 96.3% (129/134) were missense variants, with 3 non-frameshift deletions, 1 nonsense variant, and 1 splice site altering variant composing the remaining percentage. For genes harbouring VUSs, 40.6% carried only a single variant (26/64 genes), with 25.0% (16/64 genes), 14.1% (9/64 genes), and 9.37% (6/64 genes) harbouring two, three and four variants across the sample set, respectively. The remaining genes each carried five or more variants classified as VUS (*CDKN2A* = 13, *ERCC5* = 10, *ALK* = 9, *ATM* = 9, *TSC2* = 6, *ERCC3* = 5 and *ERCC4* = 5). VUS variants were found at a rate of 1.40 per individual (range 0-4). VUS variants occurred less frequently in samples harbouring P-LP variants at 1.05 compared to 1.48 variants per sample, though it did not reach statistical significance (p=0.08; Student's t-test). Comparisons of InterVar-assigned pathogenicity to Clinvar status reported in the VUS variants identified 10 variants in which Clinvar indicates clear lack of pathogenicity, marked as benign or likely benign. Conversely, no variants designated as VUS by InterVar were classified as P-LP variant by Clinvar.

A single missense variant was found in *SMARCB1*, a gene encoding a component of the SWI/SNF complex which contains *PBRM1* (389), which is shown to be altered in papillary RCC (158). The variant is located in the 4th exon (NM_001317946: c.C497G: p.T166S) and appears to be relatively common compared to other VUSs in the set (AF=1.0E-03 nc-gnomAD) and is predicted to be tolerated or benign by all in silico predictive tools.

Several missense VUS variants were present in genes significantly affected in somatic RCC sequencing. The variants include two missense variants in *EGFR* which is amplified in somatic papillary RCC as part of chromosome 7 duplications (274). Neither of the *EGFR* variants fall within functional domains or have evidence to suggest they would result in constitutive activation of the epidermal growth factor receptor. *EGFR* variant p.Pro20Arg (NM_005228: c.C59G: p.P20R) is reported only once in gnomAD but is predicted to be tolerated or benign by in silico predictive tools whereas the second variant (NM_005228: c.G2024A: p.R675Q) is reported more frequently (AF= 2.1E-04) but predicted to be deleterious by in silico predictive tools.

Two additional VUS variants were identified in *TP53* and *CDKN2A*, both of which are described in somatic sequencing. The variant in *TP53* (NM_000546: c.G124A: p.D42N) is present as a singleton in gnomAD and is located in the Cellular tumour antigen p53, transactivation domain 2 region but in silico predictive tools suggest the amino acid change is tolerated. Lastly, a missense variant in *CDKN2A* was present in 13 individuals (NM_000077: c.A221C: p.D74A). While passing all filtering and quality control criteria, the inflated allele count for this variant is anomalous given the size of the cohort sequenced and the expected rarity of causal variants. Review of data regarding this variant suggested that it is present as a sequencing artefact and failed random forest filtering, as part of ExAC (390) and as such this variant was not evaluated further.

Several samples carried non-missense VUS variants across multiple genes. An individual carried both a *BRCA2* non-frameshift deletion and a MSH6 splice site altering variant. The *BRCA2* variant (NM_000059:exon11: c.4142_4144del: p.1381_1382del) has multiple conflicting interpretations of pathogenicity, reported as both likely benign and a VUS. The variant is reported at an allele frequency which conforms with potential pathogenicity (AF=8.E-05) and functional studies have demonstrated a loss of function of the BRCA2 protein (391) but additional Clinvar submissions report co-occurrence with known pathogenic variants reported in breast cancer. The splice site affecting deletion in *MSH6* (NM_000179: c.4001+12_4001+15delACTA) is present in gnomAD at an allelic frequency of 1.2E-03, which is relatively frequent for a pathogenic variant and expert panel review in Clinvar regards it as a true VUS without further evidence to support pathogenic or benign classification.

Two related genes, *FANCL* and *FANCD2*, were shown to be present in one individual each. A non-frameshift deletion in *FANCL* (NM_001114636: c.1022_1024del: p.341_342del) was classified as a VUS but functional studies have demonstrated the variant results in a null allele (392), and subsequent incorporation of this data in ACMG shifts the classification for VUS to likely pathogenic. The *FANCD2* non-frameshift deletion (NM_033084: c.877_885del: p.293_295del) has no published studies regarding its likely effect on protein function but it does result in the loss of 3 amino acids within a region suggested to interact with FANCE and the variant is only present as a singleton in gnomAD. Lastly, an individual carried a nonsense variant in *CEBPA*. *CEBPA* is an intronless gene with a complex series of differential initiation codons, including both ATG and non-ATG start sites. The variant *CEBPA* (NM_001287424: exon1: c.C16T: p.R6X), is only a stop gain in isoform C, resulting in a 5'-UTR variant in other isoforms, making interpretation difficult (393).

4.3 Table 2

*V*ariants identified as pathogenic or likely pathogenic by ACMG guideline classifications assigned by InterVar

GENE	Pos (GRCh38)	rsID	CONSEQUENCE	Transcript (Canonical)	DNA	Exon	AA	Genomad AF	InterVar classification
BRCA1	chr17:43074505	N/a	frameshift deletion	NM_007300	c.4563delA	exon15	p.Lys1521Asnfs*5	NS	Likely pathogenic
BRIP1	chr17:61780325	rs587781321	nonsense	NM_032043	c.1871C>A	exon13	p.Ser624*	1.86E-05	Pathogenic
BRIP1	chr17:61799278	N/a	frameshift insertion	NM_032043	c.1161dupA	exon9	p.Gln388Thrfs*7	NS	Likely pathogenic
BRIP1	chr17:61716051	rs137852986	nonsense	NM_032043	c.2392C>T	exon17	p.Arg798*	1.40E-04	Pathogenic
CHEK2	chr22:28694066	rs142763740	nonsynonymous	NM_007194	c.1427C>T	exon13	p.Thr476Met	3.00E-04	Likely pathogenic
CHEK2	chr22:28695238	rs587780174	frameshift deletion	NM_007194	c.1263delT	exon12	p.Ser422Valfs*15	4.49E-05	Pathogenic
ERCC2	chr19:45352315	rs746618110	nonsynonymous	NM_000400	c.2084G>A	exon22	p.Arg695His	1.19E-05	Likely pathogenic
ERCC2	chr19:45353112	rs140522180	nonsynonymous	NM_000400	c.1802G>A	exon19	p.Arg601Gln	1.81E-04	Likely pathogenic
ERCC2	chr19:45364278	rs767916267	nonsynonymous	NM_000400	c.772C>T	exon9	p.Arg258Trp	4.00E-06	Likely pathogenic
FANCE	chr6:35455763	rs752690798	nonsense	NM_021922	c.265C>T	exon2	p.Arg89*	3.98E-06	Pathogenic
MITF	chr3:69964940	rs149617956	nonsynonymous	NM_000248	c.952G>A	exon9	p.Glu318Lys	1.37E-03	Likely pathogenic
MUTYH	chr1:45331556	rs36053993	nonsynonymous	NM_012222	c.1178G>A	exon13	p.Gly393Asp	3.06E-03	Likely pathogenic
MUTYH	chr1:45332803	rs34612342	nonsynonymous	NM_012222	c.527A>G	exon7	p.Tyr176Cys	1.54E-03	Likely pathogenic
PMS2	chr7:5982932	rs1254554953	nonsynonymous	NM_000535	c.2066C>T	exon12	p.Thr689Ile	4.63E-06	Likely pathogenic
PMS2	chr7:6002670	rs200029834	nonsense	NM_001322015	c.11C>G	exon5	p.Ser4*	2.48E-04	Likely pathogenic
SBDS	chr7:66994210	rs113993993	splice site affecting	NC_000007.13	c.258+2T>C	intron 3	N/a	3.88E-03	Pathogenic
SLX4	chr16:3597655	rs774532876	frameshift insertion	NM_032444	c.1406dupC	exon7	p.Leu470Ilefs*8	3.55E-06	Likely pathogenic
XPA	chr9:97687186	N/a	nonsense	NM_000380	c.464delT	exon4	p.Leu155*	NS	Likely pathogenic
XPC	chr3:14172946	N/a	frameshift deletion	NM_004628	c.219delG	exon2	p.Val75Trpfs*4	NS	Likely pathogenic

4.3 Table 3

RCC samples carrying variants identified as pathogenic or likely pathogenic by ACMG guideline classifications assigned by InterVar.

Variants	Sex	Subtype	Histology	Age	Gene
SBDS:NC_000007.13:c.258+2T>C *XPA*:c.464delT:p.Leu155*	F	Early onset	ccRCC	46	*SBDS* *XPA*
BRCA1:c.4563delA:p.Lys1521Asnfs*5	M	Early onset	pRCC	40	*BRCA1*
CHEK2:c.1263delT:p.Ser422Valfs*15	F	Bi/Multi	nsRCC	56	*CHEK2*
XPC:c.219delG:p.Val75Trpfs*4	M	Familial	pRCC	44	*XPC*
BRIP1:c.1161dupA:p.Gln388Thrfs*7	F	Familial	nsRCC	64	*BRIP1*
SLX4:c.1406dupC:p.Leu470Ilefs*8	F	Early onset	nsRCC	15	*SLX4*
CHEK2:c.1427C>T:p.Thr476Met	M	Familial	nsRCC	58	*CHEK2*
ERCC2:c.2084G>A:p.Arg695His	F	Bi/Multi	ccRCC	40	*ERCC2*
ERCC2:c.1802G>A:p.Arg601Gln	F	Familial	nsRCC	N/A	*ERCC2*
ERCC2:c.772C>T:p.Arg258Trp	F	Bi/Multi	nsRCC	61	*ERCC2*
MITF:c.952G>A:p.Glu318Lys	M	Familial	ccRCC	74	*MITF*
CHEK2:c.1263delT:p.Ser422Valfs*15 *MUTYH*:c.1178G>A:p.Gly393Asp	M	Bi/Multi	nsRCC	56	*CHEK2* *MUTYH*
MUTYH:c.527A>G:p.Tyr176Cys	F	Early onset	nsRCC	45	*MUTYH*
PMS2:c.2066C>T:p.Thr689Ile	M	Early onset	nsRCC	27	*PMS2*
BRIP1:c.1871C>A:p.Ser624*	M	Bi/Multi	nsRCC	46	*BRIP1*
FANCE:c.265C>T:p.Arg89*	M	Early onset	nsRCC	N/A	*FANCE*
PMS2:c.11C>G:p.Ser4*	M	Familial	nsRCC	38	*PMS2*
BRIP1:c.1871C>A:p.Ser624*	M	Bi/Multi	pRCC	54	*BRIP1*
PMS2:c.11C>G:p.Ser4*	F	Familial	ccRCC	47	*PMS2*
PMS2:c.11C>G:p.Ser4*	F	Early onset	nsRCC	34	*PMS2*
BRIP1:c.2392C>T:p.Arg798*	M	Familial	ccRCC	39	*BRIP1*

4.4 Discussion

In many centres, individuals presenting with confirmed or indicative features of inherited RCC are screened for pathogenic germline variants in a panel of RCC-predisposing syndrome genes that will typically include *VHL*, *MET*, *FLCN*, *FH*, and *SDHB* and more recent studies have identified further genes associate with RCC predisposition (*SDHC*, *SDHA*, *BAP1*, and *PBRM1*). Despite this, many individuals undergoing screening harbour no causative variant in known predisposition genes suggesting an undiscovered proportion of heritability for RCC.

Here, a targeted cancer gene sequencing panel, including 94 genes and 284 cancer-related SNPs, was used to assess the presence of pathogenic or likely pathogenic variants in individuals with either early onset, familial history, or multiple focal / bilateral presentation of RCC. At least one pathogenic or likely pathogenic variant was identified in 21 of 118 patient (17.8%), as classified by InterVar using the ACMG guidelines (325) including truncating variants in *CHEK2*, *BRIP1*, and *BRCA1*. The results reported here conform with recent assessments of clinically relevant pathogenic variants in cancer genes in multiple primary tumour cases which identified a comparable number of variants (15.2%), in which 42% of those variants did not occur in genes which correlate with the presenting cancer (376).

CHEK2 and *BRCA1* variants have been reported in RCC cases previously but no known association has been established between pathogenic variants in these genes and RCC predisposition. Single cases have reported pathogenic *BRCA1* variants (394) and recent results in a Chinese cohort of early onset sporadic cases also identified pathogenic variants in *BRCA1* (395). In difference to this study, the rate of pathogenic variant detection was only 9.5% though this may be due to a reduced scope, in terms of genes assessed, and inclusion of known RCC predisposing genes.

CHEK2 has been reported as being a multi-cancer susceptibility gene, with variants predisposing to a number of different cancers, including RCC, (396,397) but most strongly associated with breast cancer (398), though neither of the affected individuals carrying the *CHEK2* variants had a family history of breast cancer. Interpretation of either *BRCA1* or *CHEK2* variants is difficult and should be assessed conservatively. The lack of demonstrable enrichment of *CHEK2* and *BRCA1* variants does not support the involvement of these genes in RCC predisposition. In particular, the assessment of *BRCA1* and *BRCA2* mutations in have been demonstrated to drive tumourigenesis in *BRCA*-associated cancer lineages but biologically neutral in non-*BRCA* tumour lineages (399).

The occurrence of *BRIP1* rare truncating variants in this series is an interesting finding given that inactivating variants in *BRIP1* are not currently associated with RCC but have been previously implicated in predisposition to ovarian (400) and breast cancer (401), though more recent studies have questioned the legitimacy of the association with breast cancer predisposition (379,402). The data reported here suggests an association between rare *BRIP1* truncating variants, being statistically enriched compared to control and disease datasets, and segregating with affected family members in one pedigree. Equally, this finding should be interpreted cautiously given the limited statistical power and series size and further validation and follow-up in similarly screened independent cohorts would be needed to confirm the association. Interestingly, recent publications demonstrated no association between breast cancer and *BRIP1* truncations (379) and in comparison to the studies described in the aforementioned publication, *BRIP1* truncations were statistically enriched in our series, but again restrained interpretation is necessary.

As with previous studies, the assessment of VUS variants continues to be a challenging endeavour. Population minor allele frequencies and in silico predictive tools may aid prediction of pathogenicity but are not robust enough to reliably state whether a VUS is of consequence. For variants such as the *FANCL* (NM_001114636: c.1022_1024del: p.341_342del) in-frame deletion identified, pathogenicity may be ascertained from analysis of functional studies but this is unruly for all identified variants and most do not have any additional supporting information to inform classification. Variants in genes related to PCC (*SDHAF2* and *RET*) and variants in *TSC2* are potentially interesting candidates for further assessment given the genotypic overlaps between PCC/PGLs and RCC and the occurrence of RCC in Tubular sclerosis complex (232), caused by inactivating variants in *TSC1* and *TSC2* (403), but most are categorised as benign and functional studies would be needed to confirm loss of function in those with unknown consequences. The nonsense variant in *CEBPA* (NM_001287424: c.C16T: p.R6X) may also be an interesting candidate given its related function to the SWI/SNF complex (404), multiple components of which are mutated somatically in RCC and includes *PBRM1* which is already associated with RCC predisposition (331).

Further limitations of the experimental design utilised in this chapter include the systematic differences in sequencing sensitivity for the detection of variants, inclusion of individuals with non-white British/Caucasian ethnographic backgrounds, and estimated tolerance to truncating variants seen for *BRIP1*. Targeted panel sequencing had mean number of variants per sample of 38.2, whereas variants generated from whole exome sequencing carried 22.5 variants per sample. For all intents and purposes, sequencing methodology and bioinformatic processing for both targeted sequencing and whole exome sequencing datasets are equivalent, utilising the same hybridisation probes and whole exome data limited to genomic regions defined by targeted sequencing loci. As such the primary differentiating factor is the read depth coverage for each methodology; Targeted sequencing had a mean read depth across all samples of 327X coverage in comparison to 120X coverage for exome samples and differing variant calling sensitivity may contribute to the difference detection rates seen between targeted and exome sequencing datasets. This is particularly important given the statistical comparison between the variants identified in this chapter to control datasets generated from whole exome sequencing data.

A further limitation is ethnographic backgrounds in this chapter were not elucidated and statistical comparisons of genotype rates between non-concordant ethnic groups can lead to confounding results due to geography-specific genotypes and allele frequencies. In this instance, prior knowledge from further analysis of exome data analysed in chapter 5 negate this limitation, as all of the identified pathogenic variants occurred in individuals of European (non-Finnish) decent, but this is an important caveat to consider had this study been performed in isolation.

Lastly, assessment of the likely impact of pathogenicity of truncating variants identified within *BRIP1* is potentially a limitation on the conclusions that can be drawn from an enrichment of truncating variants in *BRIP1*. Computational assessment of *BRIP1* and its tolerance for truncating variants (propensity to negatively select truncating variants) is that *BRIP1* is highly tolerant of truncating variants, suggesting that any given truncating variant in *BRIP1* is unlikely to result in a phenotypic change (pLI = 0) (321). Conversely, caution should be taken when assessing tolerance to inactivating variants across an entire gene loci, as specific residues or features can carry greater or less tolerance for alterations than the gene region as a whole, as exemplified by assessment of constrained regions across the genome (405).

This assessment of pathogenic or likely pathogenic variants in inherited RCC also highlights the current limitations of automated pipelines for the application of ACMG guidelines. With a number of VUS variants being known benign variants through ClinVar consensus and misclassification of a variant classified as VUS to likely pathogenic (*FANCL*: NM_001114636: c.1022_1024del: p.341_342del) due to published functional studies (392). Discordance within ClinVar is already well noted (406) and without proper integration of both in silico metrics, population minor allele frequency, known functional studies, and consensus interpretations by other labs then annotation by automated pipelines without robust downstream manual assessment will only compound the issue.

4.5 Conclusion

In conclusion, the targeted next generation sequencing of a series of cancer related genes and risk SNPs using a pre-built cancer gene panel has uncovered a series of pathogenic and likely pathogenic variants in a range of genes associated with both the monoallelic and biallelic predisposition. Assessment of pathogenicity is challenging, particularly for VUS variants, without functional follow up and additional evidence but familial segregation and statistical enrichment of truncating variants in *BRIP1* may suggest a new association between individuals with pathogenic truncating variants in *BRIP1* and RCC predisposition, though additional validation studies would be beneficial to corroborate the evidence provided here. Designing of high-throughput functional analyses of identified variants, such as effects on DNA repair function by variants in DNA repair-related genes. Furthermore, large-scale population wide sequencing cohorts (such as Genomics England 100K genomes) will greatly increase the ability to improve confidence in potentially pathogenic variants by excluding pathogenicity based on population frequency.

5.0 Germline whole exome sequencing of individuals with features of inherited renal cell carcinoma

5.0.1 Table of contents

5.1 Introduction

Investigations into the missing heritability seen in RCC have largely involved familial co-segregation studies or targeted sequencing of known RCC associated genes and while whole exome sequencing (WES) methods can be analytically more complex due to increased genomic coverage, that same coverage can be leveraged to investigate the entire coding region and perform analyses which are impractical in targeted sequencing panels. Utilising a subset of samples investigated in Chapter 4 (see section 2.1.3), WES was performed to investigate novel causes of RCC predisposition across all coding regions and exploit multiple modes of analysis to discover unreported variants and mechanisms associated inherited RCC.

5.1.1 Single nucleotide variant analysis

As performed with the cancer gene panel sequencing study (chapter 4), detection of rare pathogenic variants across all individuals is a first route of investigation in uncovering new associations with RCC predisposition. Analysis in this set will attempt to utilise multiple gene clusters to narrow down and isolate potentially causal variants while effectively removing the vast number of non-pathogenic variants carried in all individuals. Variant analysis will focus on 3 gene clusters; genes altered somatically in RCC (after exclusion of known RCC predisposition genes), genes encoding complex components of the tricarboxylic acid (TCA) cycle due to links with HLRCC and succinate dehydrogenase deficient RCC (SDH-RCC), as well as phaeochromocytomas (PCC) and paragangliomas (PGL) (155,212,214), and variant analysis of ultra-rare (AF < 0.001) truncating variants (nonsense, frameshift deletions/insertions, or splice-site affecting) to determine if any novel genes harbour variants which are most likely to be pathogenic compared to more frequent truncating alterations. An allele frequency of 0.001 was selected as most individuals harbour, on average, 90-100 truncating variants but most occur at non-pathogenic allele frequencies greater than 0.005 in the general population (390). This methodology allows for a robust analysis of candidate variants in relevant genes whilst maintaining a systematic and repeatable approach to variant detection.

5.1.2 Copy number detection

While a large proportion of genetic variation is attributable to single base variants, small or single base insertions and deletions, there is an array of other genomic alterations that can result in a disease phenotype. Cytogenetic or sub-microscopic insertions and deletions, chromosome translocations and inversions, and copy number alterations all contribute to genetic variance within a genome to varying degrees, some of which are pathogenic in nature. Typically, structural and copy number alterations are detected and captured through means other than NGS-based sequencing platforms, such as comparative genomic hybridisation arrays, due to NGS-based methods having restrictive capture/target regions (i.e. whole exome sequencing or panel sequencing). Whilst many of these alterations can be detected from whole genome sequencing with high specificity and sensitivity, the prohibitive cost of whole genome sequencing and lower sequencing coverage in comparison to targeted approaches makes this approach challenging. While whole exome sequencing is restrictive in terms of genomic regions available to interrogate, many algorithms have been designed to attempt to utilise and leverage the read depth and single nucleotide variant information from this data to predict and make copy number variation (CNV) calls across targeted regions. XHMM was chosen as the CNV detection tool of choice based on various metrics and data availability, including portability, detection rates, and control requirements as reviewed by Tan *et al* (2014) (407). Copy number alteration detection in this series may uncover unreported losses or gains in both genes known to be associated with RCC predisposition or novel genes in which an association with inherited RCC has yet to be established.

5.1.3 Gene burden analysis

With exome-wide sequencing, the amount of alleles genotyped allows for the opportunity to perform relatively robust case-control analysis to identify loci which are statistically associated with cases (in this instance individuals with features of inherited RCC) compared to a control set of healthy individuals. In addition to inferring statistical associations, statistical testing provides an unbiased framework for candidate variant detection without a need for gene lists and complex interpretation of *in silico* predictive metrics and biological relevance.

Typically, association studies are performed on a genotype scale where individual variants are compared by frequency between cases and controls, particularly in genome-wide association studies (GWAS) which focus on common SNPs conferring a low risk for the case phenotype. For rare disease, genotype-genotype comparisons are often not effective due to low sample numbers and, in the case of WES, poor coverage of non-coding variant sites. More recent approaches to overcome these limitations in rare disease is the development of collapsing or clustered statistical ‘burden’ testing, in which rare variants are assessed over specified genomic features or loci (e.g. genes, pathways) to determine the presence of statistical enrichment (i.e. genetic burden) in comparison to control sets, increasing the potential statistical power to detect an association.

Many bioinformatic tools and statistical models have been developed to perform these analyses such as Combined Minor Allele test (CMAT) (408) and Combined Multivariate and Collapsing test (CMC) (409) which collapse genotypes over a genomic loci into a single ‘score’, or more complex models such as statistical kernel association test (SKAT) (310) which function to identify over-dispersion in the calculated variance across a given genomic region. Lastly, statistical models have been developed which combine the two approaches and include variant weighting (typically by minor allele frequency) to improve modelling in assessing potential gene mutational burden, including tests such as the optimal statistical kernel association test (SKAT-O) (410), as reviewed by Lee *et al* (2014) (411).

Gene burden has been effectively used to identify increased occurrences of rare variants in specific genes in both non-cancer syndromes (412,413) and germline cancer predisposition cases (414) and may prove useful in the identification of novel genes in RCC predisposition which harbour a greater mutational burden compared to healthy controls. In this study, the SKAT-O combined gene burden and variance test was selected due to having greater statistical power when assessing variant sets where causal direction of a given variant is unknown and a low proportion of variant are presumed to be causal, though the SKAT-O test is less statistically powerful than either burden or variance-based tests independently.

5.1.4 Additional detection methods

While not conventionally considered as causes of genetic disorders, particularly in cancer predisposition syndromes, the role of mobile genetic elements (i.e. transposons) and short tandem repeat expansions are rarely explored in germline sequencing for their potential involvement in the disruption of genes associated with cancer predisposition.

Transposons are mobile DNA sequences which are capable of 'jumping' between different genetic loci and form a substantial proportion of the human genome (415). Due to the mobile nature of transposons, movement of a transposon into a coding region, exonic or intronic, can result in a disease phenotype as seen in haemophilia A (416), retinitis pigmentosis (417), and cancer predisposition (418) by disrupting the coding region, affecting exon splicing, or interfering with promotor regions upstream of transcription start sites (419). Recent bioinformatics tools, such as mobile element locator tool (MELT) (420), allow for the detection of common classes of transposons in WES data based on reference positions and subsequent mismapping of reads to mobile elements which have reinserted themselves into different genomic loci.

Short tandem repeats are present throughout the human genome (421) and expansion of these repeat motifs has been associated with multiple genetic diseases such as myotonic dystrophy type 2 (422), myoclonic epilepsy (423), and Huntingdon's disease (424). Only a small number of studies have linked germline short tandem repeat expansions to cancer predisposition or gene regulation (425), but disruption of intronic or exonic regions by motif expansion or contraction could lead to altered gene function. Tools aimed at leveraging short read data have been developed to model and estimate known short tandem repeats, such as gangSTR (426), and detect expansion or contractions compared to reference repeat numbers.

5.1.5 Aims

- Identify germline alterations in genes associated with somatic alterations in RCC, genes associated with TCA cycle, and investigate rare truncating variants as a cause of RCC predisposition.
- Use a hypothesis-free statistical approach to identify potential associations in both genes and pathways in order to determine potential causes of RCC predisposition.
- Explore underutilised methods of WES data analysis to identify novel causes of RCC predisposition caused by copy number alterations, mobile element insertions, and repeat expansion changes.

5.2 Materials and methods

5.2.1 Patients

Samples included as part of this study were selected as a subset of the samples analysed in chapter 4 and as such were selected for the same clinical features as previously described; Patients were recruited if they matched one of the following criteria 1) Patient had at least one first or second degree relative with RCC 2) Presented with no family history but two or more separate primary RCC before age 60 years, or 3) Presenting with RCC at age 45 years or less. Patients with confirmed or likely mutations in *BAP1, FH, FLCN, MET, SDHB* and *VHL* were excluded from the study. The subset of samples from the primary cohort is described in section 2.13, where patients with clinically relevant variants from Chapter 4 were excluded.

5.2.2 DNA extraction and quantification

DNA extraction from whole blood lymphocytes, quantification and quality control was performed as described in material and methods (section 2.1).

5.2.3 Library preparations and sequencing

WES library preparations were performed as described in materials and methods (section 2.6.3) performed by the SMCL sequencing service.

5.2.4 Sequencing bioinformatics

Primary bioinformatics (BCL to VCF) was performed as described in materials and methods (section 2.7) by the SMCL sequencing service.

5.2.5 Variant filtering and prioritisation

Variant filtering, annotation, and prioritisation was performed as described in the materials and methods (section 2.8) including Intervar variant interpretation using ACMG guidelines (325). Gene lists were curated as follows; gene lists for TCA cycle genes were obtained from Reactome pathway data (427). Genes frequently altered somatically in RCC tumours were selected from genes with alterations occurring at a rate of 3% or greater within the TCGA provisional sample sets for clear cell RCC, papillary RCC, and chromophobe RCC (25). The list was then assessed by NCG (version 6.0) (428) and false positive genes, as flagged by Bailey *et al* (2018) (429), were removed as well as known RCC predisposing genes retaining 41 genes (see appendix 9.4.1). Analysis of all known coding genes was excluded as a SNV investigatory route due to a large proportion of uninformative gene annotations for many genes.

5.2.6 Copy number variation detection

Copy number alterations were detected from BAM file read depth discrepancies identified utilising XHMM (430) across WES aligned and sorted BAM files. Additional WES BAM files from other read depth matched (mean depth within 1 Standard deviation) were jointly called to improve call rate and identification of common CNVs. CNV calling utilising a modified version of the analysis pipeline was also performed on all ICR birth control cohort cases to generate a reference set of commonly called CNVs (Allele frequency > 0.05) to filter experimental data against. Default CNV calls were modified to provide exon-level copy number calls and calls were filtered based on frequency (allele frequency < 0.01) and Q_some quality (Q_some > 60), as described in the XHMM documentation (430).

CNV pipeline calibration was performed against a subset of samples sequenced as part of the HapMap / 1000 genomes project with both comparative genomic hybridisation array-based copy number calls and WES data (431) (Sample list provided in appendix section 9.4.2). The primary script used to run CNV calling with XHMM, xhmm_CNV.sh, is provided in the appendix section 9.4.3a. Additional scripts, including pre-processing steps to generate reference files and parameter files, annotation steps, and plotting is described in appendix section 9.4.3b. HapMap WES data was downloaded in FASTQ format from EBI (ftp://ftp.1000genomes.ebi.ac.uk/vol1/ftp/) and aligned to GRCh38 as described in materials and methods (section 2.7), after which the CNV pipeline described herein was run across all HapMap WES BAM files.

Due to the data format of the HapMap calibration set additional pre-processing was required prior to CNV analysis. HapMap CNV array data was downloaded from ftp://ftp.ncbi.nlm.nih.gov/hapmap and remapped to GRCh38 from hg18 using NCBI remap service, discarding calls that failed to map to GRCh38. HapMap CNV array genotypes were called bi-allelically and as such genotypes were merged to match the mono-allelic calls provided by XHMM (e.g. -2 to 2 to -1 to 1). Genomic positions were merged based on overlapping loci and unique intervals were retained. HapMap CNV data was intersected with the genomic exome probe intervals as provided by Illumina to select only CNVs overlapping with regions sequenced by WES by 5% or more. Intersected WES targets were then filtered to remove regions with only reference or missing calls and the data was coerced into a pseudo-XHMM output format for comparison.

5.2.7 Population stratification and sample concordance

Sample population structure and genetic background were calculated and assigned from ADMIXTURE software (432) modelling, which allows for a higher resolution decomposition of genetic ethnic background. Case variants were merged with high quality genotypes from the 1000 Genomes data set which was used as the training set. Genotypes were pruned and separated by a minimum of 2000 bp to reduced linkage effects, selecting only bi-allelic sites present in a minimum of 2 samples, and restricted to autosomal chromosomes. Further restrictions for minor allele frequency (MAF > 0.05) and missingness per site (missingness < 5%) were subsequently applied. ADMIXTURE algorithm was designated k = 5, corresponding to the number of population groups to assign, which is equivalent to 1000 Genomes super population groups (320). Population structure scripts, including plotting scripts are provided in the appendix (section 9.4.4). For samples in which both WES and cancer gene sequencing had been performed, genotype concordance was performed to assess if WES data adequately captured the same genotype information as the previously sequenced cancer gene panel. The tool bcftools gtcheck (version 1.8) was used to compare genotype calls across the pan-cancer gene panel targets (see chapter 4.2) to determine if sequencing between WES and cancer gene panel sequencing were in concordance.

5.2.8 Burden analysis

Genomic region burden analysis was performed across all genes containing genetic variants utilising sequence kernel association testing (SKAT) R package (version 1.3.2.1), as described by Wu *et al* (310) utilising allele frequency as the weighting criteria after logistic weight conversion with the “optimal” implementation. Principle components (PC) 1 and PC2 were generated using the same variant pruning and filtering as discussed in 5.2.7 for ADMIXTURE analysis and were used as covariates in the regression model. Cases in this series were joint called using GATK Unified Genotyper (see materials and methods section 2.7) with control samples from the ICR UK 1000 birth control cohort (433). Given that population structures in both sets should be of non-Finnish western European origin PCA components PC1, PC2 and PC3 were used as sample exclusion criteria for outliers falling outside of the primary PCA cluster (see section 5.3.9).

Joint called genotypes were filtered for variant consequence type, minor allele frequency (applied independently to both cases, controls and both sets to reduce the interference of batch effects and sequencing artefacts), minor allele frequency compared to the ExAC data set (390), genotype quality, site QUAL, and missingness. Several iterative analyses were performed utilising differing filtering and covariate combinations and burden testing results were assessed based on minimum achievable p-value (MAP) adjusted Q-Q plot distributions to determine the best performing test, where MAP values are generated during resampling of the burden input data as described by Lee *et al* (2016) (434). Q-Q plots are frequently used as a metric of goodness of fit for association tests, principally in GWAS studies (435), to determine if inflation of significance levels is presence between the observed p values versus the theoretical p value quantiles and observe confounding features such as population stratification. Filtering parameters and covariates for the optimised parameters are described in 5.2 Table 1.

Results were corrected for multiple testing using false discovery rate adjustment (FDR) and genes meeting significance thresholds, either p-value or corrected p-values where specified in the text, were assessed for gene ontology and pathway enrichment using WebGestalt (436), Gene Ontology/Panther analysis (Panther GO-slim biological process set; fishers exact method) (437), and Reactome (427) in order to detect biological function or pathway enrichment in genes with significant genetic burden compared to controls. Full burden testing script is provided in appendix section 9.4.5. Additional comparisons were made to Network of Cancer Genes database set to assess the proportion of genes identified as known or candidate cancer genes (428).

5.2 Table 1

Table of optimised parameters used for gene burden association testing including filtering values and included covariates. PC1 = principal component 1. PC2 = principal component.

Metric		Value
Minor allele frequency (AF < value)		
	Global (ExAC)	0.0025
	Internal (Both)	0.05
	Internal (case)	0.2
	Internal (control)	0.2
Site metrics (Metric > value)		
	Genotype quality	30
	Read depth	15
	QUAL	100
	Non-missing	0.9
Consequences included		
frameshift deletions nonsense frameshift insertions splice site variants missense variants		
Covariates included		
	PC1	✓
	PC2	✓

5.2.9 Short tandem repeat detection

Detection of short tandem repeats was performed using the GRCh38 BAM files with GangSTR (version 1.4) using the default parameters as described by Mousavi *et al* (2018)(426), with only adjustments made for non-uniform coverage. Repeat expansion calls were filtered for read depth (DP > 10) and Quality metric 'Q' (Q > 3). Calls were annotated by gene region and only calls falling within known RCC predisposing genes and novel genes identified in this thesis were analysed (see appendix 9.4.1).

5.2.10 Mobile element insertion detection

Mobile element insertions were detected using the mobile element locator tool (MELT; version 2.1.5) across all BAM files to determine the presence of non-reference mobile element insertions into coding regions. Analysis was performed against LINE1, ALU, HERVK, and SVA mobile element reference sets for GRCh38. Variant calls were filtered by "PASS" status and split read support > 2. Calls for mobile insertion types were merged into a single VCF file and filtered against known RCC predisposing genes and novel genes identified in this thesis (see appendix 9.4.1).

5.2.11 Statistical methods

Q values (FDR corrected p values) after SKAT-O burden analysis were generated using p.adjust() function with method "fdr" in base R (version 3.5). Fishers exact test was performed using the fishers.test() function in base R (version 3.5). Chi-squared test was performed using function chisq.test()in base R (version 3.5).

5.3 Results

5.3.1 Clinical features

A total of 72 unrelated individuals matching the selection criteria for RCC predisposition and were grouped clinically as follows: 33 cases with a family history and 39 cases with either early onset or bilateral/multifocal disease (23 and 16 cases, respectively). Median age of onset across all cases was 41 years (range 23-74). Median age of onset in familial cases was 51 years (range 24-74), 48 years (range 31-60) in multifocal/bilateral cases and 34 years (range 23-46) in early onset cases only cases.

Histological subtype was available for 36 of 72 cases (50%) and comprised 25 (69.4%) clear cell RCC, 8 (22.2%) papillary RCC and 3 (8.3%) chromophobe RCC, approximately consistent with previous assessments of histological frequencies. RCC presentation by sex was consistent with sporadic and heritable cases across all individuals and subgroups (male to female ratio 1.5-2.2) except for early onset which had significantly different distribution (male to female ratio 0.92; fishers exact p=0.004). Summary of the distribution of clinical features are given in 5.3 Table 2.

Population structure analysis by admixture demonstrated that 66/72 individuals were of European origin, with the remaining population being African (1/72), East Asian (1/72), and European-south Asian (4/72) by admixture proportions (see 5.3 Figure 1).

5.3 Table 2

Table of clinical features associated with the case series in this chapter. Percentages are calculated based on the entire cohort apart from histologies. Percentages for ccRCC, pRCC, and chRCC are calculated excluding nsRCC cases.

Feature		Number
Age, Median (range)		
	All	41 (23-74)
	Familial	51 (24-74)
	Early onset	34 (23-46)
	Bi/Multi	48 (31-60)
Histology, Number (%)		
	nsRCC	36 (50.0%)
	pRCC	8 (22.2%)
	ccRCC	25 (69.4%)
	chRCC	3 (8.33%)
Sex, Number (%)		
	M	44 (61.1%)
	F	28 (38.9%)
Type, Number (%)		
	Familial	33 (45.8%)
	Early onset	23 (31.9%)
	Bi/Multi	16 (22.2%)
Family history, Num. (%)		
	1st degree	21 (63.6)
	2nd degree	5 (15.2)
	Unspecified	7 (21.2)

5.3 Figure 1

Graph visualising the genetic admixture of samples within the cases attributed to 5 sub groupings with equivalence to the 1000 genomes super population groupings (European, African, East Asian, South Asian, and American). Coloured proportions represent the genetic proportion to which an individual sample is attributed (e.g. entirely red indicates close to, if not completely European genetic origin). The right hand side of the plot demonstrates 6 individuals with either mixed or non-European ethnographic backgrounds.

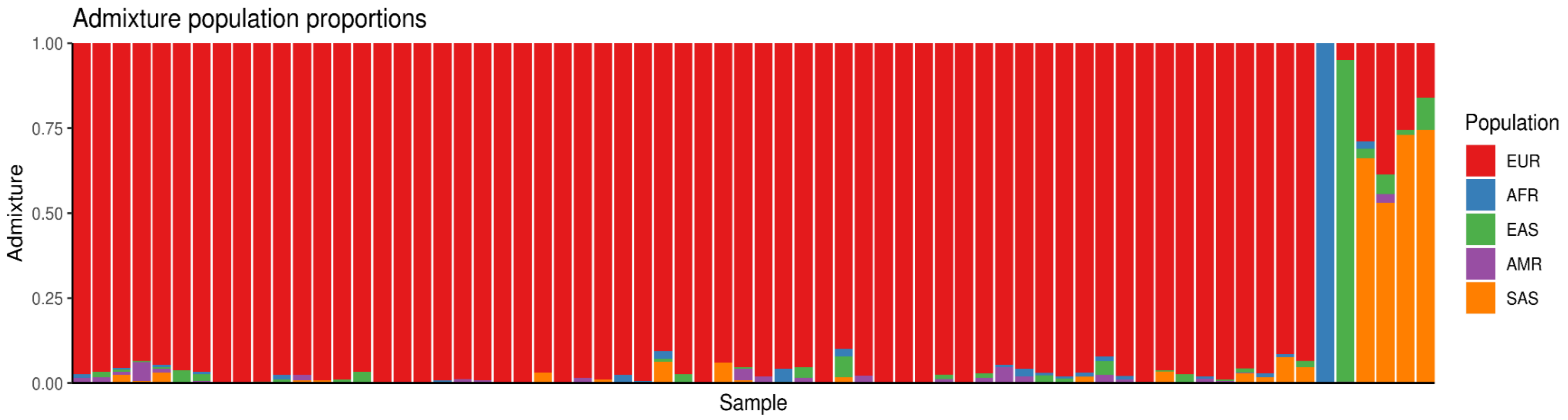

5.3.2 Quality control and variant filtering

Given the number of variants identified by whole exome sequencing, stringent and appropriate variant filtering criteria are required, as well as appropriate quality control metrics for read alignment, read depth, and variant calls. Read alignment rates a mean of 99.81% across all samples, with a mean coverage of 120X. PCR duplicates across all samples were present at a mean rate of 13.7% (range 7.2-30.2%) (5.3 Figure 2-3).

Comparisons for genotype discordance between samples sequenced on both the pan-cancer gene sequencing panel and WES was available for 75.0% (54/72) of sequenced cases, of which no samples demonstrated genotype discordance between the two sequencing data sets. The remaining proportion had WES data but not pan-cancer sequencing panel data available.

Variant calling was performed and resulted in 337,021 variant calls (304,231 SNVs and 32,790 indels) including 12,704 multi-allelic sites with a resulting transition/transversion (Ts/Tv) ratio of 2.23. After filtering for variant quality metrics (read depth, QUAL, genotype quality, missingness and minor allele frequency), as described in the materials and methods section, and left alignment and normalisation the number of variants retained was 194,367 (175,756 SNVs and 18,611 indels), demonstrating an increased Ts/Tv ratio of 2.43. Indel size distributions, and variant substitution types are shown in 5.3 Figure 4.

Variant filtering, as described in materials and methods (section 2.8) removed 113,663 variants occurring in intergenic regions, intronic regions more than 2 bp from splice site consensus sequences, and a further 34,445 variants which resulted in synonymous amino acid changes. Variants were filtered for global minor allele frequency in both 1000 genomes and ExAC to exclude sites present above 1%, resulting in 25,022 rare protein affecting variants being retained. Allelic depth was assessed and variants with insufficient alternative allele depth (AD < 0.3) in at least one sample per site were removed, reducing the final number of filtered sites to 22,384. Variants identified as part of chapter 4 were excluded from reported variants but included in variant counts and association testing.

5.3 Figure 2

Plot of mean read coverage calculated for all probe targets used in the WES library. Bars represent individual samples and mean read depth is given on the y-axis. Dashed line indicates the cohort-wide mean read depth.

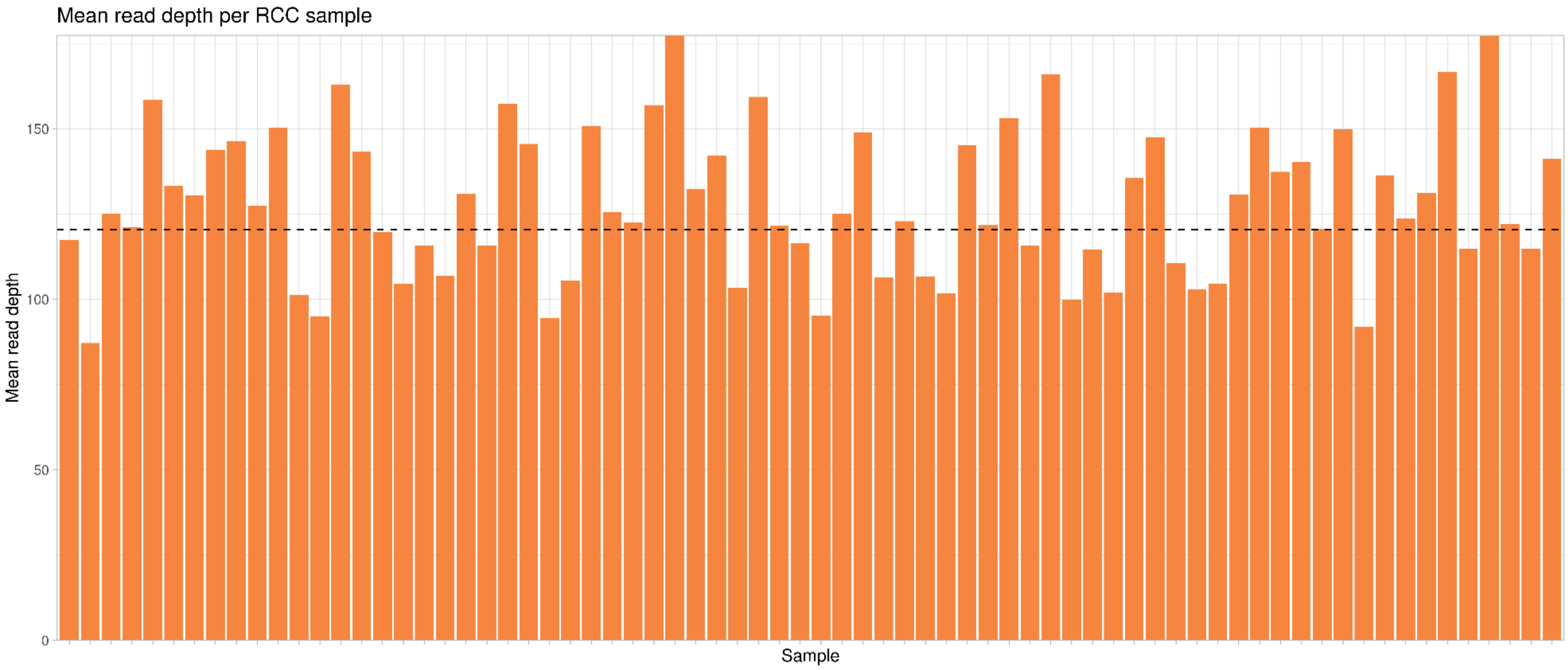

5.3 Figure 3

Plot of PCR duplicate rates occurring in WES library preparation per individual. Blue colouration represents the proportion of reads not assigned as PCR duplicate reads and orange represents reads which were marked as PCR duplicates. Relative proportions are given as a percentage of total number of reads.

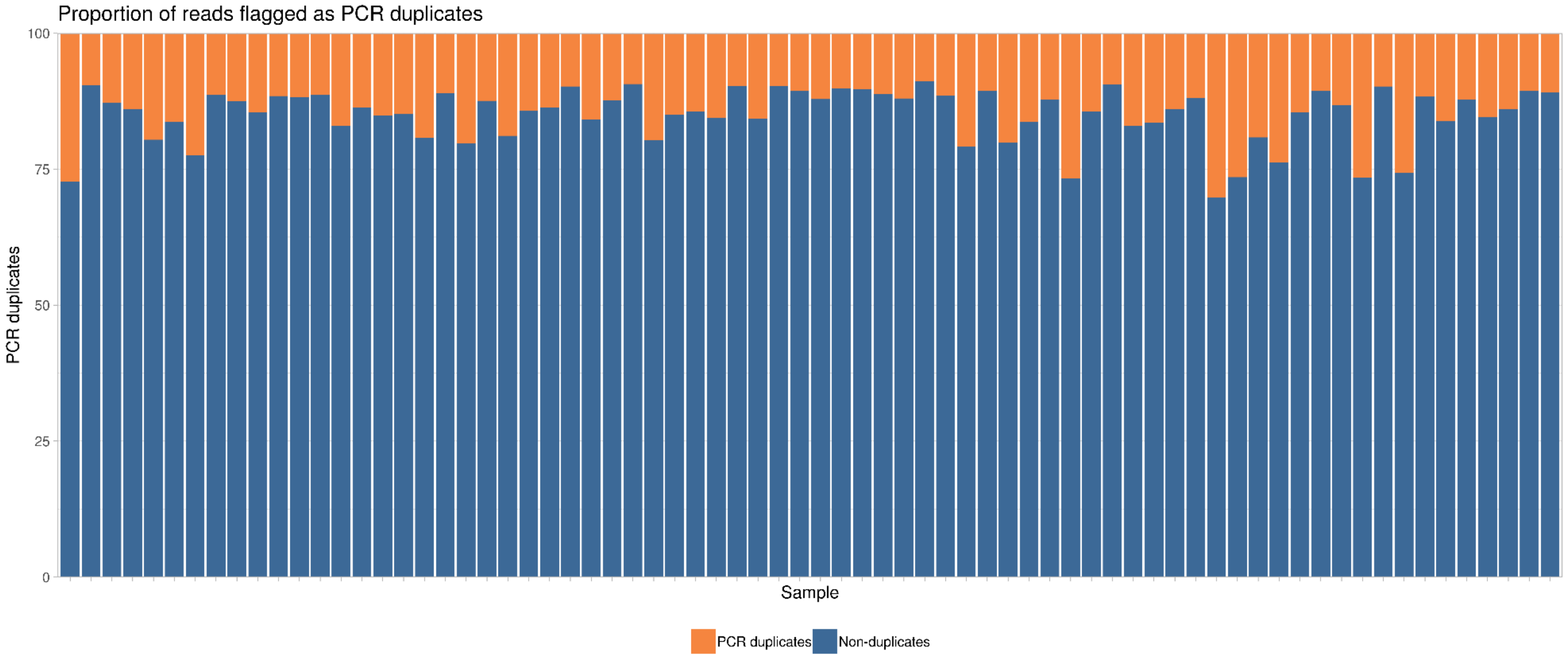

5.3 Figure 4

Variant calling metrics from the WES data. 4A plots the indel size distribution for all indels called passing low site quality filters (not rarity filters). Deletions are presented with negative values and insertions as positive values. A majority of indels are seen to be 5 bases or less in length, which is typical in WES data. 4B depicts the frequency of different base substitutions present in the low-site quality filtered call set demonstrating a standard distribution with more than twice as many transition changes compared to transversions. Substitutions on opposite strands are counted (e.g. A>G and T>C) demonstrate no variant calling strand bias.

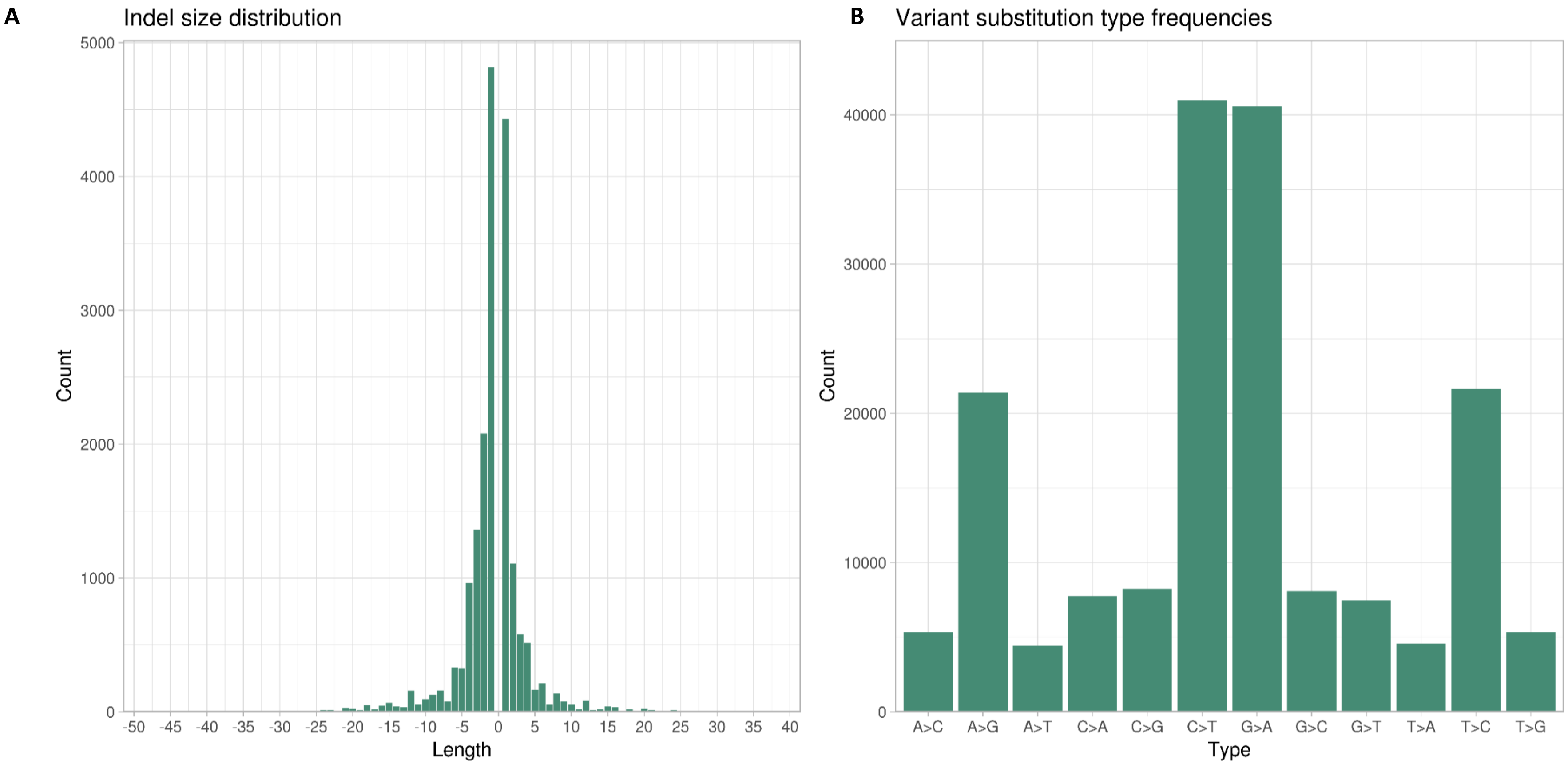

Given the volume of genetic alterations called and meeting default filtering parameters, in-depth analysis of all sites is an impractical methodology to determine potential candidate variants in RCC predisposition. This is exemplified by applying ACMG classifications to the filtered call set which categorises 84.4% (18,884/22,384) of the sites as variants of uncertain significance. As such, SNV analysis was segregated into distinct analysis sets; Ultra rare truncating or splice site-affecting variants, somatically altered genes in RCC, and genes related to the TCA cycle, as described in the methods.

5.3.3 Truncating and splice site-affecting variants across all genes

Variants were filtered to retain only the most potentially damaging variant consequences (nonsense variant, frameshift insertions or deletion, and splice site-affecting variants) in order to determine if any rare or novel truncating variants disrupted genes which may function in predisposition to RCC. After filtering a total of 1,134 variants were kept (5.1%), which consisted of 450 nonsense variants, 145 frameshift insertions, 310 frameshift deletions, and 229 splice site-affecting variants. Due to the number of truncating variants identified, further filtering criteria were applied to reduce the candidate number including removal of variants present in a non-reference homozygous state, variants identified as known benign or likely benign alterations by ClinVar, and reducing the minor allele frequency in ExAC to 0.001 which retained 758 variants. ACMG criteria (325) were applied to the remaining variants utilising InterVar (326) as previously described and assigned 99 variants as pathogenic or likely pathogenic (P/LP) and 608 variants as variants of uncertain significance. A residual 51 variants failed to be parsed correctly by InterVar and as such were not assigned ACMG classifications.

For sites designated as P/LP, genes were assessed by the Network of Cancer Genes platform (NCG) (428) to determine if they have previously been related to cancer and in what capacity. The 99 variants contained 94 unique genes, of which 20 genes were suggested to be associated with cancer as assigned by the NCG v6.0 analysis (428) (4 genes were flagged as potential false positives in cancer and were excluded). This resulted in a final set of 21 sites with truncating alteration in candidate cancer genes assigned as P/LP (5.3 Table 3).

All variants categorised as ultra-rare truncating variants were present in only a single individual and occurred at allele frequencies in ExAC at 8.00E-04 or lower. Interpretation of these variants is highly dependent upon gene function and established associations with other genetic disorders. Most *In silico* predictions for these variants were not designated, except for CADD, which suggested all were deleterious in nature. Interestingly, all the genes in which variants were identified in this subset were altered somatically in RCC on average 1.83% (range 0.1-9%) of cases, though specific selection of genes altered in RCC was not performed. Enrichment analysis biological processes associated with the genes in this set using Panther gene ontologies did not identify any significantly enriched groups.

Several variants are worth noting, including the *PKHD1* nonsense variant (NM_138694: c.C5323T: p.R1775X) which is a known pathogenic variant associated with autosomal recessive polycystic kidney disease. The variant is carried by an individual with early onset clear cell RCC. The variant occurs midway through the protein coding sequence and is reported as loss of function intolerant by gnomAD classifications (353). Lastly, *PKHD1* is reported as a frequently altered (3%) across the TCGA renal cancer set, though most are VUS missense variants. The truncating variant in *DIAPH1* (NM_005219: c.C1261T: p.R421X) is associated with autosomal dominant deafness. *DIAPH1* is highly mutated somatically in RCC (9%) but is nearly exclusively amplified and only one truncating variant is reported, occurring concurrently with an broad amplification (25). This would suggest that truncating variants in *DIAPH1* are unlikely to result in RCC predisposition despite the variant being likely pathogenic.

RNF43 which harbours a frameshift deletion (NM_001305544: c.1410delC: p.P470fs) is also reported frequently somatically (1.8%) but with a high degree of amplification though it has been demonstrated to have tumour suppressor functions complicating variant interpretation in the context of RCC predisposition. The splice site variant identified in *NUP93* (NM_014669) affects the first base of splice donor site after exon 2, potentially disrupting exon splicing. While no reports implicate *NUP93* in cancer, *NUP93* inactivating variants are associated with autosomal recessive nephrotic syndrome.

5.3 Table 3

Table of truncating variants identified in candidate cancer genes and classified as pathogenic or likely pathogenic by InterVar interpretation of ACMG guidelines.

Chr	Pos	rsID	Red	Alt	QUAL	Gene	Transcript	cDNA	AA	Consequence	ExAC	InterVar
chr6	135463145	rs779410126	G	GT	339	*AHI1*	NM_001134830	c.910dupA	p.T304fs	frameshift insertion	2.00E-04	Pathogenic
chr10	71797103		G	A	1740	*CDH23*				splice site	0	Pathogenic
chr13	24892780		G	A	2524	*CENPJ*	NM_018451	c.C3079T	p.Q1027X	nonsense	0	Pathogenic
chr2	237388132	rs780921503	TC	T	3618	*COL6A3*	NM_004369	c.761delG	p.G254fs	frameshift deletion	9.97E-05	Pathogenic
chr5	141577494		G	A	3348	*DIAPH1*	NM_005219	c.C1261T	p.R421X	nonsense	0	Pathogenic
chr6	56618195		CGAGTGGA	C	5566	*DST*	NM_001723	c.5832_5838del	p.A1944fs	frameshift deletion	0	Likely pathogenic
chr7	74046187		G	C	1967	*ELN*				splice site	0	Pathogenic
chr12	101764367		CT	C	3783	*GNPTAB*	NM_024312	c.2549delA	p.K850fs	frameshift deletion	0	Likely pathogenic
chr18	23763403	rs756617534	A	G	2785	*LAMA3*				splice site	8.28E-06	Pathogenic
chr18	23773638	rs187997925	C	T	575	*LAMA3*	NM_001302996	c.C1324T	p.R442X	nonsense	8.00E-04	Likely pathogenic
chr12	40364845	rs281865056	G	GGT	4046	*LRRK2*	NM_198578	c.7185_7186insGT	p.E2395fs	frameshift insertion	9.18E-06	Likely pathogenic
chr14	74516943		T	A	1499	*LTBP2*				splice site	0	Pathogenic
chr1	43338704	rs587778515	CT	C	2462	*MPL*	NM_005373	c.376delT	p.F126fs	frameshift deletion	4.12E-05	Pathogenic
chr1	211674515	rs201869074	T	C	1404	*NEK2*				splice site	2.00E-04	Pathogenic
chr16	56748427		G	A	376	*NUP93*				splice site	0	Pathogenic
chr6	52022858	rs770522674	G	A	3005	*PKHD1*	NM_138694	c.C5323T	p.R1775X	nonsense	8.25E-06	Pathogenic
chr1	13786522	rs769738759	CT	C	2498	*PRDM2*	NM_001007257	c.4442delT	p.L1481fs	frameshift deletion	8.25E-06	Likely pathogenic
chr19	40395498		C	CA	6780	*PRX*	NM_181882	c.2853dupT	p.G952fs	frameshift insertion	0	Likely pathogenic
chr17	58358365		AG	A	1967	*RNF43*	NM_001305544	c.1410delC	p.P470fs	frameshift deletion	0	Likely pathogenic
chr22	37735350	rs200045032	G	T	2041	*TRIOBP*	NM_001039141	c.G5014T	p.G1672X	nonsense	6.00E-04	Likely pathogenic
chr14	92011057		C	A	5148	*TRIP11*	NM_004239	c.G1243T	p.E415X	nonsense	0	Pathogenic

5.3.4 Detection of SNVs in sporadic renal cell carcinoma genes

After variant filtering and quality control, variants were selected based on gene list incorporating genes which are described as being frequently altered in sporadic RCC tumours, as described in the materials and methods Assessment of variants passing filter identified 331 variants falling within the coding regions of genes associated with sporadic RCC tumours (See appendix 9.4.1; excluding known inherited RCC genes). Intervar was used to apply ACMG guidelines to all 331 variants and found 3 pathogenic or likely pathogenic variants across 3 genes, all of which were previously identified in the previous analysis (COL6A3: NM_004369: c.761delG: p.G254fs, DST: NM_001723: c.5832_5838del: p.A1944fs, and PKHD1: NM_170724: c.C5323T: p.R1775X) and 227 VUS variants. Variants were cross referenced with ClinVar data to remove conflicting reports and variants presenting in a non-reference homozygous state were also removed, resulting in a final count of 202 variants.

Protein alterations incurred by the variants identified in this set consisted of 194 missense variants, 2 frameshift deletions, 2 frameshift insertions, 2 non-frameshifting deletions, 2 nonsense variants, and 1 stop loss variant. Variants, excluding missense variants, are in 5.3 Table 4. Overall, few non-nonsynonynmous variants were identified in genes which are frequently somatically altered in RCC and of the 7 genes that were identified, 3 were recapitulations of variants identified without somatic RCC-specific gene list filtering. The remaining 5 variants, 3 of which were truncating, only revealed one variant of particular interest in *SETD2* (NM_014159: c.579_587del: p.193_196del) which is one of the most frequently somatically altered genes in RCC, though the pathogenicity of this variant is uncertain given it does not result in a premature stop codon or frameshift. The deletion of 3 amino acids (p193-196) may result in protein dysfunction but does not occur in any known critical functional domain.

Analysis of VUS assigned missense variants is difficult, particularly given the number identified in this instance (194 sites). Application of restraining *in silico* predictive metrics to filter variants further still resulted in a large set of VUS missense variants being retained where selecting variants only predicted to be likely pathogenic by SIFT and PolyPhen, as well as a CADD score greater than 25 was true for 132 variant sites. For the genes identified in 5.3 Table 4, *AHNAK2, COL6A3, DST, KIAA1109, PKHD1, SETD2*, and *XIRP2*, also harboured rare VUS missense variants after *in silico* filtering parameters were applied (*AHNAK2* = 18, *COL6A3* = 4, *DST* = 5, *KIAA1109* = 1, *PKHD1* = 1, *SETD2* = 2, and *XIRP2* = 7).

Further sub setting of VUS missense variants in the *in silico* filtered set uncovered missense variants in biologically relevant somatic RCC-linked or cancer-associated genes such as *ATM, KDM6A*, *KMT2C*, *KMT2D*, *MTOR*, *NF2*, and *SMARCA4* in addition to *SETD2* (See 5.3 Table 5).

5.3 Table 4

Table of variants identified in frequently somatically altered genes in RCC tumours (TCGA data) after exclusion of all 194 missense substitution variants present in the set.

Chr	Pos	rsID	Ref	Alt	Gene	Transcript	Exon	cDNA	AA	Consequence	ExAC	InterVar
chr14	104945007	rs755948408	AGGGCATC TTGAACTT	A	AHNAK2	NM_138420	exon7	c.10429_10443del	p.3477_3481del	non-frameshift deletion	0.003	Uncertain significance
chr2	237388132	rs780921503	TC	T	COL6A3	NM_004369	exon4	c.761delG	p.G254fs	frameshift deletion	9.97E-05	Pathogenic
chr6	56618195	N/A	CGAGTGGA	C	DST	NM_001723	exon23	c.5832_5838del	p.A1944fs	frameshift deletion	0	Likely pathogenic
chr4	122238178	rs780100006	C	T	KIAA1109	NM_015312	exon26	c.C3661T	p.Q1221X	nonsense	1.66E-05	Uncertain significance
chr6	52022858	rs770522674	G	A	PKHD1	NM_138694	exon33	c.C5323T	p.R1775X	nonsense	8.25E-06	Pathogenic
chr3	47124048	rs764288610	AGGTGGAGGC	A	SETD2	NM_014159	exon3	c.579_587del	p.193_196del	non-frameshift deletion	1.00E-04	Uncertain significance
chr2	167248077	N/A	G	GA	XIRP2	NM_152381	exon9	c.6686dupA	p.E2229fs	frameshift insertion	0	Uncertain significance
chr2	167248353	rs553644411	G	GA	XIRP2	NM_152381	exon9	c.6962dupA	p.E2321fs	frameshift insertion	0.0013	Uncertain significance

5.3 Figure 5

Oncoprint plot generated from the TCGA renal cancer dataset for the genes described in 5.3 Table 4. Plot was automatically generated by the cBioPortal cancer data analysis platform (438).

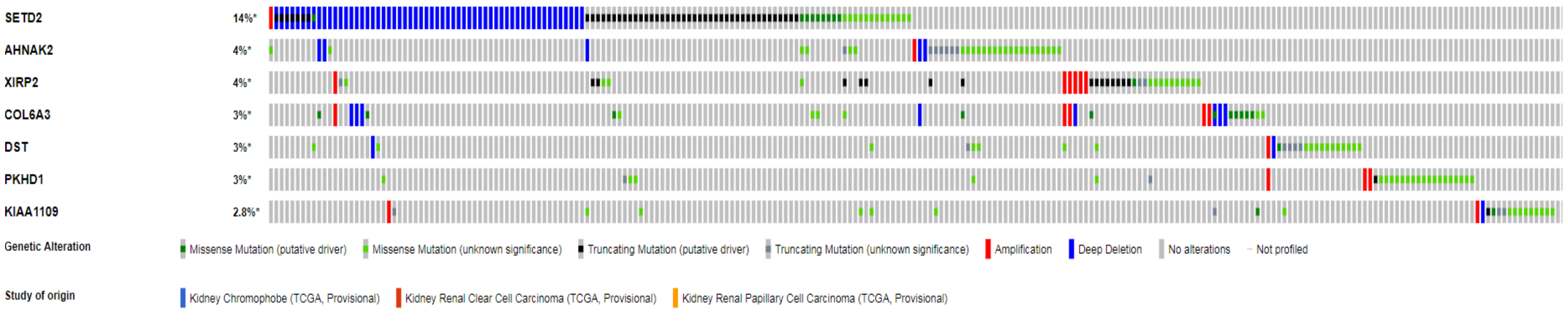

5.3 Table 5

Missense variants of uncertain significance identified in a subset of selected somatically altered RCC genes which passed *in silico* filtering criteria

Chr	Pos	rsID	Ref	Alt	Gene	Transcript	Exon	cDNA	AA	EXAC	CADD	SIFT	Poly Phen	CLINVAR	InterVar
chr11	108292716		G	A	ATM	NM_000051	exon30	c.G4534A	p.A1512T	0	23.7	D	P	Uncertain significance	Uncertain significance
chr11	108293341		T	C	ATM	NM_000051	exon31	c.T4640C	p.I1547T	0	26.9	D	P	Uncertain significance	Uncertain significance
chrX	45070327		C	G	KDM6A	NM_021140	exon17	c.C2672G	p.P891R	0	22.7	D	D	N/A	Uncertain significance
chr7	152151453	rs139111507	G	C	KMT2C	NM_170606	exon50	c.C12655G	p.L4219V	0.0031	0.002	D	B	N/A	Uncertain significance
chr7	152187411		G	A	KMT2C	NM_170606	exon33	c.C4859T	p.P1620L	0	26.9	D	B	N/A	Uncertain significance
chr7	152199279	rs746270757	C	T	KMT2C	NM_170606	exon27	c.G4273A	p.G1425S	8.35E-06	26.2	D	D	N/A	Uncertain significance
chr7	152252613	rs140919432	G	T	KMT2C	NM_170606	exon10	c.C1402A	p.P468T	9.00E-04	25.3	D	B	N/A	Uncertain significance
chr7	152252671	rs149250254	C	A	KMT2C	NM_170606	exon10	c.G1344T	p.Q448H	4.00E-04	26.5	D	B	N/A	Uncertain significance
chr12	49042232	rs754420100	G	A	KMT2D	NM_003482	exon28	c.C5966T	p.T1989M	0	23.9	T	D	N/A	Uncertain significance
chr1	11126781		G	C	MTOR	NM_004958	exon46	c.C6367G	p.L2123V	0	27.9	D	D	N/A	Uncertain significance
chr22	29674892	rs866689896	G	A	NF2	NM_000268	exon13	c.G1397A	p.R466Q	0	27.1	T	B	Uncertain significance	Uncertain significance
chr3	47083880	rs143991928	C	T	SETD2	NM_014159	exon12	c.G5900A	p.G1967D	3.00E-04	22.2	D	P	N/A	Uncertain significance
chr3	47088188	rs141847082	C	G	SETD2	NM_014159	exon10	c.G5202C	p.Q1734H	2.47E-05	23.4	T	D	N/A	Uncertain significance
chr19	10984204		C	T	SMARCA4	NM_003072	exon2	c.C53T	p.P18L	0	24.4	D	D	Uncertain significance	Uncertain significance

5.3.5 Detection of SNVs in metabolic genes associated with Krebs cycle

Variants from the filtered set were demarcated by genes associated with the TCA cycle (see appendix 9.4.1) in order to identify novel or rare likely damaging variants in components the genes encoding proteins involved in the TCA cycle and its supporting complexes. After gene list filtering (22 genes) a total of 13 sites were retained. All sites identified within the genes present on the TCA cycle gene list were nonsynonymous variants and InterVar interpretation of clinical significance assigned 76.9% (10/13) as VUS variants, with the remaining categorised as likely benign.

Of the 13 variants identified, 10 sites occurred within known protein domains or functional sites, though variants outside of protein domains did not correlate with variants assigned as likely benign. Genes carrying variants included direct components of the TCA cycle complexes (*ACO1, ACO2, DLST, CS, IDH3A, MDH2,*) and genes encoding proteins related to complex scaffolds or TCA complex-like functions (*SUCLG2, OGDHL,* and *DLD*).

5.3 Table 6

Table of variants identified in genes associated with the TCA cycle.

Chr	Pos	rsID	Ref	Alt	Gene	Transcript	Exon	cDNA	AA	Consequence	ExAC	InterVar	Interpro domain
chr9	32448908	rs375980125	G	A	*ACO1*	NM_002197	exon20	c.G2383A	p.V795I	nonsynonymous	5.77E-05	Uncertain significance	Swivel domain
chr22	41507837	rs141772938	C	G	*ACO2*	NM_001098	exon3	c.C220G	p.L74V	nonsynonymous	0.0041	Uncertain significance	Alpha/beta/alpha domain
chr14	74893399	rs199961137	G	T	*DLST*	NM_001933	exon9	c.G647T	p.G216V	nonsynonymous	9.89E-05	Uncertain significance	N/A
chr14	74892903	rs766047735	C	T	*DLST*	NM_001933	exon8	c.C512T	p.A171V	nonsynonymous	8.25E-06	Uncertain significance	N/A
chr10	49736482	rs140281439	C	A	*OGDHL*	NM_001347819	exon21	c.G2629T	p.A877S	nonsynonymous	0.002	Uncertain significance	Thiamin diphosphate-binding pyrimidine-binding domain
chr10	49736126	rs144636641	C	T	*OGDHL*	NM_001347819	exon22	c.G2806A	p.G936S	nonsynonymous	0.0018	Likely benign	Thiamin diphosphate-binding pyrimidine-binding domain
chr10	49758570	rs200629482	G	A	*OGDHL*	NM_001347819	exon2	c.C23T	p.P8L	nonsynonymous	5.88E-05	Uncertain significance	N/A
chr7	107915609	rs145670503	G	A	*DLD*	NM_000108	exon9	c.G788A	p.R263H	nonsynonymous	7.00E-04	Uncertain significance	FAD/NAD(P)-binding domain
chr12	56273709	rs149476836	T	C	*CS*	NM_004077	exon10	c.A1108G	p.N370D	nonsynonymous	3.00E-04	Uncertain significance	Citrate synthase-like alpha subdomain
chr15	78168982	rs116374996	C	T	*IDH3A*	NM_005530	exon11	c.C1078T	p.R360C	nonsynonymous	0.0022	Uncertain significance	Isopropylmalate dehydrogenase-like domain
chr15	78161708	rs61752770	T	A	*IDH3A*	NM_005530	exon5	c.T417A	p.D139E	nonsynonymous	0.0048	Likely benign	Isopropylmalate dehydrogenase-like domain
chr7	76058064	rs111879470	G	A	*MDH2*	NM_005918	exon4	c.G415A	p.V139I	nonsynonymous	0.0038	Likely benign	NAD(P)-binding domain
chr3	67520559	N/A	G	T	*SUCLG2*	NM_001177599	exon5	c.C493A	p.P165T	nonsynonymous	0	Uncertain significance	ATP-grasp fold

5.3.6 Copy number alterations - Calibration of copy number pipeline

In order to assess the necessary changes to default parameters provided by XHMM for the calling of CNVs in unmatched whole exome data, calibration was performed on a subset of HapMap samples with both whole exome sequencing and CNV calls from comparative genomic array data (see materials and methods 5.2).

Comparisons in calling rate and genotype for overlapping targets in both whole exome and array data were performed across 23 samples to assess the calling efficiency, genotyping accuracy, and ability to replicate results found in CGH array data, considered the gold standard for high-throughput detection of copy number alterations. Analysis was replicated 95 times utilising differential parameters regarding target size, target read depth, sample read depth, read depth standard deviation, and PCA variance normalisation. Of 95 replicates attempted, 73 successfully produced CNV calls and used to generate summary and comparison data.

5.3.7 Copy number alterations calibration - Evaluation of call rate, type I, and type II errors

When comparing exome targets which intersected with genomic regions with available array data, the true positive rate was 68.53 ± 2.89% when restricted to all experimental iterations for which targets were called in both exome data and array data. False positives occurred at a mean rate of 5.69 ± 0.63% in which XHMM called an alteration in copy number but array data was discordant. The remaining percentage was attributable to false negative calls, where XHMM failed to genotype a non-neutral copy number alteration identified by the array data at a rate of 25.77 ± 3.30%. Distributions across all samples are given in 5.3 Figure 6A.

A majority of algorithm parameters, independently, had little to no impact on call rates in the calibration set with the exception of ‘minimum mean target read depth’, that is to say the threshold below which exome targets are excluded on the basis of mean read depth across the analysed samples (5.3 Figure 6B). No analysis was performed to assess call rate effects due to combinatorial parameter modifications.

5.3 Figure 6

CNV calibration results across all HapMap WES data sets compared to array data. 6A visualisation of the relative proportion of calls and the detection rates by colour. True positives (blue), false positives (red), and false negatives (green). 6B Line plot grid for each altered XHMM algorithm metric and the change to TP, FP, and FN rates over different iterations.

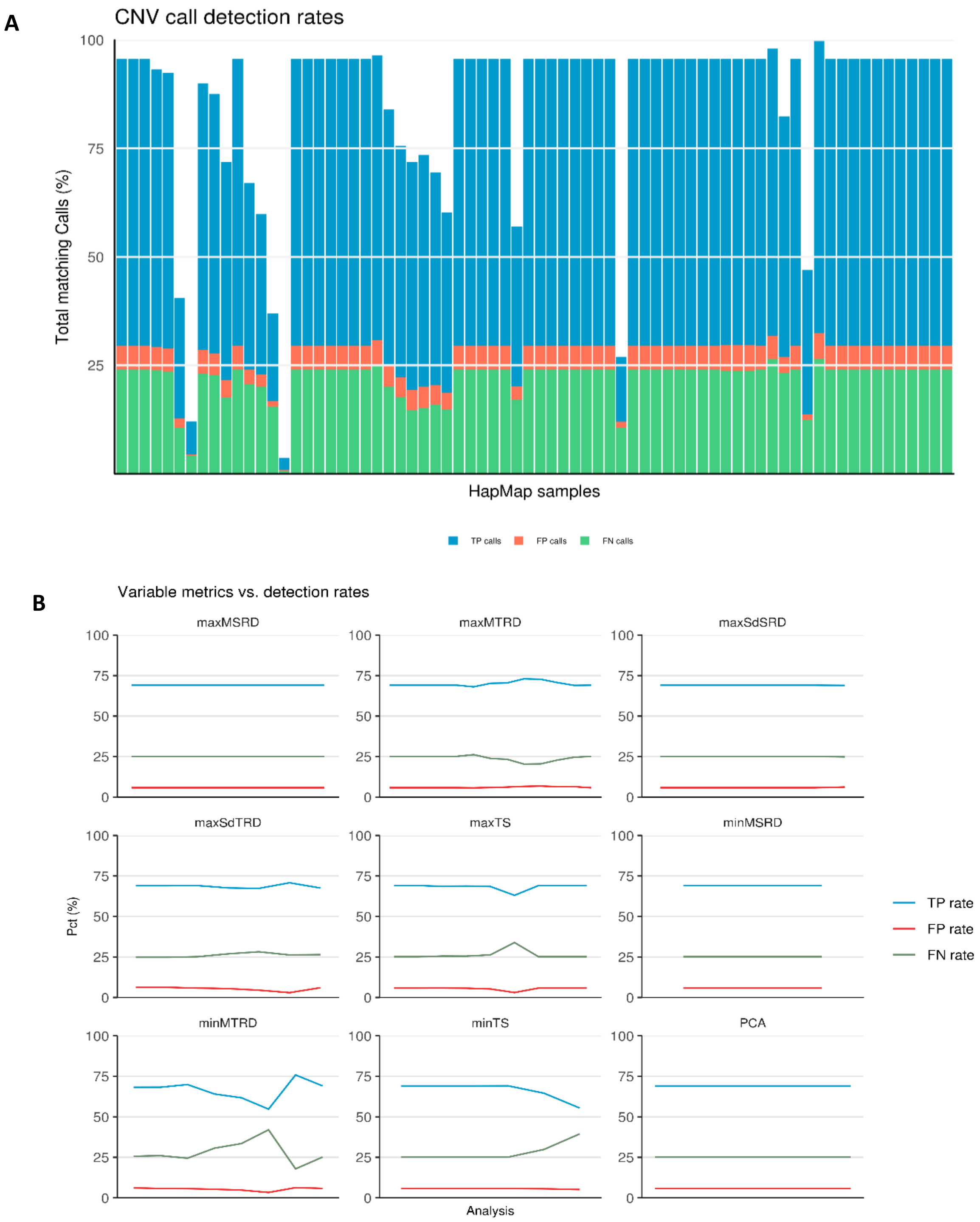

5.3.8 Copy number alterations – RCC copy number analysis

CNV calling utilising the CNV pipeline was performed on all 72 RCC WES cases with an additional 74 read depth-matched WES samples. The sample set was normalised on the second principle component, removing variance up to the 70% threshold, as specified in the XHMM methodology (430).

Initial calling by XHMM called 9,310 copy number altered regions across all samples. After annotation and exon extraction, a total of 13,072 exons were called as having altered copy numbers across 146 samples equating to 78,942 altered genotypes over all samples. These calls were split evenly between deletions and duplications, with 39,378 duplications and 39,564 deletions (deletion to duplication ratio = 1.004). The median number of duplication calls was 249 (range 53-780) per sample and the mean number of deletions was 249 (range 116-1085). Stringent call filtering (see materials and methods 5.2) filtered 7,418 sites and the removal of 27 samples in which no CNV calls remained, resulting in the retention of 5,654 individual genotypes, 3,536 (62.5%) were duplications and 2,118 (37.5%) were deletions. The mean duplication and deletion call rates across the retained samples were 29.7 (range 0-591) and 17.8 (range 0-437), respectively.

Lastly, samples were subset to exclude the non-case samples used to improve calling. This caused 2,275 additional sites to be filtered causing a reduction in genotype calls to 3,379 (2,024 duplications and 1,355 deletions). Median CNV calls per sample was 23 (range 1-441), with duplications having a median of 15 (range 0-337) and deletions a median of 4 (range 0-437). Of the samples assessed, 5 individuals harboured call rates exceeding 1 standard deviation from the mean rate across all samples, and 3 samples exceeded 2 standard deviations. These samples accounted for 46.6% (1,576/3,379) of all CNV calls (See 5.3 Figure 7A).

Given that germline CNVs should occur at low rates, samples with an excessive number of CNVs were excluded on the premise that the CNV calls were artefactual. Samples with CNV calls exceeding one standard deviation greater than the cohort mean were removed. Exclusion of these outlier samples resulted in attenuated call rates with a total of 5,654 sites called across 56 samples for a total of 1,803 genotype calls (5.3 Figure 7B). Removal of the outlier samples resolved to stabilise the CNV call rates across all samples with a median of 21 (range 1-127) CNV calls (1,179 duplications and 624 deletions). Median duplication and deletion rates in the final sample set were 12.5 (range 0-103) and 3 (range 0-123), respectively.

5.3 Figure 7

Stacked bar plot of exon call types and counts across all RCC samples where duplication proportion is indicated in yellow and deletions in blue. Solid line represents the mean count, dotted represents the upper standard deviation, and dashed represents two times the upper standard deviation. 7A Stacked bar plot including outlier samples which exceeded 2 standard deviations from mean number of target exons called. 7B Stacked bar plot identical to that in 7A but after the removal of the outlier samples.

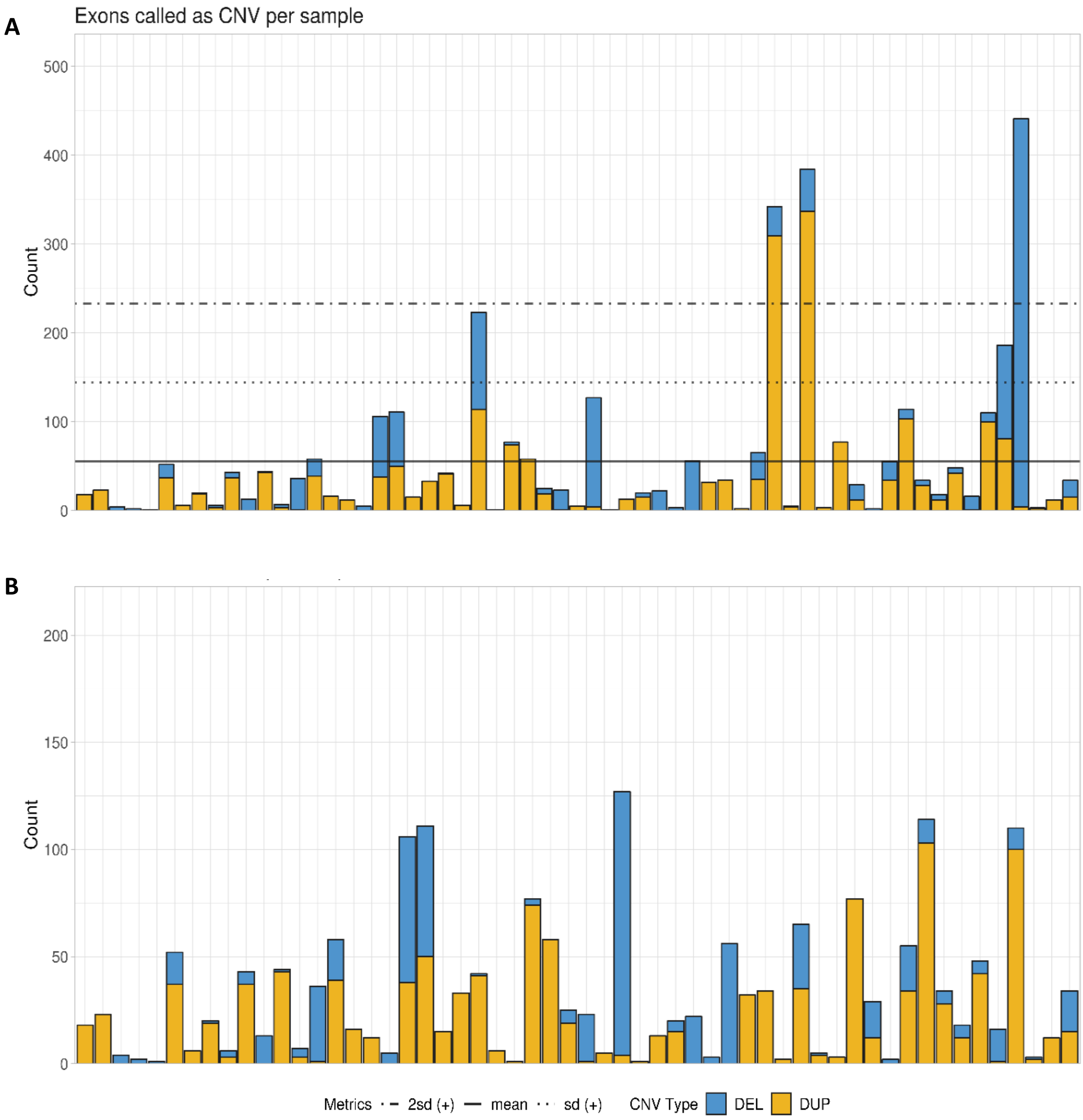

Analysis of affected genes was performed by first identifying CNV calls in protein coding genes and subsequently the application of gene lists as utilised for SNV analysis. Analysis of CNV calls discovered copy number duplications in 274 genes and copy number deletions in 137. A total of 18 genes had both copy gain and copy loss calls and were excluded on the basis that genes carrying both duplications and deletions are unlikely to be associated with the same phenotypic presentation.

Filtering of CNV calls using a broad pan-cancer gene list (572 cancer-related genes curated from the COSMIC cancer consensus gene lists (378) reduced the call set to 75 CNV calls which, when exon overlapping calls were merged, collapsed to 10 distinct calls in 10 samples (5.3 Table 7). These CNV calls were divided into 5 duplications and 5 deletions, 2 were full coding region alterations and the remaining calls were partial. All calls occurred only once, detected in a single individual across the entire unfiltered sample set. Many calls were partial duplications of known tumour suppressor genes and therefore likely to be false positives or not assumed to have functional effects (*TSC2*, *CARD11*, *PMS2*), as well as the full coding region of *MUTYH*. Deletions were broadly partial in nature, resulting in copy number losses of a subset of exonic regions and only a single gene demonstrated a copy loss of the entire coding region (*EP300*).

5.3 Table 7

Table of high quality filtered CNV calls made across the RCC set collapsed by gene and copy number alteration type.

CNV	Gene	Chr	Start	End	Size (Bp)	Q Some	Allele frequency	Allele count	Region
DEL	*PDE4DIP*	chr1	149030194	149030314	120	99	6.90E-03	1	Exon 46
DEL	*COL2A1*	chr12	47976750	47978819	2069	63	6.90E-03	1	Exon 42-48
DEL	*NF1*	chr17	31358907	31360764	1857	97	6.90E-03	1	Exon 55-56
DEL	*EP300*	chr22	41117125	41176589	59464	69	6.90E-03	1	Exon 1-30
DEL	*HNRNPA2B1*	chr7	26197302	26197908	606	79	6.90E-03	1	Exon 2-4
DUP	*MUTYH*	chr1	45329244	45340348	11104	99	6.90E-03	1	Exon 1-16
DUP	*TSC2*	chr16	2087801	2088671	870	97	6.90E-03	1	Exon 39-42
DUP	*APOBEC3B*	chr22	38982402	38982522	120	76	6.90E-03	1	Exon 1
DUP	*CARD11*	chr7	2910037	2947799	37762	94	6.90E-03	1	Exon 3-24
DUP	*PMS2*	chr7	5986697	5990016	3319	88	6.90E-03	1	Exon 10-11

5.3.9 Gene burden analysis

Gene burden analysis was performed utilising 66 cases with features of RCC predisposition and 999 control samples from the ICR UK exome (433) (as described in materials and methods 5.2). As such, patients identified as not having non-Finnish European admixtures were excluded from downstream analysis. Burden analysis was restricted to truncating and nonsynonymous variants (excluding in-frame deletions and insertions, non-coding, intronic, and synonymous alterations) and after filtering resulted in 497,138 variants across 1,071 samples.

PCA was performed to assess for batch effects and determine appropriate covariates to include the gene burden model (See 5.3 Figure 8). Further interrogation of the PCA plot and its variance profile demonstrated a likely batch effect due to library and data preparation methods between control and case samples, driven by variance in PC1 and intra-case variance from both P1 and PC2 collectively. In PCA plots utilising principle components 3 or greater, samples broadly overlapped, suggesting no variance between cases and controls, or intra-case variability.

The magnitude of any variance to a single principle component is an important factor when determining the degree to which it will affect downstream analysis. A plot of cumulative variance was generated for all computed principle components in order to quantify the contributed variance for each principle component (see 5.3 Figure 9). Principle component 1 and 2 contributed 1.03% and 0.55% of total variance derived from the principle component analysis, respectively. All the remaining variance was spread equally across all remaining principle components at percentages between 0 - 0.47% (mean = 0.09%). Formally, the contributed variance for each principle component broadly correlated with the amount of variance contributed individually by each sample. Given the minimal about of variance contributed by each principle component, downstream analysis was carried out with both principle component 1 and 2 as covariates in the SKAT-O model with all remaining principle components contributing an increasingly low amount of variance.

5.3 Figure 8

Scatter plots of principle components 1 – 5 grouped by case and control; cases from this study in blue, control samples from ICR1958 birth control cohort in red. A) Scatter plot of principle component 1 against principle component 2. B) Scatter plot of principle component 2 against principle component 3. C) Scatter plot of principle component 3 against principle component 4. D) Scatter plot of principle component 4 against principle component 5.

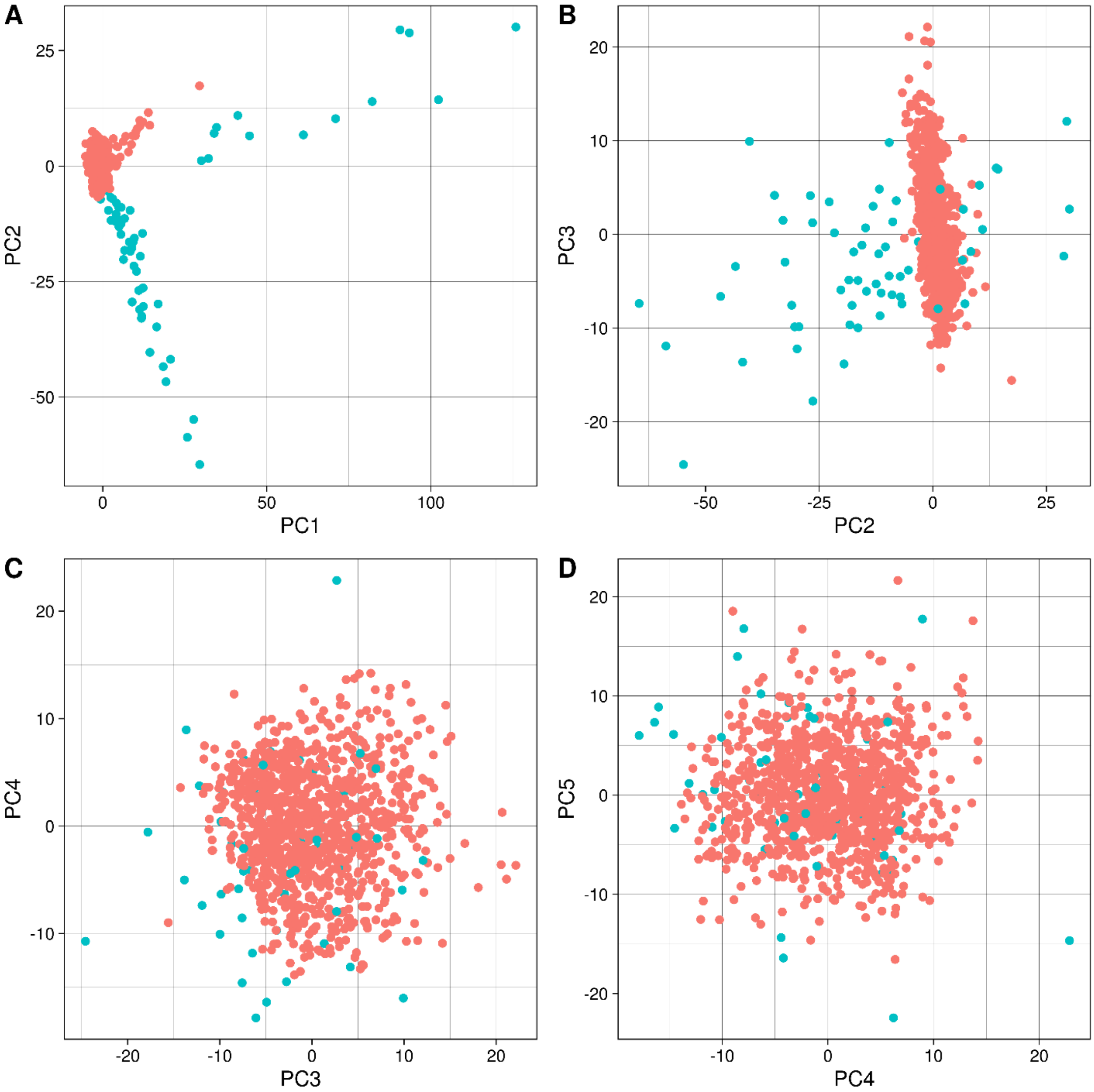

5.3 Figure 9

Contributed variance across all principle components. X-axis presents all principle components generated by principle component analysis; y-axis presents the amount of total variance within the data contributed by a given principle component. Graphs A and B display the same data but with different y-axis scaling. A) Contributed variance with y-axis scaled to the highest amount of variance contributed by a single principle component. B) Contributed variance with y-axis scaled to 100% contributed variance.

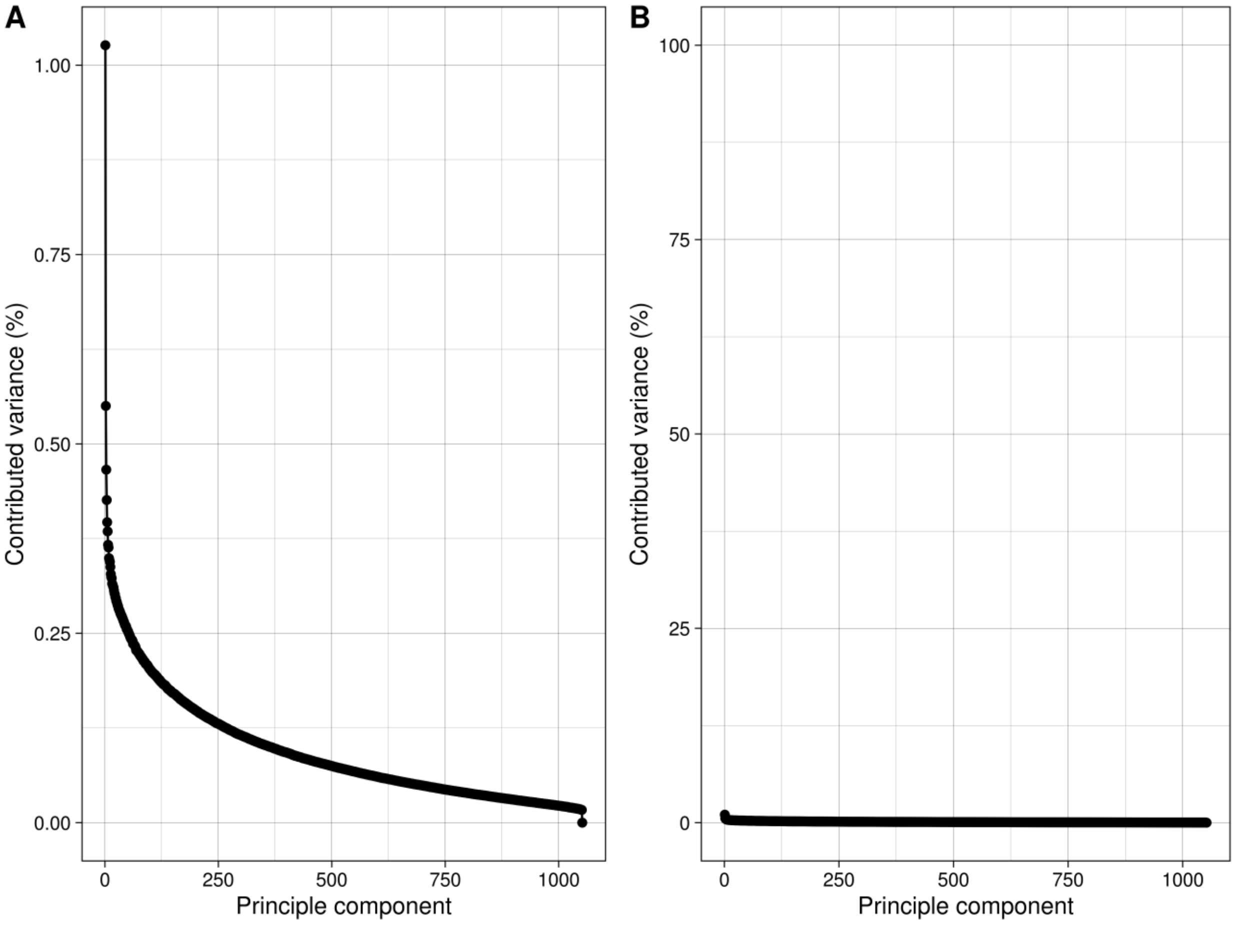

5.3 Figure 10

Q-Q plot for the described SKAT-O implementation depicting the quantile p value spread against the theoretical quantiles. Upwards deviation of points from the theoretical distribution (centre line) indicate an inflation of p values.

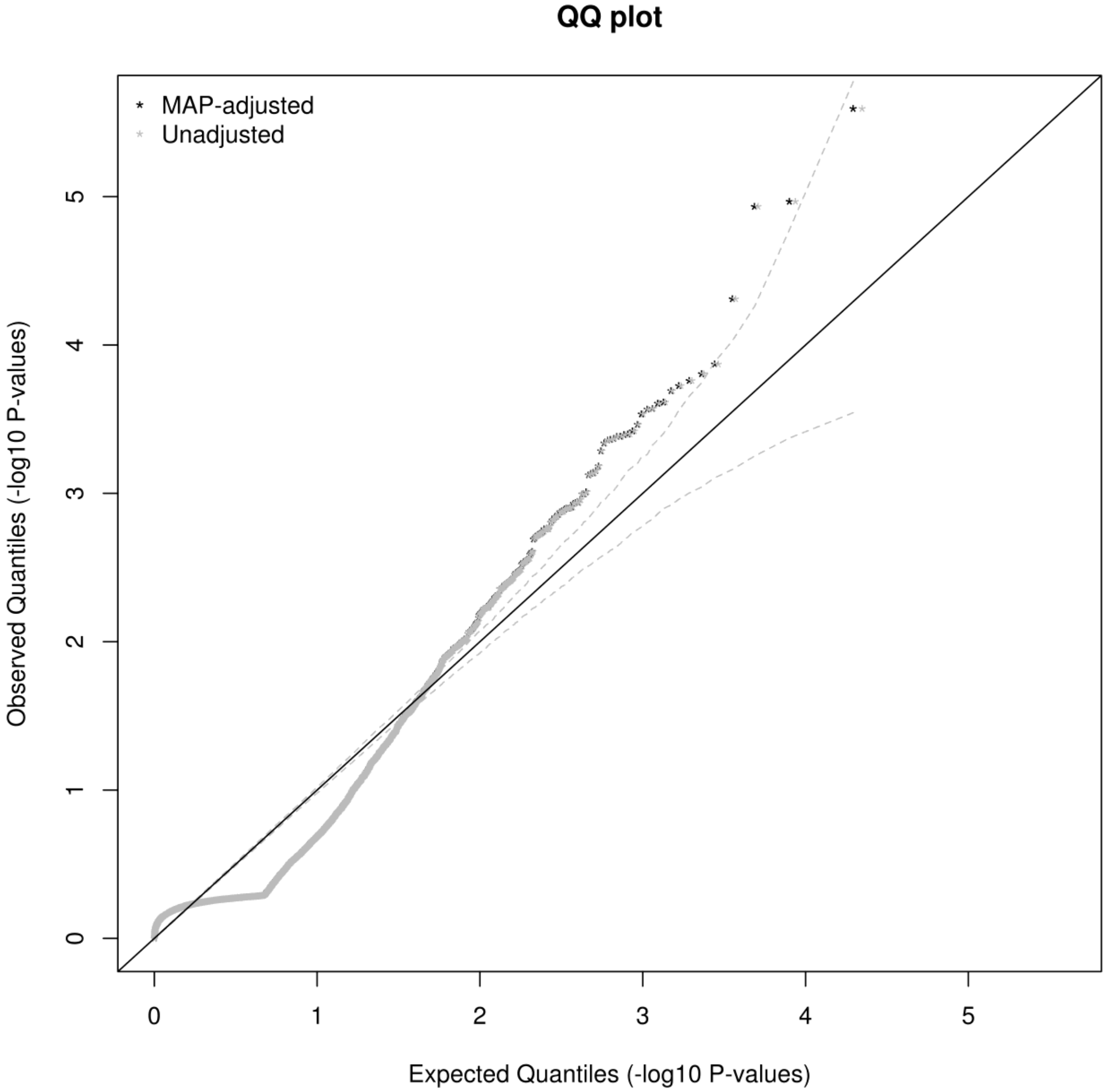

SKAT-O burden analysis was performed across all genes containing variants with the optimised parameters with covariates (5.3 Figure 10 and 5.2 Table 1). Analysis of SKAT-O output revealed 532 genes with a significant mutational burden compared to controls at $p < 0.05$ and 180 genes at significance $p < 0.01$ (See appendix section 9.4.6). A single gene was significant after multiple testing correction by FDR (*FBLIM1*, q value = 0.035). The correction was applied across all assessed genes (n = 13,959) and the false discovery rate was set to 5%, as such multiple testing correction was statistically conservative for false positive associations. Genes occurring with p values < 0.01 included 12 known cancer associated genes as defined by network of cancer genes (v6.0) (428), including *HIF1A* (p = 3.28E-04). Analysis of the genes associated with mutational burden ($p < 0.01$) by the Network of Cancer Genes (NCG v6.0; (428)) identified a statistical enrichment of known or candidate cancer genes in the burden-associated genes compared to global rates with 6.67% (12/180) genes in the burden associated set being known or candidate cancer genes compared to 12.6% (2372/18833) across the genome (χ^2 test p = 0.040).

Gene enrichment analysis was performed on various gene set analysis platforms for genes with p values < 0.01 in order to identify enriched biological processes, pathways, or regions. Analysis for overrepresented gene ontologies (GOs) using WebGestalt detected no enriched GOs after FDR correction. Gene enrichment performed by Reactome to detect statistically overrepresented pathways did not detect any pathways in which genes (or their protein products) were enriched. It is worth noting that Reactome failed to find matching gene identifiers for 70/180 (38.9%) genes despite using multiple gene/protein identifiers (NCBI, Entrez gene, gene symbol, and Uniprot) which may have impacted pathway enrichment analysis. Lastly, GO enrichment analysis using Panther and GO-slim biological process ontology set also did not result in any FDR corrected biological processes being enriched in genes with p values < 0.01.

5.3.10 Short tandem repeat expansion analysis

Short tandem repeat expansion (or contraction) (STRE) analysis was performed on BAM files for all 72 individuals in the case set to determine if known tandem repeat alterations could be detected in germline sequencing from WES data, and if those alterations could impact genes known to result in RCC predisposition. STREs were called at a mean rate of 34,925 calls per sample (median = 33,343; range 20,776-69,571). STRE calls were filtered for both read depth and quality (Q) and restricted to calls within known RCC predisposition genes (see appendix 9.4.1), as well as *BRIP1*, as identified in chapter 4.

After filtering and genomic region restriction the mean number of STRE calls per sample was 1.78 (median = 1.5; range 1-5). Calls across all samples were collapsed into a single VCF resulting in a total of 31 STRE calls passing filtering criteria. A further 24 sites were excluded for occurring at an allele frequency greater than 5% (allele frequency > 0.05) and were therefore likely to be either false positive calls or natural fluctuations in short tandem repeat lengths.

The remaining 7 sites (5.3 Table 11) occurred in 6 individual samples, with a single individual harbouring both large STRE calls in *SDHA* and *TSC1* (chr5:250296 A/$(AGG)^{272}$ and chr9:132903602 C/$(CAAAA)^{163}$). Of the 7 STRE calls made by gangSTR which passed all filtering criteria, 6 were present within gene introns and none occurred in the disruption or in proximity to a spice site consensus sequence. A single STRE call was present within exon 20 of *BRIP1* (chr17:61684053 T/TTTGT), occurring at amino acid 998 within the *BRCA1* binding domain in an individual with familial RCC and no other known candidate variants from previous analysis.

5.3 Table 8

STRE calls after filtering and joint allelic frequency assessment identified in 72 RCC predisposition-related WES samples

Chr	Position	REF	ALT	Allele count	Allele frequency	Gene	Type	Exon	Intron	Strand
chr1	161319223	A	AAATA	1	1.370E-02	*SDHC*	Intronic		1/5	1
chr17	61684053	T	TTTGT	1	1.370E-02	*BRIP1*	Exonic	20/20		-1
chr17	61780729	A	AACA	1	1.370E-02	*BRIP1*	Intronic		1/12	-1
chr3	52566049	CAAAAC	C	1	1.370E-02	*PBRM1*	Intronic			-1
chr5	250296	A	(AGG)X272	1	1.370E-02	*SDHA*	Intronic		1/11	1
chr7	116792457	ACACACACA	A	1	1.370E-02	*MET*	Intronic		19/20	1
chr9	132903602	C	(CAAAA)X163	1	1.370E-02	*TSC1*	Intronic		17/22	-1

5.3.11 Mobile element analysis

Analysis of mobile element insertion was performed using MELT for all 72 samples present in the WES data set. Initial calling of mobile element insertions (MEIs) was independently identified per sample for each of the 4 transposable element types and jointly genotyped, describe in the materials and methods section. Prior to site filtering MEIs the following number of MEIs were detected per transposable element type; ALU = 1,645, HERVK = 1, LINE1 = 152, SVA = 73.

Filtering parameters for MELT calls were applied (PASS status and split read support > 2) to each transposable element type resulting in the retention of 35 ALU sites, 0 HERVK sites, 5 LINE1 sites, and 1 SVA sites. Transposon-specific VCF files were concatenated and region filtering of calls to genes present in known RCC predisposition genes (and *BRIP1*), as described previously, did not result in any sites being retained. Intersection of the sites present in the multi-transposon VCF file with all known gene coding regions returned 41 sites with MEI calls. Removal of common (AF > 0.05) MEI calls across the sample set retained 18 sites, only 1 of which was within a gene exon, *ZNF763* (5.3 Table 9).

5.3 Table 9

Table of rare mobile element insertion calls generated by filtered MELT analysis

Chromosome	Start	Gene	Ref	Alt	Transcript	Type	Class	RA	SR	AF
chr1	59849339	*HOOK1*	T	AAAAATGACTTACATCT	NM_015888	Intronic	ALU	1.585	7	4.110E-02
chr1	83950029	*TTLL7*	T	AAAATACTTCT	NM_024686	Intronic	ALU	4.585	13	6.849E-03
chr1	71072427	*ZRANB2*	G	AAGAATTTTTTCTG	NM_203350	Intronic	LINE1	1.322	3	6.849E-03
chr10	16876712	*CUBN*	A	null	NM_001081	Intronic	ALU	-1	16	2.740E-02
chr12	40398001	*MUC19*	T	AAAATTAGTGTGTTTCTT	NM_173600	Intronic	LINE1	4.459	8	6.849E-03
chr14	80206464	*DIO2*	T	null	NM_000793	Intronic	ALU	3.17	25	1.370E-02
chr14	75886876	*TTLL5*	G	null	NM_015072	Intronic	ALU	2.807	15	2.055E-02
chr19	11978162	*ZNF763*	T	null	NM_001012753	Exon 4	ALU	-2.585	23	6.849E-03
chr2	159462354	*BAZ2B*	C	null	NM_001289975	Intronic	LINE1	-2.322	8	6.849E-03
chr4	169737924	*C4orf27*	T	GAAAATCAGCT	NM_017867	Intronic	ALU	2.459	19	4.795E-02
chr4	55954168	*CEP135*	T	null	NM_025009	Intronic	ALU	-2.322	28	6.849E-03
chr5	157490513	*ADAM19*	C	GCAGATTTC	NM_033274	Intronic	ALU	2	3	6.849E-03
chr5	173609434	*BOD1*	C	null	NM_138369	Intronic	LINE1	3.7	3	6.849E-03
chr6	110627236	*CDK19*	G	null	NM_001300964	Intronic	ALU	3.585	40	2.740E-02
chr6	54354449	*TINAG*	T	null	NM_014464	Intronic	ALU	-2	6	6.849E-03
chr7	82117243	*CACNA2D1*	T	null	NM_001302890	Intronic	ALU	4.858	9	6.849E-03
chr7	104168669	*ORC5*	T	TAAACATGTTT	NM_181747	Intronic	ALU	4.087	4	4.795E-02

5.4 Discussion

In this study the use of multiple analysis types has been utilised to identify potential candidate genes which may be associated with RCC predisposition. Identification of genes with strong associations with somatic RCC alterations in histone modifying and chromatin remodelling pathways such as *SMARCA4*, *SETD2*, *KDM6A*, *KMT2C*, and *KMT2D* are potential candidate genes given the recent association of *PBRM1* and *BAP1* with RCC predisposition (263,264) and in regard to the details discussed in chapter 3 section 3.1.3. *SMARCA4* encodes a component of the same complex as *PBRM1* and is frequently somatically altered in RCC and has been reported in predisposition to other cancer (439).

Variants in *SETD2*, including a non-frameshift deletion, are interesting potential candidates given the frequency of somatic alterations in *SETD2* seen somatically, with 18% of clear cell RCC cases having either copy loss or putative driver mutations (25) and has been demonstrated to act as tumour suppressor via epigenetic regulation (440). Histopathological information was available for one of the three individuals with *SETD2* variants and had multifocal clear cell RCC at age 48 years, which would correlate with *SETD2* mutational status. Heterozygous loss of function *SETD2* mutations have been described as a cause of the intellectual disability disorder, Luscan-Lumish syndrome (MIM: 616831) which is characterised by developmental and speech delay, dysmorphic facial features, macrocephaly and autistic features (441,442). Luscan-Lumish syndrome is a rare disorder and predisposition to RCC has not been described and, to my knowledge, the individuals in our RCC cohort with *SETD2* variants did not have features of Luscan-Lumish syndrome. Variants in *KMT2C* and *KMT2D* have been broadly discussed in previous chapters but they do occur frequently somatically and should not be removed from consideration, particularly *KMT2C* given the sequencing issues and potential false positives that may occur, as such further analysis would be necessary.

Lastly, *KDM6A* is a further gene coding a histone modifying protein, lysine demethylase 6A, and is also altered somatically, though at a lower rate than the other genes mentioned (1.8%). *KDM6A* is closely linked to *KMT2D*, both of which are associated with Kabuki syndrome 2 and 1, respectively (MIM: 300867 and 147920) and therefore is open to the same points discussed in chapter 3 in regard to the inheritance of a variant associated with an autosomal dominant condition. It is worth noting that *KDM6A* is present on chromosome X and demonstrates X linked inheritance which complicates variant interpretation. In this case the individual was a female presenting a chromophobe RCC at age 27 years so adherence to a two-hit model is still feasible. Overall variants in these genes are interesting candidates given the rate of somatic alterations, where 26% of RCC cases across all histological subtypes carry at least one alteration in one of the genes discussed. While interesting candidates, additional studies to confirm function implication of the variants identified and tumour studies to demonstrate LOH which would support their role in RCC predisposition.

Variants were identified after analysis of genes associated with TCA cycle complex components and supporting proteins. Interpretation of these variants in genes such as *ACO1* and *CS* is difficult without functional assessment of the variants and effect on the TCA cycle. Variants in these genes may act similarly to *FH* in HLRCC or *SDH* genes by results in the intracellular accumulation of substrates of the TCA cycle and intermediates such as 2-oxoglutarate which result in the disruption of alpha-ketoglutarate-dependent dioxygenase enzymes such as TET and KDM proteins (229), as well as potential inhibition of PHD proteins in a manner similar to that seen with fumarate and succinate (175). Histopathology in these cases, where available, was 50% papillary RCC, which would be consistent with HLRCC-like tumours if the mechanisms were similar (443). While protein function experiments could be labour intensive, metabolic testing of tumours for accumulated metabolites has been demonstrated for *SDH*-deficient and *FH*-deficient tumours (444) and, in combination with immunohistochemistry for the affected TCA complexes, could rapidly confirm or refute the potential detrimental nature of the variants in this set.

SNV analysis also identified several putative causal variants in genes linked to genetic renal diseases known pathogenic variants associated with renal-related autosomal recessive conditions. The nonsense variant in *PKHD1* (NM_138694: c.C5323T: p.R1775X) which is a known pathogenic variant associated with autosomal recessive polycystic kidney disease. While determining if this variant is causal for the predisposition seen in this individual, it is interesting that an individual harbouring a pathogenic allele for polycystic kidney disease would develop RCC given that cystic disease is a risk factor for RCC (36) and a reported increased susceptibility in autosomal dominant polycystic kidney disease (445), especially given the rate at which somatic alterations occur across RCC tumours (3%). Conversely, whether the loss of the second wild type allele would induce RCC or renal cysts only would require further investigation and that this may be an incidental finding of an individual who is a carrier for autosomal recessive polycystic kidney disease. Assessed in the same manner, the splice variant seen in *NUP93* (NM_014669) could, in autosomal dominant inheritance pattern, confer a risk to RCC but *NUP93* inactivating variants have only been associated with autosomal recessive nephrotic syndrome and though nephrotic syndrome has been associated with increased cancer risk (446) in affected individuals, carriers have not been assessed for increased cancer risk and are infrequently seen somatically. It is also important to note that acquired cystic disease can develop in patients with renal failure and is associated with an increased risk of RCC (447), as such drawing correlations between inherited renal cystic disease, RCC predisposition and renal failure can be difficult.

Gene burden association testing demonstrated reasonably robust statistical metrics given the limited sample size and case-control size discrepancy. Only a single gene reached statistical significance after multiple test correction (FDR) and only a handful of genes were statistically significant prior to FDR correction and known to be associated with cancer. Gene ontology analysis of genes with significant burden, with or without multiple testing correction, failed to identify any relevant biological processes that were enriched in the gene set. The clear limitation in the gene burden analysis is the lack of association after multiple testing correction and the presence of an overabundance of genes surpassing uncorrected significance level due to the observed p value inflation, seen in 5.3 Figure 9. Indications from both the gene burden outcomes and gene ontology enrichment suggest that underlying issues with statistical power and clear issues regarding control of variance between the cases and controls persist. Overall a limited number of conclusions can be drawn from the results presented. Conversely, the gene burden analysis was performed on all coding sequence affecting variants, utilising differing subsets of variant consequences, such as only missense variants may yield different associations though refitting of the model is required. The statistical power of the analysis performed here using SKAT-O could be greatly improved with increased sample size which may allow for statistical associations to be detected and allow for absolute associations between increased gene mutational burden and RCC predisposition.

Finally copy number, short tandem repeat expansion, and mobile element analyses collectively identified very few candidate alterations which could be plausibly linked to RCC predisposition. CNV analysis generated only 10 high quality calls, many of which were partial duplications that are unlikely to result in an altered phenotype. Remaining calls such as the partial deletion of exons 55 and 56 of *NF1* are potentially interesting due to links with predisposition to PCC in neurofibromatosis 1 (MIM: 162200)(448) and the known phenotypic connections between those diseases and RCC (212,385). Conversely, the deletion of those specific exons would result in the truncation of the 2nd and 3rd exons from the final 57th exon which does not appear to harbour any functional domains, though there are two modified phosphoserine residues on the C terminus which may have a function during mitosis (449).

The full coding region deletion of *EP300* due to it encoding the histone acetyltransferase enzyme p300 which regulates chromatin structure and truncating mutations are seen relatively frequently in somatic RCC (2.8%), although heterozygous inactivating variants in *EP300* are associated with Rubinstein–Taybi syndrome (450) and offsetting evidence is available for p300 and its function or role in cancer. The WES-based CNV pipeline has clear limitations, particularly regarding false negatives, which limits this study's ability to detect CNVs. Additionally, the presence of a significant false positive rate means any copy number alteration would need to be validated by conventional methods (i.e. array-based of multiplex-ligation dependent probe amplification) and as such should be interpreted with caution.

The exploratory investigations into the potential for short tandem repeat expansions or mobile elements to be associated with RCC failed to reveal any substantial results and genetic diseases caused by these mechanisms are rare. While these methods did not yield clear and obvious associations, exploring all potential avenues to discover the heritability in RCC utilising rare and under measured sources of genetic alterations may prove critical to identifying factors linked to predisposition which fall outside of the typical paradigms assessed routinely.

5.5 Conclusion

WES analysis of individuals with features of RCC predisposition has uncovered a range of potentially pathogenic or likely pathogenic variants outside of those discovered in chapter 4, as well as a series of VUS variants in genes associated with somatic RCC, other renal-related diseases, and metabolic pathways seen to be altered in both syndromic RCC and PCC. Conversely, case control mutational burden analysis and exploration into copy number alterations and other genetic alteration types did not reveal strong candidates for causes of inherited RCC. Limitations of reduced genomic coverage, poor variant interpretation, and sample sizes have confounded the identification of any robust associations. In particular, power to detect associations given the limited sample size and prior probability of an individual having a monogenic disorder is the major limiting factor and it is likely that only substantially increased sample sizes would be capable of identifying alleles that contribute to RCC predisposition at moderate to low risk rates.

6.0 Characterisation of RCC-associated constitutional chromosomal abnormalities by whole genome sequencing

6.0.1 Table of contents

6.1 Introduction

Constitutional translocations are detected prenatally at a rate of 1 in 109-238 births (0.42-0.92%) (451–453), and large structural variants occur relatively frequently in the general population (454). Chromosomal translocations are subdivided into 3 primary types; balanced, unbalanced, and Robertsonian, each of which result in differential retention or loss of genomic information depending upon the size and type of translocation. Though most translocations are not known to cause genetic disorders, a subset of translocations, particularly those that are unbalanced, have been associated with a number of different diseases including cancer, infertility, neuropsychiatric disorders, and Intellectual/developmental disorders (455–458).

6.1.1 Constitutional translocations in RCC

Four decades ago, Cohen et al (1979) described a large kindred in which clear cell RCC segregated with a constitutional translocation between the short arm of chromosome 3 and the long arm of chromosome 8, t(3;8)(p14.2;q24.1) such that the risk of RCC in translocation carriers was estimated to be 80% at age 60 years (259). Subsequently, somatic deletions of the short arm of chromosome 3 (3p) were found to be the most common cytogenetic abnormality in sporadic clear cell RCC suggesting the presence of critical renal tumour suppressor genes on 3p (126). These developments led to the suggestion that identification of individuals with suspected inherited forms of RCC should be screened for constitutional translocations involving 3p and that the characterisation of RCC-associated translocation breakpoints might lead to the identification of novel inherited RCC genes (459). Subsequent research studies have confirmed that chromosome 3p does indeed harbour several tumour suppressor genes (TSGs) that are frequently inactivated in sporadic RCC (e.g. *VHL, PBRM1, BAP1, RASSF1A*) (25,128,277,389,460–463).

Unlike normal RCC syndromes, which conform to either a two hit hypothesis or constitutional activation of an oncogene, constitutional translocations are suggested to cause RCC predisposition via a three-hit model. The three-hit model of tumourigenesis in translocation-related renal cell carcinomas is theorized as follows: I) presence of constitutional translocations lead to a genomic instability, II) Loss of genomic stability results in the loss of the chromosome 3p region on the derivative chromosome, III) Secondary loss of an allele from genes on the wildtype 3p region, usually *VHL*, leads to complete loss of one or more tumour suppressor genes. Under this model, initial genomic instability is insufficient to induce cancer development and two additional hits are still required to induce neoplastic cell growth, frequently including the loss of tumour suppressors (i.e. *VHL*), although the precise mechanism of the genomic instability is not known.

Translocations may also confer a generalised genomic instability, in which specific loss of 3p is not required, and further inactivation of unknown genes are responsible for tumourigenesis. Alternatively, translocations may result in positional-effect variegation, resulting in differential expression patterns for coding regions under differential chromatin regulation (464). Generalising the model to all translocations, particularly those outside of chromosome 3 has proven more challenging. The lack of known tumour suppressors, intergenic break points, and no relation to commonly lost regions in sporadic RCC cases suggests that other mechanisms are involved in predisposition and tumour progression.

6.1.2 Constitutional translocations in other cancers

Constitutional translocations have been documented in leukaemia (465–468). Recently an overlap between blood-derived cancers and RCC was described with a report of an individual with both RCC and Hodgkin lymphoma concomitantly, in which germline testing identified a constitutional t(6;11)(p21;q12) translocation (469), though the clinical significance is difficult to interpret. Furthermore, translocations have also been linked with a predisposition to Wilm's tumours (470–472) and though translocations are not common in Wilm's tumours, evidence for a non-stochastic mechanism of tumourigenesis via constitutional translocations seems to be present for these cases, implicating genes such as *HACE1* and *BBS9* as a susceptibility genes in Wilm's tumour development (470,472). Many additional studies have shown idiosyncratic presentations of constitutional translocations in cases of oncogenesis, including but not limited to, testicular cancer (473), teratomas (474), thymomas (475), appendiceal carcinomas (476), rhabdomyosarcomas (477), meningiomas (478), retinoblastomas (479), and neuroblastomas (480–482).

6.1.3 Methods for translocation characterisation

Classically, translocations have been identified and characterised by performing an admixture of techniques (including array painting, comparative genomic hybridisation arrays, flow cytogenetic sorting, Fluorescent *in-situ* hybridisation, and YAC/BAC hybridisation), allowing for a steady increase in genomic resolution to a juncture at which break points can be accurately mapped. These techniques, whilst reliable, are laborious and have limited utility for further applications outside of break point mapping.

Comparatively, newer techniques utilising next-generation sequencing at whole genome scale have been used to identify and characterise constitutional translocations, utilising the increased genomic coverage, paired read discordance, and local reassembly to characterise break points (470,483) but have been widely underutilised. The significant drawback of these methods is the financial burden of parallel sequencing, but further utility is provided in WGS approaches to allow for a greater breadth and depth for data interrogation (e.g. single nucleotide variant, structural variation, and copy-number aberrations). Clinical diagnostics may well benefit from a personalised but holistic approach to genomic analysis by providing a greater volume of genetic information with which to interpret disease, including but not limited to detection and analysis of structural rearrangements.

6.1.4 Summary

As discussed above and previously (Introduction section 1.4.10), constitutional translocations have previously been associated with a predisposition to RCC having been identified in numerous families and individuals harbouring translocations, most frequently chromosome 3 and other chromosome partners. Though rare, these translocations have implications for understanding the molecular mechanisms of RCC through characterisation of the chromosomal breakpoints, affected genomic loci, and subsequent observations in RCC tumours. In this chapter, a review of all known RCC-associated translocation cases to-date is performed, assessing the clinical and genetic features across these cases and characterise the breakpoints and molecular genetics of novel RCC-associated translocation cases. Lastly, the use of WGS and new bioinformatics approaches is explored as a methodology for a robust and efficient method of breakpoint characterisation without using techniques used previously in translocation characterisation studies.

6.1.5 Aims

- Determine the clinical, genetic, and molecular features and characteristics of known RCC-associated translocation cases
- Perform molecular and clinical characterisation of 5 novel RCC-associated translocation cases
- Assess the viability of WGS-based and 3rd generation NGS methods for translocation breakpoint characterisation

6.2 Materials and methods

6.2.1 Literature review

Reports of cases of RCC with a constitutional chromosome rearrangement were identified through a search of PubMed using the search terms “renal cell carcinoma” or “renal cancer” or “kidney cancer/tumour” and “rearrangement/inversion/translocation or chromosome” and by searching previously published reports. When previous reports had suggested candidate genes that were either close to or disrupted by the relevant chromosomal breakpoints, evidence to suggest that the genes were implicated in human cancer was sought by reviewing curated data from the Network of Cancer Genes data portal (NCG; http://ncg.kcl.ac.uk/ version 6) (428). Where genes were classified as either ‘known cancer genes’, ‘candidate cancer genes’, or ‘non-cancer genes’. Genes flagged as ‘false positive cancer genes’ were designated as ‘non-cancer genes’.

6.2.2 Clinical studies

Individuals presenting with RCC and with constitutional rearrangements were ascertained through Regional Clinical Genetics Units in the United Kingdom.

6.2.3 Sequence alignment and variant calling

DNA from four probands was sequenced at Novogene as described in materials and methods section 2.6.4. WGS bioinformatics was performed as described in materials and methods section 2.7.

DNA from one proband underwent WGS as part of the NIHR BioResource Rare Diseases study with sequencing and primary bioinformatics performed as previously described in Whitworth *et al* (2018) (376). Data in this instance had been aligned to genome build GRCh37 and all subsequent analysis was performed identically with appropriate adjustments for differences in genome build. All genomic coordinates are reported in GRCh38 and GRCh37 coordinates were remapped using the NCBI remap tool (https://www.ncbi.nlm.nih.gov/genome/tools/remap). Called SNVs were processed and filtered for various quality control metrics and allelic frequency as described in materials and methods section 2.8.

6.2.4 WGS Analysis: Candidate gene analysis and Breakpoint identification

The WGS results were analysed for evidence for rare, potentially pathogenic, SNVs and copy number abnormalities in previously reported inherited RCC genes (VHL, MET, FH, SDHB, SDHD, SDHC, BAP1, CDKN2B) (98,484). Copy number detection was performed using Canvas Copy Number Variant Caller (version 1.39.0.1598) (485), copy number variants were filtered to include calls only marked as “PASS” (See appendix section 9.51). Structural rearrangements and breakpoints were identified using Manta Structural Variant Caller (version 1.3.1) (486). Manta structural variants were filtered to include only calls marked as “PASS”, number of supporting spanning/split reads > 5, QUAL > 100, and call frequency (See appendix section 9.5.1. Breakpoints called on chromosomes matching cytogenetic reports were visually inspected using Integrative Genomics Viewer (IGV - version 2.3.93) to confirm the presence of split and spanning reads (See appendix section 9.5.2).

6.2.5 Nanopore sequencing of translocation breakpoints

Long read sequencing of translocation breakpoint PCR amplicons was performed as described in the materials and methods section 2.9.

6.2.6 Sanger sequencing

Sanger sequencing was performed as described in materials and methods section 2.4 using breakpoint spanning primer pairs (Appendix section 9.5.3). Primer pairs were constructed for each chromosomal breakpoint to span the break point region by inversing the primer pairing (i.e. ChrA-forward ←→ ChrB-reverse & ChrB-forward ←→ ChrA-reverse), in this instance only PCR products specific to the translocation break point should be amplified. Sanger traces are provided in appendix section 9.5.3.

6.2.7 Statistical tests

All statistical tests were performed using R project for statistical computing (version 3.5). Welch’s t-test was performed using the package BSDA (version 1.2.0) with the function tsum.test(). Kruskal–Wallis rank sum test was performed using the base R function kruskal.test(). Fisher’s exact test was performed using the base R function fisher.test(). Statistical testing was undertaken on data from confirmed translocation carriers only.

6.3 Results

6.3.1 Literature review of previously reported cases

A total of 17 previously published distinct constitutional chromosome rearrangements were identified from searches of the biomedical literature (see 6.3 Table 1) (260,459,495–499,487–494). In 15 cases (88%) chromosome 3 was involved (all of which were reciprocal translocations) and there were a variety of partner chromosomes in the 15 translocation cases (e.g. 3 with chromosome 6, 3 with chromosome 8 – see 6.3 Table 1 and 6.3 Figure 1). For the RCC-associated chromosome 3 translocation cases, the breakpoints were almost evenly distributed between the long arm (3q), n=8) and short arm (3p; n=7) and were heterogeneous (see 6.3 Figure 2).

Review of the clinical and pathological data in the previously reported cases demonstrated 9 kindreds with at least 2 related individuals with RCC. In the 4 cases without a family history and available clinical information, multiple RCC was described in 2 individuals. The mean age at diagnosis of a renal tumour in those cases known to carry a constitutional chromosomal rearrangement was 50 years (range 25-82 years). Histopathological details were available for 43 cases and clear cell RCC was reported in 42 cases (98%).

Previous studies have demonstrated that cases of sporadic and familial RCC differ by mean age of diagnosis, with RCC presenting earlier in familial cases (30,129). Comparison of the mean age of diagnosis of RCC in translocation cases to familial and sporadic RCC cases (as reported previously by Maher *et al.* (30)) were 50.2 (SD=12.7), 48.2 (SD=12.3), and 61.8 (SD=10.8) years of age, respectively. Translocation cases have a statistically lower age of diagnosis than those with sporadic disease (Welch's t-test, p=9.84x10-7) but no significant difference between translocation and familial cases was observed (Welch's t-test, p=0.522). Though age of diagnosis across all affected translocation carriers is variable there was no significant difference in age when comparing between familial (with 2 or more related individuals) translocation families (Kruskal–Wallis test, p=0.174).

6.3 Table 1

Clinical features of RCC in individuals from families with a constitutional chromosome rearrangement.

Individuals marked (*) were presumed to be carriers of the relevant rearrangement but were not tested.

Publication(s)	Cytology	Histology	Type (foci = n)	Sex	Age
Cohen et al. [1979]	t(3;8)(pl4.2;q24.1)	clear cell RCC	Bilateral (n=2)	M	37
		clear cell RCC	Bilateral (n=3)	M	45
		clear cell RCC	Unilateral (n>2)	M	59
		clear cell RCC	Unilateral (n=3)	F	46
		clear cell RCC	Unilateral (n=1)	M	44
		clear cell RCC	Unilateral (n=1)	F	50
		clear cell RCC	Bilateral (n>3)	F	41
		clear cell RCC *	Bilateral (n>2)	M	47
		clear cell RCC *	Bilateral (n=9)	F	44
		RCC	Bilateral (n=7)	F	39
Kovacs & Hoene [1988]	t(3;12)(q13.2;q24.1)	clear cell RCC	Unilateral (n=1)	M	50
Kovacs et al [1989]	t(3;6)(p13;q25.1)	clear cell RCC	Bilateral (n = 5)	M	53
Koolen et al. [1998]	t(2;3)(q35;q21)	clear cell RCC	Bilateral (n=3)	M	54
		RCC	N/a	F	53
		clear cell RCC	Unilateral (n=3)	F	68
		clear cell RCC	Unilateral (n=1)	M	40
		clear cell RCC	Bilateral (n=2)	M	30
Van Kessel et al. [1999]	t(3;4)(p13;p16)	clear cell RCC	N/a	M	52
Eleveld et al [2001]	t(3;6)(q11.2;6q13)	clear cell RCC	Unilateral	F	59
		clear cell RCC	Unilateral	F	41

		clear cell RCC	Unilateral	F	63
		clear cell RCC	Unilateral	M	67
Kanayama et al. [2001]	t(1;3)(q32;q13.3)	clear cell RCC	Unilateral (n=1)	F	79
		clear cell RCC	Bilateral (n=4)	M	56
		clear cell RCC *	Unilateral (n=1)	M	70
		clear cell RCC	Unilateral (n=1)	M	62
Podolski et al [2001]	t(2;3)(q33;q21)	clear cell RCC	N/a	M	45
		clear cell RCC	N/a	M	38
		clear cell RCC *	N/a	M	51
		clear cell RCC *	N/a	F	51
		clear cell RCC *	N/a	F	51
		clear cell RCC *	Bilateral	M	51
		clear cell RCC *	N/a	F	63
Meléndez et al. [2003]	t(3;8)(p14.1;q24.23)	clear cell RCC	Bilateral (n = 2)	M	46
		clear cell RCC	Bilateral (n = N/a)	F	56
		clear cell RCC *	N/a	M	68
		clear cell RCC	Bilateral (n = N/a)	M	25
		clear cell RCC	Bilateral (n = N/a)	M	66
		clear cell RCC	Bilateral (n = N/a)	M	82
		clear cell RCC	Bilateral (n = N/a)	M	44
		clear cell RCC	Bilateral (n = N/a)	F	39
		clear cell RCC	Unilateral (n = N/a)	F	44
Bonne et al [2007]	t(3;15)(p11;q21)	clear cell RCC	N/a	F	49
	ins(3;13)(p24.2;q32q21.2)	clear cell RCC	N/a	N/a	74

Foster et al. [2007]	t(3;6)(q22;q16.2)	clear cell RCC papillary RCC	Bilateral (n=3)	M	49
Poland et al. [2007]	t(3;8)(p14;q24.1)	clear cell RCC	Bilateral (n = N/a)	F	47
		clear cell RCC	Bilateral (n = N/a)	M	39
Kuiper et al. [2009]	t(3;4)(q21;q31)	clear cell RCC	N/a	N/a	45
McKay et al [2010]	t(2;3)(q36.3;q13.2)	clear cell RCC	Bilateral (n = 8)	M	54
		clear cell RCC	N/a	M	50
		clear cell RCC	Unilateral (n > 1)	F	35
Doyen et al [2012]	t(11;22)(q23-24;q11.2-12)	clear cell RCC	Unilateral (n = 1)	M	72
Wake et al. [2013]	t(5;19)(p15.3;q12)	oncocytoma chromophobe RCC	Unilateral (n = 2)	F	35
		clear cell RCC chromophobe RCC oncocytoma	Bilateral (n > 2)	F	36

6.3 Figure 1

Circos plots visualising constitutional chromosomal rearrangements. Previously published translocations shown in blue and rearrangements identified in this study shown in orange. Width of the region at the ends of each ribbon represents the proportion of each chromosome which is translocated with its corresponding translocation partner. 1A contains all previously published translocations and translocations in the current series, 1B contains only rearrangements in this series, and 1C contains only previously published translocations.

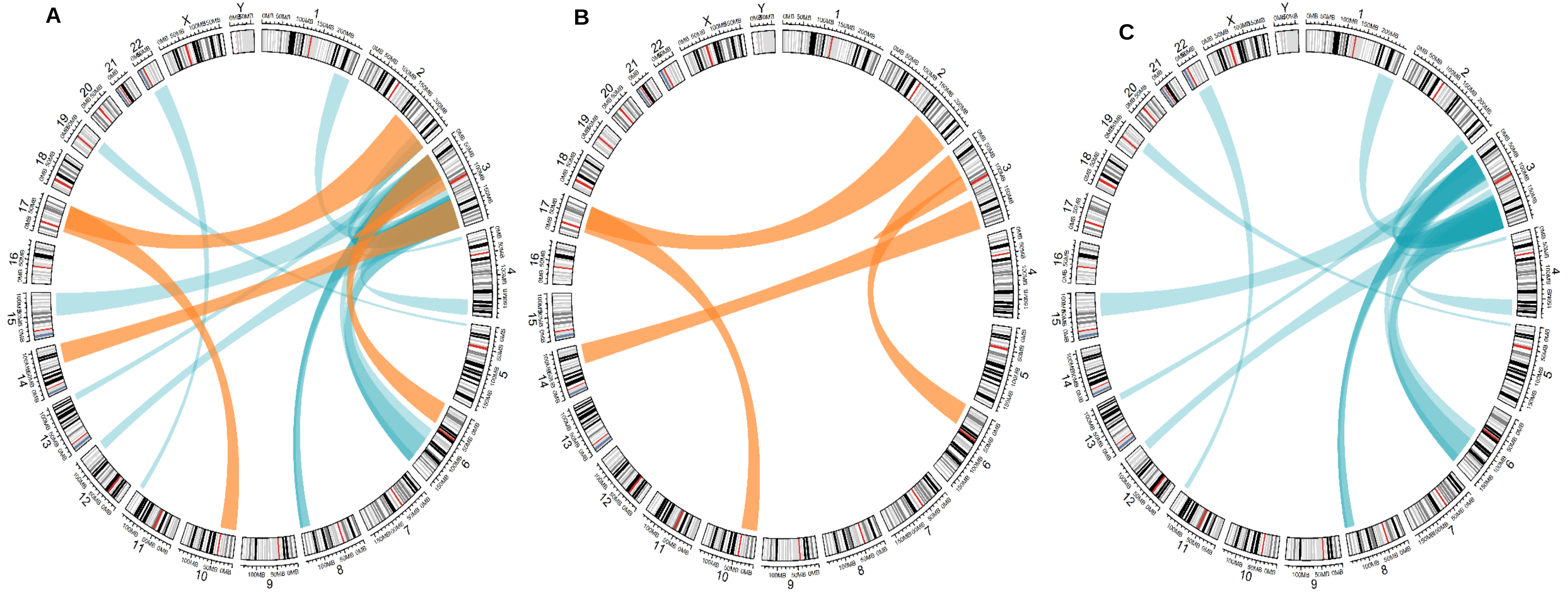

6.3 Figure 2

Diagram illustrating the position of chromosome 3 translocation breakpoints across the p and q arms. Differentially shaded portions represent different cytobands, the red region represent the centromeric region. Positions given in cases without base pair resolution are presented with a horizontal bar across the given cytoband in the translocation karyotype.

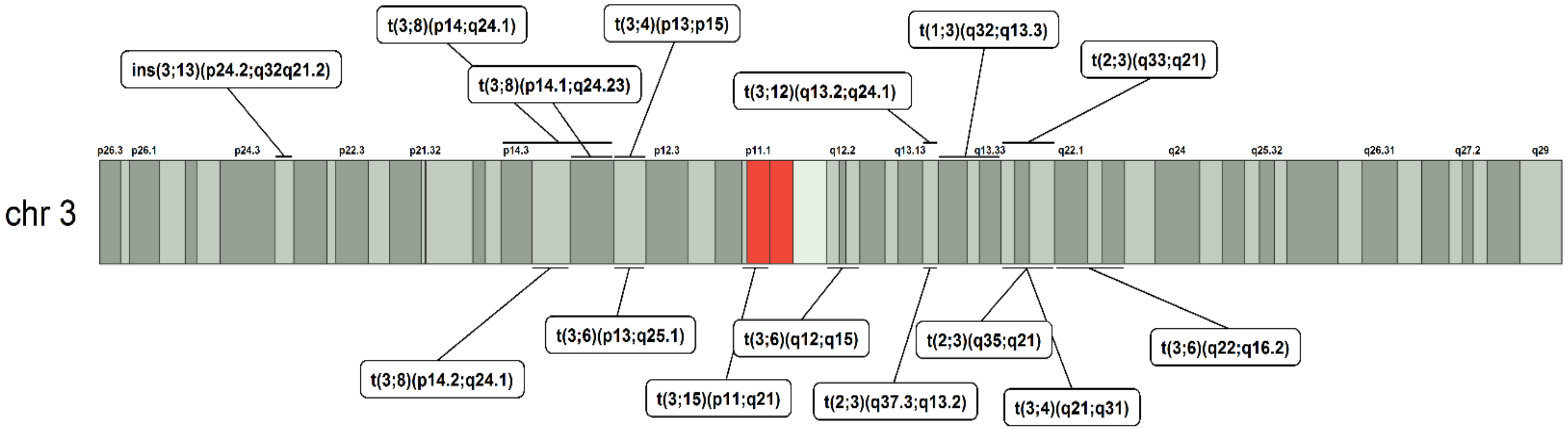

The chromosomal rearrangement breakpoints had been mapped in 15 of 17 previously reported cases and a total of 10 candidate genes had been reported to be disrupted by the relevant rearrangement breakpoints (6.3 Table 2). Additionally, 21 genes found to be in the vicinity of translocation breakpoints and cited as relevant genes by the authors of the original report were also assessed (6.3 Table 3). The evidence for implicating the various genes in RCC predisposition was assessed using NCG data portal (6.3 Table 2 & 3).

Of the 10 genes directly disrupted by translocation breakpoints, 20% (2/10) are classified as known cancer genes (of a total of 2372 curated cancer genes), with all remaining genes having no evidence supporting their role in cancer. Regarding genes stated to be in the vicinity of translocation breakpoint, 2 were designated as known cancer genes and 4 were classified as candidate cancer genes.

6.3 Table 2

Reassessment of genes disrupted by translocation breakpoints in RCC-associated translocations reported previously. Genes were categorised according to their current status in NCG v6.0 (428)

Original publication	Affected genes	Position (GRCh38)	Known cancer gene (NCG 6.0)
Cohen et al. [1979]	*FHIT*	chr3:59747587-61251459	Known cancer gene
Cohen et al. [1979]	*RNF139 (TRC8)*	chr8:124474738-124488618	Non-cancer gene
Kovacs et al [1989]	*STXBP5*	chr6:147204358-147390476	Non-cancer gene
Koolen et al. [1998]	*SLC49A4 (DIRC2)*	chr3:122794795-122881139	Non-cancer gene
van Kessel et al. [1999]	*KCNIP4*	chr4:20728606-21948801	Non-cancer gene
Kanayama et al. [2001]	*LSAMP*	chr3:115802363-117139389	Non-cancer gene
Kanayama et al. [2001]	*RASSF5 (NORE1)*	chr1:206507530-206589448	Non-cancer gene
Podolski et al [2001]	*DIRC1*	chr2:188733738-188839420	Non-cancer gene
Kuiper et al. [2009]	*FBXW7*	chr4:152320544-152536095	Known cancer gene
Wake et al. [2013]	*UBE2QL1*	chr5:6437347-6496721	Non-cancer gene

6.3 Table 3

Reassessment of genes highlighted as being close to translocation breakpoints in RCC-associated translocations reported previously. Genes were categorised according to their current status in NCG v6.0 (428)

Original publication	Affected genes	Position (GRCh38)	Known cancer gene (NCG 6.0)
Meléndez et al 2003	*LRIG1*	chr3:66378797-66501263	Candidate cancer gene
Wake et al 2013	*CCNE1*	chr19:29811898-29824312	Known cancer gene
Kuiper et al 2009	*C3orf56*	chr3:127193131-127198185	Non-cancer gene
Foster et al 2007	*PPP2R3A*	chr3:135965673-136147891	Non-cancer gene
Foster et al 2007	*PCCB*	chr3:136250306-136337896	Non-cancer gene
Foster et al 2007	*STAG1*	chr3:136336233-136752403	Known cancer gene
Foster et al 2007	*MSL2 (RNF184)*	chr3:136148922-136197241	Non-cancer gene
Foster et al 2007	*EPHB1*	chr3:134597801-135260467	Non-cancer gene
Foster et al 2007	*EPHA7*	chr6:93240020-93419547	Non-cancer gene
Podolski et al 2001	*HIBCH*	chr2:190189735-190344193	Non-cancer gene
Podolski et al 2001	*INPP1*	chr2:190343470-190371665	Non-cancer gene
Podolski et al 2001	*HNRNPC* (*HNRPC*)	chr14:21209136-21269494	Non-cancer gene
Koolen et 1998	*HSPBAP1*	chr3:122740003-122793824	Non-cancer gene
Koolen et 1998	*SEMA5B*	chr3:122909082-123028605	Candidate cancer gene
Yusenko et al 2010	*PDZRN3*	chr3:73382433-73624940	Candidate cancer gene
Yusenko et al 2010	*CNTN3*	chr3:74262568-74521140	Non-cancer gene
Yusenko et al 2010	*NECTIN3* (*PVRL3*)	chr3:111070071-111275563	Non-cancer gene
Yusenko et al 2010	*HSPB8*	chr12:119178642-119221131	Candidate cancer gene
Yusenko et al 2010	*CCDC60*	chr12:119334712-119541047	Non-cancer gene
Cohen et al 1979	*TRMT12*	chr8:124450820-124462150	Non-cancer gene
Cohen et al 1979	*TATDN1*	chr8:124488485-124539458	Non-cancer gene

6.3.2 Clinical features of previously unreported cases

Five previously unreported constitutional chromosomal rearrangements ascertained through a patient presenting with RCC were identified through UK genetics services. The cytogenetic, clinical features and pathological features of the five probands and (when relevant) their affected relatives are described in 6.3 Table 4. There were 4 translocations (involving chromosome 3 in two cases) and a pericentric inversion of chromosome 3 (see 6.3 Table 4 and 6.3 Figure 1). Two or more individuals developed RCC in 3 kindreds:

In the kindred with the t(3;14)(q13.3;q22) 5 individuals developed RCC (four of whom were confirmed or obligate translocation carriers). The proband presented with bilateral RCC at age 75 years, his daughter (an obligate carrier) died from RCC at age 36 years, his mother and two of his brothers were reported to have developed RCC at ages 51, 41 and 79 years respectively. The proband's mother and brother with RCC at ages 51 and 79 years were also obligate t(3;14)(q13.3;q22) carriers and the son of the latter developed RCC at age 67 years and was confirmed to have inherited the t(3;14)(q13.3;q22).

In the kindred with the t(3;6)(p14.2;p12) rearrangement, the proband presented with RCC at age 72 years and four relatives were demonstrated to also harbour the translocation. Three had not developed RCC (age at last follow up 47-52 years) but one (the proband's brother) had developed bilateral clear cell RCC age 55 years with unilateral recurrent disease and an adrenal metastasis age 74 years and his son died from RCC at age 40 years without any record of his status for the t(3;6)(p14.2;p12).

The index case carrying the inv(3)(p21.1q12) was unaffected but was ascertained following a report that her cousin had developed clear cell RCC at age 39 and harboured the chromosome 3 inversion. Other carriers of the inversion in the family who were reported to carry the inversion, but were unaffected, included her paternal aunt and father, whilst her grandfather was also a carrier and died of carcinomatosis at age 80 years. The proband's brother was diagnosed with RCC at age 48 but was not tested for the inversion.

The t(2q21.1; 17q11.2) was identified in a 37 year old man with a poorly differentiated clear cell RCC who died from metastatic disease shortly thereafter. The translocation was maternally inherited and was detected in three unaffected family members (mother and two siblings) aged between 30 and 58 years of age.

In the kindred with the t(10;17)(q11.21;p11.2) the proband and their sibling were found to have features of suggestive Birt-Hogg-Dubé syndrome (BHD; OMIM: 135150) (pneumothoraces, and fibrofolliculomas in the proband and multiple pulmonary cysts and fibrofolliculomas in his sister) after the diagnosis of RCC in the proband and the detection of the translocation.

6.3 Table 4

Clinical details of families harbouring RCC-related translocations cases in this series

Patient	Carrier	Sex	Age	RCC histology	Sanger	Break points	Additional notes
t(2;17)(q21;q11.2)	Yes	M	37	Clear cell RCC	Yes	chr2:130693727 chr17:28031855	
t(2;17)(q21;q11.2) Grandfather	Unknown	M	?	RCC		N/a	
t(3;6)(p14.2;p12)	Yes	M	72	N/a	Yes	chr3:66680663 chr6:54817716	
t(3;6)(p14.2;p12) Relative 1	Yes	N/a	55	Clear cell RCC	No	N/a	Recurrent RCC Adrenal metastasis
t(3;6)(p14.2;p12) Relative 2	Yes	N/a	?	RCC		N/a	
inv(3)(p21.1q12)	Yes	F	N/a	Unaffected	No	N/a	
inv(3)(p21.1q12) Cousin	Yes	N/a	39	Clear cell RCC		N/a	
inv(3)(p21.1q12) Brother	Unknown	M	48	RCC		N/a	
t(3;14)(q13.3;q22)	Yes	M	75	Clear cell RCC	Yes	chr3:125771297 chr14:59009871	Bladder carcinoma
t(3;14)(q13.3;q22) Nephew	Yes	M	67	RCC	Yes	chr3:125771297 chr14:59009871	
t(3;14)(q13.3;q22) Brother-obligate	Obligate	M	41	Clear cell RCC	No	N/a	
t(3;14)(q13.3;q22) Daughter	Obligate	F	36	RCC	No	N/a	
t(3;14)(q13.3;q22) Brother	Obligate	M	79	RCC	No	N/a	
CAMB-AL-GM13.12941 Mother	Obligate	F	51	RCC	No	N/a	
t(10;17)(q11.21;p11.2)	Yes	M	53	Clear cell RCC	Yes	N/a	Fibrofolliculomas Pneumothoraces
t(10;17)(q11.21;p11.2) Relative	Yes	F	N/a	Unaffected		N/a	Fibrofolliculomas Lung cysts Renal cysts

6.3.3 Whole genome sequencing and bioinformatics

Sequencing metrics were assessed to confirm data reliability and suitability for downstream SNV, SV, and CNV analysis. Mean sequence alignment rates across all samples was 99.7%, indicating a high-quality sequence mapping. WGS coverage analysis demonstrated a mean coverage of 28.9X across all genomes, though the genome analysed as part of NIHR Rare diseases bioresource study had mean coverage of 35X due to a different sequencing methodology. For variant calling, the transition / transversion ratio (Ts/Tv) after minimal genotype filtering (depth > 10 and QUAL > 30) was reported as 1.93, suggesting no variant calling bias across the genome.

6.3.4 Characterisation of constitutional rearrangements in previously unreported cases

WGS did not identify any plausible likely pathogenic or pathogenic SNVs or CNVs variants in previously reported inherited RCC genes (*VHL, SDHB, SDHC, SDHD, MET, FLCN, TSC1, TSC2, FH, PTEN, PBRM1, BAP1,* or *CDKN2B*) in the four probands who were affected by RCC. A novel missense variant of uncertain significance by ACMG criteria (325) was identified in *PBRM1* (NM_018313.4:c.2446A>T p.Asn816Tyr) in the t(3;6)(p14.2;p12) translocation case. DNA from an affected individual was not available for sequencing in the family carrying the inv(3)(p21.1q12) inversion, as such sequencing was performed solely to identify candidate breakpoints. Candidate rearrangement breakpoints were identified from the WGS data by the Manta structural variation detection algorithm in all five cases:

Breakpoints for translocation t(3;14)(q13.3;q22) were resolved to be present at the loci chr3:125771297 and chr14:59009871. The candidate breakpoints were supported by 7 and 9 spanning and split reads, respectively (Appendix section 9.5.4). The candidate breakpoint locations identified by WGS differed from those suggested previously by cytogenetic studies: the 3q breakpoint at chr3:125771297 is within cytoband 3q21 and the WGS-identified 14q breakpoint at chr14:59009871 maps to 14q23.1. Sanger sequencing confirmed the presence of the translocation breakpoints. Sanger sequencing in a DNA sample from his affected nephew confirmed identical breakpoints to the proband. The 3q breakpoint intersects with *LOC105374312*, an uncharacterised non-coding RNA gene and the 14q breakpoint disrupts the last intron of *LINC01500*, a long intergenic non-coding RNA gene, and is predicted to result in a truncated transcript lacking the final exon.

WGS in the second chromosome 3 associated translocation case t(3;6)(p14.2;p12) revealed candidate breakpoints at chr3:66680663 and chr6:54817716 within an AT-rich repetitive region. Breakpoint calls were supported by 4 and 7 spanning and split read calls, respectively (Appendix section 9.5.4). Sanger sequencing confirmed the presence of the translocation breakpoints. The 3p chromosomal breakpoint identified by WGS mapped within 3p14.1 and disrupted *LOC105377142*, an uncharacterised non-coding RNA. The 6p breakpoint did not disrupt a predicted gene but was 29 kb upstream of *FAM83B*.

The candidate breakpoints in the inv(3)(p21.1q12) were identified by Manta with 11 spanning and 11 split reads supporting the presence of this inversion, though the number of reference spanning reads was only 2 (Appendix section 9.5.4). The two candidate breakpoints mapped to chr3:59964935 at 3p14.2 (interrupting intron 7 of *FHIT*) and chr3:98667603 (3q12), 47 kb upstream of *ST3GAL6-AS1*, a non-coding RNA gene. Though cytogenetics and Manta calls support the presence of the inv(3)(p21.1q12), Sanger sequencing under multiple experimental conditions failed to generate any PCR products and the candidate breakpoints could not be independently confirmed.

WGS in the first of the two non-chromosome 3 translocations (t(2;17)(q21.1;q11.2)) localised the breakpoints to chr2:130693728 (2q21.1) and chr17:28030855 (17q11.2). The translocation breakpoint was supported by 9 spanning and 10 split reads as called by Manta (Appendix section 9.5.4). Sanger sequencing confirmed the genomic coordinates and breakpoint as a single base translocation without local rearrangement, insertions, or deletions. The breakpoint present on chromosome 2 disrupted the coding region of two overlapping pseudogenes *KLF2P3* and *FAR2P3*, as well as interrupting a CpG island spanning chr2:130693485-130693839. The nearest coding genes were *POTEJ*, *AMER3*, and *GPR148* which were 35 kb upstream, 34 kb downstream and 62 kb downstream, respectively. The junction on chromosome 17 did not disrupt any known coding region but was 1.7 kb upstream of a reported H3K27Ac element covering chr17:28,033,593-28,035,092, and 9.9 kb upstream of the *NLK* gene.

The second non-chromosome 3 translocation t(10;17)(q11.22;p12) underwent sequencing as part of the NIHR BioResource Rare Diseases BRIDGE project (see methods 6.2) and was analysed previously as part of a multiple primary tumour cohort (34) with a history facial fibrofolliculomas, recurrent pneumothoraces and RCC. At that time no abnormality was detected but subsequently reanalysis identified candidate translocation breakpoints that were supported by two overlapping Manta calls for the chromosome 10 and chromosome 17 breakpoints at chr17:17218211-17218214 (17p11.2) and chr10:43236047-43236050 (10q11.21) that were supported by 22 spanning and 10 split reads and a secondary call at chr17:17218216-17218217 and chr10:43236058-43236059 by 15 spanning and 18 split reads (Appendix section 9.5.4). Given the proximity of the assigned breakpoint regions, a single translocation was presumed with an additional nested structural variation resulting in divided calling. Sanger sequencing confirmed the presence of the translocation breakpoint in the proband. The chromosome 17 breakpoint prediction disrupted the coding region of *FLCN*, falling within intron 9 (ENST00000285071). The chromosome 10 breakpoint disrupted the first intron of *RASGEF1A* (the first exon encodes 5' untranslated region only proximal to the translation initiation site (ENST00000395810). Sanger sequencing of DNA from the proband's sibling (who was known to carry the t(10;17)(q11.22;p12)) confirmed that translocation breakpoint and that she had evidence of BHD syndrome (multiple lung and renal cysts and facial fibrofolliculomas).

6.3.5 Characterisation of translocation breakpoints utilising Nanopore sequencing

While Sanger sequencing of translocation breakpoints can effectively confirm the presence or absence of a breakpoint, and in some instances provide characterisation of breakpoints, many translocation break points are complex or involve additional genomic alterations such as deletions and insertions of additional bases, particularly in repetitive regions. Herein demonstrates the utility of Nanopore sequencing for the base-level characterisation of one of the newly reported translocation cases, t(3;14)(q13.3;q22), which contained an ambiguous region at the break site by multiple sequence alignment of breakpoint-spanning PCR products due to increased sequencing read sizes.

Assessment of Nanopore sequencing metrics determined the sequencing run generated 46,431 reads across the translocation breakpoint with a median read length of 815 bp from 474 of 512 active sequencing channels from breakpoint-spanning PCR products. Mean read qualities were most frequent at 8-12, suggesting high quality sequencing was generated (6.3 Figure 3). Nanopore sequencing was aligned to GRCh38 and generated 75,096 mapped reads. Discrepancy between number of sequenced reads and the number of mapped reads is due to the presence of supplementary read alignments, which are defined as reads with two distinct but split mapping positions, as would be expected from a translocation breakpoint. Of those reads 71,927 (95.8%) reads intersected the translocation breakpoints (chr3:125771297 and chr14:59009871) determined by Manta.

Read alignments were visualised using IGV (6.3 Figure 4) which demonstrated the translocation breakpoint succinctly, showing aligned reads split evenly between chromosome 3 and 14. Comparisons between Nanopore alignments and Sanger sequencing alignments allowed for the resolution of a 5 bp deletion on chromosome 14 (5’-ATGTGTGG) at the breakpoint site whereas chromosome 3 did not appear to have any additional structural rearrangements.

6.3 Figure 3

Quality metrics from Nanopore sequencing metrics for the t(3;14)(q13.3;q22) translocation PCR amplicon. 3A Histogram plot binning the mean read quality for all generated Nanopore sequencing reads. 3B Plot shows the cumulative number of Kb of sequencing generated over time during Nanopore sequencing until the run was stopped. 3C Histogram plot shows the binning of read lengths generated by Nanopore sequencing, most reads match the size of the PCR breakpoint amplicon. 3D A channel map of the Nanopore sequencing channels depicting the number of Kb generated by each pore/channel. All sequencing metrics shown here are suggestive of high-quality sequencing data.

D

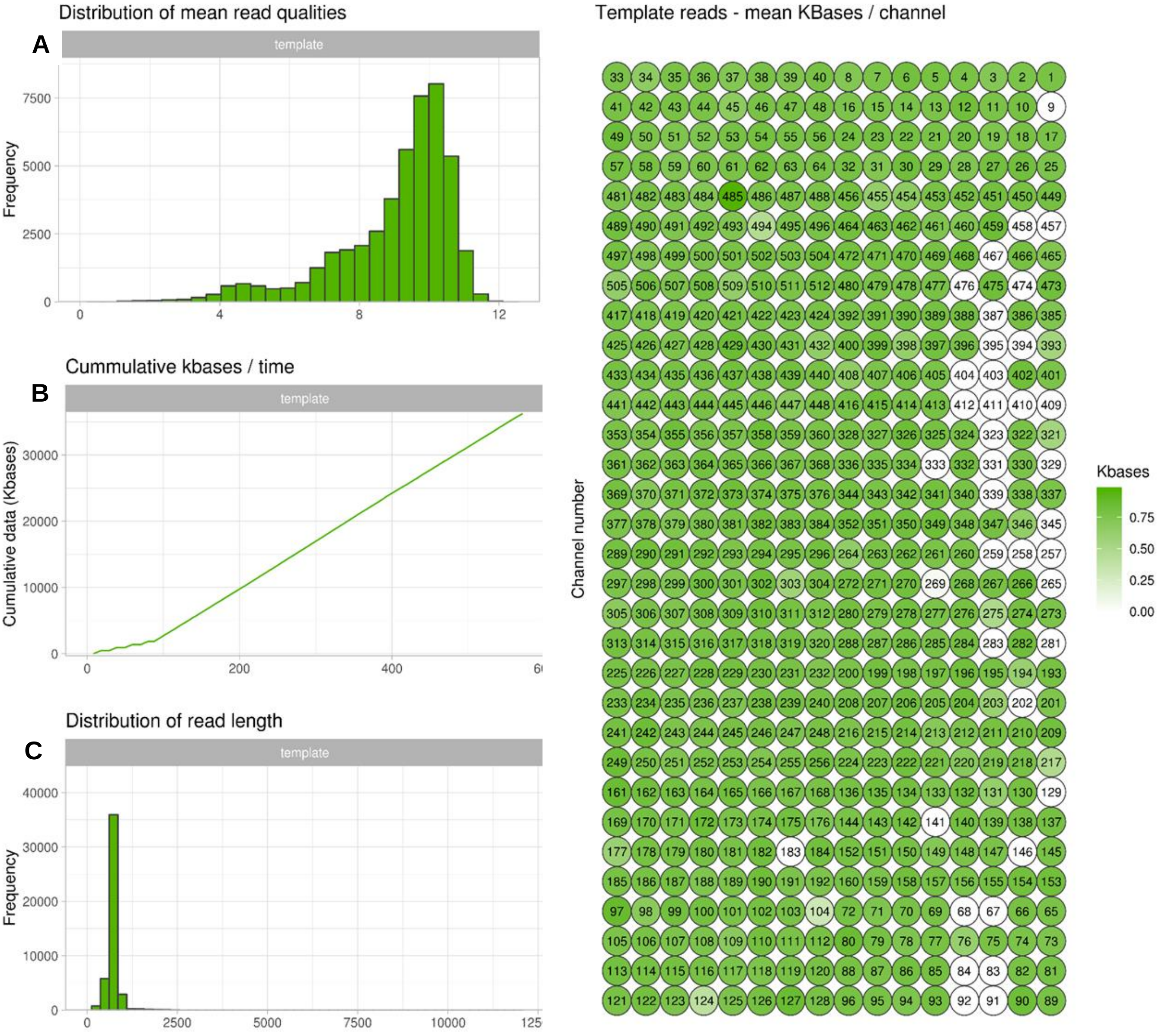

33	34	35	36	37	38	39	40	8	7	6	5	4	3	2	1
41	42	43	44	45	46	47	48	16	15	14	13	12	11	10	9
49	50	51	52	53	54	55	56	24	23	22	21	20	19	18	17
57	58	59	60	61	62	63	64	32	31	30	29	28	27	26	25
481	482	483	484	485	486	487	488	456	455	454	453	452	451	450	449
489	490	491	492	493	494	495	496	464	463	462	461	460	459	458	457
497	498	499	500	501	502	503	504	472	471	470	469	468	467	466	465
505	506	507	508	509	510	511	512	480	479	478	477	476	475	474	473
417	418	419	420	421	422	423	424	392	391	390	389	388	387	386	385
425	426	427	428	429	430	431	432	400	399	398	397	396	395	394	393
433	434	435	436	437	438	439	440	408	407	406	405	404	403	402	401
441	442	443	444	445	446	447	448	416	415	414	413	412	411	410	409
353	354	355	356	357	358	359	360	328	327	326	325	324	323	322	321
361	362	363	364	365	366	367	368	336	335	334	333	332	331	330	329
369	370	371	372	373	374	375	376	344	343	342	341	340	339	338	337
377	378	379	380	381	382	383	384	352	351	350	349	348	347	346	345
289	290	291	292	293	294	295	296	264	263	262	261	260	259	258	257
297	298	299	300	301	302	303	304	272	271	270	269	268	267	266	265
305	306	307	308	309	310	311	312	280	279	278	277	276	275	274	273
313	314	315	316	317	318	319	320	288	287	286	285	284	283	282	281
225	226	227	228	229	230	231	232	200	199	198	197	196	195	194	193
233	234	235	236	237	238	239	240	208	207	206	205	204	203	202	201
241	242	243	244	245	246	247	248	216	215	214	213	212	211	210	209
249	250	251	252	253	254	255	256	224	223	222	221	220	219	218	217
161	162	163	164	165	166	167	168	136	135	134	133	132	131	130	129
169	170	171	172	173	174	175	176	144	143	142	141	140	139	138	137
177	178	179	180	181	182	183	184	152	151	150	149	148	147	146	145
185	186	187	188	189	190	191	192	160	159	158	157	156	155	154	153
97	98	99	100	101	102	103	104	72	71	70	69	68	67	66	65
105	106	107	108	109	110	111	112	80	79	78	77	76	75	74	73
113	114	115	116	117	118	119	120	88	87	86	85	84	83	82	81
121	122	123	124	125	126	127	128	96	95	94	93	92	91	90	89

6.3 Figure 4

Composite image of read alignments mapped in t(3;14)(q13.3;q22) translocation cases. Mapped reads show split (supplemental) alignments to both chromosome 3 and 14 breakpoint regions. Soft clipped bases (highlighted in multiple colours) correspond to the regions mapped to the opposite chromosome.

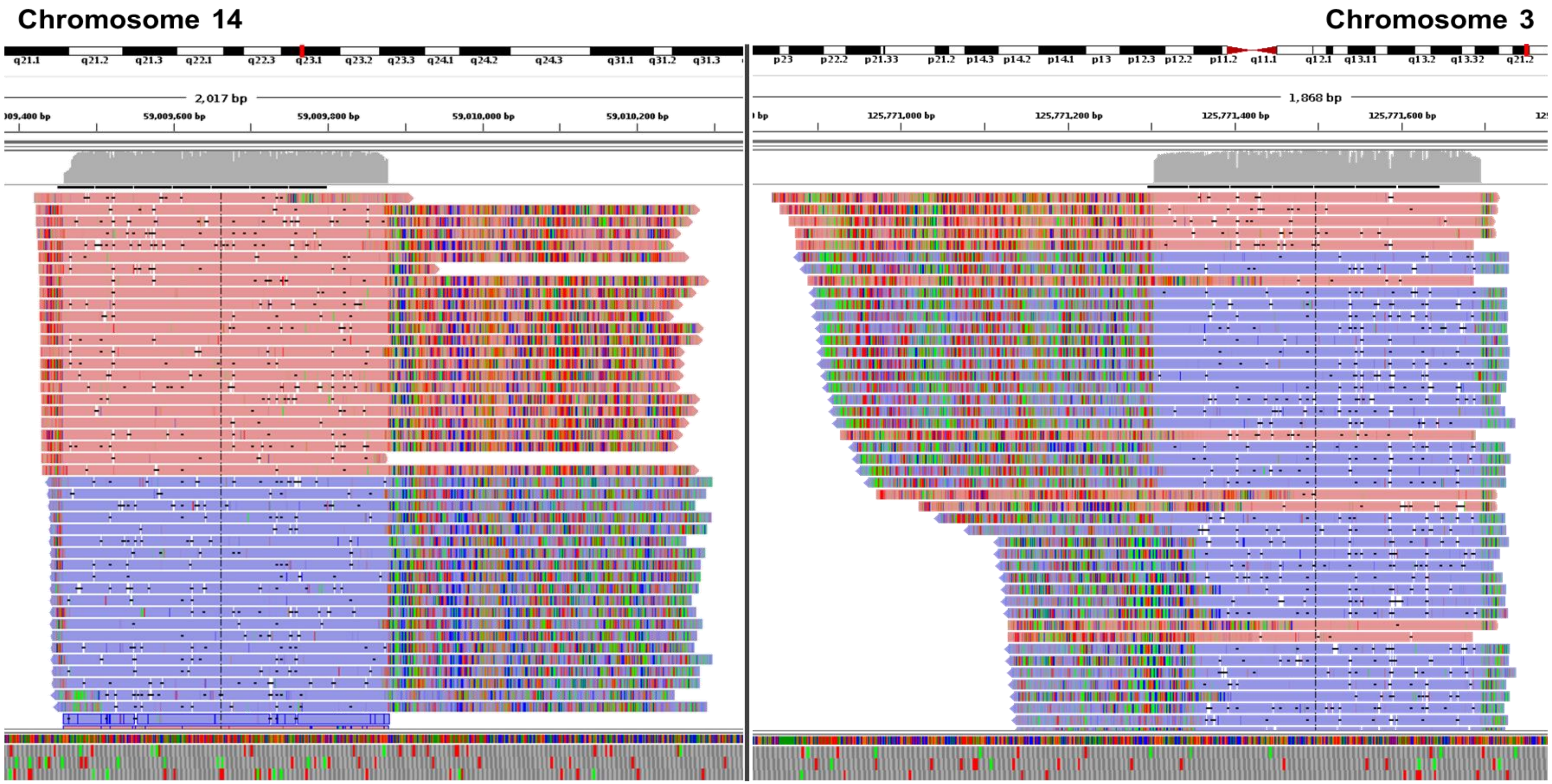

6.3.6 Computational evaluation of breakpoint-related genes

The five constitutional rearrangements were confirmed or postulated to disrupt three protein coding genes (*FHIT*, *FLCN* and *RASGEF1A*) and to map within 50 kb of four more genes (*FAM83B*, *POTEJ*, *AMER3*, *NLK*). Two of these genes, *FHIT* and *FLCN* have been previously implicated as renal tumour suppressor genes (191,195) and potential evidence for a role of *RASGEF1A*, *FAM83B*, *POTEJ*, *AMER3* and *NLK* in hereditary cancer predisposition and/or somatic tumourigenesis was sought from the NCG data portal (6.3 Table 5). On the NCG data portal both *FHIT* and *FLCN* were classified as “known cancer genes”, *RASGEF1A* as a “candidate cancer gene” and the other genes were categorised as “non-cancer genes”.

6.3 Table 5

Assessment of genes disrupted by (*) or close to breakpoints in RCC-associated rearrangement reported in the current series. Genes were categorised according to their current status in NCG v6.0 (428)

Affected genes	Position (GRCh38)	Consensus (NCG 6.0)
FHIT *	chr3:59747587-61251459	Known cancer gene
FLCN *	chr17:17206924-17237188	Known cancer gene
FAM83B	chr6:54846643-54945099	Non-cancer gene
POTEJ	chr2:130611413-130658448	Non-cancer gene
AMER3	chr2:130755435-130768134	Non-cancer gene
NLK	chr17:28041737-28205140	Non-cancer gene
RASGEF1A *	chr10:43194533-43266919	Candidate cancer gene

6.4 Discussion

This study reports five previously unreported RCC-associated constitutional chromosomal rearrangements that increase the total number of rearrangements reported to 22 and the number of cases in which the breakpoints have been characterised to 20. WGS enabled both the identification of candidate translocation breakpoints and simultaneously excluded coincidental pathogenic SNVs and CNVs in known hereditary cancer genes. With the increasing availability and reducing cost of WGS it will become increasingly feasible to characterise the molecular pathology of RCC-associated constitutional chromosomal rearrangements. This will improve our understanding of the relevance to individual RCC-associated constitutional chromosomal rearrangements to the RCC tumourigenesis and we found that the breakpoint location reported on routine cytogenetic analysis often did not correspond to the breakpoint locations identified by WGS.

The majority (21/22, 95.5%) of RCC-associated constitutional chromosomal rearrangements reported to date have been associated with the clear cell variant of RCC. This is the most common histological subtype of sporadic RCC (75-80%) and is characterised by somatic inactivation of *VHL* and deletions of chromosome 3p (25,128,460,500). The mean age at diagnosis of RCC in the cases reported to date (51 years, range 25-82, n=57, SD=13.25) is younger than the average age for sporadic RCC (61.8 years) (30). Whilst this is a feature of other forms of hereditary RCC (and many other inherited cancer types) there may also be an element of ascertainment bias with early onset cases more likely to be investigated for a genetic cause. Given the loss of the derivative chromosomes is reported as the potential initiator of tumourigenesis in chromosome 3 translocations, the loss of der(3) in the t(3;14) translocation would also result in the loss of 14q which would include the *HIF1A* coding region, a candidate 14q TSG (501).

In both this series and the previously published literature series, most RCC-associated constitutional chromosome rearrangements involved chromosome 3. Whilst this is consistent with the high frequency of 3p allele loss in sporadic clear cell RCC, the fundamental role of somatic inactivation of the *VHL* TSG in clear cell RCC and the incidence of somatic mutations of *PBRM1*, *BAP1* and *SETD2* in RCC, to date most RCC-associated constitutional chromosome 3 rearrangements do not appear to disrupt known RCC TSGs mapping to 3p. A potential explanation for this is the observation that RCC from individuals with a constitutional chromosome 3 translocation can show a somatic *VHL* mutation on the wild-type chromosome 3 and loss of the derivative chromosome containing 3p (resulting in biallelic inactivation of the *VHL* TSG).

This mechanism of tumourigenesis would imply that the susceptibility to RCC might have resulted from instability of the translocated chromosome rather than disruption of a specific RCC TSG at the translocation breakpoint on chromosome 3 (261) and would be consistent with the variability of the RCC-associated chromosome 3 rearrangement breakpoints described to date (6.3 Table 1). However, it is interesting that the chromosome 3 inversion described it was associated with a breakpoint within the *FHIT* gene. Previously it was demonstrated in two apparently unrelated families with a RCC-associated t(3;8)(p14.2;q24.1) harboured breakpoints that disrupted *FHIT* and *RNF139* (*TRC8*) on 3p and 8q respectively (16,22). *FHIT* is listed as a Tier 1 known cancer gene in the Cancer Gene Census (https://cancer.sanger.ac.uk/cosmic/census) however the presence of a somatic *VHL* mutation and loss of the translocated chromosome 3 in a previous t(3;8)(p14.2;q24.1)-associated RCC was unexpected (259,492) indicating multiple routes of pathogenicity for RCC-associated translocations.

It is possible that the recurrent involvement of *FHIT* in RCC-associated chromosome 3 rearrangements reflects the presence of palindromic AT-rich repeats at the t(3;8)(p14.2;q24.1) breakpoint and causes a propensity to recurrent rearrangements at this locus (502), but note that only a fraction of chromosome 3 translocations are associated with predisposition to RCC (503). It is therefore conceivable that both instability of the translocated chromosome and mono-allelic inactivation of *FHIT* contribute to RCC susceptibility. Other genes that have been previously reported to be located at or close to the breakpoints of RCC-associated chromosome 3 rearrangements (see 6.3 Table 2, 3 and 5) were reviewed to determine which were included in recently compiled lists of known cancer genes which are based on the results of recent large scale cancer genomics projects and 8 genes (*FHIT, LRIG1, FBXW7, CCNE1, STAG1, SEMA5B, PDZRN3, HSPB8*) were identified as known or candidate cancer genes. In addition, genes that were disrupted (*FHIT, FLCN, RASGEF1A*) or close to (*FAN83B, POTEJ, AMER3, NLK*) the breakpoints of the novel RCC-associated translocations reported here were also assessed and the three genes that were disrupted were classified as known (*FLCN* and *FHIT*) or candidate cancer genes (*RASGEF1A*) (6.3 Table 5).

Relatively few RCC-associated constitutional translocations not involving chromosome 3 have been reported. In addition to the two novel cases reported here, there are two previously reported cases (498,499) and the translocation breakpoints were characterised in only one of these cases. It is entirely possible that non-chromosome 3 constitutional translocations and RCC may occur coincidentally and, though there was an early age at onset (37 years) in the proband with t(2q21.1; 17q11.2) and an unconfirmed family history of RCC in his paternal grandfather, the translocation was also found in his mother and two siblings who were unaffected at ages 58, 40 and 31 years. However, identification of a translocation breakpoint that disrupted the *FLCN* gene in a patient with a t(10;17)(q11.22;p12) illustrated the value of characterising all RCC-associated constitutional rearrangements. Inactivating mutations in *FLCN* cause BHD syndrome which is characterised by facial fibrofolliculomas, pulmonary cysts and pneumothorax and RCC (191,504). The occurrence of fibrofolliculomas is age-dependent and pneumothorax occur in minority of cases and so BHD may present with RCC without other features being present (265), although rarely. However in the family reported here the t(10;17)(q11.22;p12) was associated with other evidence of BHD syndrome. To my knowledge this is the first description of a constitutional translocation causing BHD syndrome.

The other novel translocation case did not disrupt a known cancer gene but occurred close to *Nemo-Like Kinase* (*NLK*) a serine/threonine-protein kinase that has been associated with the non-canonical WNT and MAPK signalling pathways. Whilst *NLK* is currently not designated as a known cancer gene, evidence of tumour suppressor activity has been reported (505–507) and a role for NLK protein in the stabilisation of p53 has been suggested (508). Interestingly, NLK appears to collaborate with FBXW7 in the ubiquitination of c-Myb by enhancing ligation of additional ubiquitin molecules via NLK phosphorylation, leading to downregulation of cellular proliferation (509) and previously a RCC-associated constitutional translocation, t(3;4)(q21;q31), was demonstrated to interrupt *FBXW7* (496). Furthermore, *FBXW7* is a designated tumour suppressor gene that is mutated in multiple types of primary cancers (25) and encodes an F-box protein that is part of a SCF complex thought to target cyclin E and mTOR for ubiquitin-mediated degradation (510,511). Additionally, it was demonstrated FBXW7 interacts with Ubiquitin-conjugating enzyme E2Q-like protein 1 (UBE2QL1), the gene of which is known to be disrupted in another previously reported RCC translocation case (499), suggesting an interesting connection between multiple interacting gene products in translocation-related RCC.

While studies demonstrated complete loss of der(3p) in tumours tested (259,496,512–515), partial loss (489,516,517) or no loss of der(3p) in assessed tumours (493,495,518) has also been documented. Furthermore, studies including assessment for loss of heterozygosity or inactivating mutations in the remaining wildtype allele of *VHL* have also been conflicted with experimental data demonstrating presence in all samples (489,495,496,515), some samples (516,517), and no demonstrable loss (493,497,518).

The lack of known tumour suppressors, intergenic break points, and no relation to commonly lost regions in sporadic RCC cases suggests that other mechanisms are involved in predisposition and tumour progression. Translocations may confer a generalised genomic instability, in which specific loss of 3p is not required, and further inactivation of unknown genes are responsible for tumourigenesis. Alternatively, translocations may result in positional-effect variegation, resulting in differential expression patterns for coding regions under differential chromatin regulation (464). It is reasonable, given the atypical presentations and lack of familial history for non-chromosome 3 cases, that pathways responsible for oncogenesis in these individuals are case-specific and no generalised model exists. Given the atypical presentations and lack of familial history for non-chromosome 3 cases, that pathways responsible for oncogenesis in these individuals are case-specific and no generalised model exists.

6.5 Conclusion

In conclusion, this study reports five new cases of RCC-associated constitutional chromosome rearrangements characterised by WGS. These include the first example of a chromosome 3 inversion associated with RCC, the first case of a major inherited RCC gene disrupted by a translocation and a third example of an RCC constitutional chromosome rearrangement that disrupts *FHIT*. Review of the five novel cases reported here and previously reported cases demonstrates that RCC-associated constitutional chromosome rearrangements: 1) mostly involve chromosome 3 but rearrangements that solely involve other chromosomes may also be causally linked to RCC, 2) may predispose to RCC by a variety of mechanisms including disruption of a tumour suppressor gene (e.g. *FLCN*) and/or chromosomal instability (as with chromosome 3 translocations), 3) can be efficiently characterised by WGS and 4) can identify candidate pathways for RCC tumourigenesis. For chromosome 3 translocations it is unclear why most cases that are not ascertained because of a personal or family history of RCC appear to be associated with a very low risk of RCC (493). In those translocations that do predispose to RCC there may be a combination of factors involved including instability of the translocated chromosome during cell division together with disruption of a TSG (e.g. *FHIT*) and/or polygenic effects that increase RCC susceptibility.

7.0 Discussion

7.0.1 Table of contents

The set of studies presented in this thesis have focused on the heritability of RCC and the proportion of undiscovered genetic inheritance which exists in families and individuals with features of predisposition (early onset, family history, or multifocal or bilateral presentation), but in which no genetic cause can be determined based on known RCC predisposition syndromes and genes. Each chapter has concentrated on specific genetic sequencing technique, successively increasing in scope and coverage; beginning with single gene and exon sequencing with Sanger sequencing and ending with whole genome sequencing and 3rd generation sequencing methods, exploiting the advantages of each method when used in the correct context.

7.1 Results chapters: Consequences, associations, and limitations

Chapter 3 utilised target Sanger sequencing and small scale amplicon-based WGS in order to identify putative pathogenic variants in genes frequently altered in somatic RCC, genes in genetically linked phenotypes, and replicate associations seen in more recent germline RCC studies (266). The study effectively recapitulated previous findings for *CDKN2B* and its potential role in RCC predisposition and findings of functionally detrimental variants in *EPAS1* are strong candidates given the role of *EPAS1* in PCC and PGL and GWAS SNP associations in RCC, where a phenotypic expansion of *EPAS1* variants to include RCC would not be unexpected (111,339,342), but limited inferences can be made in regard to the variants identified in *KMT2C* and *KMT2D* without additional functional investigations and replication studies (and detailed clinical phenotyping). The most demonstrable limitation of the targeted sequencing studies is the lack of a comparable control sets to compare allele frequencies between RCC cases and the general population. Additionally, selection criteria for patients recruited into this chapter were more broad than the selection criteria for chapters 4, 5, and 6, which allows for individuals with lesser or minimal features of predisposition to be present within the case cohort and reduce the detection of potentially pathogenic variants. Further limitations include sequencing failures, stemming from methodical limitations or the intrinsic nature of DNA sequencing. PCR amplification success rates are typically determined by various factors, including primer design, reaction mixture constituents, cycling conditions and DNA template. In this study, the limitations were derived from the latter in which the nature of the region assessed (*KMT2C)* or the DNA integrity itself (*CDKN2B* and *EPAS1*) prevented optimal application of the proposed methods.

It is important to note that the methods applied in this chapter are effective and reliable when used in conjunction with high quality DNA, genomic regions without increased alignment complexity, such as that seen with *KMT2C* and the *BAGE* genes (519), and an appropriate comparison to control datasets. These methods reduce the necessity for large scale targeted or whole genome sequencing which complicate bioinformatic and analytical approaches and make Sanger sequencing or small scale amplicon-based NGS sequencing projects ideal for validation studies or clinical genetic testing where reliability, replicability, and efficiency are critical.

Targeted sequencing of a panel of genes and SNPs associated with cancer used in Chapter 4 unveiled potentially the most intriguing result from the perspective of unreported heritability in RCC. Through assessment of 118 individuals, the identification of an enrichment of pathogenic truncating variants in *BRIP1* indicate that *BRIP1* may be a new RCC predisposition gene in subset of rare inherited RCC cases. The statistical enrichment of *BRIP1* truncation carriers compared to both healthy control sets (ICR birth control cohort, gnomAD and ExAC non-tcga (321,433)) and disease sets with known associations provide strong evidence for a legitimate genetic link between RCC predisposition and *BRIP1* which is strengthened further by the co-segregation of the truncating variant in one of the assessed families (though extensive kindreds were not available). Though the evidence is persuasive for the demonstrated association, caution should still be taken before causally implicating heterozygous *BRIP1* truncating variants in non-syndromic inherited RCC. As BRIP1 functions in DNA double strand break repair (520), and as such acts as a tumour suppressor, confirmation of LOH or inactivation of the remaining wildtype allele in tumours from the affected carriers would add additional support and demonstration that the initial variants do in fact result in protein ablation or functional loss, as not all truncating variant result in complete loss of protein function. This especially relevant given that *BRIP1* truncating variants were initially associated as low penetrance risk alleles in breast cancer (401) but more recent epidemiological studies have cast doubt on that affiliation, suggesting truncating *BRIP1* variants do not confer any risk to breast cancer (379).

The investigation into a subset of the same samples selected for matching criteria of features of RCC predisposition utilising WES methods in chapter 5 provided an increased scope for the identification of novel candidate variants and genes but also introduced additional complications. The study identified potentially pathogenic truncating variants, as well as variants in both frequently somatically altered genes and genes involved in the TCA cycle but the interpretation of these variants and determining their impact in RCC predisposition is difficult without functional studies, segregation within large families, or statistical enrichment in comparison to a control data set. Case-control analysis performed well based on the model metrics assessed considering the prior assumptions and innate limitations of the case data set. The case control testing over genomic regions failed to identify any associations after multiple testing correction and genes genes demonstrated a trend towards significance failed to demonstrate any enrichment in biological pathways. The major limitation to this approach is that given the number of cases, the likely risk associated with variants, and the requirement for conservative statistical association mean that the number of cases required to have reasonable power to detect a causal variant greatly exceeds the number of cases that could be reasonably ascertained from public genetic referral services. For example, given the incidence rates of RCC in the general population, estimated occurrence of inherited RCC, and a variant effect size (OR) of 2, the number of cases required to be powered at 80% is in excess of 1200 under liberal false discovery correction.

Variants identified within genes associated with TCA cycle components are potentially the most viable candidates for functional assessment given the recent use of metabolite concentrations as a proxy for SDH complex function (444) and whether or not this could be applied to other TCA cycle components is an intriguing and potential clinically useful application of this methodology as well as uncovering pathogenicity of missense variants, particularly given most of these variants were not classified as pathogenic or likely pathogenic.

Exploratory analysis of WES data utilising algorithms and bioinformatic tools for the identification of copy number alterations, short tandem repeats, and mobile elements did not result in substantial findings across the examined cohort which could be due to several factors. Detection of these genetic alterations is limited by the bioinformatic tools, experimental design, and sequencing method used. In particular, the copy number calling was limited by complications conferred by unmatched WES data without the presence of internal controls to account for read depth variability and a high rate of false negative calls, an issue which is compounded by limited genomic coverage in WES data. Copy number detection in WGS is more reliable and replicable which was aptly demonstrated in the use of WGS copy number analysis in chapter 6 (485). Additionally the tool used, XHMM, is widely utilised for copy number calling including in large scale projects such as ExAC (321) but more recently developed methods have since improved on calling rates and handling of sample and target normalisation, including development of simulation pipelines and comparison benchmarks to establish optimal calling parameters (521,522). The alternative hypothesis is that these types of genetic alterations are rare causes of RCC predisposition, like that of chromosome 3 translocations, and cases are likely to be infrequently detected in unrelated proband studies compared to specific analysis of large pedigrees. Compared to copy number alterations, short tandem repeats and mobile element insertions are very rarely causes of genetic disorders in general and identification of any pathogenic alteration specifically in RCC predisposition was low, especially given the sample size.

More investigations have continued to sequence unrelated individuals with or without clinical features of RCC predisposition utilising cancer gene panels or whole exome sequencing with variable outcomes. Assessment of advanced RCC patients without selection for features of heritability showed 16% carried germline variants in genes not otherwise associated with RCC predisposition, such as *CHEK2*, *APC*, *MUTYH*, *BRCA2,* and *RECQL4*, amongst others. Additionally, it reiterated previous investigations, identifying pathogenic variants in *SDHA* and *BAP1*, which currently have limited support and require further validation (523). An investigation in a Chinese cohort of early onset RCC cases documented 9.5% carried germline pathogenic variants, most of which (66%) were in known RCC predisposition genes (*VHL*, *TSC1*, *TSC2*, *FH*, *FLCN*, *BAP1*, *PBRM1*), with the remaining variants in *BRCA2, BRCA1*, and *CDKN2A*, though only *BRCA1* demonstrated LOH in the tumour (395).

These most recent investigations were recapitulated by the results of the cancer gene panel sequencing and WES studies described in this thesis. The number of potential new candidates identified appears to be limited, particularly when focused on SNVs, and variants identified as potentially associated with RCC predisposition are occurring in genes with known associations to other cancer predisposition (e.g. *BRCA1*, *BRCA2*, *CHEK2* with breast cancer (27,383)) or genes altered somatically at high frequency, supporting the results described by Whitworth *et al* (2018)(376) in multiple primary malignant tumours which pathogenic variants found in individuals with unrelated cancer type suggests a phenotypic expansion, which may be the case in inherited RCC as well.

Furthermore, while the identification of candidate genes has been limited this is the largest cohort of pre-screened individuals with features of inherited RCC to be sequenced and interrogated for putative genetic factors that are causal in RCC predisposition. Other sequencing projects have utilised selection criteria (e.g. early onset, advanced disease, family history) (395,523) but none previously implemented comprehensive pre-screening for known RCC predisposition genes. The application and removal of individuals identified with pathogenic variants in known RCC genes is in some respects a double-edged sword in that it potentially enriches novel genetic factors linked to RCC predisposition but simultaneously reduces the number of available samples for analysis in an already rare sample set.

Lastly, the study and review of RCC-associated translocation cases both previously published and investigated in this thesis in chapter 6 reconfirmed and strengthened the link between specific chromosomal alterations and RCC risk and determined the specific clinical characteristics of RCC-associated translocation cases. While the identification and characterisation of constitutional translocations in this study did not identify any likely novel candidate genes associated with RCC predisposition, it did discover several novel occurrences not previously reported in other RCC translocation studies. Firstly, a translocation interrupting *FLCN* was the most clinically relevant finding which demonstrated BHD syndrome can be because of a translocation break point within the *FLCN* coding region in an individual with classical features of BHD syndrome. This is the first reported case of BHD syndrome caused by a translocation and may be important in assessing additional individuals with features of BHD who do not demonstrate obvious pathogenic SNVs or copy number alterations. Secondly, the identification of a chromosomal inversion, also involving chromosome 3, is the first non-reciprocal balanced chromosomal alteration described in RCC-associated chromosomal alteration cases. Finally, the study established a framework for the identification and characterisation of translocation break points utilising WGS and 3rd generation sequencing methodologies or Sanger sequencing to reduce the required workload to resolve karyotyping reports to the base pair resolution, as well as providing genetic alterations to rule out additional causes of inheritance such as pathogenic SNVs, CNVs, or other structural variants. Utilising this analytical pipeline should reduce analysis cost and improve interrogation of further samples identified as RCC-association chromosomal alteration cases.

7.2 General limitations in next generation sequencing projects

The results of this thesis are limited by a series of features which are common to all genetic association studies, as well as limitations which are specific to targeted next generation sequencing methodology. Primarily, the sample size in any given rare disease study is a limiting factor in the ability to identify novel causes of genetic disorders, particularly in unrelated proband studies which are unable to rely on familial segregation. By increasing sample sizes, statistical power and case control analyses can be more effectively leveraged and identification of rarer idiosyncratic presentations of predisposition can be detected.

This limitation is present across rare disease studies and germline cancer predisposition but is particularly difficult in RCC. In comparison to the assessment of heritability of cancers such as colorectal and breast cancers, which are relatively common, RCC is a rarer cancer subtype. Only an estimated 12,500 new cases of RCC are diagnosed in the UK per year (31) which, when combined with the low prevalence of heritability, currently estimated at 3% of cases (98), it limits the potential UK wide cases to less than 400 individuals as a maximum sample size and that is without screening for known RCC predisposition genes. Recent studies into the application of genetic referral criteria suggest that the number of individuals eligible for genetic testing may be greater than previously estimated which may improve the available samples for research study recruitment but closer integration of clinical and research studies, as well as global collaboration efforts, are needed to facilitate larger sample sizes to improve detection and discovery rates of the factors associated with RCC predisposition. Additional benefits could be gained from clinical follow up and detailed phenotyping of individuals with candidate variants and use familial segregation to determine if the disease phenotype segregates with the putative variant in question.

One of the larger issues faced in large scale next generation sequencing projects such as the cancer gene panel sequencing study and the whole exome sequencing study is the inability to resolve the variant consequences of rare variants occurring across the genome and in candidate RCC predisposition genes. This issue is exemplified by the WES study which, as stated in the study results, identified more than 18,000 variants of uncertain significance, almost all of which were missense variants. Use of ClinVar as a source of additional variant pathogenicity evidence can be useful but availability is limited for most variants and many variants consist of conflicting or uncorroborated reports (406,524). The development of the ACMG variant classification framework, including its improved derivatives, have allowed for a more stringent and systematised approach for variant interpretation (325,525). High-throughput tools such as InterVar have allowed for the rapid application of those described classification (326), but the framework is limited and often inadequate when not accompanied by additional evidence from functional molecular studies, incorporation of reliable *in silico* predictive metrics, and integration of previously published data. Manual classification of variants utilising these frameworks can be more effective but manual curation of publications and functional studies for thousands of variants is unrealistic.

While thorough and detailed functional investigations into all known variants present in the human genome would be the ultimate resource for variant interpretation, the scale and cost of even a fraction of such an endeavour would be unobtainable. Integration of *in silico* predictive tools such as SIFT, PolyPhen, and CADD amongst many others, could improve automated ACMG classifications but their prediction accuracy has been shown to be unreliable in certain instances. Outside of variant classification based on conservation and function consequence to the amino acid sequence, several recently published features of genetic inheritance and mutational selection could prove useful for future interpretation of variant pathogenicity and high-throughput functional experiments for subsets of variants are being proposed.

Use of genomic features like genetic constraint, in which specific regions are under positive or negative selection pressure, have been used across genes to predict intolerance or tolerance (353) but constraint averages over an entire coding region may mask specific conserved domains or regions with the coding space, including intronic regions. More recent developments and increased whole genome sequencing datasets have enabled the calculation of base pair scale assessments of mutational constraint (405) independent of gene loci, which may be a more representative proxy for evolutionary purifying selection in regions that are presumably more critical to gene function. By filtering variants in regions of low constraint (i.e. loci not under purifying selection) it may act to reduce candidate variants to only those present in regions were constraint is high and identify variants more likely to result in a functional alteration and assist in the interpretation of synonymous and intronic variants in relation to disease.

Minor allele frequencies of variants in control populations are commonly used as a first pass filter for the removal of SNPs and low-quality variants. This process is effective at removing many biologically irrelevant variants but a vast majority of variants in any given individual are rarer than the standard allele frequency cut-offs such as 5% and 1% and thus many rare non-pathogenic variants are retained (526). Even assessment of 'ultra-rare' variants in chapter 5 at a minor allele frequency of 0.1% discovered many more variants than could be easily assessed for pathogenicity. Furthermore, allele frequency filtering cut-offs are not disease specific, the likely allele frequency of a variant causing a common disorder is likely different to that of one causing a rare disorder. Use of maximal population allele frequencies, described by Whiffin *et al* (2017), which estimate the maximum tolerated allele frequency at which a causal variant could occur in a control population and still be disease causing may provide disease-specific allele frequency filtering thresholds (527), though the model requires accurate estimates of population prevalence and likely genetic variability, allelic variability, and likely penetrance which can be challenging to estimate in rare diseases.

Lastly, the development of systems such as CRISPR-Cas9 have enabled high capacity, high-throughput screening libraries using gene specific RNA guides and cell line libraries. More recent attempts are aimed at identifying therapeutic targets for specific cancer tumour types but an extension of this system would be feasible and may help prioritise candidate genes more effectively based on the effect of induced truncation in specific cell lines (528), allowing for the integration of *in vitro* functional data into variant interpretation.

7.3 Future directions for the detection of heritability in RCC

In this series of studies, several interesting candidate variants, genes, and mechanisms were discovered in association with RCC predisposition but only a small number of individuals carried putative predisposition variants or presented with rare inherited subtypes (i.e. RCC-associated translocation). The ability to identify candidate variants in individuals with features of RCC predisposition echoes previous studies and results seen in clinical diagnostic labs in which pathogenic variants are not identified in most tested individuals. While some of this missing heritability could be due to the difficulties in variant interpretation, as described above, a proportion may be missed due to not interrogating the genomic regions, variant consequences, or alterations that are truly responsible for heritability in RCC and several other factors may help form future studies which are able to effectively capture the heritable traits of RCC predisposition. Here I summarise a non-exhaustive list of potential research directions and experimental study designs that could be utilised to identify these genetic features which does not rely on solely increasing sample numbers, which would be the most effective method of improving detection rates.

This thesis focused on the assessment of protein-affecting variant and excluded synonymous variants and intronic variants which are becoming more established as disease causing even in known RCC predisposition genes such as *VHL* (137). Variants in regulatory elements such as promotor and enhancer regions, as well as intergenic regions could also be sources of heritability in RCC and should be investigated. Use of WGS would allow for the discovery of variants in these genomic areas but interpretation of pathogenicity is potentially more difficult than protein-affecting variants. The advantage of WGS is that it would allow the exploration of structural and copy number alterations with a much greater degree of accuracy and coverage than that provided by targeted sequencing.

Combinatorial analysis of WES for SNV detection and low coverage WGS, which has been demonstrated to be effective in the detection of copy number variants even at coverages as low as 1X to 5X (529), could provide significant computational and economic savings compared to full coverage WGS. Conversely, a more comprehensive sequencing method, such as WGS long read sequencing (e.g. PacBio SMRT sequencing), would allow for the examination of multiple DNA alterations and remove many of the limitations of 2nd generation short read sequencing methods (see Introduction chapter section 1.7) and allow for comprehensive SNV, structural, CNV, and phasing data across the entire genome. Additionally, the assumption is that inheritance of RCC predisposition is autosomal dominant and the likelihood that a proportion of inheritance is due to low penetrance or polygenic traits is becoming relatively high. Investigations into these features, while complex, should be performed to ascertain the proportion of heritability which can be attributed to complex polygenic traits and risk loci which may help develop methods for assessing polygenic risk scores as utilised in breast cancer (530).

An alternative to increased genomic coverage is the integration of different "–omics" and tumour mutational, metabolic, and expression data to improve variant prioritisation and interpretation. Use of epigenetic data, such as promotor methylation, may uncover germline methylation defects in known or novel genes which are associated with RCC predisposition. Though inactivation of RCC genes is frequently reported somatically (280,283,531), very few investigations have fully assessed the methylation status of genes constitutionally. By identifying hypermethylation of promotor regions or key regulatory elements which correlate with RCC heritability it may demonstrate new genetic features involved in inherited RCC which would not be detected through DNA sequencing alone.

Inclusion of tumour SNV data would allow for the validation of candidate variant by assessing features such as LOH, which provides support for two-hit hypothesis driven loss of tumour suppressors, and tumour mutational signatures which may help identify if putative variants in genes involved in DNA repair pathways, among others, result in the mutational signatures associated with dysfunction in those pathways (532). The availability of fresh frozen tumour material collected prospectively during study recruitment would also enable the use of immunohistochemistry and metabolic investigations to determine and assess germline variant pathogenicity, improving interpretation and reducing ambiguity when attempting to assess variants in genes with functions in metabolism, such as those present in the TCA cycle. Integration of multiple "–omic" types could be further expanded to the use of tumour RNA expression data which would enable the correlation of transcript and allele-specific expression with the presence of putative pathogenic variants, where pathogenicity could be refuted or supported based on whether that allele is expressed in tumours.

Counterintuitively, a proposal could be made for the reduction of study design from large scale genomic sequencing of unrelated probands to family only studies. Studies focused detailed phenotyping and genotyping of specific families may uncover pedigree-specific associations which may then more readily be detected in unrelated individuals. By exploiting familial analysis and the ability to co-segregate variants with disease status candidate variants can be more confidently determined, after which unrelated proband cohorts can be screened for the genes identified. In fact, several of the last genes associated with RCC predisposition, *PBRM1* and *BAP1* (263,331), were discovered through unrelated proband screening but the variants were discovered in individuals with strong family histories of RCC and retrospective analysis demonstrated co-segregation. By reversing this approach and assessing individuals with particularly strong family histories, it may more efficiently uncover associations which may be missed in unrelated proband studies.

7.4 Conclusion

This study has uncovered limited evidence for further associations with new genetic features and RCC predisposition. Though cautious interpretation is needed, once confirmed these findings could be utilised to inform clinical management through genetic counselling, increasing screening procedures, or the development of targeted therapeutics. Furthermore, progressive molecular sequencing methodologies were applied to improve detection and characterisation of causal events in RCC predisposition which may act to increase the efficiency and analysis strategies of genomic data in both research and clinical environments. While much of the genetic components related to predisposition of RCC remains undiscovered, the results of this body of work may act as a foundation for follow up studies which might lead to confirmation of the findings, or novel associations derived from, those results described within this thesis.

8.0 Bibliography

1. Mendel, G. (1865) EXPERIMENTS IN PLANT HYBRIDIZATION (1865). *EXPERIMENTS IN PLANT HYBRIDIZATION (1865)*; (1865) .

2. Maher, E. R., Webster, A. R., Richards, F. M., et al. (1996) Phenotypic expression in von Hippel-Lindau disease: correlations with germline VHL gene mutations. *J. Med. Genet.*, **33**, 328–32.

3. McKusick, V. A. (2000) Ellis-van Creveld syndrome and the Amish. *Nat. Genet.*, **24**, 203–204.

4. López, C., Saravia, C., Gomez, A., et al. (2010) Mechanisms of genetically-based resistance to malaria. *Gene*, **467**, 1–12.

5. Forsberg, L. A., Gisselsson, D. and Dumanski, J. P. (2017) Mosaicism in health and disease — clones picking up speed. *Nat. Rev. Genet.*, **18**, 128–142.

6. Kong, A., Frigge, M. L., Masson, G., et al. (2012) Rate of de novo mutations and the importance of father’s age to disease risk. *Nature*, **488**, 471–5.

7. Alderuccio, F., Chan, J., Scott, D. W., et al. (2009) Gene therapy and bone marrow stem-cell transfer to treat autoimmune disease. *Trends Mol. Med.*, **15**, 344–51.

8. Relling, M. V. and Evans, W. E. (2015) Pharmacogenomics in the clinic. *Nature*, **526**, 343–350.

9. Huang, M., Shen, A., Ding, J., et al. (2014) Molecularly targeted cancer therapy: some lessons from the past decade. *Trends Pharmacol. Sci.*, **35**, 41–50.

10. Alton, E. W. F. W., Armstrong, D. K., Ashby, D., et al. (2015) Repeated nebulisation of non-viral CFTR gene therapy in patients with cystic fibrosis: a randomised, double-blind, placebo-controlled, phase 2b trial. *Lancet Respir. Med.*, **3**, 684–691.

11. Dai, W.-J., Zhu, L.-Y., Yan, Z.-Y., et al. (2016) CRISPR-Cas9 for in vivo Gene Therapy: Promise and Hurdles. *Mol. Ther. Nucleic Acids*, **5**, e349.

12. Ciccia, A. and Elledge, S. J. (2010) The DNA damage response: making it safe to play with knives. *Mol. Cell*, **40**, 179–204.

13. Shaltiel, I. A., Krenning, L., Bruinsma, W., et al. (2015) The same, only different - DNA damage checkpoints and their reversal throughout the cell cycle. *J. Cell Sci.*, **128**, 607–20.

14. Nei, M., Suzuki, Y. and Nozawa, M. (2010) The Neutral Theory of Molecular Evolution in the Genomic Era. *Annu. Rev. Genomics Hum. Genet.*, **11**, 265–289.

15. Knudson, A. (1971) Mutation and cancer: statistical study of retinoblastoma. *Proc. Natl. Acad. Sci. U. S. A.*, **68**, 820–3.

16. Willis, A., Jung, E. J., Wakefield, T., et al. (2004) Mutant p53 exerts a dominant negative effect by preventing wild-type p53 from binding to the promoter of its target genes. *Oncogene*, **23**, 2330–2338.

17. Greaves, M. and Maley, C. C. (2012) Clonal evolution in cancer. *Nature*, **481**, 306–313.

18. Hanahan, D. and Weinberg, R. A. (2011) Hallmarks of Cancer: The Next Generation. *Cell*, **144**, 646–674.

19. Yokoyama, A., Kakiuchi, N., Yoshizato, T., et al. (2019) Age-related remodelling of oesophageal epithelia by mutated cancer drivers. *Nature*, **565**, 312–317.

20. Martincorena, I., Fowler, J. C., Wabik, A., et al. (2018) Somatic mutant clones colonize the human esophagus with age. *Science (80-.).*, **362**, 911–917.

21. Martincorena, I., Roshan, A., Gerstung, M., et al. (2015) High burden and pervasive positive selection of somatic mutations in normal human skin. *Science (80-.).*, **348**, 880–886.

22. Mitchell, T. J., Turajlic, S., Rowan, A., et al. (2018) Timing the Landmark Events in the Evolution of Clear Cell Renal Cell Cancer: TRACERx Renal. *Cell*.

23. National Cancer Registration and Analysis Service (2014) Cancer Survivial in England by stage 2014. Cancer Survivial in England by stage 2014 http://www.ncin.org.uk/publications/survival_by_stage (accessed Mar 15, 2019).

24. Li, F. P. and Fraumeni, J. F. (1969) Soft-tissue sarcomas, breast cancer, and other neoplasms. A familial syndrome? *Ann. Intern. Med.*, **71**, 747–752.

25. Network, C. G. A. R., N., J., Weinstein, J. N., et al. (2013) The Cancer Genome Atlas Pan-Cancer analysis project. *Nat. Genet.*, **45**, 1113–20.

26. Rahman, N. (2014) Realizing the promise of cancer predisposition genes. *Nature*, **505**, 302–8.

27. Petrucelli, N., Daly, M. B. and Pal, T. (1993) BRCA1- and BRCA2-Associated Hereditary Breast and Ovarian Cancer. *BRCA1- and BRCA2-Associated Hereditary Breast and Ovarian Cancer*; University of Washington, Seattle, (1993) .

28. Fitzmaurice, C., Dicker, D., Pain, A., et al. (2015) The Global Burden of Cancer 2013. *JAMA Oncol.*, **1**, 505.

29. Noone, A., Howlader, N., Krapcho, M., et al. (2017) SEER Cancer Statistics Review, 1975-2015. *SEER Cancer Statistics Review, 1975-2015*; Bethesda, (2017) .

30. Maher, E. R., Yates, J. R. and Ferguson-Smith, M. a (1990) Statistical analysis of the two stage mutation model in von Hippel-Lindau disease, and in sporadic cerebellar haemangioblastoma and renal cell carcinoma. *J. Med. Genet.*, **27**, 311–314.

31. Smittenaar, C. R., Petersen, K. A., Stewart, K., et al. (2016) Cancer incidence and mortality projections in the UK until 2035. *Br. J. Cancer*, **115**, 1147–1155.

32. Brown, K. F., Rumgay, H., Dunlop, C., et al.

(2018) The fraction of cancer attributable to modifiable risk factors in England, Wales, Scotland, Northern Ireland, and the United Kingdom in 2015. *Br. J. Cancer*, **118**, 1130–1141.

33. Wang, F. and Xu, Y. (2014) Body mass index and risk of renal cell cancer: A dose-response meta-analysis of published cohort studies. *Int. J. Cancer*, **135**, 1673–1686.

34. Cumberbatch, M. G., Rota, M., Catto, J. W. F., et al. (2016) The Role of Tobacco Smoke in Bladder and Kidney Carcinogenesis: A Comparison of Exposures and Meta-analysis of Incidence and Mortality Risks. *Eur. Urol.*, **70**, 458–466.

35. Weikert, S., Boeing, H., Pischon, T., et al. (2008) Blood Pressure and Risk of Renal Cell Carcinoma in the European Prospective Investigation into Cancer and Nutrition. *Am. J. Epidemiol.*, **167**, 438–446.

36. Matson, M. A. and Cohen, E. P. (1990) Acquired cystic kidney disease: occurrence, prevalence, and renal cancers. *Medicine (Baltimore).*, **69**, 217–26.

37. Tseng, C.-H. (2015) Type 2 Diabetes Mellitus and Kidney Cancer Risk: A Retrospective Cohort Analysis of the National Health Insurance. *PLoS One*, **10**, e0142480.

38. Li, C., Balluz, L. S., Ford, E. S., et al. (2011) Association Between Diagnosed Diabetes and Self-Reported Cancer Among U.S. Adults: Findings from the 2009 Behavioral Risk Factor Surveillance System. *Diabetes Care*, **34**, 1365–1368.

39. Cho, E., Curhan, G., Hankinson, S. E., et al. (2011) Prospective evaluation of analgesic use and risk of renal cell cancer. *Arch. Intern. Med.*, **171**, 1487–93.

40. Huang, T., Ding, P., Chen, J., et al. (2014) Dietary fiber intake and risk of renal cell carcinoma: evidence from a meta-analysis. *Med. Oncol.*, **31**, 125.

41. Zhao, J. and Zhao, L. (2013) Cruciferous Vegetables Intake Is Associated with Lower Risk of Renal Cell Carcinoma: Evidence from a Meta-Analysis of Observational Studies. *PLoS One*, **8**, e75732.

42. Kelsh, M. A., Alexander, D. D., Mink, P. J., et al. (2010) Occupational Trichloroethylene Exposure and Kidney Cancer. *Epidemiology*, **21**, 95–102.

43. Boffetta, P., Fontana, L., Stewart, P., et al. (2011) Occupational exposure to arsenic, cadmium, chromium, lead and nickel, and renal cell carcinoma: a case-control study from Central and Eastern Europe. *Occup. Environ. Med.*, **68**, 723–728.

44. NCD Risk Factor Collaboration (NCD-RisC), N. R. F. C. (2017) Worldwide trends in body-mass index, underweight, overweight, and obesity from 1975 to 2016: a pooled analysis of 2416 population-based measurement studies in 128·9 million children, adolescents, and adults. *Lancet (London, England)*, **390**, 2627–2642.

45. Swinburn, B. A., Caterson, I., Seidell, J. C., et al. (2004) Diet, nutrition and the prevention of excess weight gain and obesity. *Public Health Nutr.*, **7**, 123–46.

46. Kotchen, T. A. (2010) Obesity-Related Hypertension: Epidemiology, Pathophysiology, and Clinical Management. *Am. J. Hypertens.*, **23**, 1170–1178.

47. Hossain, P., Kawar, B. and El Nahas, M. (2007) Obesity and Diabetes in the Developing World — A Growing Challenge. *N. Engl. J. Med.*, **356**, 213–215.

48. Motzer, R. J., Bander, N. H. and Nanus, D. M. (1996) Renal-Cell Carcinoma. *N. Engl. J. Med.*, **335**, 865–875.

49. Srigley, J. R., Delahunt, B., Eble, J. N., et al. (2013) The International Society of Urological Pathology (ISUP) Vancouver Classification of Renal Neoplasia. *Am. J. Surg. Pathol.*, **37**, 1469–1489.

50. Moch, H., Gasser, T., Amin, M. B., et al. (2000) Prognostic utility of the recently recommended histologic classification and revised TNM staging system of renal cell carcinoma: a Swiss experience with 588 tumors. *Cancer*, **89**, 604–14.

51. Amin, M. B., Amin, M. B., Tamboli, P., et al. (2002) Prognostic impact of histologic subtyping of adult renal epithelial neoplasms: an experience of 405 cases. *Am. J. Surg. Pathol.*, **26**, 281–91.

52. Ericsson, J. L., Seljelid, R. and Orrenius, S. (1966) Comparative light and electron microscopic observations of the cytoplasmic matrix in renal carcinomas. *Virchows Arch. Pathol. Anat. Physiol. Klin. Med.*, **341**, 204–23.

53. Du, W., Zhang, L., Brett-Morris, A., et al. (2017) HIF drives lipid deposition and cancer in ccRCC via repression of fatty acid metabolism. *Nat. Commun.*, **8**, 1769.

54. Andreiana, B. C., Stepan, A. E., Mărgăritescu, C., et al. (2018) Histopathological Prognostic Factors in Clear Cell Renal Cell Carcinoma. *Curr. Heal. Sci. J.*, **44**, 201–205.

55. Cheville, J. C., Lohse, C. M., Zincke, H., et al. (2003) Comparisons of outcome and prognostic features among histologic subtypes of renal cell carcinoma. *Am. J. Surg. Pathol.*, **27**, 612–24.

56. Ambrosetti, D., Dufies, M., Dadone, B., et al. (2018) The two glycolytic markers GLUT1 and MCT1 correlate with tumor grade and survival in clear-cell renal cell carcinoma. *PLoS One*, **13**, e0193477.

57. Kim, H., Inomoto, C., Uchida, T., et al. (2018) Verification of the International Society of Urological Pathology recommendations in Japanese patients with clear cell renal cell carcinoma. *Int. J. Oncol.*, **52**, 1139–1148.

58. Muglia, V. F. and Prando, A. (2015) Renal cell carcinoma: histological classification and correlation with imaging findings. *Radiol. Bras.*, **48**, 166–74.

59. Lubensky, I. A., Schmidt, L., Zhuang, Z., et al.

(1999) Hereditary and Sporadic Papillary Renal Carcinomas with c-met Mutations Share a Distinct Morphological Phenotype. *Am. J. Pathol.*, **155**, 517–526.

60. Kuroda, N., Ohe, C., Kawakami, F., et al. (2014) Clear cell papillary renal cell carcinoma: a review. *Int. J. Clin. Exp. Pathol.*, **7**, 7312–8.

61. Zhong, M., De Angelo, P., Osborne, L., et al. (2012) Translocation Renal Cell Carcinomas in Adults. *Am. J. Surg. Pathol.*, **36**, 654–662.

62. Zhao, M., He, X. and Teng, X. (2015) Mucinous tubular and spindle cell renal cell carcinoma: a review of clinicopathologic aspects. *Diagn. Pathol.*, **10**, 168.

63. Adibi, M., Thomas, A. Z., Borregales, L. D., et al. (2015) Percentage of sarcomatoid component as a prognostic indicator for survival in renal cell carcinoma with sarcomatoid dedifferentiation. *Urol. Oncol. Semin. Orig. Investig.*, **33**, 427.e17-427.e23.

64. Akhtar, M., Tulbah, A., Kardar, A. H., et al. (1997) Sarcomatoid renal cell carcinoma: the chromophobe connection. *Am. J. Surg. Pathol.*, **21**, 1188–95.

65. Abrahams, N. A., Ayala, A. G. and Czerniak, B. (2003) Chromophobe renal cell carcinoma with sarcomatoid transformation. *Ann. Diagn. Pathol.*, **7**, 296–9.

66. Jones, T. D., Eble, J. N., Wang, M., et al. (2005) Clonal divergence and genetic heterogeneity in clear cell renal cell carcinomas with sarcomatoid transformation. *Cancer*, **104**, 1195–1203.

67. Mittal, V. (2018) Epithelial Mesenchymal Transition in Tumor Metastasis. *Annu. Rev. Pathol. Mech. Dis.*, **13**, 395–412.

68. Sobin, L. H., Gospodarowicz, M. K. (Mary K. ., Wittekind, C. (Christian), et al. (2009) TNM classification of malignant tumours. *TNM classification of malignant tumours*; Wiley-Blackwell, (2009) .

69. Kim, S. P., Alt, A. L., Weight, C. J., et al. (2011) Independent validation of the 2010 American Joint Committee on Cancer TNM classification for renal cell carcinoma: results from a large, single institution cohort. *J. Urol.*, **185**, 2035–9.

70. Hand, J. R. and Broders, A. C. (1932) Carcinoma of the Kidney: The Degree of Malignancy in Relation to Factors Bearing on Prognosis. *J. Urol.*, **28**, 199–216.

71. Fuhrman, S. A., Lasky, L. C. and Limas, C. (1982) Prognostic significance of morphologic parameters in renal cell carcinoma. *Am. J. Surg. Pathol.*, **6**, 655–63.

72. Delahunt, B., McKenney, J. K., Lohse, C. M., et al. (2013) A Novel Grading System for Clear Cell Renal Cell Carcinoma Incorporating Tumor Necrosis. *Am. J. Surg. Pathol.*, **37**, 311–322.

73. Delahunt, B., Sika-Paotonu, D., Bethwaite, P. B., et al. (2007) Fuhrman Grading is not Appropriate for Chromophobe Renal Cell Carcinoma. *Am. J. Surg. Pathol.*, **31**, 957–960.

74. Ljungberg, B., Albiges, L., Abu-Ghanem, Y., et al. (2019) European Association of Urology Guidelines on Renal Cell Carcinoma: The 2019 Update. *Eur. Urol.*

75. Ferrara, N. (2004) Vascular endothelial growth factor as a target for anticancer therapy. *Oncologist*, **9 Suppl 1**, 2–10.

76. Rini, B. I. and Small, E. J. (2005) Biology and clinical development of vascular endothelial growth factor-targeted therapy in renal cell carcinoma. *J. Clin. Oncol.*, **23**, 1028–43.

77. Mendel, D. B., Laird, A. D., Xin, X., et al. (2003) In vivo antitumor activity of SU11248, a novel tyrosine kinase inhibitor targeting vascular endothelial growth factor and platelet-derived growth factor receptors: determination of a pharmacokinetic/pharmacodynamic relationship. *Clin. Cancer Res.*, **9**, 327–37.

78. Abrams, T. J., Lee, L. B., Murray, L. J., et al. (2003) SU11248 inhibits KIT and platelet-derived growth factor receptor beta in preclinical models of human small cell lung cancer. *Mol. Cancer Ther.*, **2**, 471–8.

79. Sonpavde, G. and Hutson, T. E. (2007) Pazopanib: A novel multitargeted tyrosine kinase inhibitor. *Curr. Oncol. Rep.*, **9**, 115–119.

80. Podsypanina, K., Lee, R. T., Politis, C., et al. (2001) An inhibitor of mTOR reduces neoplasia and normalizes p70/S6 kinase activity in Pten+/- mice. *Proc. Natl. Acad. Sci. U. S. A.*, **98**, 10320–5.

81. Albert, S., Serova, M., Dreyer, C., et al. (2010) New inhibitors of the mammalian target of rapamycin signaling pathway for cancer. *Expert Opin. Investig. Drugs*, **19**, 919–930.

82. Saxton, R. A. and Sabatini, D. M. (2017) mTOR Signaling in Growth, Metabolism, and Disease. *Cell*, **168**, 960–976.

83. Wallace, E. M., Rizzi, J. P., Han, G., et al. (2016) A Small-Molecule Antagonist of HIF2α Is Efficacious in Preclinical Models of Renal Cell Carcinoma. *Cancer Res.*, **76**, 5491–5500.

84. Courtney, K. D., Infante, J. R., Lam, E. T., et al. (2018) Phase I Dose-Escalation Trial of PT2385, a First-in-Class Hypoxia-Inducible Factor-2α Antagonist in Patients With Previously Treated Advanced Clear Cell Renal Cell Carcinoma. *J. Clin. Oncol.*, **36**, 867–874.

85. Ribas, A. (2012) Tumor Immunotherapy Directed at PD-1. *N. Engl. J. Med.*, **366**, 2517–2519.

86. Camacho, L. H. (2015) CTLA-4 blockade with ipilimumab: biology, safety, efficacy, and future considerations. *Cancer Med.*, **4**, 661–672.

87. Ranieri, G., Patruno, R., Ruggieri, E., et al. (2006) Vascular endothelial growth factor (VEGF) as a target of bevacizumab in cancer: from the biology to the clinic. *Curr. Med. Chem.*, **13**, 1845–57.

88. Escudier, B., Eisen, T., Stadler, W. M., et al. (2007) Sorafenib in Advanced Clear-Cell Renal-Cell Carcinoma. *N. Engl. J. Med.*, **356**, 125–134.

89. Diamond, J. R., Salgia, R., Varella-Garcia, M., et al. (2013) Initial clinical sensitivity and acquired resistance to MET inhibition in MET-mutated papillary renal cell carcinoma. *J. Clin. Oncol.*, **31**, e254-8.

90. Rini, B. I. and Atkins, M. B. (2009) Resistance to targeted therapy in renal-cell carcinoma. *Lancet Oncol.*, **10**, 992–1000.

91. Gottesman, M. M., Fojo, T. and Bates, S. E. (2002) Multidrug resistance in cancer: role of ATP–dependent transporters. *Nat. Rev. Cancer*, **2**, 48–58.

92. Gotink, K. J., Broxterman, H. J., Labots, M., et al. (2011) Lysosomal Sequestration of Sunitinib: A Novel Mechanism of Drug Resistance. *Clin. Cancer Res.*, **17**, 7337–7346.

93. Casanovas, O., Hicklin, D. J., Bergers, G., et al. (2005) Drug resistance by evasion of antiangiogenic targeting of VEGF signaling in late-stage pancreatic islet tumors. *Cancer Cell*, **8**, 299–309.

94. Huang, D., Ding, Y., Zhou, M., et al. (2010) Interleukin-8 Mediates Resistance to Antiangiogenic Agent Sunitinib in Renal Cell Carcinoma. *Cancer Res.*, **70**, 1063–1071.

95. Hirschi, K. K. and D'Amore, P. A. (1997) Control of angiogenesis by the pericyte: molecular mechanisms and significance. *EXS*, **79**, 419–28.

96. Finke, J., Ko, J., Rini, B., et al. (2011) MDSC as a mechanism of tumor escape from sunitinib mediated anti-angiogenic therapy. *Int. Immunopharmacol.*, **11**, 856–861.

97. Hwang, H. S., Go, H., Park, J.-M., et al. (2019) Epithelial-mesenchymal transition as a mechanism of resistance to tyrosine kinase inhibitors in clear cell renal cell carcinoma. *Lab. Investig.*, 1.

98. Maher, E. R. (2013) Genomics and epigenomics of renal cell carcinoma. *Semin. Cancer Biol.*, **23**, 10–7.

99. Gossage, L., Eisen, T. and Maher, E. R. (2015) VHL, the story of a tumour suppressor gene. *Nat. Rev. Cancer*, **15**, 55–64.

100. Gherardi, E., Birchmeier, W., Birchmeier, C., et al. (2012) Targeting MET in cancer: rationale and progress. *Nat. Rev. Cancer*, **12**, 89–103.

101. Clague, J., Lin, J., Cassidy, A., et al. (2009) Family History and Risk of Renal Cell Carcinoma: Results from a Case-Control Study and Systematic Meta-Analysis. *Cancer Epidemiol. Biomarkers Prev.*, **18**, 801–807.

102. Nguyen, K. A., Syed, J. S., Espenschied, C. R., et al. (2017) Advances in the diagnosis of hereditary kidney cancer: Initial results of a multigene panel test. *Cancer*, **123**, 4363–4371.

103. Klatte, T., Patard, J.-J., Wunderlich, H., et al. (2007) Metachronous Bilateral Renal Cell Carcinoma: Risk Assessment, Prognosis and Relevance of the Primary-Free Interval. *J. Urol.*, **177**, 2081–2087.

104. Gudbjartsson, T., Jónasdóttir, T. J., Thoroddsen, Á., et al. (2002) A population-based familial aggregation analysis indicates genetic contribution in a majority of renal cell carcinomas. *Int. J. Cancer*, **100**, 476–479.

105. Mucci, L. A., Hjelmborg, J. B., Harris, J. R., et al. (2016) Familial Risk and Heritability of Cancer Among Twins in Nordic Countries. *JAMA*, **315**, 68–76.

106. Bertout, J. A., Majmundar, A. J., Gordan, J. D., et al. (2009) HIF2alpha inhibition promotes p53 pathway activity, tumor cell death, and radiation responses. *Proc. Natl. Acad. Sci. U. S. A.*, **106**, 14391–6.

107. Ivan, M., Kondo, K., Yang, H., et al. (2001) HIFalpha targeted for VHL-mediated destruction by proline hydroxylation: implications for O2 sensing. *Science*, **292**, 464–8.

108. Purdue, M. P., Johansson, M., Zelenika, D., et al. (2011) Genome-wide association study of renal cell carcinoma identifies two susceptibility loci on 2p21 and 11q13.3. *Nat. Genet.*, **43**, 60–5.

109. Han, S. S., Yeager, M., Moore, L. E., et al. (2012) The chromosome 2p21 region harbors a complex genetic architecture for association with risk for renal cell carcinoma. *Hum. Mol. Genet.*, **21**, 1190–1200.

110. Wu, X., Scelo, G., Purdue, M. P., et al. (2012) A genome-wide association study identifies a novel susceptibility locus for renal cell carcinoma on 12p11.23. *Hum. Mol. Genet.*, **21**, 456–62.

111. Audenet, F., Cancel-Tassin, G., Bigot, P., et al. (2014) Germline Genetic Variations at 11q13 and 12p11 Locus Modulate Age at Onset for Renal Cell Carcinoma. *J. Urol.*, **191**, 487–492.

112. Gudmundsson, J., Sulem, P., Gudbjartsson, D. F., et al. (2013) A common variant at 8q24.21 is associated with renal cell cancer. *Nat. Commun.*, **4**, 2776.

113. Henrion, M., Frampton, M., Scelo, G., et al. (2013) Common variation at 2q22.3 (ZEB2) influences the risk of renal cancer. *Hum. Mol. Genet.*, **22**, 825–31.

114. Henrion, M. Y. R., Purdue, M. P., Scelo, G., et al. (2015) Common variation at 1q24.1 (ALDH9A1) is a potential risk factor for renal cancer. *PLoS One*, **10**, e0122589.

115. Schödel, J., Bardella, C., Sciesielski, L. K., et al. (2012) Common genetic variants at the 11q13.3 renal cancer susceptibility locus influence binding of HIF to an enhancer of cyclin D1 expression. *Nat. Genet.*, **44**, 420–5, S1-2.

116. Xue, J., Qin, Z., Li, X., et al. (2017) Genetic polymorphisms in cyclin D1 are associated with risk of renal cell cancer in the Chinese population. *Oncotarget*, **8**, 80889.

117. Machiela, M. J., Hofmann, J. N., Carreras-Torres, R., et al. (2017) Genetic Variants Related to Longer Telomere Length are Associated with Increased Risk of Renal Cell Carcinoma. *Eur. Urol.*, **72**, 747–754.

118. Truong, H., Hegarty, S. E., Gomella, L. G., et al. (2017) Prevalence and Characteristics of Patients with Suspected Inherited Renal Cell Cancer: Application of the ACMG/NSGC Genetic Referral Guidelines to Patient Cohorts. *J. Genet. Couns.*, **26**, 548–555.

119. Glenn, G. M., Daniel, L. N., Choyke, P., et al. (1991) Von Hippel-Lindau (VHL) disease: distinct phenotypes suggest more than one mutant allele at the VHL locus. *Hum. Genet.*, **87**, 207–10.

120. Neumann, H. P. and Wiestler, O. D. (1991) Clustering of features of von Hippel-Lindau syndrome: evidence for a complex genetic locus. *Lancet (London, England)*, **337**, 1052–4.

121. Evans, D. G., Howard, E., Giblin, C., et al. (2010) Birth incidence and prevalence of tumor-prone syndromes: Estimates from a UK family genetic register service. *Am. J. Med. Genet. Part A*, **152A**, 327–332.

122. Binderup, M. L. M., Galanakis, M., Budtz-Jørgensen, E., et al. (2017) Prevalence, birth incidence, and penetrance of von Hippel-Lindau disease (vHL) in Denmark. *Eur. J. Hum. Genet.*, **25**, 301–307.

123. Maher, E. R., Iselius, L., Yates, J. R., et al. (1991) Von Hippel-Lindau disease: a genetic study. *J. Med. Genet.*, **28**, 443.

124. Ong, K. R., Woodward, E. R., Killick, P., et al. (2007) Genotype-phenotype correlations in von Hippel-Lindau disease. *Hum. Mutat.*, **28**, 143–149.

125. Collins, T. (1894) Intra-ocular growths: Two cases, brother and sister, with peculiar vascular new growth, probably primarily retinal, affecting both eyes. *Trans Ophthalmol.*

126. Zbar, B., Brauch, H., Talmadge, C., et al. (1987) Loss of alleles of loci on the short arm of chromosome 3 in renal cell carcinoma. *Nature*, **327**, 721–724.

127. Latif, F., Tory, K., Gnarra, J., et al. (1993) Identification of the von Hippel-Lindau disease tumor suppressor gene. *Science (80-.).*, **260**, 1317–1320.

128. Foster, K., Prowse, A., van den Berg, A., et al. (1994) Somatic mutations of the von Hippel-Lindau disease tumour suppressor gene in non-familial clear cell renal carcinoma. *Hum. Mol. Genet.*, **3**, 2169–73.

129. Woodward, E. R., Clifford, S. C., Astuti, D., et al. (2000) Familial clear cell renal cell carcinoma (FCRC): clinical features and mutation analysis of the VHL, MET, and CUL2 candidate genes. *J. Med. Genet.*, **37**, 348–53.

130. Sgambati, M. T., Stolle, C., Choyke, P. L., et al. (2000) Mosaicism in von Hippel-Lindau disease: lessons from kindreds with germline mutations identified in offspring with mosaic parents. *Am. J. Hum. Genet.*, **66**, 84–91.

131. Coppin, L., Grutzmacher, C., Crépin, M., et al. (2014) VHL mosaicism can be detected by clinical next-generation sequencing and is not restricted to patients with a mild phenotype. *Eur. J. Hum. Genet.*, **22**, 1149–52.

132. Pastore, Y., Jedlickova, K., Guan, Y., et al. (2003) Mutations of von Hippel-Lindau Tumor-Suppressor Gene and Congenital Polycythemia. *Am. J. Hum. Genet.*, **73**, 412–419.

133. Gordeuk, V. R., Sergueeva, A. I., Miasnikova, G. Y., et al. (2004) Congenital disorder of oxygen sensing: association of the homozygous Chuvash polycythemia VHL mutation with thrombosis and vascular abnormalities but not tumors. *Blood*, **103**, 3924–3932.

134. McNeill, A., Rattenberry, E., Barber, R., et al. (2009) Genotype-phenotype correlations in VHL exon deletions. *Am. J. Med. Genet. Part A*, **149A**, 2147–2151.

135. Chen, F., Kishida, T., Yao, M., et al. (1995) Germline mutations in the von Hippel-Lindau disease tumor suppressor gene: Correlations with phenotype. *Hum. Mutat.*, **5**, 66–75.

136. Nordstrom-O'Brien, M., van der Luijt, R. B., van Rooijen, E., et al. (2010) Genetic analysis of von Hippel-Lindau disease. *Hum. Mutat.*, **31**, n/a-n/a.

137. Lenglet, M., Robriquet, F., Schwarz, K., et al. (2018) Identification of a new VHL exon and complex splicing alterations in familial erythrocytosis or von Hippel-Lindau disease. *Blood*, **132**, 469–483.

138. Maxwell, P. H., Wiesener, M. S., Chang, G.-W., et al. (1999) The tumour suppressor protein VHL targets hypoxia-inducible factors for oxygen-dependent proteolysis. *Nature*, **399**, 271–275.

139. Jaakkola, P., Mole, D. R., Tian, Y. M., et al. (2001) Targeting of HIF-alpha to the von Hippel-Lindau ubiquitylation complex by O2-regulated prolyl hydroxylation. *Science*, **292**, 468–72.

140. Wenger, R. H., Stiehl, D. P. and Camenisch, G. (2005) Integration of Oxygen Signaling at the Consensus HRE. *Sci. Signal.*, **2005**, re12–re12.

141. Keith, B., Johnson, R. S. and Simon, M. C. (2012) HIF1α and HIF2α: sibling rivalry in hypoxic tumour growth and progression. *Nat. Rev. Cancer*, **12**, 9–22.

142. Raval, R. R., Lau, K. W., Tran, M. G. B., et al. (2005) Contrasting properties of hypoxia-inducible factor 1 (HIF-1) and HIF-2 in von Hippel-Lindau-associated renal cell carcinoma. *Mol. Cell. Biol.*, **25**, 5675–86.

143. Shen, C., Beroukhim, R., Schumacher, S. E., et al. (2011) Genetic and functional studies implicate HIF1α as a 14q kidney cancer suppressor gene. *Cancer Discov.*, **1**, 222–35.

144. Morris, M. R., Hughes, D. J., Tian, Y.-M., et al. (2009) Mutation analysis of hypoxia-inducible factors HIF1A and HIF2A in renal cell carcinoma. *Anticancer Res.*, **29**, 4337–43.

145. Roe, J.-S., Kim, H.-R., Hwang, I.-Y., et al. (2011) von Hippel–Lindau protein promotes Skp2 destabilization on DNA damage. *Oncogene*, **30**, 3127–3138.

146. Thoma, C. R., Toso, A., Gutbrodt, K. L., et al. (2009) VHL loss causes spindle misorientation and chromosome instability. *Nat. Cell Biol.*, **11**, 994–1001.

147. Roe, J.-S., Kim, H., Lee, S.-M., et al. (2006) p53 Stabilization and Transactivation by a von Hippel-Lindau Protein. *Mol. Cell*, **22**, 395–405.

148. Haase, V. H., Glickman, J. N., Socolovsky, M., et al. (2001) Vascular tumors in livers with targeted inactivation of the von Hippel-Lindau tumor suppressor. *Proc. Natl. Acad. Sci.*, **98**, 1583–1588.

149. Kleymenova, E., Everitt, J. I., Pluta, L., et al. (2003) Susceptibility to vascular neoplasms but no increased susceptibility to renal carcinogenesis in Vhl knockout mice. *Carcinogenesis*, **25**, 309–315.

150. Kapitsinou, P. P. and Haase, V. H. (2008) The VHL tumor suppressor and HIF: insights from genetic studies in mice. *Cell Death Differ.*, **15**, 650–9.

151. Velickovic, M., Delahunt, B. and Grebe, S. K. (1999) Loss of heterozygosity at 3p14.2 in clear cell renal cell carcinoma is an early event and is highly localized to the FHIT gene locus. *Cancer Res.*, **59**, 1323–6.

152. Nargund, A. M., Pham, C. G., Dong, Y., et al. (2017) The SWI/SNF Protein PBRM1 Restrains VHL-Loss-Driven Clear Cell Renal Cell Carcinoma. **18**, 2893–2906.

153. Reed, W. B., Walker, R. and Horowitz, R. (1973) Cutaneous leiomyomata with uterine leiomyomata. *Acta Derm. Venereol.*, **53**, 409–16.

154. Launonen, V., Vierimaa, O., Kiuru, M., et al. (2001) Inherited susceptibility to uterine leiomyomas and renal cell cancer. *Proc. Natl. Acad. Sci.*, **98**, 3387–3392.

155. Toro, J. R., Nickerson, M. L., Wei, M.-H., et al. (2003) Mutations in the fumarate hydratase gene cause hereditary leiomyomatosis and renal cell cancer in families in North America. *Am. J. Hum. Genet.*, **73**, 95–106.

156. Shuch, B., Vourganti, S., Ricketts, C. J., et al. (2014) Defining early-onset kidney cancer: implications for germline and somatic mutation testing and clinical management. *J. Clin. Oncol.*, **32**, 431–7.

157. Grubb, R. L., Franks, M. E., Toro, J., et al. (2007) Hereditary Leiomyomatosis and Renal Cell Cancer: A Syndrome Associated With an Aggressive Form of Inherited Renal Cancer. *J. Urol.*, **177**, 2074–2080.

158. Linehan, W. M., Spellman, P. T., Ricketts, C. J., et al. (2015) Comprehensive Molecular Characterization of Papillary Renal-Cell Carcinoma. *N. Engl. J. Med.*, **374**, 135–45.

159. Tomlinson, I. P. M., Alam, N. A., Rowan, A. J., et al. (2002) Germline mutations in FH predispose to dominantly inherited uterine fibroids, skin leiomyomata and papillary renal cell cancer. *Nat. Genet.*, **30**, 406–410.

160. Alam, N. A., Rowan, A. J., Wortham, N. C., et al. (2003) Genetic and functional analyses of FH mutations in multiple cutaneous and uterine leiomyomatosis, hereditary leiomyomatosis and renal cancer, and fumarate hydratase deficiency. *Hum. Mol. Genet.*, **12**, 1241–52.

161. Wei, M.-H., Toure, O., Glenn, G. M., et al. (2006) Novel mutations in FH and expansion of the spectrum of phenotypes expressed in families with hereditary leiomyomatosis and renal cell cancer. *J. Med. Genet.*, **43**, 18–27.

162. Alam, N. A., Bevan, S., Churchman, M., et al. (2001) Localization of a Gene (MCUL1) for Multiple Cutaneous Leiomyomata and Uterine Fibroids to Chromosome 1q42.3-q43. *Am. J. Hum. Genet.*, **68**, 1264–1269.

163. MASSEY, V. (1953) Studies on fumarase. 4. The effects of inhibitors on fumarase activity. *Biochem. J.*, **55**, 172–7.

164. Vander Heiden, M. G., Cantley, L. C. and Thompson, C. B. (2009) Understanding the Warburg effect: the metabolic requirements of cell proliferation. *Science*, **324**, 1029–33.

165. Tong, W.-H., Sourbier, C., Kovtunovych, G., et al. (2011) The glycolytic shift in fumarate-hydratase-deficient kidney cancer lowers AMPK levels, increases anabolic propensities and lowers cellular iron levels. *Cancer Cell*, **20**, 315–27.

166. D'Angelo, G., Duplan, E., Boyer, N., et al. (2003) Hypoxia Up-regulates Prolyl Hydroxylase Activity. *J. Biol. Chem.*, **278**, 38183–38187.

167. Isaacs, J. S., Jung, Y. J., Mole, D. R., et al. (2005) HIF overexpression correlates with biallelic loss of fumarate hydratase in renal cancer: Novel role of fumarate in regulation of HIF stability. *Cancer Cell*, **8**, 143–153.

168. Pollard, P. J., Brière, J. J., Alam, N. A., et al. (2005) Accumulation of Krebs cycle intermediates and over-expression of HIF1α in tumours which result from germline FH and SDH mutations. *Hum. Mol. Genet.*, **14**, 2231–2239.

169. Pollard, P., Wortham, N., Barclay, E., et al. (2005) Evidence of increased microvessel density and activation of the hypoxia pathway in tumours from the hereditary leiomyomatosis and renal cell cancer syndrome. *J. Pathol.*, **205**, 41–49.

170. Sudarshan, S., Sourbier, C., Kong, H.-S., et al. (2009) Fumarate Hydratase Deficiency in Renal Cancer Induces Glycolytic Addiction and Hypoxia-Inducible Transcription Factor 1 Stabilization by Glucose-Dependent Generation of Reactive Oxygen Species. *Mol. Cell. Biol.*, **29**, 4080–4090.

171. Alderson, N. L., Wang, Y., Blatnik, M., et al. (2006) S-(2-Succinyl)cysteine: A novel chemical modification of tissue proteins by a Krebs cycle intermediate. *Arch. Biochem. Biophys.*, **450**, 1–8.

172. Ooi, A., Wong, J.-C., Petillo, D., et al. (2011) An Antioxidant Response Phenotype Shared between Hereditary and Sporadic Type 2 Papillary Renal Cell Carcinoma. *Cancer Cell*,

20, 511–523.

173. Lenaz, G. (1998) Role of mitochondria in oxidative stress and ageing. *Biochim. Biophys. Acta - Bioenerg.*, **1366**, 53–67.

174. Xiao, M., Yang, H., Xu, W., et al. (2012) Inhibition of -KG-dependent histone and DNA demethylases by fumarate and succinate that are accumulated in mutations of FH and SDH tumor suppressors. *Genes Dev.*, **26**, 1326–1338.

175. Laukka, T., Mariani, C. J., Ihantola, T., et al. (2016) Fumarate and Succinate Regulate Expression of Hypoxia-inducible Genes via TET Enzymes. *J. Biol. Chem.*, **291**, 4256–65.

176. Bourgeron, T., Chretien, D., Poggi-Bach, J., et al. (1994) Mutation of the fumarase gene in two siblings with progressive encephalopathy and fumarase deficiency. *J. Clin. Invest.*, **93**, 2514–8.

177. Coughlin, E. M., Christensen, E., Kunz, P. L., et al. (1998) Molecular Analysis and Prenatal Diagnosis of Human Fumarase Deficiency. *Mol. Genet. Metab.*, **63**, 254–262.

178. Benusiglio, P. R., Giraud, S., Deveaux, S., et al. (2014) Renal cell tumour characteristics in patients with the Birt-Hogg-Dubé cancer susceptibility syndrome: a retrospective, multicentre study. *Orphanet J. Rare Dis.*, **9**, 163.

179. Houweling, A. C., Gijezen, L. M., Jonker, M. A., et al. Renal cancer and pneumothorax risk in Birt–Hogg–Dubé syndrome; an analysis of 115 FLCN mutation carriers from 35 BHD families. *Br. J. Cancer*, **105**, 1912–1919.

180. Toro, J. R., Wei, M.-H., Glenn, G. M., et al. (2007) BHD mutations, clinical and molecular genetic investigations of Birt-Hogg-Dubé syndrome: a new series of 50 families and a review of published reports. *J. Med. Genet.*

181. Gatalica, Z., Lilleberg, S. L., Vranic, S., et al. (2009) Novel intronic germline FLCN gene mutation in a patient with multiple ipsilateral renal neoplasms. *Hum. Pathol.*, **40**, 1813–1819.

182. Pavlovich, C. P., Walther, M. M., Eyler, R. A., et al. (2002) Renal tumors in the Birt-Hogg-Dubé syndrome. *Am. J. Surg. Pathol.*, **26**, 1542–52.

183. Kuroda, N., Furuya, M., Nagashima, Y., et al. (2014) Intratumoral peripheral small papillary tufts: a diagnostic clue of renal tumors associated with Birt-Hogg-Dubé syndrome. *Ann. Diagn. Pathol.*, **18**, 171–176.

184. Benusiglio, P., Gad, S., Massard, C., et al. (2014) Case Report: Expanding the tumour spectrum associated with the Birt-Hogg-Dubé cancer susceptibility syndrome. *F1000Research*, **3**.

185. Dong, L., Gao, M., Hao, W., et al. (2016) Case Report of Birt–Hogg–Dubé Syndrome. *Medicine (Baltimore).*, **95**, e3695.

186. Pradella, L. M., Lang, M., Kurelac, I., et al. (2013) Where Birt–Hogg–Dubé meets Cowden Syndrome: mirrored genetic defects in two cases of syndromic oncocytic tumours. *Eur. J. Hum. Genet.*, **21**, 1169–1172.

187. Raymond, V. M., Long, J. M., Everett, J. N., et al. (2014) An oncocytic adrenal tumour in a patient with Birt-Hogg-Dubé syndrome. *Clin. Endocrinol. (Oxf).*, **80**, 925–927.

188. Mota-Burgos, A., Acosta, E. H., Márquez, F. V., et al. (2013) Birt-Hogg-Dubé syndrome in a patient with melanoma and a novel mutation in the *FCLN* gene. *Int. J. Dermatol.*, **52**, 323–326.

189. Kean Khoo, S., Bradley, M., Wong, F. K., et al. (2001) Birt-Hogg-DubeÂ syndrome: mapping of a novel hereditary neoplasia gene to chromosome 17p12-q11.2. *Birt-Hogg-DubeÂ syndrome: mapping of a novel hereditary neoplasia gene to chromosome 17p12-q11.2*; (2001) .

190. Nahorski, M. S., Reiman, A., Lim, D. H. K., et al. (2011) Birt Hogg-Dubé syndrome-associated FLCN mutations disrupt protein stability. *Hum. Mutat.*, **32**, 921–929.

191. Nickerson, M. L., Warren, M. B., Toro, J. R., et al. (2002) Mutations in a novel gene lead to kidney tumors, lung wall defects, and benign tumors of the hair follicle in patients with the Birt-Hogg-Dubé syndrome. *Cancer Cell*, **2**, 157–164.

192. Schmidt, L. S., Nickerson, M. L., Warren, M. B., et al. (2005) Germline BHD-Mutation Spectrum and Phenotype Analysis of a Large Cohort of Families with Birt-Hogg-Dubé Syndrome. *Germline BHD-Mutation Spectrum and Phenotype Analysis of a Large Cohort of Families with Birt-Hogg-Dubé Syndrome*; (2005) ; Vol. 76.

193. Ding, Y., Zhu, C., Zou, W., et al. (2015) FLCN intragenic deletions in Chinese familial primary spontaneous pneumothorax. *Am. J. Med. Genet. Part A*, **167**, 1125–1133.

194. Okimoto, K., Sakurai, J., Kobayashi, T., et al. (2004) A germ-line insertion in the Birt-Hogg-Dubé (BHD) gene gives rise to the Nihon rat model of inherited renal cancer. *Proc. Natl. Acad. Sci. U. S. A.*, **101**, 2023–7.

195. Vocke, C. D., Yang, Y., Pavlovich, C. P., et al. (2005) High Frequency of Somatic Frameshift BHD Gene Mutations in Birt-Hogg-Dubé-Associated Renal Tumors. *J. Natl. Cancer Inst.*, **97**.

196. Van Steensel, M. A. M., Verstraeten, V. L. R. M., Frank, J., et al. (2007) Novel Mutations in the BHD Gene and Absence of Loss of Heterozygosity in Fibrofolliculomas of Birt-Hogg-Dubé Patients. *J. Invest. Dermatol.*, **127**, 588–593.

197. Baba, M., Hong, S.-B., Sharma, N., et al. (2006) Folliculin encoded by the BHD gene interacts with a binding protein, FNIP1, and AMPK, and is involved in AMPK and mTOR signaling. *Proc. Natl. Acad. Sci. U. S. A.*, **103**, 15552–7.

198. Hasumi, H., Baba, M., Hong, S.-B., et al. (2008) Identification and characterization of a novel folliculin-interacting protein FNIP2. *Gene*, **415**, 60–7.

199. Shaw, R. J. (2009) LKB1 and AMP-activated protein kinase control of mTOR signalling and growth. *Acta Physiol. (Oxf).*, **196**, 65–80.

200. Hasumi, Y., Baba, M., Ajima, R., et al. (2009) Homozygous loss of BHD causes early embryonic lethality and kidney tumor development with activation of mTORC1 and mTORC2. *Proc. Natl. Acad. Sci.*, **106**, 18722–18727.

201. Hong, S.-B., Oh, H., Valera, V. A., et al. (2010) Inactivation of the FLCN tumor suppressor gene induces TFE3 transcriptional activity by increasing its nuclear localization. *PLoS One*, **5**, e15793.

202. Zbar, B., Tory, K., Merino, M., et al. (1994) Hereditary papillary renal cell carcinoma. *J. Urol.*, **151**, 561–6.

203. Schmidt, L., Junker, K., Weirich, G., et al. (1998) Two North American families with hereditary papillary renal carcinoma and identical novel mutations in the MET proto-oncogene. *Cancer Res.*, **58**, 1719–22.

204. Schmidt, L., Duh, F.-M., Chen, F., et al. (1997) Germline and somatic mutations in the tyrosine kinase domain of the MET proto-oncogene in papillary renal carcinomas. *Nat. Genet.*, **16**, 68–73.

205. Zbar, B., Glenn, G., Lubensky, I., et al. (1995) Hereditary papillary renal cell carcinoma: clinical studies in 10 families. *J. Urol.*, **153**, 907–12.

206. Ornstein, D. K., Lubensky, I. A., Venzon, D., et al. (2000) Prevalence of microscopic tumors in normal appearing renal parenchyma of patients with hereditary papillary renal cancer. *J. Urol.*, **163**, 431–3.

207. Schmidt, L., Junker, K., Nakaigawa, N., et al. (1999) Novel mutations of the MET proto-oncogene in papillary renal carcinomas. *Oncogene*, **18**, 2343–2350.

208. Miller, M., Ginalski, K., Lesyng, B., et al. (2001) Structural basis of oncogenic activation caused by point mutations in the kinase domain of the MET proto-oncogene: modeling studies. *Proteins*, **44**, 32–43.

209. Basilico, C., Arnesano, A., Galluzzo, M., et al. (2008) A High Affinity Hepatocyte Growth Factor-binding Site in the Immunoglobulin-like Region of Met. *J. Biol. Chem.*, **283**, 21267–21277.

210. Trusolino, L. and Comoglio, P. M. (2002) Scatter-factor and semaphorin receptors: cell signalling for invasive growth. *Nat. Rev. Cancer*, **2**, 289–300.

211. MATSUMURA, A., KUBOTA, T., TAIYOH, H., et al. (2013) HGF regulates VEGF expression via the c-Met receptor downstream pathways, PI3K/Akt, MAPK and STAT3, in CT26 murine cells. *Int. J. Oncol.*, **42**, 535–542.

212. Bardella, C., Pollard, P. J. and Tomlinson, I. (2011) SDH mutations in cancer. *Biochim. Biophys. Acta - Bioenerg.*, **1807**, 1432–1443.

213. Vanharanta, S., Buchta, M., McWhinney, S. R., et al. (2004) Early-Onset Renal Cell Carcinoma as a Novel Extraparaganglial Component of SDHB-Associated Heritable Paraganglioma. *Am. J. Hum. Genet.*, **74**, 153–159.

214. Ricketts, C., Woodward, E. R., Killick, P., et al. (2008) Germline SDHB mutations and familial renal cell carcinoma. *J. Natl. Cancer Inst.*, **100**, 1260–1262.

215. Ricketts, C. J., Forman, J. R., Rattenberry, E., et al. (2010) Tumor risks and genotype-phenotype-proteotype analysis in 358 patients with germline mutations in SDHB and SDHD. *Hum. Mutat.*, **31**, 41–51.

216. Malinoc, A., Sullivan, M., Wiech, T., et al. (2012) Biallelic inactivation of the SDHC gene in renal carcinoma associated with paraganglioma syndrome type 3. *Endocr. Relat. Cancer*, **19**, 283–290.

217. McEvoy, C. R., Koe, L., Choong, D. Y., et al. (2018) SDH-deficient renal cell carcinoma associated with biallelic mutation in succinate dehydrogenase A: comprehensive genetic profiling and its relation to therapy response. *npj Precis. Oncol.*, **2**, 9.

218. Nicolas, E., Demidova, E. V., Iqbal, W., et al. (2019) Interaction of germline variants in a family with a history of early-onset clear cell renal cell carcinoma. *Mol. Genet. Genomic Med.*, e556.

219. Bayley, J.-P., Kunst, H. P., Cascon, A., et al. (2010) SDHAF2 mutations in familial and sporadic paraganglioma and phaeochromocytoma. *Lancet Oncol.*, **11**, 366–372.

220. Gill, A. J., Hes, O., Papathomas, T., et al. (2014) Succinate Dehydrogenase (SDH)-deficient Renal Carcinoma. *Am. J. Surg. Pathol.*, **38**, 1588–1602.

221. Williamson, S. R., Eble, J. N., Amin, M. B., et al. (2014) Succinate dehydrogenase-deficient renal cell carcinoma: detailed characterization of 11 tumors defining a unique subtype of renal cell carcinoma. *Mod. Pathol.*, **28**, 80–94.

222. Gill, A. J., Pachter, N. S., Chou, A., et al. (2011) Renal tumors associated with germline SDHB mutation show distinctive morphology. *Am. J. Surg. Pathol.*, **35**, 1578–85.

223. Benn, D. E., Zhu, Y., Andrews, K. A., et al. (2018) Bayesian approach to determining penetrance of pathogenic SDH variants. *J. Med. Genet.*, **55**, 729–734.

224. Maniam, P., Zhou, K., Lonergan, M., et al. (2018) Pathogenicity and Penetrance of Germline SDHA Variants in Pheochromocytoma and Paraganglioma (PPGL). *J. Endocr. Soc.*, **2**, 806–816.

225. Andrews, K. A., Ascher, D. B., Pires, D. E. V., et al. (2018) Tumour risks and genotype-phenotype correlations associated with germline variants in succinate dehydrogenase subunit genes SDHB, SDHC and SDHD. *J. Med. Genet.*, **55**, 384–394.

226. Casey, R. T., Warren, A. Y., Rodrigues, J. E., et al. (2017) Clinical and Molecular Features of

Renal and Phaeochromocytoma/Paraganglioma Tumour Association Syndrome (RAPTAS): Case Series and Literature Review. *J. Clin. Endocrinol. Metab.*

227. Douwes Dekker, P., Hogendoorn, P., Kuipers-Dijkshoorn, N., et al. (2003) SDHD mutations in head and neck paragangliomas result in destabilization of complex II in the mitochondrial respiratory chain with loss of enzymatic activity and abnormal mitochondrial morphology. *J. Pathol.*, **201**, 480–486.

228. Lussey-Lepoutre, C., Hollinshead, K. E. R., Ludwig, C., et al. (2015) Loss of succinate dehydrogenase activity results in dependency on pyruvate carboxylation for cellular anabolism. *Nat. Commun.*, **6**, 8784.

229. Xiao, M., Yang, H., Xu, W., et al. (2012) Inhibition of α-KG-dependent histone and DNA demethylases by fumarate and succinate that are accumulated in mutations of FH and SDH tumor suppressors. *Genes Dev.*, **26**, 1326–1338.

230. Van Coster, R., Seneca, S., Smet, J., et al. (2003) Homozygous Gly555Glu mutation in the nuclear-encoded 70 kDa flavoprotein gene causes instability of the respiratory chain complex II. *Am. J. Med. Genet.*, **120A**, 13–18.

231. Piruat, J. I. and Millán-Uclés, A. (2014) Genetically modeled mice with mutations in mitochondrial metabolic enzymes for the study of cancer. *Front. Oncol.*, **4**, 200.

232. Yang, P., Cornejo, K. M., Sadow, P. M., et al. (2014) Renal cell carcinoma in tuberous sclerosis complex. *Am. J. Surg. Pathol.*, **38**, 895–909.

233. Rakowski, S. K., Winterkorn, E. B., Paul, E., et al. (2006) Renal manifestations of tuberous sclerosis complex: Incidence, prognosis, and predictive factors. *Kidney Int.*, **70**, 1777–1782.

234. McGuire, B. B. and Fitzpatrick, J. M. (2010) The diagnosis and management of complex renal cysts. *Curr. Opin. Urol.*, **20**, 349–54.

235. Seyam, R. M., Alkhudair, W. K., Kattan, S. A., et al. (2017) The Risks of Renal Angiomyolipoma: Reviewing the Evidence. *J. kidney cancer VHL*, **4**, 13–25.

236. Ebrahimi-Fakhari, D., Mann, L. L., Poryo, M., et al. (2018) Incidence of tuberous sclerosis and age at first diagnosis: new data and emerging trends from a national, prospective surveillance study. *Orphanet J. Rare Dis.*, **13**, 117.

237. Guo, J., Tretiakova, M. S., Troxell, M. L., et al. (2014) Tuberous sclerosis-associated renal cell carcinoma: a clinicopathologic study of 57 separate carcinomas in 18 patients. *Am. J. Surg. Pathol.*, **38**, 1457–67.

238. Dabora, S. L., Jozwiak, S., Franz, D. N., et al. (2001) Mutational analysis in a cohort of 224 tuberous sclerosis patients indicates increased severity of TSC2, compared with TSC1, disease in multiple organs. *Am. J. Hum. Genet.*, **68**, 64–80.

239. Tyburczy, M. E., Dies, K. A., Glass, J., et al. (2015) Mosaic and Intronic Mutations in TSC1/TSC2 Explain the Majority of TSC Patients with No Mutation Identified by Conventional Testing. *PLOS Genet.*, **11**, e1005637.

240. Inoki, K., Li, Y., Zhu, T., et al. (2002) TSC2 is phosphorylated and inhibited by Akt and suppresses mTOR signalling. *Nat. Cell Biol.*, **4**, 648–657.

241. Zhang, Y., Gao, X., Saucedo, L. J., et al. (2003) Rheb is a direct target of the tuberous sclerosis tumour suppressor proteins. *Nat. Cell Biol.*, **5**, 578–581.

242. Long, X., Lin, Y., Ortiz-Vega, S., et al. (2005) Rheb Binds and Regulates the mTOR Kinase. *Curr. Biol.*, **15**, 702–713.

243. Tan, M.-H., Mester, J. L., Ngeow, J., et al. (2012) Lifetime Cancer Risks in Individuals with Germline PTEN Mutations. *Clin. Cancer Res.*, **18**, 400–407.

244. Bubien, V., Bonnet, F., Brouste, V., et al. (2013) High cumulative risks of cancer in patients with *PTEN* hamartoma tumour syndrome. *J. Med. Genet.*, **50**, 255–263.

245. Nieuwenhuis, M. H., Kets, C. M., Murphy-Ryan, M., et al. (2014) Cancer risk and genotype–phenotype correlations in PTEN hamartoma tumor syndrome. *Fam. Cancer*, **13**, 57–63.

246. Mester, J. L., Zhou, M., Prescott, N., et al. (2012) Papillary Renal Cell Carcinoma Is Associated With PTEN Hamartoma Tumor Syndrome. *Urology*, **79**, 1187.e1-1187.e7.

247. Bennett, K. L., Mester, J. and Eng, C. (2010) Germline Epigenetic Regulation of KILLIN in Cowden and Cowden-like Syndrome. *JAMA*, **304**, 2724.

248. Orloff, M. S., He, X., Peterson, C., et al. (2013) Germline PIK3CA and AKT1 mutations in cowden and cowden-like syndromes. *Am. J. Hum. Genet.*, **92**, 76–80.

249. Shibata, Y., Yamazaki, M., Takei, M., et al. (2015) Early-onset, severe, and recurrent primary hyperparathyroidism associated with a novel &lt;i&gt;CDC73&lt;/i&gt; mutation. *Endocr. J.*, **62**, 627–632.

250. van der Tuin, K., Tops, C. M. J., Adank, M. A., et al. (2017) CDC73-Related Disorders: Clinical Manifestations and Case Detection in Primary Hyperparathyroidism. *J. Clin. Endocrinol. Metab.*, **102**, 4534–4540.

251. Haven, C. J., Wong, F. K., van Dam, E. W. C. M., et al. (2000) A Genotypic and Histopathological Study of a Large Dutch Kindred with Hyperparathyroidism-Jaw Tumor Syndrome [1]. *J. Clin. Endocrinol. Metab.*, **85**, 1449–1454.

252. Yart, A., Gstaiger, M., Wirbelauer, C., et al. (2005) The HRPT2 Tumor Suppressor Gene Product Parafibromin Associates with Human PAF1 and RNA Polymerase II. *Mol. Cell. Biol.*, **25**, 5052–5060.

253. Rozenblatt-Rosen, O., Hughes, C. M., Nannepaga, S. J., et al. (2005) The

Parafibromin Tumor Suppressor Protein Is Part of a Human Paf1 Complex. *Mol. Cell. Biol.*, **25**, 612–620.

254. Woodard, G. E., Lin, L., Zhang, J.-H., et al. (2005) Parafibromin, product of the hyperparathyroidism-jaw tumor syndrome gene HRPT2, regulates cyclin D1/PRAD1 expression. *Oncogene*, **24**, 1272–1276.

255. Lin, L., Zhang, J.-H., Panicker, L. M., et al. (2008) The parafibromin tumor suppressor protein inhibits cell proliferation by repression of the c-myc proto-oncogene. *Proc. Natl. Acad. Sci.*, **105**, 17420–17425.

256. Zhang, C., Kong, D., Tan, M.-H., et al. (2006) Parafibromin inhibits cancer cell growth and causes G1 phase arrest. *Biochem. Biophys. Res. Commun.*, **350**, 17–24.

257. Zhao, J., Yart, A., Frigerio, S., et al. (2007) Sporadic human renal tumors display frequent allelic imbalances and novel mutations of the HRPT2 gene. *Oncogene*, **26**, 3440–3449.

258. Hahn, M. A., Howell, V. M., Gill, A. J., et al. (2010) CDC73/HRPT2 CpG island hypermethylation and mutation of 5′-untranslated sequence are uncommon mechanisms of silencing parafibromin in parathyroid tumors. *Endocr. Relat. Cancer*, **17**, 273–282.

259. Cohen, A. J., Li, F. P., Berg, S., et al. (1979) Hereditary renal-cell carcinoma associated with a chromosomal translocation. *N. Engl. J. Med.*, **301**, 592–595.

260. Gemmill, R. M., West, J. D., Boldog, F., et al. (1998) The hereditary renal cell carcinoma 3;8 translocation fuses FHIT to a patched-related gene, TRC8. *Proc. Natl. Acad. Sci. U. S. A.*, **95**, 9572–7.

261. Bodmer, D., Eleveld, M. J., Ligtenberg, M. J. L., et al. (1998) An Alternative Route for Multistep Tumorigenesis in a Novel Case of Hereditary Renal Cell Cancer and a t(2;3)(q35;q21) Chromosome Translocation. *Am. J. Hum. Genet*, **62**, 1475–1483.

262. Bertolotto, C., Lesueur, F., Giuliano, S., et al. (2011) A SUMOylation-defective MITF germline mutation predisposes to melanoma and renal carcinoma. *Nature*, **480**, 94–98.

263. Farley, M. N., Schmidt, L. S., Mester, J. L., et al. (2013) A novel germline mutation in BAP1 predisposes to familial clear-cell renal cell carcinoma. *Mol. Cancer Res.*, **11**, 1061–71.

264. Benusiglio, P. R., Couvé, S., Gilbert-Dussardier, B., et al. (2015) A germline mutation in *PBRM1* predisposes to renal cell carcinoma. *J. Med. Genet.*, **52**, 426–430.

265. Woodward, E. R., Ricketts, C., Killick, P., et al. (2008) Familial Non-VHL Clear Cell (Conventional) Renal Cell Carcinoma: Clinical Features, Segregation Analysis, and Mutation Analysis of FLCN. *Clin. Cancer Res.*, **14**, 5925–5930.

266. Jafri, M., Wake, N. C., Ascher, D. B., et al. (2015) Germline Mutations in the CDKN2B Tumor Suppressor Gene Predispose to Renal Cell Carcinoma. *Cancer Discov.*, **5**, 723–9.

267. Creighton, C. J., Morgan, M., Gunaratne, P. H., et al. (2013) Comprehensive molecular characterization of clear cell renal cell carcinoma. *Nature*, **499**, 43–49.

268. Dalgliesh, G. L., Furge, K., Greenman, C., et al. (2010) Systematic sequencing of renal carcinoma reveals inactivation of histone modifying genes. *Nature*, **463**, 360–3.

269. Sato, Y., Yoshizato, T., Shiraishi, Y., et al. (2013) Integrated molecular analysis of clear-cell renal cell carcinoma. *Nat. Genet.*, **45**, 860–7.

270. Turajlic, S., Xu, H., Litchfield, K., et al. (2018) Deterministic Evolutionary Trajectories Influence Primary Tumor Growth: TRACERx Renal. *Cell*.

271. Davis, C. F., Ricketts, C. J., Wang, M., et al. (2014) The somatic genomic landscape of chromophobe renal cell carcinoma. *Cancer Cell*, **26**, 319–30.

272. Chen, F., Zhang, Y., Şenbabaoğlu, Y., et al. (2016) Multilevel Genomics-Based Taxonomy of Renal Cell Carcinoma. *Cell Rep.*, **14**, 2476–89.

273. Li, L., Shen, C., Nakamura, E., et al. (2013) SQSTM1 is a pathogenic target of 5q copy number gains in kidney cancer. *Cancer Cell*, **24**, 738–50.

274. Ricketts, C. J., De Cubas, A. A., Fan, H., et al. (2018) The Cancer Genome Atlas Comprehensive Molecular Characterization of Renal Cell Carcinoma. *Cell Rep.*, **23**, 313-326.e5.

275. Tsai, H.-C. and Baylin, S. B. (2011) Cancer epigenetics: linking basic biology to clinical medicine. *Cell Res.*, **21**, 502–517.

276. Herman, J. G., Latif, F., Weng, Y., et al. (1994) Silencing of the VHL tumor-suppressor gene by DNA methylation in renal carcinoma. *Proc. Natl. Acad. Sci. U. S. A.*, **91**, 9700–4.

277. Morrissey, C., Martinez, A., Zatyka, M., et al. (2001) Epigenetic inactivation of the RASSF1A 3p21.3 tumor suppressor gene in both clear cell and papillary renal cell carcinoma. *Cancer Res.*, **61**, 7277–7281.

278. Awakura, Y., Nakamura, E., Ito, N., et al. (2008) Methylation-associated silencing of TU3A in human cancers. *Int. J. Oncol.*, **33**, 893–9.

279. Kvasha, S., Gordiyuk, V., Kondratov, A., et al. (2008) Hypermethylation of the 5′CpG island of the FHIT gene in clear cell renal carcinomas. *Cancer Lett.*, **265**, 250–257.

280. Dulaimi, E., Ibanez de Caceres, I., Uzzo, R. G., et al. (2004) Promoter hypermethylation profile of kidney cancer. *Clin. Cancer Res.*, **10**, 3972–9.

281. Costa, V. L., Henrique, R., Ribeiro, F. R., et al. (2007) Quantitative promoter methylation analysis of multiple cancer-related genes in renal cell tumors. *BMC Cancer*, **7**, 133.

282. Morris, M. R., Hesson, L. B., Wagner, K. J., et al. (2003) Multigene methylation analysis of Wilms' tumour and adult renal cell carcinoma. *Oncogene*, **22**, 6794–6801.

283. Bennett, K. L., Campbell, R., Ganapathi, S., et al. (2011) Germline and somatic DNA methylation and epigenetic regulation of KILLIN in renal cell carcinoma. *Genes, Chromosom. Cancer*, **50**, 654–661.

284. Gumz, M. L., Zou, H., Kreinest, P. A., et al. (2007) Secreted Frizzled-Related Protein 1 Loss Contributes to Tumor Phenotype of Clear Cell Renal Cell Carcinoma. *Clin. Cancer Res.*, **13**, 4740–4749.

285. Yoo, K. H., Park, Y.-K., Kim, H.-S., et al. (2010) Epigenetic inactivation of HOXA5 and MSH2 gene in clear cell renal cell carcinoma. *Pathol. Int.*, **60**, 661–666.

286. Shenoy, N., Vallumsetla, N., Zou, Y., et al. (2015) Role of DNA methylation in renal cell carcinoma. *J. Hematol. Oncol.*, **8**, 88.

287. McRonald, F. E., Morris, M. R., Gentle, D., et al. (2009) CpG methylation profiling in VHL related and VHL unrelated renal cell carcinoma. *Mol. Cancer*, **8**, 31.

288. Morris, M. R., Ricketts, C. J., Gentle, D., et al. (2011) Genome-wide methylation analysis identifies epigenetically inactivated candidate tumour suppressor genes in renal cell carcinoma. *Oncogene*, **30**, 1390–401.

289. Ricketts, C. J., Morris, M. R., Gentle, D., et al. (2012) Genome-wide CpG island methylation analysis implicates novel genes in the pathogenesis of renal cell carcinoma View supplementary material. *Epigenetics*, **7**, 278–290.

290. Hu, C. Y., Mohtat, D., Yu, Y., et al. (2014) Kidney Cancer Is Characterized by Aberrant Methylation of Tissue-Specific Enhancers That Are Prognostic for Overall Survival. *Clin. Cancer Res.*, **20**, 4349–4360.

291. Lasseigne, B. N. and Brooks, J. D. (2018) The Role of DNA Methylation in Renal Cell Carcinoma. *Mol. Diagn. Ther.*, **22**, 431–442.

292. Dodd, K. M., Yang, J., Shen, M. H., et al. (2015) mTORC1 drives HIF-1α and VEGF-A signalling via multiple mechanisms involving 4E-BP1, S6K1 and STAT3. *Oncogene*, **34**, 2239–2250.

293. Ricketts, C. J., Crooks, D. R., Sourbier, C., et al. (2016) SnapShot: Renal Cell Carcinoma. *Cancer Cell*, **29**, 610-610.e1.

294. Sanger, F., Nicklen, S. and Coulson, A. R. (1977) DNA sequencing with chain-terminating inhibitors. *Proc. Natl. Acad. Sci. U. S. A.*, **74**, 5463–7.

295. Swerdlow, H., Wu, S. L., Harke, H., et al. (1990) Capillary gel electrophoresis for DNA sequencing. Laser-induced fluorescence detection with the sheath flow cuvette. *J. Chromatogr.*, **516**, 61–7.

296. Consortium, I. H. G. S. (2001) Initial sequencing and analysis of the human genome. *Nature*, **409**, 860–921.

297. Morin, R. D., Bainbridge, M., Fejes, A., et al. (2008) Profiling the HeLa S3 transcriptome using randomly primed cDNA and massively parallel short-read sequencing. *Biotechniques*, **45**, 81–94.

298. Li, Y. and Tollefsbol, T. O. (2011) DNA methylation detection: bisulfite genomic sequencing analysis. *Methods Mol. Biol.*, **791**, 11–21.

299. Robertson, G., Hirst, M., Bainbridge, M., et al. (2007) Genome-wide profiles of STAT1 DNA association using chromatin immunoprecipitation and massively parallel sequencing. *Nat. Methods*, **4**, 651–657.

300. Cretu Stancu, M., van Roosmalen, M. J., Renkens, I., et al. (2017) Mapping and phasing of structural variation in patient genomes using nanopore sequencing. *Nat. Commun.*, **8**, 1326.

301. Choi, Y., Chan, A. P., Kirkness, E., et al. (2018) Comparison of phasing strategies for whole human genomes. *PLOS Genet.*, **14**, e1007308.

302. Flusberg, B. A., Webster, D. R., Lee, J. H., et al. (2010) Direct detection of DNA methylation during single-molecule, real-time sequencing. *Nat. Methods*, **7**, 461–5.

303. Simpson, J. T., Workman, R. E., Zuzarte, P. C., et al. (2017) Detecting DNA cytosine methylation using nanopore sequencing. *Nat. Methods*, **14**, 407–410.

304. Hoenen, T., Groseth, A., Rosenke, K., et al. (2016) Nanopore Sequencing as a Rapidly Deployable Ebola Outbreak Tool. *Emerg. Infect. Dis.*, **22**, 331–4.

305. Quick, J., Grubaugh, N. D., Pullan, S. T., et al. (2017) Multiplex PCR method for MinION and Illumina sequencing of Zika and other virus genomes directly from clinical samples. *Nat. Protoc.*, **12**, 1261–1276.

306. Payne, A., Holmes, N., Rakyan, V., et al. (2018) BulkVis: a graphical viewer for Oxford nanopore bulk FAST5 files. *Bioinformatics*.

307. Coster, W. De, Roeck, A. De, Pooter, T. De, et al. (2018) Structural variants identified by Oxford Nanopore PromethION sequencing of the human genome. *bioRxiv*, 434118.

308. Kraft, F., Wesseler, K., Begemann, M., et al. (2019) Novel familial distal imprinting centre 1 (11p15.5) deletion provides further insights in imprinting regulation. *Clin. Epigenetics*, **11**, 30.

309. Mitsuhashi, S., Frith, M. C., Mizuguchi, T., et al. (2018) Robust detection of tandem repeat expansions from long DNA reads. *bioRxiv*, 356931.

310. Wu, M. C., Lee, S., Cai, T., et al. (2011) Rare-variant association testing for sequencing data with the sequence kernel association test. *Am. J. Hum. Genet.*, **89**, 82–93.

311. Tataurov, A. V., You, Y. and Owczarzy, R. (2008) Predicting ultraviolet spectrum of single stranded and double stranded deoxyribonucleic acids. *Biophys. Chem.*, **133**, 66–70.

312. Borgström, E., Paterlini, M., Mold, J. E., et al. (2017) Comparison of whole genome amplification techniques for human single cell exome sequencing. *PLoS One*, **12**, e0171566.

313. Kent, W. J., Sugnet, C. W., Furey, T. S., et al. (2002) The Human Genome Browser at UCSC. *Genome Res.*, **12**, 996–1006.

314. Lander, E. S., Linton, L. M., Birren, B., et al. (2001) Initial sequencing and analysis of the human genome. *Nature*, **409**, 860–921.

315. Untergasser, A., Cutcutache, I., Koressaar, T., et al. (2012) Primer3--new capabilities and interfaces. *Nucleic Acids Res.*, **40**, e115.

316. Ye, J., Coulouris, G., Zaretskaya, I., et al. (2012) Primer-BLAST: a tool to design target-specific primers for polymerase chain reaction. *BMC Bioinformatics*, **13**, 134.

317. Danecek, P., Auton, A., Abecasis, G., et al. (2011) The variant call format and VCFtools. *Bioinformatics*, **27**, 2156–2158.

318. McKenna, A., Hanna, M., Banks, E., et al. (2010) The Genome Analysis Toolkit: a MapReduce framework for analyzing next-generation DNA sequencing data. *Genome Res.*, **20**, 1297–303.

319. Wang, K., Li, M. and Hakonarson, H. (2010) ANNOVAR: functional annotation of genetic variants from high-throughput sequencing data. *Nucleic Acids Res.*, **38**, e164–e164.

320. Auton, A., Abecasis, G. R., Altshuler, D. M., et al. (2015) A global reference for human genetic variation. *Nature*, **526**, 68–74.

321. Ruderfer, D. M., Hamamsy, T., Lek, M., et al. (2016) Patterns of genic intolerance of rare copy number variation in 59,898 human exomes. *Nat. Genet.*, **48**, 1107–1111.

322. Kumar, P., Henikoff, S. and Ng, P. C. (2009) Predicting the effects of coding non-synonymous variants on protein function using the SIFT algorithm. *Nat. Protoc.*, **4**, 1073–1081.

323. Adzhubei, I., Jordan, D. M. and Sunyaev, S. R. (2013) Predicting Functional Effect of Human Missense Mutations Using PolyPhen-2. *Current Protocols in Human Genetics*, John Wiley & Sons, Inc., Hoboken, NJ, USA, Vol. Chapter 7, pp. 7.20.1-7.20.41.

324. Kircher, M., Witten, D. M., Jain, P., et al. (2014) A general framework for estimating the relative pathogenicity of human genetic variants. *Nat. Genet.*, **46**, 310–315.

325. Richards, S., Aziz, N., Bale, S., et al. (2015) Standards and guidelines for the interpretation of sequence variants: a joint consensus recommendation of the American College of Medical Genetics and Genomics and the Association for Molecular Pathology. *Genet. Med.*, **17**, 405–423.

326. Li, Q. and Wang, K. (2017) InterVar: Clinical Interpretation of Genetic Variants by the 2015 ACMG-AMP Guidelines. *Am. J. Hum. Genet.*, **100**, 267–280.

327. Loman, N. J., Quick, J. and Simpson, J. T. (2015) A complete bacterial genome assembled de novo using only nanopore sequencing data. *Nat. Methods*, **12**, 733–735.

328. Loman, N. J. and Quinlan, A. R. (2014) Poretools: a toolkit for analyzing nanopore sequence data. *Bioinformatics*, **30**, 3399–3401.

329. De Coster, W., D'Hert, S., Schultz, D. T., et al. (2018) NanoPack: visualizing and processing long-read sequencing data. *Bioinformatics*, **34**, 2666–2669.

330. Li, H. (2018) Minimap2: pairwise alignment for nucleotide sequences. *Bioinformatics*, **34**, 3094–3100.

331. Benusiglio, P. R., Couvé, S., Gilbert-Dussardier, B., et al. (2015) A germline mutation in PBRM1 predisposes to renal cell carcinoma. *J. Med. Genet.*, **52**, 426–430.

332. Ortega, S., Malumbres, M. and Barbacid, M. (2002) Cyclin D-dependent kinases, INK4 inhibitors and cancer. *Biochim. Biophys. Acta - Rev. Cancer*, **1602**, 73–87.

333. Roussel, M. F. (1999) The INK4 family of cell cycle inhibitors in cancer. *Oncogene*, **18**, 5311–5317.

334. Krimpenfort, P., IJpenberg, A., Song, J.-Y., et al. (2007) p15Ink4b is a critical tumour suppressor in the absence of p16Ink4a. *Nature*, **448**, 943–946.

335. Boultwood, J. and Wainscoat, J. S. (2007) Gene silencing by DNA methylation in haematological malignancies. *Br. J. Haematol.*, **138**, 3–11.

336. Arya, A. K., Bhadada, S. K., Singh, P., et al. (2017) Promoter hypermethylation inactivates CDKN2A, CDKN2B and RASSF1A genes in sporadic parathyroid adenomas. *Sci. Rep.*, **7**, 3123.

337. Spisák, S., Kalmár, A., Galamb, O., et al. (2012) Genome-Wide Screening of Genes Regulated by DNA Methylation in Colon Cancer Development. *PLoS One*, **7**, e46215.

338. Agarwal, S. K., Mateo, C. M. and Marx, S. J. (2009) Rare Germline Mutations in Cyclin-Dependent Kinase Inhibitor Genes in Multiple Endocrine Neoplasia Type 1 and Related States. *J. Clin. Endocrinol. Metab.*, **94**, 1826–1834.

339. Welander, J., Andreasson, A., Brauckhoff, M., et al. (2014) Frequent EPAS1/HIF2α exons 9 and 12 mutations in non-familial pheochromocytoma. *Endocr. Relat. Cancer*, **21**, 495–504.

340. Toledo, R. A., Qin, Y., Srikantan, S., et al. (2013) In vivo and in vitro oncogenic effects of HIF2A mutations in pheochromocytomas and paragangliomas. *Endocr. Relat. Cancer*, **20**, 349–59.

341. Yang, C., Sun, M. G., Matro, J., et al. (2013) Novel HIF2A mutations disrupt oxygen sensing, leading to polycythemia, paragangliomas, and somatostatinomas. *Blood*, **121**, 2563–2566.

342. Lorenzo, F. R., Yang, C., Ng Tang Fui, M., et

al. (2013) A novel EPAS1/HIF2A germline mutation in a congenital polycythemia with paraganglioma. *J. Mol. Med. (Berl).*, **91**, 507–12.

343. Rao, R. C. and Dou, Y. (2015) Hijacked in cancer: the KMT2 (MLL) family of methyltransferases. *Nat. Rev. Cancer*, **15**, 334–46.

344. Ibragimova, I., Maradeo, M. E., Dulaimi, E., et al. (2013) Aberrant promoter hypermethylation of PBRM1, BAP1, SETD2, KDM6A and other chromatin-modifying genes is absent or rare in clear cell RCC. *Epigenetics*, **8**, 486–93.

345. Gossage, L., Murtaza, M., Slatter, A. F., et al. (2014) Clinical and pathological impact of VHL, PBRM1, BAP1, SETD2, KDM6A , and JARID1c in clear cell renal cell carcinoma. *Genes, Chromosom. Cancer*, **53**, 38–51.

346. Lee, J.-E., Wang, C., Xu, S., et al. (2013) H3K4 mono- and di-methyltransferase MLL4 is required for enhancer activation during cell differentiation. *Elife*, **2**, e01503.

347. Rada-Iglesias, A. (2018) Is H3K4me1 at enhancers correlative or causative? *Nat. Genet.*, **50**, 4–5.

348. Ooi, S. K. T., Qiu, C., Bernstein, E., et al. (2007) DNMT3L connects unmethylated lysine 4 of histone H3 to de novo methylation of DNA. *Nature*, **448**, 714–717.

349. Lee, J., Kim, D.-H., Lee, S., et al. (2009) A tumor suppressive coactivator complex of p53 containing ASC-2 and histone H3-lysine-4 methyltransferase MLL3 or its paralogue MLL4. *Proc. Natl. Acad. Sci. U. S. A.*, **106**, 8513–8.

350. Buck, M. J., Raaijmakers, L. M., Ramakrishnan, S., et al. (2013) Alterations in chromatin accessibility and DNA methylation in clear cell renal cell carcinoma. *Oncogene*, **33**, 4961–4965.

351. Nishikawa, H., Wu, W., Koike, A., et al. (2009) BRCA1-associated protein 1 interferes with BRCA1/BARD1 RING heterodimer activity. *Cancer Res.*, **69**, 111–119.

352. Waterman, M. S. and Eggert, M. (1987) A new algorithm for best subsequence alignments with application to tRNA-rRNA comparisons. *J. Mol. Biol.*, **197**, 723–8.

353. Karczewski, K. J., Francioli, L. C., Tiao, G., et al. (2019) Variation across 141,456 human exomes and genomes reveals the spectrum of loss-of-function intolerance across human protein-coding genes. *bioRxiv*, 531210.

354. Costa-Guda, J., Soong, C. P., Parekh, V. I., et al. (2013) Germline and Somatic Mutations in Cyclin-Dependent Kinase Inhibitor Genes CDKN1A, CDKN2B, and CDKN2C in Sporadic Parathyroid Adenomas. *Horm. Cancer*, **4**, 301–307.

355. Lindberg, D., Åkerström, G. and Westin, G. (2007) Evaluation of CDKN2C/p18, CDKN1B/p27 and CDKN2B/p15 mRNA expression, and CpG methylation status in sporadic and MEN1-associated pancreatic endocrine tumours. *Clin. Endocrinol. (Oxf).*, **0**, 070907134102003-???

356. Boël, P., Wildmann, C., Sensi, M. L., et al. (1995) BAGE: a new gene encoding an antigen recognized on human melanomas by cytolytic T lymphocytes. *Immunity*, **2**, 167–75.

357. Ruault, M., van der Bruggen, P., Brun, M.-E., et al. (2002) New BAGE (B melanoma antigen) genes mapping to the juxtacentromeric regions of human chromosomes 13 and 21 have a cancer/testis expression profile. *Eur. J. Hum. Genet.*, **10**, 833–840.

358. Ruault, M., Ventura, M., Galtier, N., et al. (2003) BAGE genes generated by juxtacentromeric reshuffling in the Hominidae lineage are under selective pressure. *Genomics*, **81**, 391–399.

359. Claes, K. B. M. and Leeneer, K. De (2014) Dealing with Pseudogenes in Molecular Diagnostics in the Next-Generation Sequencing Era. 303–315.

360. Ribeiro, A., Golicz, A., Hackett, C. A., et al. (2015) An investigation of causes of false positive single nucleotide polymorphisms using simulated reads from a small eukaryote genome. *BMC Bioinformatics*, **16**, 382.

361. Li, Y., Bögershausen, N., Alanay, Y., et al. (2011) A mutation screen in patients with Kabuki syndrome. *Hum. Genet.*, **130**, 715–724.

362. Makrythanasis, P., van Bon, B., Steehouwer, M., et al. (2013) *MLL2* mutation detection in 86 patients with Kabuki syndrome: a genotype-phenotype study. *Clin. Genet.*, **84**, 539–545.

363. Koemans, T. S., Kleefstra, T., Chubak, M. C., et al. (2017) Functional convergence of histone methyltransferases EHMT1 and KMT2C involved in intellectual disability and autism spectrum disorder. *PLOS Genet.*, **13**, e1006864.

364. Niikawa, N., Kuroki, Y., Kajii, T., et al. (1988) Kabuki make-up (Niikawa-Kuroki) syndrome: A study of 62 patients. *Am. J. Med. Genet.*, **31**, 565–589.

365. Kleefstra, T., Kramer, J. M., Neveling, K., et al. (2012) Disruption of an EHMT1-associated chromatin-modification module causes intellectual disability. *Am. J. Hum. Genet.*, **91**, 73–82.

366. Rampias, T., Karagiannis, D., Avgeris, M., et al. (2019) The lysine-specific methyltransferase KMT 2C/ MLL 3 regulates DNA repair components in cancer . *EMBO Rep.*, **20**.

367. Gala, K., Li, Q., Sinha, A., et al. (2018) KMT2C mediates the estrogen dependence of breast cancer through regulation of ERα enhancer function. *Oncogene*, **37**, 4692–4710.

368. Ortega-Molina, A., Boss, I. W., Canela, A., et al. (2015) The histone lysine methyltransferase KMT2D sustains a gene expression program that represses B cell lymphoma development. *Nat. Med.*, **21**, 1199–208.

369. Guo, C., Chen, L. H., Huang, Y., et al. (2013) KMT2D maintains neoplastic cell proliferation and global histone H3 lysine 4

monomethylation. *Oncotarget*, **4**, 2144–53.

370. Carosso, G. A., Boukas, L., Augustin, J. J., et al. (2018) Transcriptional suppression from KMT2D loss disrupts cell cycle and hypoxic responses in neurodevelopmental models of Kabuki syndrome. *bioRxiv*, 484410.

371. de Billy, E., Strocchio, L., Cacchione, A., et al. (2019) Burkitt lymphoma in a patient with Kabuki syndrome carrying a novel *KMT2D* mutation. *Am. J. Med. Genet. Part A*, **179**, 113–117.

372. Teranishi, H., Koga, Y., Nakashima, K., et al. (2018) Cancer Management in Kabuki Syndrome. *J. Pediatr. Hematol. Oncol.*, **40**, 1.

373. Karagianni, P., Lambropoulos, V., Stergidou, D., et al. (2016) Recurrent giant cell fibroblastoma: Malignancy predisposition in Kabuki syndrome revisited. *Am. J. Med. Genet. A*, **170A**, 1333–8.

374. Lv, S., Ji, L., Chen, B., et al. (2018) Histone methyltransferase KMT2D sustains prostate carcinogenesis and metastasis via epigenetically activating LIFR and KLF4. *Oncogene*, **37**, 1354–1368.

375. Beebe-Dimmer, J. L., Zuhlke, K. A., Johnson, A. M., et al. (2018) Rare germline mutations in African American men diagnosed with early-onset prostate cancer. *Prostate*, **78**, 321–326.

376. Whitworth, J., Smith, P. S., Martin, J.-E., et al. (2018) Comprehensive Cancer-Predisposition Gene Testing in an Adult Multiple Primary Tumor Series Shows a Broad Range of Deleterious Variants and Atypical Tumor Phenotypes. *Am. J. Hum. Genet.*, **103**, 3–18.

377. Duggan, M. A., Anderson, W. F., Altekruse, S., et al. (2016) The surveillance, epidemiology, and end results (SEER) program and pathology: Toward strengthening the critical relationship. *Am. J. Surg. Pathol.*, **40**, e94–e102.

378. Forbes, S. A., Beare, D., Gunasekaran, P., et al. (2015) COSMIC: Exploring the world's knowledge of somatic mutations in human cancer. *Nucleic Acids Res.*, **43**, D805–D811.

379. Easton, D. F., Lesueur, F., Decker, B., et al. (2016) No evidence that protein truncating variants in *BRIP1* are associated with breast cancer risk: implications for gene panel testing. *J. Med. Genet.*, **53**, 298–309.

380. Byers, H., Wallis, Y., van Veen, E. M., et al. (2016) Sensitivity of BRCA1/2 testing in high-risk breast/ovarian/male breast cancer families: little contribution of comprehensive RNA/NGS panel testing. *Eur. J. Hum. Genet.*, **24**, 1591–1597.

381. Leongamornlert, D., Saunders, E., Dadaev, T., et al. (2014) Frequent germline deleterious mutations in DNA repair genes in familial prostate cancer cases are associated with advanced disease. *Br. J. Cancer*, **110**, 1663–72.

382. Wu, Y., Yu, H., Zheng, S. L., et al. (2018) A comprehensive evaluation of *CHEK2* germline mutations in men with prostate cancer. *Prostate*, **78**, 607–615.

383. Desrichard, A., Bidet, Y., Uhrhammer, N., et al. (2011) CHEK2 contribution to hereditary breast cancer in non-BRCA families. *Breast Cancer Res.*, **13**, R119.

384. Roeb, W., Higgins, J. and King, M.-C. (2012) Response to DNA damage of CHEK2 missense mutations in familial breast cancer. *Hum. Mol. Genet.*, **21**, 2738–44.

385. Clark, G. R., Sciacovelli, M., Gaude, E., et al. (2014) Germline FH mutations presenting with pheochromocytoma. *J. Clin. Endocrinol. Metab.*, **99**, E2046-50.

386. Hao, H.-X., Khalimonchuk, O., Schraders, M., et al. (2009) SDH5, a gene required for flavination of succinate dehydrogenase, is mutated in paraganglioma. *Science*, **325**, 1139–42.

387. Bausch, B., Schiavi, F., Ni, Y., et al. (2017) Clinical Characterization of the Pheochromocytoma and Paraganglioma Susceptibility Genes SDHA, TMEM127, MAX, and SDHAF2 for Gene-Informed Prevention. *JAMA Oncol.*, **3**, 1204–1212.

388. Huang, K., Mashl, R. J., Wu, Y. Y., et al. (2018) Pathogenic Germline Variants in 10,389 Adult Cancers. *Cell*, **173**, 355-370.e14.

389. Varela, I., Tarpey, P., Raine, K., et al. (2011) Exome sequencing identifies frequent mutation of the SWI/SNF complex gene PBRM1 in renal carcinoma. *Nature*, **469**, 539–542.

390. The Exome Aggregation Consortium (ExAC) (2015) Analysis of protein-coding genetic variation in 60,706 humans. *bioRxiv*, 030338.

391. Wu, K., Hinson, S. R., Ohashi, A., et al. (2005) Functional evaluation and cancer risk assessment of BRCA2 unclassified variants. *Cancer Res.*, **65**, 417–26.

392. Ali, A. M., Kirby, M., Jansen, M., et al. (2009) Identification and characterization of mutations in FANCL gene: a second case of Fanconi anemia belonging to FA-L complementation group. *Hum. Mutat.*, **30**, E761-70.

393. Calkhoven, C. F., Müller, C. and Leutz, A. (2000) Translational control of C/EBPalpha and C/EBPbeta isoform expression. *Genes Dev.*, **14**, 1920–32.

394. Rashid, M. U., Gull, S., Faisal, S., et al. (2011) Identification of the deleterious 2080insA BRCA1 mutation in a male renal cell carcinoma patient from a family with multiple cancer diagnoses from Pakistan. *Fam. Cancer*, **10**, 709–712.

395. Wu, J., Wang, H., Ricketts, C. J., et al. (2018) Germline mutations of renal cancer predisposition genes and clinical relevance in Chinese patients with sporadic, early-onset disease. *Cancer*, cncr.31908.

396. Cybulski, C., Górski, B., Huzarski, T., et al. (2004) CHEK2 is a multiorgan cancer susceptibility gene. *Am. J. Hum. Genet.*, **75**, 1131–5.

397. Näslund-Koch, C., Nordestgaard, B. G. and Bojesen, S. E. (2016) Increased Risk for Other Cancers in Addition to Breast Cancer for CHEK2*1100delC Heterozygotes Estimated From the Copenhagen General Population Study. *J. Clin. Oncol.*, **34**, 1208–16.

398. Nevanlinna, H. and Bartek, J. (2006) The CHEK2 gene and inherited breast cancer susceptibility. *Oncogene*, **25**, 5912–5919.

399. Jonsson, P., Bandlamudi, C., Cheng, M. L., et al. (2019) Tumour lineage shapes BRCA-mediated phenotypes. *Nature*, **571**, 576–579.

400. Rafnar, T., Gudbjartsson, D. F., Sulem, P., et al. (2011) Mutations in BRIP1 confer high risk of ovarian cancer. *Nat. Genet.*, **43**, 1104–1107.

401. Seal, S., Thompson, D., Renwick, A., et al. (2006) Truncating mutations in the Fanconi anemia J gene BRIP1 are low-penetrance breast cancer susceptibility alleles. *Nat. Genet.*, **38**, 1239–1241.

402. Weber-Lassalle, N., Hauke, J., Ramser, J., et al. (2018) BRIP1 loss-of-function mutations confer high risk for familial ovarian cancer, but not familial breast cancer. *Breast Cancer Res.*, **20**, 7.

403. DiMario, F. J., Sahin, M. and Ebrahimi-Fakhari, D. (2015) Tuberous Sclerosis Complex. *Pediatr. Clin. North Am.*, **62**, 633–648.

404. Müller, C., Calkhoven, C. F., Sha, X., et al. (2004) The CCAAT enhancer-binding protein alpha (C/EBPalpha) requires a SWI/SNF complex for proliferation arrest. *J. Biol. Chem.*, **279**, 7353–8.

405. Havrilla, J. M., Pedersen, B. S., Layer, R. M., et al. (2019) A map of constrained coding regions in the human genome. *Nat. Genet.*, **51**, 88–95.

406. Shah, N., Hou, Y.-C. C., Yu, H.-C., et al. (2018) Identification of Misclassified ClinVar Variants via Disease Population Prevalence. *Am. J. Hum. Genet.*, **102**, 609–619.

407. Tan, R., Wang, Y., Kleinstein, S. E., et al. (2014) An evaluation of copy number variation detection tools from whole-exome sequencing data. *Hum. Mutat.*, **35**, 899–907.

408. Zawistowski, M., Gopalakrishnan, S., Ding, J., et al. (2010) Extending rare-variant testing strategies: analysis of noncoding sequence and imputed genotypes. *Am. J. Hum. Genet.*, **87**, 604–17.

409. Li, B. and Leal, S. M. (2008) Methods for Detecting Associations with Rare Variants for Common Diseases: Application to Analysis of Sequence Data. *Am. J. Hum. Genet.*, **83**, 311–321.

410. Lee, S., Emond, M. J., Bamshad, M. J., et al. (2012) Optimal unified approach for rare-variant association testing with application to small-sample case-control whole-exome sequencing studies. *Am. J. Hum. Genet.*, **91**, 224–37.

411. Lee, S., Abecasis, G. R., Boehnke, M., et al. (2014) Rare-variant association analysis: study designs and statistical tests. *Am. J. Hum. Genet.*, **95**, 5–23.

412. Shaw, K. A., Cutler, D. J., Okou, D., et al. (2019) Genetic variants and pathways implicated in a pediatric inflammatory bowel disease cohort. *Genes Immun.*, **20**, 131–142.

413. Klein, K., Tremmel, R., Winter, S., et al. (2019) A New Panel-Based Next-Generation Sequencing Method for ADME Genes Reveals Novel Associations of Common and Rare Variants With Expression in a Human Liver Cohort. *Front. Genet.*, **10**, 7.

414. Leongamornlert, D. A., Saunders, E. J., Wakerell, S., et al. (2019) Germline DNA Repair Gene Mutations in Young-onset Prostate Cancer Cases in the UK: Evidence for a More Extensive Genetic Panel. *Eur. Urol.*

415. Bourque, G., Burns, K. H., Gehring, M., et al. (2018) Ten things you should know about transposable elements. *Genome Biol.*, **19**, 199.

416. Ganguly, A., Dunbar, T., Chen, P., et al. (2003) Exon skipping caused by an intronic insertion of a young Alu Yb9 element leads to severe hemophilia�A. *Hum. Genet.*, **113**, 348–352.

417. Schwahn, U., Lenzner, S., Dong, J., et al. (1998) Positional cloning of the gene for X-linked retinitis pigmentosa 2. *Nat. Genet.*, **19**, 327–332.

418. Teugels, E., De Brakeleer, S., Goelen, G., et al. (2005) De novo Alu element insertions targeted to a sequence common to the BRCA1 and BRCA2 genes. *Hum. Mutat.*, **26**, 284–284.

419. Lanikova, L., Kucerova, J., Indrak, K., et al. (2013) β-Thalassemia Due to Intronic LINE-1 Insertion in the β-Globin Gene (HBB): Molecular Mechanisms Underlying Reduced Transcript Levels of the β-GlobinL1 Allele. *Hum. Mutat.*, **34**, 1361.

420. Gardner, E. J., Lam, V. K., Harris, D. N., et al. (2017) The Mobile Element Locator Tool (MELT): population-scale mobile element discovery and biology. *Genome Res.*, **27**, 1916–1929.

421. Vergnaud, G. and Denoeud, F. (2000) Minisatellites: mutability and genome architecture. *Genome Res.*, **10**, 899–907.

422. Liquori, C. L., Ricker, K., Moseley, M. L., et al. (2001) Myotonic Dystrophy Type 2 Caused by a CCTG Expansion in Intron 1 of ZNF9. *Science (80-.).*, **293**, 864–867.

423. Ishiura, H., Doi, K., Mitsui, J., et al. (2018) Expansions of intronic TTTCA and TTTTA repeats in benign adult familial myoclonic epilepsy. *Nat. Genet.*, **50**, 581–590.

424. Pringsheim, T., Wiltshire, K., Day, L., et al. (2012) The incidence and prevalence of Huntington's disease: A systematic review and meta-analysis. *Mov. Disord.*, **27**, 1083–1091.

425. Grünewald, T. G. P., Bernard, V., Gilardi-Hebenstreit, P., et al. (2015) Chimeric EWSR1-FLI1 regulates the Ewing sarcoma susceptibility gene EGR2 via a GGAA microsatellite. *Nat. Genet.*, **47**, 1073–1078.

426. Mousavi, N., Shleizer-Burko, S., Yanicky, R., et al. (2019) Profiling the genome-wide landscape

of tandem repeat expansions. *bioRxiv*, 361162.

427. Sidiropoulos, K., Viteri, G., Sevilla, C., et al. (2017) Reactome enhanced pathway visualization. *Bioinformatics*, **33**, 3461–3467.

428. Repana, D., Nulsen, J., Dressler, L., et al. (2019) The Network of Cancer Genes (NCG): a comprehensive catalogue of known and candidate cancer genes from cancer sequencing screens. *Genome Biol.*, **20**, 1.

429. Bailey, M. H., Tokheim, C., Porta-Pardo, E., et al. (2018) Comprehensive Characterization of Cancer Driver Genes and Mutations. *Cell*, **174**, 1034–1035.

430. Fromer, M., Moran, J. L., Chambert, K., et al. (2012) Discovery and statistical genotyping of copy-number variation from whole-exome sequencing depth. *Am. J. Hum. Genet.*, **91**, 597–607.

431. (2003) The International HapMap Project. *Nature*, **426**, 789–796.

432. Zhou, H., Alexander, D. and Lange, K. (2011) A quasi-Newton acceleration for high-dimensional optimization algorithms. *Stat. Comput.*, **21**, 261–273.

433. Ruark, E., Münz, M., Renwick, A., et al. (2015) The ICR1000 UK exome series: a resource of gene variation in an outbred population. *F1000Research*, **4**, 883.

434. Lee, S., Fuchsberger, C., Kim, S., et al. (2016) An efficient resampling method for calibrating single and gene-based rare variant association analysis in case-control studies. *Biostatistics*, **17**, 1–15.

435. Ehret, G. B. (2010) Genome-Wide Association Studies: Contribution of Genomics to Understanding Blood Pressure and Essential Hypertension. *Curr. Hypertens. Rep.*, **12**, 17.

436. Wang, J., Vasaikar, S., Shi, Z., et al. (2017) WebGestalt 2017: a more comprehensive, powerful, flexible and interactive gene set enrichment analysis toolkit. *Nucleic Acids Res.*, **45**, W130–W137.

437. Mi, H., Muruganujan, A., Ebert, D., et al. (2019) PANTHER version 14: more genomes, a new PANTHER GO-slim and improvements in enrichment analysis tools. *Nucleic Acids Res.*, **47**, D419–D426.

438. Gao, J., Aksoy, B. A., Dogrusoz, U., et al. (2013) Integrative Analysis of Complex Cancer Genomics and Clinical Profiles Using the cBioPortal. *Sci. Signal.*, **6**, pl1–pl1.

439. Hasselblatt, M., Nagel, I., Oyen, F., et al. (2014) SMARCA4-mutated atypical teratoid/rhabdoid tumors are associated with inherited germline alterations and poor prognosis. *Acta Neuropathol.*, **128**, 453–456.

440. Li, J., Duns, G., Westers, H., et al. (2016) SETD2: an epigenetic modifier with tumor suppressor functionality. *Oncotarget*, **7**, 50719–50734.

441. Luscan, A., Laurendeau, I., Malan, V., et al. (2014) Mutations in *SETD2* cause a novel overgrowth condition. *J. Med. Genet.*, **51**, 512–517.

442. Lumish, H. S., Wynn, J., Devinsky, O., et al. (2015) Brief Report: SETD2 Mutation in a Child with Autism, Intellectual Disabilities and Epilepsy. *J. Autism Dev. Disord.*, **45**, 3764–3770.

443. Smit, D. L., Mensenkamp, A. R., Badeloe, S., et al. (2011) Hereditary leiomyomatosis and renal cell cancer in families referred for fumarate hydratase germline mutation analysis. *Clin. Genet.*, **79**, 49–59.

444. Casey, R. T., McLean, M. A., Madhu, B., et al. (2018) Translating In Vivo Metabolomic Analysis of Succinate Dehydrogenase–Deficient Tumors Into Clinical Utility. *JCO Precis. Oncol.*, 1–12.

445. Cachat, F. and Renella, R. (2016) Risk of cancer in patients with polycystic kidney disease. *Lancet. Oncol.*, **17**, e474.

446. Christiansen, C. F., Onega, T., Sværke, C., et al. (2014) Risk and Prognosis of Cancer in Patients with Nephrotic Syndrome. *Am. J. Med.*, **127**, 871-877.e1.

447. Kondo, T., Sasa, N., Yamada, H., et al. (2018) Acquired cystic disease-associated renal cell carcinoma is the most common subtype in long-term dialyzed patients: Central pathology results according to the 2016 WHO classification in a multi-institutional study. *Pathol. Int.*, **68**, 543–549.

448. Ferner, R. E. (2007) Neurofibromatosis 1. *Eur. J. Hum. Genet.*, **15**, 131–138.

449. Olsen, J. V, Vermeulen, M., Santamaria, A., et al. (2010) Quantitative phosphoproteomics reveals widespread full phosphorylation site occupancy during mitosis. *Sci. Signal.*, **3**, ra3.

450. Hennekam, R. C. M. (2006) Rubinstein–Taybi syndrome. *Eur. J. Hum. Genet.*, **14**, 981–985.

451. Van Dyke, D. L., Weiss, L., Roberson, J. R., et al. (1983) The frequency and mutation rate of balanced autosomal rearrangements in man estimated from prenatal genetic studies for advanced maternal age. *Am. J. Hum. Genet.*, **35**, 301–8.

452. Vasilevska, M., Ivanovska, E., Kubelka Sabit, K., et al. (2013) The incidence and type of chromosomal translocations from prenatal diagnosis of 3800 patients in the republic of macedonia. *Balkan J. Med. Genet.*, **16**, 23–8.

453. Jacobs, P. A., Browne, C., Gregson, N., et al. (1992) Estimates of the frequency of chromosome abnormalities detectable in unselected newborns using moderate levels of banding. *J. Med. Genet.*, **29**, 103–8.

454. Collins, R. L., Brand, H., Karczewski, K. J., et al. (2019) An open resource of structural variation for medical and population genetics. *bioRxiv*, 578674.

455. Brand, H., Pillalamarri, V., Collins, R. L., et al. (2014) Cryptic and complex chromosomal aberrations in early-onset neuropsychiatric disorders. *Am. J. Hum. Genet.*, **95**, 454–61.

456. Mohamed, A. M., Kamel, A., Mahmoud, W., et al. (2015) Intellectual disability secondary to a 16p13 duplication in a 1;16 translocation. Extended phenotype in a four-generation family. *Am. J. Med. Genet. Part A*, **167**, 128–136.

457. Minouk J, S., Michael E, J., Craig D, H., et al. (2018) Mortality and Cancer Incidence in Carriers of Balanced Robertsonian Translocations: a National Cohort Study. *Am. J. Epidemiol.*

458. Martin, R. H. (2008) Cytogenetic determinants of male fertility. *Hum. Reprod. Update*, **14**, 379–390.

459. Boldog, F. L., Gemmillt, R. M., Wilkes, C. M., et al. (1993) Positional cloning of the hereditary renal carcinoma 3;8 chromosome translocation breakpoint (suppresor gene/fagile site/polycystic kidney diease/lung cancer/thyroid cancer). *Genetics*, **90**, 8509–8513.

460. Gnarra, J. R., Tory, K., Weng, Y., et al. (1994) Mutations of the VHL tumour suppressor gene in renal carcinoma. *Nat. Genet.*, **7**, 85–90.

461. Young, A. C., Craven, R. A., Cohen, D., et al. (2009) Analysis of VHL Gene Alterations and their Relationship to Clinical Parameters in Sporadic Conventional Renal Cell Carcinoma. *Clin. Cancer Res.*, **15**, 7582–7592.

462. Peña-Llopis, S., Vega-Rubín-de-Celis, S., Liao, A., et al. (2012) BAP1 loss defines a new class of renal cell carcinoma. *Nat. Genet.*, **44**, 751–9.

463. Dreijerink, K., Braga, E., Kuzmin, I., et al. (2001) The candidate tumor suppressor gene, RASSF1A, from human chromosome 3p21.3 is involved in kidney tumorigenesis. *Proc. Natl. Acad. Sci. U. S. A.*, **98**, 7504–9.

464. Weiler, K. S. and Wakimoto, B. T. (1995) Heterochromatin and Gene Expression in Drosophila. *Annu. Rev. Genet.*, **29**, 577–605.

465. Panani, A. D., Pappa, V. and Raptis, S. A. (2004) Novel constitutional translocations t(3;5)(p25;q22) and t(1;14)(p31;q21) in patients with acute leukemia. *Ann. Hematol.*, **83**, 156–159.

466. Ganly, P., McDonald, M., Spearing, R., et al. (2004) Constitutional t(5;7)(q11;p15) rearranged to acquire monosomy7q and trisomy 1q in a patient with myelodysplastic syndrome transforming to acute myelocytic leukemia. *Cancer Genet. Cytogenet.*, **149**, 125–130.

467. Li, Y., Schwab, C., Ryan, S. L., et al. (2014) Constitutional and somatic rearrangement of chromosome 21 in acute lymphoblastic leukaemia. *Nature*, **508**, 98–102.

468. Russel, J., Dutta, U., Wand, D., et al. (2009) The 9p24.3 Breakpoint of a Constitutional t(6;9)(p12;p24) in a Patient with Chronic Lymphocytic Leukemia Maps Close to the Putative Promoter Region of the DMRT2 Gene. *Cytogenet. Genome Res.*, **125**, 81–86.

469. Elsaid, M. Y., Gill, K. G., Gosain, A., et al. (2017) Synchronous Presentation of Renal Cell Carcinoma and Hodgkin Lymphoma in an Adolescent. *J. Pediatr. Hematol. Oncol.*, **39**, e399–e402.

470. Slade, I., Stephens, P., Douglas, J., et al. (2010) Constitutional translocation breakpoint mapping by genome-wide paired-end sequencing identifies HACE1 as a putative Wilms tumour susceptibility gene. *J. Med. Genet.*, **47**, 342–347.

471. Hoban, P. R., Cowen, R. L., Mitchell, E. L., et al. (1997) Physical localisation of the breakpoints of a constitutional translocation t(5;6)(q21;q21) in a child with bilateral Wilms' tumour. *J. Med. Genet.*, **34**, 343–5.

472. Vernon, E. G., Malik, K., Reynolds, P., et al. (2003) The parathyroid hormone-responsive B1 gene is interrupted by a t(1;7)(q42;p15) breakpoint associated with Wilms' tumour. *Oncogene*, **22**, 1371–1380.

473. Saikevych, I. A., Mayer, M., Brooks, V. P., et al. (1987) Cytogenetic study of a testicular tumor in a translocation (13;14) carrier. *Cancer Genet. Cytogenet.*, **26**, 299–307.

474. Veltman, I. M., Vreede, L. A., Cheng, J., et al. (2005) Fusion of the SUMO/Sentrin-specific protease 1 gene SENP1 and the embryonic polarity-related mesoderm development gene MESDC2 in a patient with an infantile teratoma and a constitutional t(12;15)(q13;q25). *Hum. Mol. Genet.*, **14**, 1955–1963.

475. Nicodème, F., Geffroy, S., Conti, M., et al. (2005) Familial occurrence of thymoma and autoimmune diseases with the constitutional translocation t(14;20)(q24.1;p12.3). *Genes, Chromosom. Cancer*, **44**, 154–160.

476. Koorey, D., Basha, N. J., Tomaras, C., et al. (2000) Appendiceal carcinoma complicating adenomatous polyposis in a young woman with a de novo constitutional reciprocal translocation t(5;8)(q22;p23.1). *J. Med. Genet.*, **37**, 71–5.

477. Savaşan, S., Lorenzana, A., Williams, J. A., et al. (1998) Constitutional balanced translocations in alveolar rhabdomyosarcoma. *Cancer Genet. Cytogenet.*, **105**, 50–4.

478. Niazi, M., van Dijken, P. J. and al Moutaery, K. (1998) A patient with meningioma showing multiple cytogenetic abnormalities and a constitutional translocation (3;9)(q13.3;q22). *Cancer Genet. Cytogenet.*, **105**, 11–3.

479. Triviño, E., Guitart, M., Egozcue, J., et al. (1997) Characterization by FISH of a t(5;13) in a patient with bilateral retinoblastoma. *Cancer Genet. Cytogenet.*, **96**, 23–5.

480. Sossey-Alaoui, K., Su, G., Malaj, E., et al. (2002) WAVE3, an actin-polymerization gene, is truncated and inactivated as a result of a constitutional t(1;13)(q21;q12) chromosome translocation in a patient with ganglioneuroblastoma. *Oncogene*, **21**, 5967–5974.

481. Vandepoele, K., Andries, V., Van Roy, N., et al. (2008) A Constitutional Translocation t(1;17)(p36.2;q11.2) in a Neuroblastoma Patient Disrupts the Human NBPF1 and ACCN1 Genes. *PLoS One*, **3**, e2207.

482. Roberts, T., Chernova, O. and Cowell, J. K. (1998) NB4S, a member of the TBC1 domain family of genes, is truncated as a result of a constitutional t(1;10)(p22;q21) chromosome translocation in a patient with stage 4S neuroblastoma. *Hum. Mol. Genet.*, **7**, 1169–78.

483. Thibodeau, M. L., Steinraths, M., Brown, L., et al. (2017) Genomic and Cytogenetic Characterization of a Balanced Translocation Disrupting &lt;b&gt;&lt;i&gt;NUP98&lt;/i&gt;&lt;/b&gt; *Cytogenet. Genome Res.*, **152**, 117–121.

484. Shuch, B. and Zhang, J. (2018) Genetic Predisposition to Renal Cell Carcinoma: Implications for Counseling, Testing, Screening, and Management. *J. Clin. Oncol.*, **36**, 3560–3566.

485. Roller, E., Ivakhno, S., Lee, S., et al. (2016) Canvas: versatile and scalable detection of copy number variants. *Bioinformatics*, **32**, 2375–2377.

486. Chen, X., Schulz-Trieglaff, O., Shaw, R., et al. (2016) Manta: rapid detection of structural variants and indels for germline and cancer sequencing applications. *Bioinformatics*, **32**, 1220–1222.

487. Yusenko, M. V., Nagy, A. and Kovacs, G. (2010) Molecular analysis of germline t(3;6) and t(3;12) associated with conventional renal cell carcinomas indicates their rate-limiting role and supports the three-hit model of carcinogenesis. *Cancer Genet. Cytogenet.*, **201**, 15–23.

488. Chen, J., Lui, W.-O., Vos, M. D., et al. (2003) The t(1;3) breakpoint-spanning genes LSAMP and NORE1 are involved in clear cell renal cell carcinomas. *Cancer Cell*, **4**, 405–413.

489. Eleveld, M. J., Bodmer, D., Merkx, G., et al. (2001) Molecular analysis of a familial case of renal cell cancer and a t(3;6)(q12;q15). *Genes, Chromosom. Cancer*, **31**, 23–32.

490. Druck, T., Podolski, J., Byrski, T., et al. (2001) The DIRC1 gene at chromosome 2q33 spans a familial RCC-associated t(2;3)(q33;q21) chromosome translocation. **46**, 583–589.

491. Bodmer, D., Eleveld, M., Kater-Baats, E., et al. (2002) Disruption of a novel MFS transporter gene, DIRC2, by a familial renal cell carcinoma-associated t(2;3)(q35;q21). *Hum. Mol. Genet.*, **11**, 641–9.

492. Meléndez, B., Rodríguez-Perales, S., Martínez-Delgado, B., et al. (2003) Molecular study of a new family with hereditary renal cell carcinoma and a translocation t(3;8)(p13;q24.1). *Hum. Genet.*, **112**, 178–85.

493. Poland, K. S., Azim, M., Folsom, M., et al. (2007) A constitutional balanced t(3;8)(p14;q24.1) translocation results in disruption of theTRC8 gene and predisposition to clear cell renal cell carcinoma. *Genes, Chromosom. Cancer*, **46**, 805–812.

494. Foster, R. E., Abdulrahman, M., Morris, M. R., et al. (2007) Characterization of a 3;6 translocation associated with renal cell carcinoma. *Genes. Chromosomes Cancer*, **46**, 311–7.

495. Bonne, A., Vreede, L., Kuiper, R. P., et al. (2007) Mapping of constitutional translocation breakpoints in renal cell cancer patients: identification of KCNIP4 as a candidate gene. *Cancer Genet. Cytogenet.*, **179**, 11–18.

496. Kuiper, R. P., Vreede, L., Venkatachalam, R., et al. (2009) The tumor suppressor gene FBXW7 is disrupted by a constitutional t(3;4)(q21;q31) in a patient with renal cell cancer. *Cancer Genet. Cytogenet.*, **195**, 105–11.

497. McKay, L., Frydenberg, M., Lipton, L., et al. (2011) Case report: renal cell carcinoma segregating with a t(2;3)(q37.3;q13.2) chromosomal translocation in an Ashkenazi Jewish family. *Fam. Cancer*, **10**, 349–353.

498. Doyen, J., Carpentier, X., Haudebourg, J., et al. (2012) Renal cell carcinoma and a constitutional t(11;22)(q23;q11.2): case report and review of the potential link between the constitutional t(11;22) and cancer. *Cancer Genet.*, **205**, 603–607.

499. Wake, N. C., Ricketts, C. J., Morris, M. R., et al. (2013) UBE2QL1 is disrupted by a constitutional translocation associated with renal tumor predisposition and is a novel candidate renal tumor suppressor gene. *Hum. Mutat.*, **34**, 1650–61.

500. Banks, R. E., Tirukonda, P., Taylor, C., et al. (2006) Genetic and epigenetic analysis of von Hippel-Lindau (VHL) gene alterations and relationship with clinical variables in sporadic renal cancer. *Cancer Res.*, **66**, 2000–11.

501. Shen, C., Beroukhim, R., Schumacher, S. E., et al. (2011) Genetic and Functional Studies Implicate HIF1 as a 14q Kidney Cancer Suppressor Gene. *Cancer Discov.*, **1**, 222–235.

502. Kato, T., Franconi, C. P., Sheridan, M. B., et al. (2014) Analysis of the t(3;8) of hereditary renal cell carcinoma: a palindrome-mediated translocation. *Cancer Genet.*, **207**, 133–40.

503. Woodward, E. R., Skytte, A.-B., Cruger, D. G., et al. (2010) Population-based survey of cancer risks in chromosome 3 translocation carriers. *Genes, Chromosom. Cancer*, **49**, 52–58.

504. Menko, F. H., van Steensel, M. A., Giraud, S., et al. (2009) Birt-Hogg-Dubé syndrome: diagnosis and management. *Lancet Oncol.*, **10**, 1199–1206.

505. Emami, K. H., Brown, L. G., Pitts, T. E. M., et al. (2009) Nemo-like kinase induces apoptosis and inhibits androgen receptor signaling in prostate cancer cells. *Prostate*, **69**, 1481–1492.

506. Yasuda, J., Tsuchiya, A., Yamada, T., et al. (2003) Nemo-like kinase induces apoptosis in DLD-1 human colon cancer cells. *Biochem. Biophys. Res. Commun.*, **308**, 227–33.

507. Han, Y., Kuang, Y., Xue, X., et al. (2014) NLK, a novel target of miR-199a-3p, functions as a tumor suppressor in colorectal cancer. *Biomed. Pharmacother.*, **68**, 497–505.

508. Zhang, H.-H., Li, S.-Z., Zhang, Z.-Y., et al.

(2014) Nemo-like kinase is critical for p53 stabilization and function in response to DNA damage. *Cell Death Differ.*, **21**, 1656–63.

509. Kanei-Ishii, C., Nomura, T., Takagi, T., et al. (2008) Fbxw7 acts as an E3 ubiquitin ligase that targets c-Myb for nemo-like kinase (NLK)-induced degradation. *J. Biol. Chem.*, **283**, 30540–8.

510. Koepp, D. M., Schaefer, L. K., Ye, X., et al. (2001) Phosphorylation-Dependent Ubiquitination of Cyclin E by the SCFFbw7 Ubiquitin Ligase. *Science (80-.).*, **294**, 173–177.

511. Mao, J.-H., Kim, I.-J., Wu, D., et al. (2008) FBXW7 targets mTOR for degradation and cooperates with PTEN in tumor suppression. *Science*, **321**, 1499–502.

512. Kovacs, G. and Hoene, E. (1988) Loss of der(3) in renal carcinoma cells of a patient with constitutional t(3;12). *Hum Genet*, **78**, 148–150.

513. Kovacs, G., Brusa, P. and De Riese, W. (1989) Tissue-specific expression of a constitutional 3;6 translocation: Development of multiple bilateral renal-cell carcinomas. *Int. J. Cancer*, **43**, 422–427.

514. Podolski, J., Byrski, T., Zajaczek, S., et al. (2001) Characterization of a familial RCC-associated t(2;3)(q33;q21) chromosome translocation. *J. Hum. Genet.*, **46**, 685–693.

515. Kanayama, H., Lui, W. O., Takahashi, M., et al. (2001) Association of a novel constitutional translocation t(1q;3q) with familial renal cell carcinoma. *J. Med. Genet.*, **38**, 165–70.

516. Koolen, M. I., van der Meyden, A. P. M., Bodmer, D., et al. (1998) A familial case of renal cell carcinoma and a t(2;3) chromosome translocation. *Kidney Int.*, **53**, 273–275.

517. Valle, L., Cascón, A., Melchor, L., et al. (2005) About the origin and development of hereditary conventional renal cell carcinoma in a four-generation t(3;8)(p14.1;q24.23) family. *Eur. J. Hum. Genet.*, **13**, 570–578.

518. van Kessel, A. G., Wijnhoven, H., Bodmer, D., et al. (1999) Renal cell cancer: chromosome 3 translocations as risk factors. *J. Natl. Cancer Inst.*, **91**, 1159–60.

519. Ruault, M., Ventura, M., Galtier, N., et al. (2003) BAGE genes generated by juxtacentromeric reshuffling in the hominidae lineage are under selective pressure. *Genomics*, **81**, 391–399.

520. Cantor, S. B., Bell, D. W., Ganesan, S., et al. (2001) BACH1, a novel helicase-like protein, interacts directly with BRCA1 and contributes to its DNA repair function. *Cell*, **105**, 149–160.

521. Tolhuis, B. and Karten, H. (2018) Validation of an ultra-fast CNV calling tool for Next Generation Sequencing data using MLPA-verified copy number alterations. *bioRxiv*, 340505.

522. Sadedin, S. P., Ellis, J. A., Masters, S. L., et al. (2018) Ximmer: a system for improving accuracy and consistency of CNV calling from exome data. *Gigascience*, **7**.

523. Carlo, M. I., Mukherjee, S., Mandelker, D., et al. (2018) Prevalence of Germline Mutations in Cancer Susceptibility Genes in Patients With Advanced Renal Cell Carcinoma. *JAMA Oncol.*, **4**, 1228.

524. Landrum, M. J., Lee, J. M., Benson, M., et al. (2016) ClinVar: public archive of interpretations of clinically relevant variants. *Nucleic Acids Res.*, **44**, D862–D868.

525. Nykamp, K., Anderson, M., Powers, M., et al. (2017) Sherloc: a comprehensive refinement of the ACMG–AMP variant classification criteria. *Genet. Med.*, **19**, 1105–1117.

526. Bodian, D. L., McCutcheon, J. N., Kothiyal, P., et al. (2014) Germline variation in cancer-susceptibility genes in a healthy, ancestrally diverse cohort: implications for individual genome sequencing. *PLoS One*, **9**, e94554.

527. Whiffin, N., Minikel, E., Walsh, R., et al. (2017) Using high-resolution variant frequencies to empower clinical genome interpretation. *Genet. Med.*, **19**, 1151–1158.

528. Behan, F. M., Iorio, F., Picco, G., et al. (2019) Prioritization of cancer therapeutic targets using CRISPR–Cas9 screens. *Nature*, 1.

529. Zhou, B., Ho, S. S., Zhang, X., et al. (2018) Whole-genome sequencing analysis of CNV using low-coverage and paired-end strategies is efficient and outperforms array-based CNV analysis. *J. Med. Genet.*, **55**, 735–743.

530. Mavaddat, N., Michailidou, K., Dennis, J., et al. (2019) Polygenic Risk Scores for Prediction of Breast Cancer and Breast Cancer Subtypes. *Am. J. Hum. Genet.*, **104**, 21–34.

531. Clifford, S. C., Prowse, A. H., Affara, N. A., et al. (1998) Inactivation of the von Hippel-Lindau (VHL) tumour suppressor gene and allelic losses at chromosome arm 3p in primary renal cell carcinoma: evidence for a VHL-independent pathway in clear cell renal tumourigenesis. *Genes. Chromosomes Cancer*, **22**, 200–9.

532. Alexandrov, L. B., Kim, J., Haradhvala, N. J., et al. (2018) The Repertoire of Mutational Signatures in Human Cancer. *bioRxiv*, 322859.

9.0 Appendix

9.0.1 Table of contents

9.0.2 Notes on appendix data

The appendix figures, tables, lists, and data provided in this chapter are given in a context-free format and are intended to be read as supplemental components to the other chapters in this thesis. For scripts and code, script language is given in square brackets (e.g. [BASH]) and scripts are provided in a minimally functional state and as such most code comments, user interface components, software and server environment variables, and help utilities are removed for reduce the number of pages generated by indiscriminate copying of scripts and pipelines into the appendix.

9.1 Chapter 2 materials and methods

9.1.1 Next generation sequencing pipeline – FASTQ to VCF

FASTQ alignment - BWA mem (version 0.7.15-r1140) [BASH]

```
bwa mem -c ${BWAC} \
    -r ${BWAR} \
    -t ${CORES} -R "@RG\tID:${RG}\tLB:WGS_RCC\tSM:${SAMPLE}\tPL:ILLUMINA" \
    ${SAMPLE}_1.fq.gz ${SAMPLE}_2.fq.gz | samtools sort -O bam -l 0 -T . \
    -o ${SAMPLE}.sorted.bam
```

Remove duplicates - samtools (version 1.6-12-gc7b2f4f) [BASH]

```
samtools rmdup ${SAMPLE}.sorted.bam ${SAMPLE}.sorted.rmdup.bam
samtools index ${SAMPLE}.sorted.rmdup.bam
```

Indel realignment - GATK IndelRealigner (version 3.7-0-gcfedb67) [BASH]

```
java -Xmx40g -jar GenomeAnalysisTK.jar \
        -T RealignerTargetCreator \
        -R ${REFERENCE}.fa \
        -o ${SAMPLE}.merge.sorted.list \
        -I ${SAMPLE}.merge.sorted.bam \
        -nt ${CORES} \
        --allow_potentially_misencoded_quality_scores

java -Xmx40g -jar /data/Resources/Software/Javas/GenomeAnalysisTK.jar \
        -I ${SAMPLE}.merge.sorted.bam \
        -R ${REFERENCE}.fa \
        -T IndelRealigner \
        -targetIntervals ${SAMPLE}.merge.sorted.list \
        -o ${SAMPLE}.merge.sorted.realigned.bam \
        --allow_potentially_misencoded_quality_scores
```

Base quality recalibration - GATK BaseRecalibrator (version 3.7-0-gcfedb67) [BASH]

```
java -Xmx40g -jar GenomeAnalysisTK.jar -l INFO \
        -R ${REFERENCE}.fa \
        -I ${SAMPLE}.merge.sorted.realigned.bam \
        -T BaseRecalibrator \
        -o ${SAMPLE}.merge.sorted.realigned.table \
        -knownSites All.vcf.gz \
        -nct ${CORES} \
        --allow_potentially_misencoded_quality_scores
java -Xmx40g -jar GenomeAnalysisTK.jar -l INFO \
        -R ${REFERENCE}.fa \
        -I ${SAMPLE}.merge.sorted.realigned.bam \
        -T PrintReads \
        -BQSR ${SAMPLE}.merge.sorted.realigned.table \
        -o ${SAMPLE}.merge.sorted.realigned.recal.bam \
        -nct ${CORES} \
        --allow_potentially_misencoded_quality_scores
```

Final sort and index - samtools (version 1.6-12-gc7b2f4f) [BASH]

```
samtools sort -@ ${CORES} \
        -m 4G \
        -O bam -l 9 \
        -T . \
        -o ${SAMPLE}.sorted.final.bam ${SAMPLE}.merge.sorted.realigned.recal.bam
samtools index ${i}.sorted.final.bam
```

Variant calling - GATK unified genotyper (version 3.7-0-gcfedb67) [BASH]

```
java -Xmx60g -jar GenomeAnalysisTK.jar -glm BOTH -R ${REFERENCE}.fa \
 -T UnifiedGenotyper \
        -D All.vcf.gz \
        -o ${COHORT}.vcf \
        -stand_call_conf 30.0 \
        -A Coverage \
        -A AlleleBalance \
        --max_alternate_alleles 46 \
        -nt ${CORES} \
        -I bam.list \
        --allow_potentially_misencoded_quality_scores \
        -ip 100 \
        -dcov 1500 \

        -rf MappingQuality \

        --min_mapping_quality_score 30
```

9.1.2 Next generation sequencing pipeline – VCF filtering and annotation

Variant filtering – variant_filtering.config [BASH]

```
MEANDP  30
MAF     0.2
GQ      30
MISSING 0.8
G1000   0.01
EXAC    0.01
CADD    0
HET     15
ADEPTH  0.30
QUAL    30
SAMP_NUM       1400
```

Variant filtering – variant_filteringsh [BASH]

```
#!/bin/bash
BUILD="hg38"
ANNO="/home/pss41/resources/annovar/"
GATK="/data/Resources/Software/Javas/GenomeAnalysisTK.jar"
REF="/data/Resources/References/hg38.bwa/hg38.bwa.fa"
## config argument settings
MEANDP=$(grep MEANDP ${CONFIG} | cut -f2)
MAF=$(grep MAF ${CONFIG} | cut -f2)
GQ=$(grep GQ ${CONFIG} | cut -f2)
MISSING=$(grep MISSING ${CONFIG} | cut -f2)
G1000=$(grep G1000 ${CONFIG} | cut -f2)
EXAC=$(grep EXAC ${CONFIG} | cut -f2)
CADD=$(grep CADD ${CONFIG} | cut -f2)
HET=$(grep HET ${CONFIG} | cut -f2)
ADEPTH=$(grep ADEPTH ${CONFIG} | cut -f2)
QUAL=$(grep QUAL ${CONFIG} | cut -f2)
SAMP_NUM=$(grep SAMP_NUM ${CONFIG} | cut -f2)

## Run folder setup and config file availability
if [[ ! -d ${OUTPUT}${PROJECT}_variantfiltering ]]; then
       mkdir ${OUTPUT}${PROJECT}_variantfiltering
```

```
else
        echo -e `date +[%D-%R]` "## Variant Filter Script ## - Project folder already
exists - Overwritting content" | tee -a variantfilter.log
fi
## Migrate required ref files, config and logs to working directory
cp ${CONFIG} ${OUTPUT}${PROJECT}_variantfiltering/variant_filtering.config
cp variant_filtering.R ${OUTPUT}${PROJECT}_variantfiltering/variant_filtering.R
cp RVIS_Unpublished_ExACv2_March2017.tsv \
        ${OUTPUT}${PROJECT}_variantfiltering/RVIS_Unpublished_ExACv2_March2017.tsv
cp GDI_full_10282015.tsv \
        ${OUTPUT}${PROJECT}_variantfiltering/GDI_full_10282015.tsv
mv variantfilter.log \
        ${OUTPUT}${PROJECT}_variantfiltering/variantfilter.log
cd ${OUTPUT}${PROJECT}_variantfiltering

## Filter all sites containing ref/ref for all positions & on provided filters
cp ${INPUT} variant_orig.vcf
vcftools --vcf variant_orig.vcf \
                --non-ref-ac-any 1 \
                --min-meanDP ${MEANDP} \
                --max-maf ${MAF} \
                --minGQ ${GQ} \
                --max-missing ${MISSING} \
                --recode --out variant_orig
mv variant_orig.recode.vcf variant_filtered.vcf

## Splitting of multi-allelic sites
java -jar ${GATK} -T LeftAlignAndTrimVariants -R ${REF} \
                --variant variant_filtered.vcf \
                -o variant_filtered.bi.vcf \
                --splitMultiallelics > /dev/null 2>&1

## Removing header command & generating intermediate files with bcftools
vcftools --vcf variant_filtered.bi.vcf \
                --max-indv 0 \
                --recode --out annotate > /dev/null 2>&1
sed -n '/#CHROM/,${p}' annotate.recode.vcf > variant.table
```

```
## bcftools to extract depth/genotype/INFO_field information
bcftools query --print-header \
               -f '%CHROM\t%POS\t%REF\t%ALT[\t%GT]\n'
               -o genotype.table variant_filtered.bi.vcf
sed -i 's/\[[0-9]\+\]//g' genotype.table

bcftools query --print-header
               -f '%CHROM\t%POS\t%REF\t%ALT[\t%DP]\n' \
               -o sitedepth.table variant_filtered.bi.vcf
sed -i 's/\[[0-9]\+\]//g' sitedepth.table


bcftools query --print-header \
               -f '%CHROM\t%POS\t%REF\t%ALT[\t%AD]\n' \
               -o allelicdepth.table variant_filtered.bi.vcf
sed -i 's/\[[0-9]\+\]//g' allelicdepth.table

bcftools query --print-header \
               -f '%CHROM\t%POS\t%REF\t%ALT[\t%GQ]\n'
               -o genoqual.table variant_filtered.bi.vcf
sed -i 's/\[[0-9]\+\]//g' genoqual.table

## Removing incorrect #CHROM to CHROM for R input
sed -i 's/# CHROM/CHROM/' genotype.table
sed -i 's/# CHROM/CHROM/' sitedepth.table
sed -i 's/# CHROM/CHROM/' allelicdepth.table
sed -i 's/# CHROM/CHROM/' genoqual.table
sed -i 's/#CHROM/CHROM/' variant.table

## Removing bcftools tags
sed -i 's/:GT//g' genotype.table
sed -i 's/:DP//g' sitedepth.table
sed -i 's/:AD//g' allelicdepth.table
sed -i 's/:GQ//g' genoqual.table

## Generating annovar-annotation file for use as table
```

```
${ANNO}convert2annovar.pl -format vcf4old annotate.recode.vcf \
               --outfile annovarform > /dev/null 2>&1

${ANNO}table_annovar.pl annovarform ${ANNO}humandb/ \
               -buildver ${BUILD} \
               -out annotated \
               -remove \
               -protocol
refGene,1000g2015aug_all,exac03,avsnp150,dbnsfp35a,clinvar_20180603,cosmic70,nci60,dbscs
nv11 \
               -operation g,f,f,f,f,f,f,f,f \
               -nastring -9 > /dev/null 2>&1
mv annotated.${BUILD}_multianno.txt annovar.table

## Index all the files with header ID followed by var1-var(nrows-1)
awk -F'\t' -v OFS='\t' 'NR == 1 {print "ID", $0; next} {print "Var"(NR-1), $0}' \
               variant.table > awk.table
mv awk.table variant.table

awk -F'\t' -v OFS='\t' 'NR == 1 {print "ID", $0; next} {print "Var"(NR-1), $0}' \
               genotype.table > awk.table
mv awk.table genotype.table

awk -F'\t' -v OFS='\t' 'NR == 1 {print "ID", $0; next} {print "Var"(NR-1), $0}' \
       genoqual.table > awk.table
mv awk.table genoqual.table

awk -F'\t' -v OFS='\t' 'NR == 1 {print "ID", $0; next} {print "Var"(NR-1), $0}' \
               allelicdepth.table > awk.table
mv awk.table allelicdepth.table

awk -F'\t' -v OFS='\t' 'NR == 1 {print "ID", $0; next} {print "Var"(NR-1), $0}' \
               sitedepth.table > awk.table
mv awk.table sitedepth.table

awk -F'\t' -v OFS='\t' 'NR == 1 {print "ID", $0; next} {print "Var"(NR-1), $0}' \
               annovar.table > awk.table
```

```
mv awk.table annovar.table

###Run R script to filter variants
wd=$(pwd)
Rscript variant_filtering.R ${wd} > /dev/null 2>&1
```

Variant filtering – variant_filtering.R [R]

```
args = commandArgs(trailingOnly=TRUE)
setwd(args[1])
require("stringr")

## Import data tables from bash script
ad <- read.table("allelicdepth.table",
               header = TRUE,
               stringsAsFactors = FALSE)
anno <- read.table("annovar.table",
               header = TRUE,
               sep = "\t",
               stringsAsFactors = FALSE, quote="")
gt <- read.table("genotype.table",
               header = TRUE,
               stringsAsFactors = FALSE)
dp <- read.table("sitedepth.table",
               header = TRUE,
               stringsAsFactors = FALSE)
config <- read.table("variant_filtering.config",
               stringsAsFactors = FALSE)
vv <- read.table("variant.table",
               comment.char = "",
               header = TRUE,
               stringsAsFactors = FALSE)
## Read in genetic intolerance lists
rvis <- read.table("RVIS_Unpublished_ExACv2_March2017.tsv",
               sep="\t",
               header = TRUE,
               stringsAsFactors = FALSE,
               quote="")
gdis <- read.table("GDI_full_10282015.tsv",
               sep = "\t",
               header = TRUE,
               stringsAsFactors = FALSE)

## Remove columns that aren't needed
ad <- ad[,-(2:5)]
gt <- gt[,-(2:5)]
dp <- dp[,-(2:5)]
vv <- vv[,-(8:10)]
rvis <- rvis[c(1,4)]
gdis <- gdis[c(1,3)]

## Rename rs id col to something other than "ID" for safety - Rename cols in genetic
intolerance data
names(vv)[4] <- "rsID"
names(rvis) <- c("GENE","RVIS_Pct")
names(gdis) <- c("GENE","GDIS_Phred")

## Add annotation cols to variant file
vv$GENE <- anno$Gene.refGene
vv$TYPE <- anno$Func.refGene
vv$AA <- anno$AAChange.refGene
vv$CONSEQUENCE <- anno$ExonicFunc.refGene
vv$X1000G <- anno$X1000g2015aug_all
vv$EXAC <- anno$ExAC_ALL
vv$CADD <- anno$CADD_phred
vv$SIFT <- anno$SIFT_pred
vv$POLYPHEN <- anno$Polyphen2_HVAR_pred
vv$CLINVAR <- anno$CLNSIG

## AF - making novel results = 0 and not -9 for freq calculations
vv$X1000G[vv$X1000G == "-9"] <- 0
vv$EXAC[vv$EXAC == "-9"] <- 0

## Import config file settings
```

```
X1000g <- config$V2[config$V1 == "G1000"]
exac <- config$V2[config$V1 == "EXAC"]
CADD <- config$V2[config$V1 == "CADD"]
HET <- config$V2[config$V1 == "HET"]
ADEPTH <- config$V2[config$V1 == "ADEPTH"]
QUAL <- config$V2[config$V1 == "QUAL"]
SAMP_NUM <- config$V2[config$V1 == "SAMP_NUM"]

## Filter variants to those occuring in exonic regions and splice sites
exonic.ft <- as.data.frame(anno$ID[grepl("^exonic$",anno$Func.refGene)
                 | grepl("^splicing$",anno$Func.refGene)
                 | grepl("^exonic;splicing$",anno$Func.refGene)])
## rename col to match other ID cols
names(exonic.ft)[1] <- "ID"
## filter by functional consequence
vv.ft <- vv[vv$ID %in% exonic.ft$ID,]

## filtering on functional consequnce - ExonicFunction.refGene
func.ft <- as.data.frame(vv.ft$ID[!grepl("^synonymous SNV$",vv.ft$CONSEQUENCE)
                 & !grepl("^unknown$",vv.ft$CONSEQUENCE)])

## rename col to match other ID cols
names(func.ft)[1] <- "ID"
## filter by functional consequence
vv.ft <- vv.ft[vv.ft$ID %in% func.ft$ID,]

## filter by qual
qual.ft <- as.data.frame(vv.ft$ID[vv.ft$QUAL > QUAL])
names(qual.ft)[1] <- "ID"
vv.ft <- vv.ft[vv.ft$ID %in% qual.ft$ID,]

## corce gt data.frame into a matrix and replace non-numeric format with numeric
genotypes
gt <- gt[gt$ID %in% vv.ft$ID,]
gtm <- as.matrix(gt)
gtm[gtm == "0/0"] <- 0
gtm[gtm == "0/1"] <- 1
```

```
gtm[gtm == "1/1"] <- 2
gtm[gtm == "./."] <- -9
gt <- as.data.frame(gtm)

## apply function to sum the number of missing, het, hom and ref sites
refHOM <- apply(gtm,1, function(x) sum(x == 0))
HETp <- apply(gtm,1, function(x) sum(x == 1))
nonHOM <- apply(gtm, 1, function(x) sum(x == 2))
miss <- apply(gtm, 1, function(x) sum(x == -9))
## addition of raw counts of HET/HOM
vv.ft$HET_val <- HETp
vv.ft$HOM_val <- nonHOM
## form matrix for pct calculations
calc <- cbind(refHOM,HETp,nonHOM,miss)

## calculate hetpct & hompct (excluding missing sites) and missingness over all sites
hetpct <- ((calc[,2] / (calc[,1] + calc[,2] + calc[,3]))*100)
hompct <- ((calc[,3] / (calc[,1] + calc[,2] + calc[,3]))*100)
misspct <- ((calc[,4] / length(gt[1,-1])*100))
## append values to new columns in vv.ft
vv.ft$HET_rate <- hetpct
vv.ft$HOM_rate <- hompct
vv.ft$MISS_rate <- misspct

## filter variant ids that are below values for both 1000g & exac_all
rarity.ft <- as.data.frame(anno$ID[anno$X1000g2015aug_all < X1000g & anno$ExAC_ALL <
exac])
names(rarity.ft)[1] <- "ID"

## filter variant ids that are above cadd
cadd.ft <- as.data.frame(anno$ID[anno$CADD_phred > CADD | anno$CADD_phred < 0])
names(cadd.ft)[1] <- "ID"

## filter by rarity
vv.ft <- vv.ft[vv.ft$ID %in% rarity.ft$ID,]

## filter by cadd score
```

```
vv.ft <- vv.ft[vv.ft$ID %in% cadd.ft$ID,]


###filter by het/hom ratio and het rate (het > 0 & no het rate in cohort above 15%)
hethom.ft <- as.data.frame(vv.ft$ID[vv.ft$HET_rate < HET])
names(hethom.ft)[1] <- "ID"
#log number of variants - Het/Hom
varcount <- paste("##Variant Filter Script ## R-script Log - Variants matching Het/Hom
thresholds:",nrow(hethom.ft))
write(varcount, file = "R_log.txt", append = TRUE)


###Extract variants based on filtered list
vv.ft <- vv.ft[vv.ft$ID %in% hethom.ft$ID,]
###tidy variables and tables
###performing allelic depth transformation to allele percent
###make copy of allelicdepth(ad)
af <- ad[ad$ID %in% vv.ft$ID,]
af[af == "."] <- NA
## Indexing and generation of percent allelic depth info
af_index <- af[1]
af_mat1 <- as.data.frame(apply(af[2:ncol(af)], c(1,2),
               FUN = function(x) str_split_fixed(x, ",",2)[,1]))
af_mat2 <- as.data.frame(apply(af[2:ncol(af)], c(1,2),
               FUN = function(x) str_split_fixed(x, ",",2)[,2]))
af_mat1[af_mat1 == ""] <- NA
af_mat2[af_mat2 == ""] <- NA
## conversion to matrix and perform matrix arithematic
af_mat1 <- as.matrix(apply(af_mat1,2,function(x) as.numeric(x)))
af_mat2 <- as.matrix(apply(af_mat2,2,function(x) as.numeric(x)))
ad_pct <- af_mat2 / (af_mat1 + af_mat2)
af <- cbind(af_index, ad_pct)
## filter on variants with no af rate above threshold
af.ft <- data.frame(x=rep(0,nrow(af)))
for(i in 1:nrow(af)){
  if(max(af[i,2:ncol(af)], na.rm = TRUE) > ADEPTH){
    af.ft[i,1] <- af[i,1]}
  else{
    af.ft[i,1] <- NA
  }
}
names(af.ft)[1] <- "ID"
af.ft <- subset(af.ft, (!is.na(af.ft[,1])))
vv.ft <- vv.ft[vv.ft$ID %in% af.ft$ID,]

## Add genotype information for remaining variants
if(ncol(gt) > SAMP_NUM){
 gt.ft <- gt[gt$ID %in% vv.ft$ID,]
 vvgt <- vv.ft
 clock <- as.character(Sys.time())
 names(gt.ft)[1] <- "Id"
 write.table(gt.ft,file = "variant_filtering_results_GT.tsv",
               sep = "\t",
               row.names = FALSE,
               quote = FALSE)
} else {
 gt.ft <- gt[gt$ID %in% vv.ft$ID,]
 vvgt <- merge(vv.ft,gt.ft, sort = FALSE)
}
## rename ID col - issues with opening files in excel with "ID" as the first value
names(vvgt)[1] <- "Id"
names(af)[1] <- "Id"

## Col trimming for final tables
drop_col <- c("HET_rate","HOM_rate")
vvgt <- vvgt[ , !(names(vvgt) %in% drop_col)]
## write filtered table out
write.table(vvgt,file = "variant_filtering_results.tsv",
               sep = "\t",
               row.names = FALSE,
               quote = FALSE)
write.table(af,file = "variant_filtering_results_AD.tsv",
               sep = "\t",
               row.names = FALSE,
               quote = FALSE)
```

9.1.3 ONT Nanopore sequencing pipeline

ONT Nanopore pipeline – nano-pipe.sh [BASH]

```
#!/bin/bash
## BED HANDLING
if [[ ! -z "$BED" ]]; then
        if [[ -f "$BED" ]]; then
        #echo -e "${BED} is a file"
        if [[ $(cat "$BED" | wc -l) -lt 2 ]]; then
                #echo -e "${BED} is a file with one region"
                BED=$(cat ${BED} | sed 's/\(\S\+\)\t\(\S\+\)\t\(\S\+\)/\1:\2-\3/')
                        BED_TYPE="SINGLE"
                else
                        BED_TYPE="BED"
                fi
        fi
else
        BED_TYPE="REF"
fi

## Output directory structure and overwrite protection
cd ${OUTPUT_FOLDER}

## Base calling
if [[ "$BASE_CALLING" == "TRUE" ]]; then
        cd ${OUTPUT_FOLDER}${PROJECT}
        if [[ ! -d "base_calls" ]]; then
                mkdir base_calls
        fi
        cd base_calls




## Albacore base calling
        if [[ "$BASE_CALLER" == "ALBACORE" ]]; then
        read_fast5_basecaller.py --flowcell ${FLOWCELL} \
                        --recursive \
                        --kit ${KIT} \
                        -n 0 \
                        --output_format fast5,fastq \
                        --input ${INPUT_FOLDER}/ \
                        --save_path ${OUTPUT_FOLDER}${PROJECT}/base_calls/ \
                        --worker_threads ${CORES} \
                        --disable_pings
                        cat workspace/pass/*.fastq > ${PROJECT}_merged.fastq
                if [[ ! -d "fast5_syms" ]]; then
                        mkdir fast5_syms
                 cd fast5_syms
                 find ${OUTPUT_FOLDER}${PROJECT}/base_calls/workspace/ -type f \
                               -name "*.fast5" | xargs -n1 -I {} ln -s {} .
                cd ..
             fi
        fi
## Indexing FAST files for variant calling
        ${NANOPOLISH_PATH}nanopolish index \
                -s ${OUTPUT_FOLDER}${PROJECT}/base_calls/sequencing_summary.txt \
                -d ${OUTPUT_FOLDER}${PROJECT}/base_calls/fast5_syms/ \
                ${OUTPUT_FOLDER}${PROJECT}/base_calls/${PROJECT}_merged.fastq
fi

## Base calling QC
if [[ "$BASE_QC" == "TRUE" ]]; then
    if [[ "$LOCAL_PYTHON" == "TRUE" ]];then
        source ${PYTHON_ENV}activate
    fi
        cd ${OUTPUT_FOLDER}${PROJECT}/base_calls
    if [[ ! -d "base_QC" ]]; then
        mkdir base_QC
    fi
    cd ${OUTPUT_FOLDER}${PROJECT}/base_calls/base_QC
        Rscript ${INSTALL_FOLDER}nano-qc.R \
                ${OUTPUT_FOLDER}${PROJECT}/base_calls/fast5_syms ${PROJECT} \
                ${OUTPUT_FOLDER}${PROJECT}/base_calls/base_QC
        if [[ -f "${OUTPUT_FOLDER}${PROJECT}/base_calls/sequencing_summary.txt" ]]; then
                NanoStat --summary \
                        ${OUTPUT_FOLDER}${PROJECT}/base_calls/sequencing_summary.txt \
                        --readtype 1D
        fi

## Alignment
if [[ "$ALIGNMENT" == "TRUE" ]]; then
        cd ${OUTPUT_FOLDER}${PROJECT}
    if [[ ! -d "alignment" ]]; then
                mkdir alignment
        fi
    cd alignment
##MINIMAP2 Alignment
        if [[ "$ALIGNMENT_TYPE" == "MINIMAP" ]]; then
        minimap2 -ax map-ont \
                        ${REFERENCE} \
                        ${OUTPUT_FOLDER}${PROJECT}/base_calls/${PROJECT}_merged.fastq > \
                        ${PROJECT}_basecalled.sam
        samtools view -b \
                        -q ${MAP_Q} \
                        ${PROJECT}_basecalled.sam | samtools sort \
                        -O bam -l 0 -T . -o ${PROJECT}_basecalled.sorted.bam
        samtools index ${PROJECT}_basecalled.sorted.bam
        fi
fi
```

ONT Nanopore pipeline – nano-qc.R [R]

```
args = commandArgs(trailingOnly=TRUE)
library(rhdf5)
library(poRe)
library(ggplot2)
library(reshape2)
library(dplyr)
library(gridExtra)
## Set environment
```

```
setwd(dir = args[3])
project <- args[2]
reads_info <- read.fast5.info(dir = args[1])
## Set Nanopore channel layout
layout <- function(){
 p1 = data.frame(channel=33:64, row=rep(1:4, each=8), col=rep(1:8, 4))
 p2 = data.frame(channel=481:512, row=rep(5:8, each=8), col=rep(1:8, 4))
 p3 = data.frame(channel=417:448, row=rep(9:12, each=8), col=rep(1:8, 4))
 p4 = data.frame(channel=353:384, row=rep(13:16, each=8), col=rep(1:8, 4))
 p5 = data.frame(channel=289:320, row=rep(17:20, each=8), col=rep(1:8, 4))
 p6 = data.frame(channel=225:256, row=rep(21:24, each=8), col=rep(1:8, 4))
 p7 = data.frame(channel=161:192, row=rep(25:28, each=8), col=rep(1:8, 4))
 p8 = data.frame(channel=97:128, row=rep(29:32, each=8), col=rep(1:8, 4))
 q1 = data.frame(channel=1:32, row=rep(1:4, each=8), col=rep(16:9, 4))
 q2 = data.frame(channel=449:480, row=rep(5:8, each=8), col=rep(16:9, 4))
 q3 = data.frame(channel=385:416, row=rep(9:12, each=8), col=rep(16:9, 4))
 q4 = data.frame(channel=321:352, row=rep(13:16, each=8), col=rep(16:9, 4))
 q5 = data.frame(channel=257:288, row=rep(17:20, each=8), col=rep(16:9, 4))
 q6 = data.frame(channel=193:224, row=rep(21:24, each=8), col=rep(16:9, 4))
 q7 = data.frame(channel=129:160, row=rep(25:28, each=8), col=rep(16:9, 4))
 q8 = data.frame(channel=65:96, row=rep(29:32, each=8), col=rep(16:9, 4))
 map = rbind(p1, p2, p3, p4, p5, p6, p7, p8, q1, q2, q3, q4, q5, q6, q7, q8)
 map.matrix = acast(map, row ~ col, value.var = "channel")
 return(map.matrix)
}
channel.layout <- layout()
channel.layout <- melt(channel.layout)
## functions
## qual_plot fucntion
qual_plot <- function(input){
 dat <- input[which(colnames(input) %in% c("tmq","cmq","mq2d"))]
 #dat <- dat[!is.na(dat$tmq),]

 qual_melt <- melt(as.matrix(dat))
 qual_melt$Var2 <- as.character(qual_melt$Var2)

 names(qual_melt) <- c("Var1","read type","mean quality")
 qual_melt$`read type`[qual_melt$`read type` == "tmq"] <- "template"
 qual_melt$`read type`[qual_melt$`read type` == "cmq"] <- "complement"
 qual_melt$`read type`[qual_melt$`read type` == "mq2d"] <- "2d"

 qual_melt$`read type` <- factor(qual_melt$`read type`,
                                      levels = c("template","complement","2d"))

 lim <-round(max(hist(qual_melt$`mean quality`[qual_melt$`mean quality` > 0])$counts),-
3)



 ggplot(data = qual_melt,aes(x = `mean quality`,fill = `read type`)) +
        geom_histogram(bins = 30,color = "grey25") +
        facet_grid(. ~ `read type`) +
        labs(title = "Distribution of mean read qualities",
                       fill = "Read type",
                       y = "Frequency",
                       x = "Mean quality") +
        theme_light() +
        scale_y_continuous(limits = c(0,lim),expand = c(0,0)) +
        scale_fill_manual(values=c("#53B400", "#C49A00","#F8766D")) +
        scale_x_continuous(limits = c(0,NA))
}

## length_plot fucntion
rlength_plot <- function(input){
 dat <- input[which(colnames(input) %in% c("tlen","clen","len2d"))]
 dat <- dat[!is.na(dat$tlen),]

 rlength_melt <- melt(as.matrix(dat))
 rlength_melt$Var2 <- as.character(rlength_melt$Var2)
 #qual_melt <- qual_melt[qual_melt$value > 0,]

 names(rlength_melt) <- c("Var1","read type","read length")
 rlength_melt$`read type`[rlength_melt$`read type` == "tlen"] <- "template"
 rlength_melt$`read type`[rlength_melt$`read type` == "clen"] <- "complement"
 rlength_melt$`read type`[rlength_melt$`read type` == "len2d"] <- "2d"
 rlength_melt$`read type` <- factor(rlength_melt$`read type`,
                                     levels = c("template","complement","2d"))
 lim <- round(max(hist(rlength_melt$`read length`[rlength_melt$`read length` >
0])$counts),-3)

 ggplot(data = rlength_melt) +
               geom_histogram(aes(x = `read length`,fill = `read type`),
                      bins = 50,color = "grey25") +
               facet_grid(. ~ `read type`) +
               labs(title = "Distribution of read length",
                      fill = "Read type",
                      y = "Frequency",
                      x = "Mean length") +
                theme_light() +
               scale_y_continuous(limits = c(0,lim),expand = c(0,0)) +
               scale_fill_manual(values=c("#53B400","#C49A00","#F8766D")) +
               scale_x_continuous(limits = c(0,NA))
}
##yield plot fucntion
yield_plot <- function(input){
 dat <- input[!is.na(input$read_start_time),]

 dat$TIME_SUM <- (as.numeric(dat$exp_start +
                      dat$read_start_time) -
                      min(as.numeric(dat$exp_start + dat$read_start_time)))
 dat <- dat[order(dat$read_start_time),]
 dat <- dat[which(colnames(dat) %in% c("tlen","clen","len2d","read_start_time"))]
 dat$len2d <- cumsum(dat$len2d) / 1000
 dat$tlen <- cumsum(dat$tlen) / 1000
 dat$clen <- cumsum(dat$clen) / 1000

 yield_melt <- melt(data = dat,id.vars = c("read_start_time"))
 yield_melt$variable <- as.character(yield_melt$variable)

 names(yield_melt) <- c("time","read type","cumulative kbs")
 yield_melt$`read type`[yield_melt$`read type` == "tlen"] <- "template"
 yield_melt$`read type`[yield_melt$`read type` == "clen"] <- "complement"
 yield_melt$`read type`[yield_melt$`read type` == "len2d"] <- "2d"

 yield_melt$`read type` <- factor(yield_melt$`read type`,
                              levels = c("template","complement","2d"))
 ggplot(data = yield_melt) +
               geom_line(aes(x = `time`,y = `cumulative kbs`,color = `read type`)) +
               facet_grid(. ~ `read type`,scales = "free") +
               labs(title = "Cummulative kbases / time",
                       x = "Time",
                       y = "Cumulative data (Kbases)",
                       color = "Read type") +
               theme_light() +
               scale_y_continuous(expand = c(0.01,0)) +
               scale_color_manual(values=c("#53B400","#C49A00","#F8766D")) +
               scale_x_continuous(limits = c(0,NA))
}
## channel kb function
channel_stats_plot_tkb <- function(input){
 numeric_cols_sum <- c("len2d","tlen","clen","tcevents","channel")
 dat_sum <- input[which(colnames(input) %in% numeric_cols_sum)]
 dats <- dat_sum %>% group_by(channel) %>% summarise_all(sum)
 merged_channel <- merge(channel.layout,dats,by.x = "value",by.y = "channel",all.x = T)
 merged_channel$tlen <- merged_channel$tlen / 1000
 merged_channel$len2d <- merged_channel$len2d / 1000
 merged_channel$clen <- merged_channel$clen / 1000
 names(merged_channel) <- c("channel","Var1","Var2","2d kbases (total)",
                              "template kbases (total)",
                              "complement kbases (total)",
                              "template events (total)")
 merged_out <- melt(merged_channel,id.vars = c("channel","Var1","Var2"))
 ggplot(merged_out[merged_out$variable=="template kbases (total)",],aes(x = Var2,y =
Var1)) +
               geom_point(shape = 21,size = 9,
                       color = "grey25",stroke = 0.5,
                       aes(fill = value)) +
               geom_text(aes(label=channel),size = 3) +
               scale_y_reverse() +
               scale_fill_continuous(low = "grey95", high = "#53B400",na.value = "white",
                       limits = c(0,
                              max(merged_out$value[which(merged_out$variable %in%
                              c("2d kbases (total)",
                                     "template kbases (total)",
                                     "complement kbases (total)"))])
                       )) +
               labs(title = "Template reads - KBases / channel",y = "Channel number",
                       fill="Kbases") + theme_light() +
               theme(panel.background = element_blank(),plot.background =
element_blank(),
               panel.grid = element_blank(),axis.line = element_blank(),
               axis.title.x = element_blank(),axis.ticks = element_blank(),
               axis.text = element_blank(),panel.border = element_blank()
     )
}
## channel events function
channel_stats_plot_tevn <- function(input){
 numeric_cols_sum <- c("len2d","tlen","clen","tcevents","channel")
 dat_sum <- input[which(colnames(input) %in% numeric_cols_sum)]
 dats <- dat_sum %>% group_by(channel) %>% summarise_all(sum)

 merged_channel <- merge(channel.layout,dats,by.x = "value",
                       by.y = "channel",
                       all.x = T)
 merged_channel$tlen <- merged_channel$tlen
 merged_channel$len2d <- merged_channel$len2d
 merged_channel$clen <- merged_channel$clen
 names(merged_channel) <- c("channel","Var1","Var2",
                              "2d kbases (total)",
                              "template kbases (total)",
                              "complement kbases (total)",
                              "template events (total)")
 merged_out <- melt(merged_channel,id.vars = c("channel","Var1","Var2"))

ggplot(merged_out[merged_out$variable == "template events (total)",],
               aes(x = Var2,y = Var1)) +
               geom_point(shape = 21,
                      size = 9,
                      color = "grey25",
                      stroke = 0.5,
                      aes(fill = value)) +
               geom_text(aes(label=channel),size = 3) +
               scale_y_reverse() +
               scale_fill_continuous(low = "grey95",high = "blue2",na.value = "white") +
               labs(title = "Events / channel",y = "Channel number", fill="Events") +
               theme_light() +
               theme(panel.background = element_blank(),
                      plot.background = element_blank(),
               panel.grid = element_blank(),
                      axis.line = element_blank(),
                      axis.title.x = element_blank(),
                      axis.ticks = element_blank(),
                      axis.text = element_blank(),
                      panel.border = element_blank()
  )

}
## Chnanel mean kb function
channel_stats_plot_tmeankb <- function(input){
 numeric_cols_mean <-c("len2d","tlen","clen","channel")
 dat_mean <- input[which(colnames(input) %in% numeric_cols_mean)]
 datm <- dat_mean %>% group_by(channel) %>% summarise_all(mean)

 merged_channel <- merge(channel.layout,datm,by.x = "value",by.y = "channel",all.x = T)
 merged_channel$tlen <- merged_channel$tlen / 1000
 merged_channel$len2d <- merged_channel$len2d / 1000
 merged_channel$clen <- merged_channel$clen / 1000

 names(merged_channel) <- c("channel","Var1","Var2",
                              "2d kbases (mean)",
                              "template kbases (mean)",
                              "complement kbases (mean)")
 merged_out <- melt(merged_channel,id.vars = c("channel","Var1","Var2"))

 ggplot(merged_out[merged_out$variable == "template kbases (mean)",],aes(x = Var2,y =
Var1)) +
  geom_point(shape = 21,size = 9,color = "grey25",stroke = 0.5, aes(fill = value)) +
  geom_text(aes(label=channel),size = 3) +
  scale_y_reverse() +
  scale_fill_continuous(low = "white",high = "#53B400",na.value = "white",
             limits = c(0,max(merged_out$value[which(merged_out$variable %in%
                              c("2d kbases (mean)",
                                      "template kbases (mean)",
                                      "complement kbases (mean)"))],na.rm = T))) +
  labs(title = "Template reads - mean KBases / channel",
                       y = "Channel number",
                       fill="Kbases") +
  theme_light() +
  theme(panel.background = element_blank(),
               plot.background = element_blank(),
        panel.grid = element_blank(),
               axis.line = element_blank(),
        axis.title.x = element_blank(),
               axis.ticks = element_blank(),
        axis.text = element_blank(),
               panel.border = element_blank()
  )
}

## channel temp function
channel_stats_plot_temp <- function(input){

 numeric_cols_mean <-c("channel","heatsink_temp")
 dat_mean <- input[which(colnames(input) %in% numeric_cols_mean)]
 datm <- dat_mean %>% group_by(channel) %>% summarise_all(mean)

 merged_channel <- merge(channel.layout,datm,by.x = "value",
                              by.y = "channel",
                              all.x = T)

 names(merged_channel) <- c("channel","Var1","Var2","temp (C)")

 merged_out <- melt(merged_channel,id.vars = c("channel","Var1","Var2"))

 ggplot(merged_out[merged_out$variable == "temp (C)",],aes(x = Var2,y = Var1)) +
  geom_point(shape = 21,
                      size = 9,
                      color = "grey25",
                      stroke = 0.5,
                      aes(fill = value)) +
  geom_text(aes(label=channel),size = 3) +
  scale_y_reverse() +
  scale_fill_continuous(low = "green",
               high = "red",
               na.value = "white",
               limits = c(0,60)) +
  labs(title = "Mean temperature / channel",
               y = "Channel number",
               fill="Temp (C)") +
  theme_light() +
  theme(panel.background = element_blank(),
               plot.background = element_blank(),
        panel.grid = element_blank(),
               axis.line = element_blank(),
        axis.title.x = element_blank(),
               axis.ticks = element_blank(),
        axis.text = element_blank(),
               panel.border = element_blank()
  )
}
## Channel quality function
channel_stats_plot_tmeanq <- function(input){

 numeric_cols_mean <-c("tmq","cmq","mq2d","channel")
 dat_mean <- input[which(colnames(input) %in% numeric_cols_mean)]
 dat_mean[is.na(dat_mean)] <- 0
 datm <- dat_mean %>% group_by(channel) %>% summarise_all(mean)
 merged_channel <- merge(channel.layout,datm,by.x = "value",
                       by.y = "channel",
                       all.x = T)
 names(merged_channel) <- c("channel","Var1","Var2",
                              "template quality (mean)",
                              "complement quality (mean)",
                              "2d quality (mean)")

 merged_out <- melt(merged_channel,id.vars = c("channel","Var1","Var2"))

 ggplot(merged_out[merged_out$variable == "template quality (mean)",],
                       aes(x = Var2,y = Var1)) +
  geom_point(shape = 21,size = 9,color = "grey25",
               stroke = 0.5, aes(fill = value)) +
  geom_text(aes(label=channel),size = 3) +
  scale_y_reverse() +
  scale_fill_continuous(low = "grey95",high = "#53B400",na.value = "white",
  limits = c(0,max(merged_out$value[which(merged_out$variable %in%
               c("2d quality (mean)",
               "template quality (mean)",
               "complement quality (mean)"))],
               na.rm = T))) +
  labs(title = "Template reads - mean quality / channel",
               y = "Channel number", fill="Quality") +
  theme_light() +
  theme(panel.background = element_blank(),
               plot.background = element_blank(),
        panel.grid = element_blank(),
               axis.line = element_blank(),
        axis.title.x = element_blank(),
               axis.ticks = element_blank(),
        axis.text = element_blank(),
               panel.border = element_blank()
  )
}
```

```
## Plotting
png(filename = paste(project,"_channelQC_kb_events.png",sep = ""),width = 23.5,
               height = 10,
               units = "in",
               res = 600)
grid.arrange(channel_stats_plot_tkb(reads_info),channel_stats_plot_tevn(reads_info),ncol
=2)
dev.off()
png(filename = paste(project,"_channelQC_meanKB.png",sep = ""),width = 17.5,
               height = 10,
               units = "in",
               res = 600)
grid.arrange(channel_stats_plot_tmeankb(reads_info),ncol=1)
dev.off()
png(filename = paste(project,"_channelQC_meanQuality.png",sep = ""),width = 17.5,
               height = 10,
               units = "in",
               res = 600)
grid.arrange(channel_stats_plot_tmeanq(reads_info), ncol=1)
dev.off()
png(filename = paste(project,"_channelQC_temp.png",sep = ""),width = 6,
               height = 10,
               units = "in",
               res = 600)
channel_stats_plot_temp(reads_info)
dev.off()
png(filename = paste(project,"_readQC.png",sep = ""),width = 16,
               height = 10,
               units = "in",
               res = 600)
grid.arrange(qual_plot(reads_info),yield_plot(reads_info),rlength_plot(reads_info),nrow=
3)
dev.off()
write.table(reads_info,paste(project,"_qcdata.txt",sep = ""),append = FALSE, quote = F,
               sep = "\t",
               na = "NA",
               row.names = T, col.names = T)
```

9.2 Chapter 3 Targeted Sanger and amplicon sequencing

9.2.1 Sanger sequencing and long range PCR primers

Gene Name	Primer Name	Forward Primer	Reverse Primer	TmF (°C)	TmR (°C)	PCR size (bp)	Exons
KMT2C	KMT2C-Exon 1	GTCACCATGCCAGGCTAATT	TTGCTGGTCCTTGTAATGACA	58.23	57.5	7909	1
KMT2C	KMT2C-Exon 2	GCAAAACATGGGTCTGAGAGA	AGGAGTATGTTTGGTGGGCT	58.22	58.63	7950	2
KMT2C	KMT2C-Exon 3	GATGATGAGGTTGCGCAGTT	CAGGAGAATCGCGCGAAC	58.91	59	7854	3
KMT2C	KMT2C-Exon 4-6	CTGGTCTCGAACTTCCACCT	TTTGAAAGCTTTGCCTATGTTCT	59.03	57.21	7457	4-6
KMT2C	KMT2C-Exon 7	AAATTTGGAGCATGGGGAGC	GAGGCAGGAGAAATCGCATG	58.8	59.06	5668	7
KMT2C	KMT2C-Exon 8-9	CCACCACACCCTGCTAATTT	AGGGGAGACAGAACAAGCT	58.08	57.83	7826	8-9
KMT2C	KMT2C-Exon 10-14	GTGCAGATTTTGTGAGGCCA	GCTTACCGTTCTACTAGTTGGC	59.04	58.81	7896	10-14
KMT2C	KMT2C-Exon 15-16	CCCCACTGCCTACCACTAAA	CCCCACAAAGAAAATTTCAGGC	59.01	58.6	7243	15-16
KMT2C	KMT2C-Exon 17-18	TCGAACTCCTGATCCACCTG	GAGGAGAGAGAATGCGGGAA	58.81	58.88	4806	17-18
KMT2C	KMT2C-Exon 19-20	GCCAAAAGAAACAAAACAAGTGT	TTACGTAGGGAGGGCAGAAG	57.39	58.52	6219	19-20
KMT2C	KMT2C-Exon 21-23	TTCTTGGGACTCTGGCTACT	TGCAGGCCCACTTACATACA	57.67	59.01	8008	21-23
KMT2C	KMT2C-Exon 24-27	GGTGGGGAACTAGATAGGAGC	TGCCCACCAAAACCAAAAGG	59.03	59.46	9375	24-27
KMT2C	KMT2C-Exon 28-31	GGATTGAAATTGGACAGAGAACA	TCCTTGAAACTGGTCCCTGG	57.04	59.23	7832	28-31
KMT2C	KMT2C-Exon 32-37	GTTCACACCCTGGGCTTTTG	CTCCTGAGTAGCCGCGAATA	59.61	59.05	9205	32-37
KMT2C	KMT2C-Exon 38-41	TCCCATCATCAAACCTGTGC	GGGACCCCTGCAAATAACTAG	58.16	58.07	9776	38-41
KMT2C	KMT2C-Exon 42-44	ATGTAGTTTGGCTTGTGGGTT	TACCACCACGCCCAGTAAAT	58.04	59.01	9047	42-44
KMT2C	KMT2C-Exon 45-52	ACTGTTAAGCTGGGAGAGGT	TCCCCAATGCAAATGACAGG	57.97	58.44	9169	45-52
KMT2C	KMT2C-Exon 53-58	AGTATGTGGAGCTGCTTTCTT	CCACACCTGAACTGCTGAAG	57.29	58.77	8924	53-58
KMT2C	KMT2C-Exon 59	TCCTGGAAAGCTGTCACTGA	AACAAACTGCAAGCACCTGT	58.58	58.81	8076	59
KMT2D	KMT2D-Exon 1-14	GCACAGACTGGCCTCTAGAA	CACGATGGTCCTGAACTCCT	59.1	59.1	8151	1-14
KMT2D	KMT2D-Exon 15-18	GGAGGCCTAGTCTCTGCATT	AGACCATGGTGCCTGATGAA	57	57	1518	15-18

Gene Name	Primer Name	Forward Primer	Reverse Primer	TmF (°C)	TmR (°C)	PCR size (bp)	Exons
KMT2D	KMT2D-Exon 19-34	TTCACCGTGTTA GCCAGGAT	TCAATCAACTCTCCT GCCTCA	59.02	58.74	8880	19-34
KMT2D	KMT2D-Exon 35-47	AGATCGCCTCAT TGCACTCC	CGCCTGGCTACTGT TTTGTT	58	56	8064	35-47
KMT2D	KMT2D-Exon 48-54	AGATTGTGCCAC TGGATCCA	CCTGCGCTCTCAAA CCTCTA	59.01	59.47	9125	48-54
CDKN2B	CDKN2B-1A-PS	TAGCATCTTTGG GCAGGCTT	CACCTTCTCCACTA GTCCCC	59.67	58.8	598	1
CDKN2B	CDKN2B-1B-PS	CTAGGAAGGAGA GAGTGCGC	TCGTTGAAAGCAGA CAGACA	59.62	57.4	597	1
CDKN2B	CDKN2B-2A-PS	GAGACCTGAACA CCTCTGCA	GTCGAGGGCCAGAT AAGACA	59.32	58.89	600	2
CDKN2B	CDKN2B-2B-PS	CCGCCCACAACG ACTTTATT	CAGGGCTTCCAGAG AGTGT	58.84	58.63	595	2
EPAS1	ORF-EPAS1-Ex12	TGACACAGCCAA GTCTGAGG	ACATGGCTTGAGGT GATTCC	60.02	59.93	829	12
EPAS1	ORF-EPAS1-Ex9	TCCATGGCTCAC ACACTTCT	GGAGCGTGTGGTGT TCTTTT	58.94	58.98	565	9

9.2.2 Sequence identity comparisons

KMT2C-BAGE2 gene

Command line:

```
matcher –auto –stdout –asequence emboss_matcher-I20160128-160222-0718-19876421-
oy.asequence –bsequence emboss_matcher-I20160128-160222-0718-19876421-oy.bsequence –
datafile EDNAFULL –gapopen 16 –gapextend 4 –alternatives 1 -aformat3 pair –snucleotide1 –
snucleotide2
```

Align format: pair | Aligned sequences: 2

ENSG00000055609

ENSG00000187172

Matrix: EDNAFULL | Gap penalty: 16 | Extend penalty: 4 | Length: 93385 | Identity: 80878/93385 (86.6%) | Similarity: 80878/93385 (86.6%) | Gaps: 8361/93385 (8.0%)

KMT2C-BAGE2 mRNA

Command line:

```
matcher –auto –stdout –asequence emboss_matcher-I20190325-143621-0347-48066866-
p2m.asequence –bsequence emboss_matcher-I20190325-143621-0347-48066866-
p2m.bsequence –datafile EDNAFULL –gapopen 16 –gapextend 4 –alternatives 1 -aformat3 pair –
snucleotide1 –snucleotide2
```

Align format: pair | Aligned sequences: 2

- NM_170606.3
- NM_182482.2

Matrix: EDNAFULL | Gap penalty: 16 | Extend penalty: 4

Length: 2109 | Identity: 1539/2109 (73.0%) | Similarity: 1539/2109 (73.0%) | Gaps: 535/2109 (25.4%)

9.2.3 Sequence alignment and quality metrics – KMT2C/KMT2C sequencing

Read mapping percentages for KMT2C and KMT2D (orange) compared to off target mapping (blue). Figure A shows read mapping proportion of both KMT2C and KMT2D. Figure B shows read mapping proportion for KMT2C only. Figure C shows the read mapping proportion for KMT2D only and Figure D shows the read mapping proportion for BAGE2.

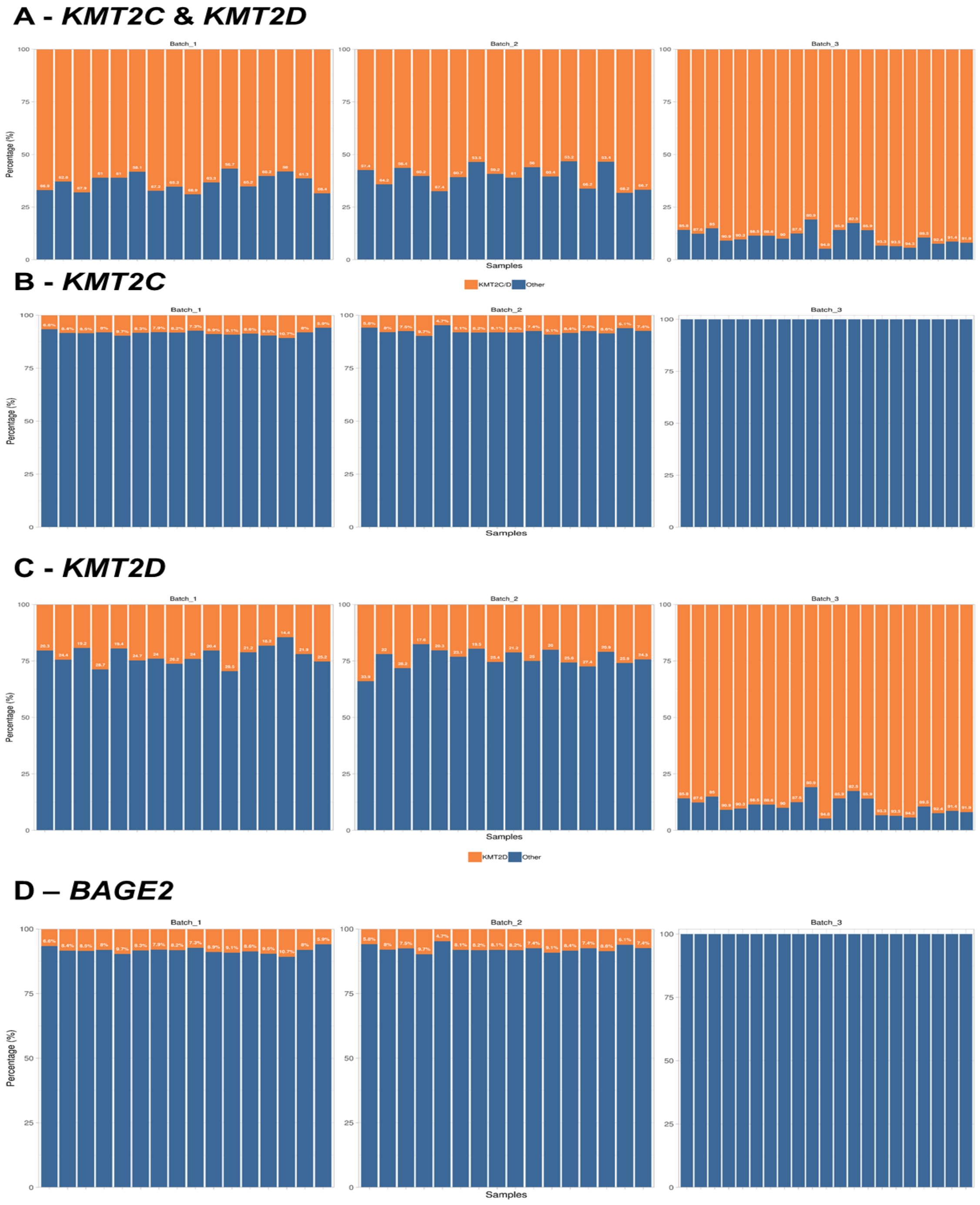

9.2.4 BAGE-family genes table

Gene	Loci	Location/Scaffold (GRCh38)	Lenth (bp)	Length (AA)	Aliases	Notes
BAGE	21p11.1	NW_001839676.1 Not in current release	1,004	43	*BAGE1* *CT2.1* *B Melanoma Antigen Family, Member 1*	No full gene length - cDNA (132bp) reported far smaller than mRNA - 2 reported exons
BAGE2	21p11.2	chr21:10,413,477-10,516,431	102,955	109	*Cancer/Testis Antigen 2.2* *CT2.2* *B Melanoma Antigen Family, Member 2*	Reported as protein producing, processed transcript & unknown locus type; 10 reported exons; 3 Transcripts
BAGE3	21p11.2	NC_000021.8 (Hg37) Not in current release	1,891	109	*Cancer/Testis Antigen 2.3* *CT2.3* *B Melanoma Antigen Family, Member 3*	8 exons reported - Full gene length unknown - orientation unknown - cDNA (330bp) far smaller than mRNA
BAGE4	21p11.1	AC_000153.1 Not in current release	1,840	39	*Cancer/Testis Antigen 2.4* *CT2.4* *B Melanoma Antigen Family, Member 4*	2 exons reported - No full gene length - cDNA (120bp) far smaller than reported mRNA - protein coding (inference)
BAGE5	13cen	chr13:76,210-170,143 (NW_011332699.1)	1,589	43	*Cancer/Testis Antigen 2.5* *CT2.5* *B Melanoma Antigen Family, Member 5*	9 exons reported - Split build information for loci - mRNA sequence longer than reported gene

9.2.5 KMT2C/BAGE2 conservation

KMT2C / BAGE2 conservation plot – Top track highlights the sequence regions of *BAGE2* with identical sequence identity to *KMT2C* aligned across the *KMT2C* coding region

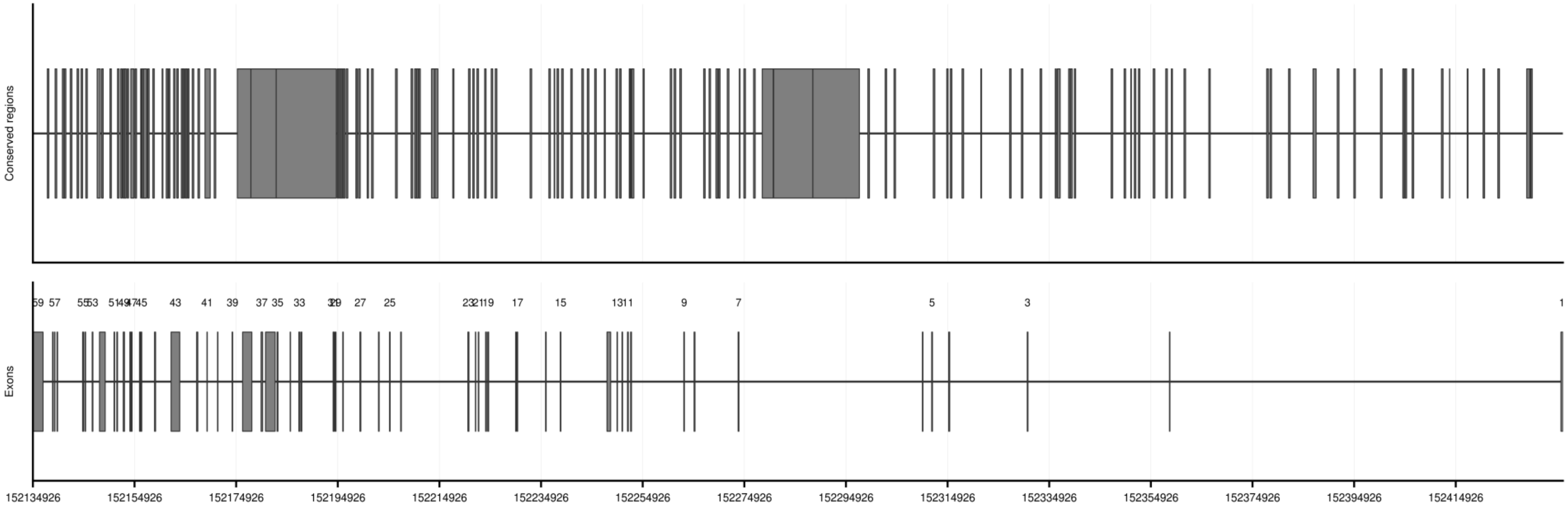

9.3 Chapter 4 Cancer gene panel sequencing

9.3.1 Cancer gene panel target list

SNPs (287)						
rs17401966	rs710521	rs3117582	rs4242384	rs110419	rs7176508	rs1327301
rs9430161	rs2131877	rs204999	rs7837688	rs1945213	rs8034191	rs5945572
rs7538876	rs798766	rs9268542	rs9642880	rs11228565	rs1051730	rs5945619
rs11249433	rs1494961	rs6903608	rs2019960	rs7931342	rs8042374	rs5919432
rs7412746	rs12500426	rs2395185	rs10088218	rs10896449	rs3803662	rs1321311
rs3790844	rs17021918	rs2858870	rs891835	rs7130881	rs4784227	rs3824999
rs6691170	rs1229984	rs674313	rs4295627	rs7105934	rs3112612	rs5934683
rs6687758	rs971074	rs28421666	rs2294008	rs614367	rs9929218	rs2283873
rs801114	rs7679673	rs2647012	rs7040024	rs1393350	rs391525	rs807624
rs1465618	rs10069690	rs10484561	rs755383	rs1801516	rs258322	rs1027643
rs7579899	rs2242652	rs9275572	rs3814113	rs3802842	rs1805007	rs3755132
rs1432295	rs2736100	rs210138	rs7023329	rs498872	rs4785763	rs790356
rs721048	rs2853676	rs10484761	rs2157719	rs735665	rs4795519	rs5955543
rs10187424	rs4635969	rs339331	rs1412829	rs2900333	rs4430796	rs10974944
rs17483466	rs4975616	rs2180341	rs1011970	rs718314	rs7501939	rs1210110
rs12621278	rs401681	rs9485372	rs4977756	rs10875943	rs7210100	rs7555566
rs2072590	rs31489	rs2046210	rs965513	rs11169552	rs1859962	rs1364054
rs13016963	rs12653946	rs651164	rs865686	rs902774	rs17674580	rs6734275
rs13393577	rs2255280	rs9364554	rs505922	rs995030	rs7238033	rs7584993
rs3768716	rs13361707	rs7758229	rs10795668	rs3782181	rs4939827	rs17272796
rs6435862	rs2121875	rs4487645	rs11012732	rs4474514	rs8170	rs1155741
rs13387042	rs4415084	rs11978267	rs3123078	rs11066015	rs8102137	rs161792
rs966423	rs889312	rs4132601	rs10993994	rs671	rs10411210	rs11940551
rs13397985	rs10052657	rs6465657	rs10821936	rs4767364	rs8102476	rs9293511
rs7584330	rs20541	rs1495741	rs7089424	rs2074356	rs11083846	rs9352613
rs2292884	rs4624820	rs1512268	rs10822013	rs11066280	rs2735839	rs685449
rs757978	rs10058728	rs2439302	rs10995190	rs4765623	rs961253	rs7808249
rs4973768	rs872071	rs16892766	rs224278	rs1572072	rs910873	rs1106334
rs1052501	rs12210050	rs1016343	rs704010	rs9510787	rs4925386	rs11017876
rs2660753	rs4712653	rs1456315	rs3765524	rs753955	rs6010620	rs9572094
rs9284813	rs6939340	rs16901979	rs2274223	rs9600079	rs4809324	rs4905366
rs17181170	rs4324798	rs2456449	rs3781264	rs9573163	rs372883	rs4775699
rs9841504	rs29232	rs16902094	rs17119461	rs9543325	rs2014300	rs1528601
rs10934853	rs3129055	rs445114	rs12413624	rs7335046	rs45430	rs11655512
rs6763931	rs2860580	rs13281615	rs11199874	rs944289	rs1547374	rs4793172
rs6774494	rs2517713	rs1562430	rs2981579	rs116909374	rs738722	rs242076
rs10936599	rs6457327	rs10505477	rs2981575	rs4444235	rs36600	rs6603251
rs10936632	rs130067	rs6983267	rs1219648	rs4779584	rs2284063	AMG_mid100
rs4488809	rs2894207	rs7014346	rs2981582	rs4924410	rs1014971	rs149617956
rs10937405	rs2596542	rs1447295	rs3817198	rs4775302	rs5759167	
rs17505102	rs2248462	rs4242382	rs7127900	rs8030672	rs5768709	rs138213197

Genes (94)

AIP
ALK
APC
ATM
BAP1
BLM
BMPR1A
BRCA1
BRCA2
BRIP1
BUB1B
CDC73
CDH1
CDK4
CDKN1C
CDKN2A
CEBPA
CEP57
CHEK2
CYLD
DDB2
DICER1
DIS3L2
EGFR
EPCAM
ERCC2
ERCC3
ERCC4
ERCC5
EXT1
EXT2
EZH2
FANCA
FANCB
FANCC
FANCD2
FANCE
FANCF
FANCG
FANCI
FANCL
FANCM
FH
FLCN
GATA2
GPC3
HNF1A
HRAS
KIT
MAX
MEN1
MET
MLH1
MSH2
MSH6
MUTYH
NBN
NF1
NF2
NSD1
PALB2
PHOX2B
PMS1
PMS2
PRF1
PRKAR1A
PTCH1
PTEN
RAD51C
RAD51D
RB1
RECQL4
RET
RHBDF2
RUNX1
SBDS
SDHAF2
SDHB
SDHC
SDHD
SLX4
SMAD4
SMARCB1
STK11
SUFU
TMEM127
TP53
TSC1
TSC2
VHL
WRN
WT1
XPA
XPC

9.3.2 Sanger sequencing primers – BRIP1

Position (GRCh38)	Variant (*BRIP1*)	Forward primer	Reverse primer	Tm-F (°C)	Tm-R (°C)	Size (bp)
chr17:61716051	p.Arg798*	ACCAGTTCCTATGGTTCCAGT	TGCTTGAGATCACACAGCTG	58.37	58.2	462
chr17:61799278	p.Gln388Thrfs*7	TCCCAAGAAGCCTAGTTAACCA	TGTAGAGCTGATATTTGGTTGGC	58.75	58.8	498
chr17:61780325	p.Ser624*	TGCATCCCAAGTGACTGGAT	CAGACTCCTAGACTCAAGCGA	59.01	58.64	467

9.4 Chapter 5 Whole exome sequencing

9.4.1 WES gene lists

Frequently somatically altered

Gene	Chr	Start (bp)	End (bp)	Gene description
ABCA13	chr7	48171458	48647497	*ATP binding cassette subfamily A member 13*
ADGRV1	chr5	90529344	91164437	*adhesion G protein-coupled receptor V1*
AHNAK2	chr14	104937244	104978374	*AHNAK nucleoprotein 2*
ANK2	chr4	112818109	113383740	*ankyrin 2*
ANK3	chr10	60026298	60733490	*ankyrin 3*
ARID1A	chr1	26693236	26782104	*AT-rich interaction domain 1A*
ATM	chr11	108222484	108369102	*ATM serine/threonine kinase*
COL6A3	chr2	237324003	237414375	*collagen type VI alpha 3 chain*
DNAH2	chr17	7717354	7833744	*dynein axonemal heavy chain 2*
DNAH8	chr6	38715341	39030529	*dynein axonemal heavy chain 8*
DNAH9	chr17	11598470	11969748	*dynein axonemal heavy chain 9*
DST	chr6	56457987	56954649	*dystonin*
FAT1	chr4	186587794	186726722	*FAT atypical cadherin 1*
HERC1	chr15	63608618	63833948	*HECT and RLD domain containing E3 ubiquitin protein ligase family member 1*
KDM5C	chrX	53191321	53225422	*lysine demethylase 5C*
KDM6A	chrX	44873177	45112602	*lysine demethylase 6A*
KIAA1109	chr4	122152333	122362758	*KIAA1109*
KIF1B	chr1	10210805	10381603	*kinesin family member 1B*
KMT2C	chr7	152134922	152436005	*lysine methyltransferase 2C*
KMT2D	chr12	49018975	49059774	*lysine methyltransferase 2D*
LRP1	chr12	57128493	57213351	*LDL receptor related protein 1*
MACF1	chr1	39081316	39487177	*microtubule-actin crosslinking factor 1*
MTOR	chr1	11106535	11262507	*mechanistic target of rapamycin kinase*
MUC17	chr7	101020072	101058745	*mucin 17, cell surface associated*
NF2	chr22	29603556	29698598	*neurofibromin 2*
NFE2L2	chr2	177227595	177392697	*nuclear factor, erythroid 2 like 2*
OBSCN	chr1	228208130	228378874	*obscurin, cytoskeletal calmodulin and titin-interacting RhoGEF*
PIK3CA	chr3	179148114	179240093	*phosphatidylinositol-4,5-bisphosphate 3-kinase catalytic subunit alpha*
PKHD1	chr6	51615300	52087625	*PKHD1, fibrocystin/polyductin*
RANBP2	chr2	108719482	108785809	*RAN binding protein 2*
RYR1	chr19	38433699	38587564	*ryanodine receptor 1*
RYR3	chr15	33310945	33866121	*ryanodine receptor 3*
SETD2	chr3	47016429	47163967	*SET domain containing 2, histone lysine methyltransferase*
SMARCA4	chr19	10960825	11079426	*SWI/SNF related, matrix associated, actin dependent regulator of chromatin, subfamily a, member 4*

Gene	Chr	Start (bp)	End (bp)	Gene description
SMARCB1	chr22	23786931	23838008	*SWI/SNF related, matrix associated, actin dependent regulator of chromatin, subfamily b, member 1*
SRRM2	chr16	2752626	2772538	*serine/arginine repetitive matrix 2*
STAG2	chrX	123960212	124422664	*stromal antigen 2*
SYNE2	chr14	63852983	64226433	*spectrin repeat containing nuclear envelope protein 2*
TP53	chr17	7661779	7687550	*tumor protein p53*
UBR4	chr1	19074510	19210266	*ubiquitin protein ligase E3 component n-recognin 4*
XIRP1	chr3	39183210	39192620	*xin actin binding repeat containing 1*

TCA cycle genes

Gene	Chr	Start (bp)	End (bp)	Gene description
ACO1	chr9	32384603	32454769	*aconitase 1*
ACO2	chr22	41469117	41528989	*aconitase 2*
CS	chr12	56271699	56300391	*citrate synthase*
DLD	chr7	107891162	107931730	*dihydrolipoamide dehydrogenase*
DLST	chr14	74881891	74903743	*dihydrolipoamide S-succinyltransferase*
FH	chr1	241497603	241519761	*fumarate hydratase*
IDH1	chr2	208236227	208266074	*isocitrate dehydrogenase (NADP(+)) 1, cytosolic*
IDH2	chr15	90083045	90102504	*isocitrate dehydrogenase (NADP(+)) 2, mitochondrial*
IDH3A	chr15	78131498	78171945	*isocitrate dehydrogenase 3 (NAD(+)) alpha*
IDH3B	chr20	2658395	2664219	*isocitrate dehydrogenase 3 (NAD(+)) beta*
IDH3G	chrX	153785766	153794523	*isocitrate dehydrogenase 3 (NAD(+)) gamma*
MDH1	chr2	63588609	63607197	*malate dehydrogenase 1*
MDH2	chr7	76048051	76067508	*malate dehydrogenase 2*
OGDH	chr7	44606572	44709066	*oxoglutarate dehydrogenase*
OGDHL	chr10	49734641	49762379	*oxoglutarate dehydrogenase like*
SDHA	chr5	218241	257082	*succinate dehydrogenase complex subunit A*
SDHB	chr1	17018722	17054170	*succinate dehydrogenase complex subunit B*
SDHC	chr1	161314257	161375340	*succinate dehydrogenase complex subunit C*
SDHD	chr11	112086824	112120013	*succinate dehydrogenase complex subunit D*
SUCLA2	chr13	47745736	48037968	*succinate-CoA ligase ADP-forming beta subunit*
SUCLG1	chr2	84423528	84460045	*succinate-CoA ligase alpha subunit*
SUCLG2	chr3	67360460	67654614	*succinate-CoA ligase GDP-forming beta subunit*

Known RCC genes

Gene	Chr	Start (bp)	End (bp)	Gene description
BAP1	chr3	52401013	52410350	*BRCA1 associated protein 1*
BRIP1	chr17	61681266	61863521	*BRCA1 interacting protein C-terminal helicase 1*
CDKN2B	chr9	22002903	22009363	*cyclin dependent kinase inhibitor 2B*
FH	chr1	241497603	2.42E+08	*fumarate hydratase*
FLCN	chr17	17212212	17237188	*folliculin*
MET	chr7	116672390	1.17E+08	*MET proto-oncogene, receptor tyrosine kinase*
MITF	chr3	69739435	69968337	*melanocyte inducing transcription factor*
PBRM1	chr3	52545352	52685917	*polybromo 1*
PTEN	chr10	87863113	87971930	*phosphatase and tensin homolog*
SDHA	chr5	218241	256700	*succinate dehydrogenase complex flavoprotein subunit A*
SDHB	chr1	17018722	17054170	*succinate dehydrogenase complex iron sulfur subunit B*
SDHC	chr1	161314257	1.61E+08	*succinate dehydrogenase complex subunit C*
SDHD	chr11	112086773	1.12E+08	*succinate dehydrogenase complex subunit D*
TSC1	chr9	132891348	1.33E+08	*TSC complex subunit 1*
TSC2	chr16	2047465	2089487	*TSC complex subunit 2*
VHL	chr3	10141008	10152220	*von Hippel-Lindau tumor suppressor*

9.4.2 HapMap sample list

Sample ID			
NA06985	NA07051	NA11832	NA11918
NA06986	NA07056	NA11840	NA11919
NA06989	NA10847	NA11881	NA11920
NA06994	NA11829	NA11892	NA11931
NA07000	NA11830	NA11893	NA11992
NA07037	NA11831	NA11894	

9.4.3a CNV pipeline - main

Primary pipeline – xhmm_CNV.sh [BASH]

CNV_xhmm.sh acts as a wrapper bash script for the XHMM C++ binary executable that acts to pass tar-get BAM alignment files in batches to GATK DepthOfCoverage and subsequently XHMM sub-programmes ‘xhmm –matrix’, ‘xhmm –normalize’, ‘xhmm –PCA’, ‘xhmm –discover’, and ‘xhmm –genotype’.

```bash
#!/bin/bash
## Generating work-environment folder
if [ -d "${outputfolder}cnv_analysis" ]; then
        echo -e "## CNV Pipeline ## - Root folder exists - folder not generated"
else
        mkdir ${outputfolder}cnv_analysis
fi
cp cnvPCA.R ${outputfolder}cnv_analysis/
cp cnvANNO.R ${outputfolder}cnv_analysis/
cp cnvPLOTS.R ${outputfolder}cnv_analysis/
cp ref_CNVs.txt ${outputfolder}cnv_analysis/
cd ${outputfolder}cnv_analysis

### Output directory
if [ -d "xhmm_analysis_${cohort}" ]; then
        echo -e "## CNV Pipeline ## - Analysis folder exists - folder not generated"
else
        mkdir xhmm_analysis_${cohort}
fi
mv cnvPCA.R xhmm_analysis_${cohort}/temp
mv cnvANNO.R xhmm_analysis_${cohort}
mv cnvPLOTS.R xhmm_analysis_${cohort}
mv ref_CNVs.txt xhmm_analysis_${cohort}
cd xhmm_analysis_${cohort}/temp


## folder setup
cp ${int} xhmm.intervals
vim -c "%s/\(\S\+\)\t\(\S\+\)\t\(\S\+\)\t\(\S\+\)/\1:\2-\3/g|wq" xhmm.intervals
```

```
interval="xhmm.intervals"
ls ${inputfolder}*.bam > bam_list_xhmm

## XHMM Analysis
echo -e "## CNV Pipeline ## - XHMM started..."
if [[ ${call} = "FALSE" ]]; then
        echo -e "## XHMM ANALYSIS ## - Bam files split into 6 sets...(Stage 1 of 10)"
        split -a 1 --numeric-suffixes=1 --additional-suffix=.list -n l/6 bam_list_xhmm
        bam_chunk


java -Xmx30g -jar ${gatk} -T DepthOfCoverage \                   |
 -I bam_chunk1.list \                                     |
 -L ${interval} \                                                |
 -R ${ref} \                                                     |
 -dt BY_SAMPLE \                                                 |
 -dcov 5000 \                                                    |
        -l INFO \                                                |
        --omitDepthOutputAtEachBase \                            |
        --omitLocusTable \                                       | Process replicated
6
        --minBaseQuality 0 \                                     | times for 6 sample
        --minMappingQuality 20 \                                 | chucks (one shown)
        --start 1 \                                              |
        --stop 5000 \                                            |
        --nBins 200 \                                            |
        --includeRefNSites \                                     |
        --countType COUNT_FRAGMENTS \                            |
        --allow_potentially_misencoded_quality_scores \          |
        -o bam_chunkOUT1 > /dev/null 2>&1 &                      |
## Allow for all child processes in parallel to complete
        wait
        sleep 5
## Combines GATK Depth-of-Coverage outputs for multiple samples (at same loci):
        xhmm --mergeGATKdepths -o xhmmCNV.mergeDepths.txt \
        --GATKdepths bam_chunkOUT1.sample_interval_summary \
        --GATKdepths bam_chunkOUT2.sample_interval_summary \
        --GATKdepths bam_chunkOUT3.sample_interval_summary \
        --GATKdepths bam_chunkOUT4.sample_interval_summary \
        --GATKdepths bam_chunkOUT5.sample_interval_summary \
        --GATKdepths bam_chunkOUT6.sample_interval_summary > /dev/null 2>&1

## calculates the GC Content of the exome intervals
java -Xmx30g -jar ${gatk} -T GCContentByInterval \
        -L ${interval} \
        -R ${ref} \
        -o DATA_GC_percent.txt > /dev/null 2>&1

## Concatenates and assess GC content (if less than 0.1 or more than 0.9
cat DATA_GC_percent.txt | \
awk '{if ($2 < 0.1 || $2 > 0.9) print $1}' > extreme_gc_targets.txt

## Centres the data about the mean and filters high/low GC intervals
xhmm --matrix -r xhmmCNV.mergeDepths.txt --centerData --centerType target \
        -o xhmmCNV.filtered_centered.RD.txt \
        --outputExcludedTargets xhmmCNV.filtered_centered.RD.txt.filtered_targets.txt \
        --outputExcludedSamples xhmmCNV.filtered_centered.RD.txt.filtered_samples.txt \
        --excludeTargets extreme_gc_targets.txt --minTargetSize ${minTargetSize} \
        --maxTargetSize ${maxTargetSize} --minMeanTargetRD ${minMeanTargetRD} \
        --maxMeanTargetRD ${maxMeanTargetRD} --minMeanSampleRD ${minMeanSampleRD} \
        --maxMeanSampleRD ${maxMeanSampleRD} \
        --maxSdSampleRD ${maxSdSampleRD} > /dev/null 2>&1

## Performs PCA to generate component variation
xhmm --PCA -r xhmmCNV.filtered_centered.RD.txt \
        --PCAfiles xhmmCNV.mergeDepths_PCA > /dev/null 2>&1



wd=$(pwd)
Rscript cnvPCA.R ${wd} ${PVE_mean_factor} > /dev/null 2>&1

## Normalises the mean centered data using the PCA data
xhmm --normalize -r xhmmCNV.filtered_centered.RD.txt \
        --PCAfiles xhmmCNV.mergeDepths_PCA \
        --normalizeOutput xhmmCNV.PCA_normalized.txt \
        --PCnormalizeMethod PVE_mean \
        --PVE_mean_factor ${PVE_mean_factor} > /dev/null 2>&1

## Generates and asseses z-score distribution of mean centered-normalised
## read depth data and filters inappropriate intervals
xhmm --matrix -r xhmmCNV.PCA_normalized.txt \
        --centerData --centerType sample --zScoreData \
        -o xhmmCNV.PCA_normalized.filtered.sample_zscores.RD.txt \
        --outputExcludedTargets xhmmCNV.PCA_normalized.filtered_targets.txt \
        --outputExcludedSamples xhmmCNV.PCA_normalized..filtered_samples.txt \
        --maxSdTargetRD ${maxSdTargetRD} > /dev/null 2>&1



## applies the normalisation and z-scoring to the standard non-normalised
xhmm --matrix -r xhmmCNV.mergeDepths.txt \
        --excludeTargets xhmmCNV.filtered_centered.RD.txt.filtered_targets.txt \
        --excludeTargets xhmmCNV.PCA_normalized.sample_zscores.filtered_targets.txt \
        --excludeSamples xhmmCNV.filtered_centered.RD.txt.filtered_samples.txt \
        --excludeSamples xhmmCNV.PCA_normalized.sample_zscores.filtered_samples.txt \
        -o xhmmCNV.same_filtered.RD.txt > /dev/null 2>&1

## assessment of the z-score to identify high levels of statistical deviation
xhmm --discover -p ${params} \
        -r xhmmCNV.PCA_normalized.filtered.sample_zscores.RD.txt \
        -R xhmmCNV.same_filtered.RD.txt -c xhmmCNV.xcnv \
        -a xhmmCNV.aux_xcnv -s xhmmCNV > /dev/null 2>&1

## genotypes indentified CNV during prior discovery steps
xhmm --genotype -p ${params} \
        -r xhmmCNV.PCA_normalized.filtered.sample_zscores.RD.txt \
        -R xhmmCNV.same_filtered.RD.txt -g xhmmCNV.xcnv -F ${ref} \
        -v xhmmCNV.vcf > /dev/null 2>&1

if (( $(cat xhmmCNV.xcnv | wc -l) < '2' )); then
    echo -e "## CNV Pipeline ## - ERROR: No CNVs called"
    echo -e "## CNV Pipeline ## - XHMM analysis exiting"
    exit
fi
mv xhmmCNV.xcnv ../xhmmCNV.xcnv
mv xhmmCNV.vcf ../xhmmCNV.vcf
mv bam_list_xhmm ../xhmm_samplelist.txt
if [[ ${PCA_plot} == "TRUE" ]]; then
        mv PCA_Scree.png ../PCA_Scree.png
        mv PCA_summary.txt ../PCA_summary.txt
fi
mv xhmmCNV.aux_xcnv ../xhmmCNV.aux_xcnv
mv cnv.log ../cnv.log
cd ../
Rscript cnvANNO.R ${int} > /dev/null 2>&1
```

XHMM annotation – cnvPCA.R [R]

cnvPCA.R script uses GATK DepthOfCoverage output to generate a principle component graph used for dimensional reduction of variance in read depth across the read depth matrix, where the value of the i-th row and j-th column of the matrix correspond to the mean read depth at genomic target i in sample j.

```
args = commandArgs(trailingOnly=TRUE)
setwd(args[1])
PCA <- args[2]
PCA <- as.numeric(PCA) * 100
library(ggplot2)
library(data.table)
## read in filtered and centered read depth data from xhmm
t <- fread("xhmmCNV.filtered_centered.RD.txt",sep = "\t",header = TRUE)
t1 <- t[,-1]
p <- prcomp(t1)

## generate SVD eigen values from SD data in PCA output
## Coerce into a dataframe with index values for each PC
scr <- as.data.frame(p$sdev^2/sum(p$sdev^2)*100)
scr$PC <- seq.int(nrow(scr))
```

```
names(scr)[1] <- "Eigen"
for(i in 1:nrow(scr)){
 c <- sum(scr$Eigen[1:i])
 if(c >= PCA){
  val <- i
  break
  }
}

## plot the data of eigen value against PC
png("PCA_Scree.png", width = 5, height = 5, units = 'in', res = 600)
ggplot(scr, aes(x=PC, y=Eigen)) + geom_line() + geom_point() +
        geom_vline(xintercept=val, linetype = "dashed", color="red") +
        scale_y_continuous(name="Eigen Value - Contributed Variance (%)",
 breaks = pretty(scr$Eigen, n = 10)) +
 scale_x_continuous(name="Princple Component",
 breaks = pretty(scr$PC, n = 10)) +
 ggtitle(label="PCA Scree Plot", subtitle="Cummulative Contributed Variance") +
 geom_text(data=NULL, x=val+3, y=max(scr$Eigen),label="Contributed Variance cut off",
        size=2.5) +
 theme(panel.border = element_blank(),axis.line = element_line(colour="black")) +
 theme(panel.background = element_blank(),
 panel.grid.major = element_line(size = 0.1,colour = "grey50"))
dev.off()
```

XHMM annotation – cnvANNO.R [R]

The cnvANNO.R script performs a secondary calling, annotation, and filtering steps on the default output files from XHMM. Utilising the .xcnv output file, the .aux_xcnv auxiliary calling file, and the target bed file, calling data from ‘xhmm –PCA’, ‘xhmm –discover’, and ‘xhmm –genotype’ sub-programmes, cnvANNO.R converts from genomic region calls to target region resolution calls. Target calls are then annotated using the initial bed file to allow for gene/exon mapping and analysis. A series of filtering steps are also applied during this process to remove upstream and downstream targets with neutral copy changes, remove low quality calls (using the Q_SOME metric), and CNV allele frequency (internal and external).

Output is an 11+N column tab-delimited file (where N is the number of samples in the analysis set), each call being annotated with originating CNV identification number, original CNV call region, name of affected exon, genomic positions of target, non-normalised read depth and mean read depths, Quality score and mean quality score, and internal minor allele frequency for the associated call.

```
args = commandArgs(trailingOnly=TRUE)
options(digits=3)
require(methods)
library(ggplot2)
library(stringr)
library(tidyr)
library(dplyr)

int_af_value <- 0.05
ref_af_value <- 0.05

## Read in files for CNV annotation script
cnv <- read.table("xhmmCNV.xcnv", sep = "\t", header = TRUE, stringsAsFactors = FALSE)
intv <- read.table(args[1], sep = "\t", stringsAsFactors = FALSE)
colnames(intv) <- c("chr","start","stop","exon")
aux <- read.table("xhmmCNV.aux_xcnv", sep = "\t", header = TRUE, stringsAsFactors =
FALSE)

ref.list <- read.table("ref_CNVs.txt", sep = "\t", stringsAsFactors = FALSE)
colnames(ref.list) <- c("EXON","CNV","AF_ref")
f.aux <- aux[!aux$TARGET_IND == "U-2" & !aux$TARGET_IND == "U-1" &
     !aux$TARGET_IND == "D+1" & !aux$TARGET_IND == "D+2",]
intv$id <- paste(intv$chr,":", intv$start, "-", intv$stop, sep="")
x <- merge(f.aux, intv, by.x = "TARGET", by.y = "id", all.x = TRUE)
x$cnv_id <- as.numeric(as.factor(x$FULL_INTERVAL))
x <- cbind(x$cnv_id,x$SAMPLE,x$CHR,x$TARGET,
 x$FULL_INTERVAL,x$CNV,x$exon,x[,8:10])

colnames(x) <- c("CNV_ID","SAMPLE","CHR","TARGET",
"FULL_INTERVAL","CNV","EXON","POSTERIOR","RD","ORIG_RD")
## Remove unmapped exons from interval files
```

```
x <- x[!is.na(x$EXON),]
x <- droplevels.data.frame(x)

## Add Q_SOME field from CNV file and number of targets per full interval
q.value <- data.frame(x=rep(0,nrow(x)))
for(i in 1:nrow(x)){
  q <- cnv[cnv$SAMPLE == as.character(x[i,2]) &
     cnv$INTERVAL == as.character(x[i,5]),]
  q.value[i,] <- q[10]
}
q.tar <- q.value
colnames(q.tar) <- "Q_SOME"
x <- cbind(x,q.tar)
rm(q.value,q.tar,q,i)

## Remove redundant columns
x <- x[,-c(5,8:9)]

## Conversion to vcf sytyle genotype annotation
t <- unique(x[c("EXON","CNV")])
t <- cbind(t,seq.int(1,nrow(t),1))
colnames(t)[3] <- "EXON_CNV_ID"
x <- merge(x,t,by.y = c("CNV","EXON"), all.x = TRUE)
x$GT <- 1
x <- x[!duplicated(x),]
x <- spread(x,SAMPLE,GT,fill=0)
x %>% mutate_if(is.factor, as.character) -> x
#na replaced as 0 in ref genotype field
x[is.na(x)] <- 0

## Selecting columns with constant values across rows & collapsing
x_const <- x[,c(8,1,2,4,5)]
x_const <- x_const %>% group_by(EXON_CNV_ID) %>%
       summarise_all(funs(paste(unique(.), collapse=",")))

## Selecting columns with variable values and concatenating them into cells
x_var <- x[,c(8,3,6,7)]
x_var <- x_var %>% group_by(EXON_CNV_ID) %>%
      summarise_all(funs(paste(., collapse=",")))

## Collapsing genotype information into single row for each unique "site"
x_geno <- x[,c(8:ncol(x))]
x_geno <- as.data.frame(x_geno %>% group_by(EXON_CNV_ID) %>%
       summarise_all(funs(sum(as.numeric(.)))))
## Confirming only 1 or 0 present
x_geno[-1][x_geno[-1] > 0] <- 1

## Reconstructing db into single dataframe
x <- cbind(x_const,x_var,x_geno)
x <- x[-c(6,10)]

## Adding mean Q_some for each row
x$Mean_Q_Some <- sapply(str_split(x$Q_SOME, ","),
          function(x) mean(as.numeric(x)))
x$Mean_Orig_RD <- sapply(str_split(x$ORIG_RD, ","),
          function(x) mean(as.numeric(x)))
x <- cbind(x[1:7],x[ncol(x)],x[9:ncol(x)-1])
x <- cbind(x[1:9],x[ncol(x)],x[11:ncol(x)-1])

## Addition of AF internal to file
AF_all <- apply(x[11:ncol(x)],1, function(y) (sum(y == 1)/sum(y == 0)))
x <- cbind(x[1:10],AF_all,x[11:ncol(x)])

## Adding REF_AF
x <- merge(x, ref.list, by = c("EXON","CNV"), all.x = TRUE, fill = 0)
x[is.na(x)] <- 0
x <- cbind(x[1:11],x[ncol(x)],x[13:ncol(x)-1])
#remove commonly altered exons in ref Cohort
x <- x[x$AF_ref < ref_af_value,]

## String split Exon into gene and exon
gene_exon <- as.data.frame(str_split(as.character(x$EXON),
                    "_",
                    simplify = TRUE),
              stringsAsFactors = FALSE)
gene_exon <- gene_exon[-3]
colnames(gene_exon) <- c("GENE","EXON")
x <- x[-1]
x <- cbind(gene_exon,x[1:ncol(x)])

## Make sure chr positions are unified as numeric - not containing "chr"
x$CHR <- gsub("chr","",x$CHR)
x$TARGET <- gsub("chr","",x$TARGET)
## write output
write.table(x, file="cnv_xhmm_annotated.tsv", sep="\t",
       quote = FALSE, row.names = FALSE, col.names = TRUE, na = "-9")
save.image(file="cnvANNO.RData")
```

9.4.3b CNV pipeline - Reference interval file generation

While implemented in its standard deployment, XHMM was limited in its ability to call CNVs at the exon-level resolution and provided no reference files for exome target regions. Generation of an accurate and curated target file is critical to calculating accurate CNV calls from therefore a series of selection criteria were applied to all exome target regions.

Reference intervals

Exon bed file was downloaded from BioMart (1) in TSV format, returning unique entries for the following fields:

- "Chromosome/scaffold name"
- "Exon region start (bp)"
- "Exon region end (bp)"
- "Gene name"
- "Exon rank in transcript"

Exon intervals were reformatted to fit BED4 (chr, chromStart, chromEnd, Label) specifications.

Repeat region filtering

An important component of the interval file used is that is appropriately filtered for regions that are of interest; this excludes regions overlapping low-complexity regions of the genome. These regions act to add excessive noise to CNV calling due to systemic sequencing bias and technical issue, so can be justifiably removed from genomic target lists. The site repeatmasker.org provides categorical fasta files for each type and span of these regions.

Fasta files containing the type and genomic position of repeat-masked regions can be downloaded from repeatmasker.org. The repeat-mask fasta is not immediately appropriate for use so some minor pre-processing steps were required to allow for interval comparisons (i.e. delimiter alterations, repeat type selection, and sorting by chromosome and position).

Generating list of overlapping intervals

Filtering out intervals with any amount of repeat-mask overlap would be overly stringent so only exome intervals harbouring an overlap of 25% or more are excluded. The command below compares the exome interval set to the repeat-masked interval set generating a list of exons that are overlapped by repeat-masked regions by > 25%

Nextera probe positions were downloaded from Illumina to match library preparation kit used for sequencing run and regions overlapping with 50% of matching targets from the library preparation probes were retained using Bedtools intersect. The preceding files are loaded into R for filtering and target merging, after which 10bp padding is applied to each target interval. This is intended to increase the fidelity of calls over target sets by incorporating more reads that align to the edges of target regions. The subsequent file is then sorted and merged to collapse overlapping intervals into a single interval, resulting in a final exome interval bed file containing only targets of interest.

XHMM reference interval – Exome_CNV_reference_intervals_1.sh [BASH]

```
sed -i '1d' exons.txt
sed -i 's/\(\S\+\)\t\(\S\+\)\t\(\S\+\)\t\(\S\+\)\t\(\S\+\)/\1\t\2\t\3\t\4_\5/g' >
exons.txt

sort -k1,1 -k2,2n exons.txt > exons.sorted.bed
wget -c LINK_TO_REPEATMASKER_FA_FILE
gunzip REPEATMASKER.fa.out.gz

awk -v OFS="\t" '$1=$1' REPEATMASKER.fa.out > REPEATMASKER _tab.fa.out
grep "Simple_repeat" REPEATMASKER _tab.fa.out >> lowcomplex_simpreps.REPEATMASKER.bed
grep "Low_complexity" REPEATMASKER _tab.fa.out >> lowcomplex_simpreps.REPEATMASKER.bed
cut -f5-7 lowcomplex_simpreps.REPEATMASKER.bed >
lowcomplex_simpreps.cut.REPEATMASKER.bed

sort -k1,1 -k2,2n lowcomplex_simpreps.cut.REPEATMASKER.bed > \
                       lowcomplex_simpreps.sorted.REPEATMASKER.bed
bedtools intersect -wb -v -F 0.25 -a exons.sorted.bed
                       -b lowcomplex_simpreps.sorted.REPEATMASKER.bed > exons.masked.bed
sort -k1,1 -k2,2n exons.masked.bed > exons.masked.sorted.bed
bedtools intersect -loj -wb -F 0.5 -b exons.masked.sorted.bed \
          -a nextera_exome_targets.bed > intersect.txt
```

XHMM reference interval – Exome_CNV_reference_interval.R [R]

```
library(dplyr)
library(stringr)
options(scipen = 999)

# Load data and remove empty fields
bed <- read.table("intersect.txt",sep="\t",comment.char = "",quote = "",fill = T,
          stringsAsFactors = F)
bed <- bed[bed$V1 != ".",]
bed <- bed[bed$V4 != ".",]
bed <- bed[,-c(4:6)]

# Keep unique and remove misencoded exons
```

```
bed <- unique(bed)
bed <- bed[which(!grepl(bed$V7,perl = T,pattern = "\\S+_\\S+_\\S+")),]



# Collapse on genomic position
bed_col <- bed %>% group_by(V1,V2,V3) %>%
      summarise_all(funs(paste(unique(.),collapse = ",")))
# Add padding
bed_col$V2 <- bed_col$V2 - 10
bed_col$V3 <- bed_col$V3 + 10
# Write output
write.table(bed_col, "cnv_targets_masked_pad_.bed",sep="\t",quote=FALSE,
row.names=FALSE,
      col.names=FALSE)
```

XHMM reference interval – Exome_CNV_reference_intervals_2.sh [BASH]

```
sort -k1,1 -k2,2n cnv_targets_masked_pad.bed > cnv_targets_masked_pad_sort.bed
bedtools merge -i cnv_targets_masked_pad_sort.bed -c 4 \
                      -o collapse > COLLAPSE.cnv_targets_masked_pad_sort.bed
mv COLLAPSE.cnv_targets_masked_pad_sort.bed cnv_targets_masked_pad_sort.bed
```

9.4.4 Miscellaneous scripts

Discordance – genotype_discord.sh [BASH]

```
#!/bin/bash
## Compress and index for bcftools format
bgzip INPUT_1.vcf; tabix INPUT_1.vcf.gz
bgzip INPUT_2.vcf ;tabix INPUT_2.vcf.gz

## Calculate discordance with bcftools
bcftools gtcheck -R ${REGION} -G 1 -g INPUT_1.vcf.gz INPUT_2.vcf.gz | \
  cut -f2,4 | tail -n1 > discord_out

## Convert and calculate percentage of GTs discordant
SCI_NUMER=$(cut -f1 discord_out) # removes scientific notation for calculations
NUMER=$(printf "%.0f\n" ${SCI_NUMER})
DENOM=$(cut -f2 discord_out)
PCT=$(bc <<< "scale=4; $NUMER / $DENOM * 100" | sed -r 's/^(-?)\./\10./' | \
   awk ' sub("\\.*0+$","") ')

## Convert target file paths to useable sample names
ECHO_1=$(echo ${INPUT1} | sed 's%\S\+/\(\S\+\)_\S\+%\1%')
ECHO_2=$(echo ${INPUT2} | sed 's%\S\+/\(\S\+\)_\S\+%\1%')
```

Population scripts – population.sh [BASH]

```
#!/bin/bash
cat ${VCF} | grep -m 1 "#C" | tr '\t' '\n' | sed -e '1,9d' > sample_list_pop
bcftools view -h ${REF_VCF} | grep -m 1 "#C" | tr '\t' '\n' | \
sed -e '1,9d' >> sample_list_pop

bgzip -c ${VCF} > ${NAME}.vcf.gz
tabix ${NAME}.vcf.gz
bcftools merge -Oz -o ${NAME}_REF.vcf.gz ${NAME}.vcf.gz ${REF_VCF}

vcftools --gzvcf ${NAME}_REF.vcf.gz --thin 2000 --chr chr1 --chr chr2 --chr chr3 --chr
chr4 \
               --chr chr5 --chr chr6 --chr chr7 --chr chr8 --chr chr9 --chr chr10 --chr
chr11 \
               --chr chr12 --chr chr13 --chr chr14 --chr chr15 --chr chr16 --chr chr17 \
               --chr chr18 --chr chr19 --chr chr20 --chr chr21 --chr chr22 --chr chrX \
               --min-alleles 2 --max-alleles 2 --non-ref-ac 2 --recode --out ${NAME}_REF

plink1.90 --vcf ${NAME}_REF.recode.vcf --out ${NAME}_REF.maf0.05 --make-bed --maf 0.05 \
               --vcf-half-call 'm' --const-fid --biallelic-only --geno 0.05

${ADMIXTURE} ${NAME}_REF.maf0.05.bed 5
Rscript admixture_plotting.R ${NAME}_REF.maf0.05.5.Q
```

Population scripts – admixture_plot.R [R]

```
rm(list = ls())
## Enable cmd line args
args = commandArgs(trailingOnly=TRUE)

library(ggplot2)
library(reshape2)
library(plotly)
library(RColorBrewer)

q.table <- read.table(args[1])
colnames(q.table) <- c("SAS","EUR","EAS","AFR","AMR")

sample.table <- read.table("sample_list_pop")
colnames(sample.table) <- c("Sample")

pop.table <- read.table("1KG_samplePopulations.tsv",header = T)

plot.table <- cbind(sample.table,q.table)

merge.table <- merge(plot.table,pop.table[,c(2,4)],
by = "Sample",all.x = T,all.y = F,sort = F)
merge.table$pred <- apply(merge.table[2:6],1,function(x) names(which.max(x)))

lapply(sort(unique(merge.table$pred)),
function(x){print(table(merge.table$Super_population[merge.table$pred == x]))})
```

```
merge.table <- merge.table[with(merge.table, order(pred)),]

merge.table$Sample <- factor(merge.table$Sample,levels = merge.table$Sample)


merge.table.cases <- merge.table[is.na(merge.table$Super_population),]

write.table(merge.table.cases[,-7],"admixture_unknowns.tsv",

sep = "\t",quote = F,col.names = T,row.names = F)


data.json <- t(merge.table.cases[,1:6])

data.json <- cbind(rownames(data.json),data.json)

save(data.json,file = "admixture_pop.RData")


melt.table <- melt(merge.table,id.vars = c("Sample","Super_population","pred"))

names(melt.table) <- c("Sample","SuperPop","Pred","Population","Admixture")


P <- ggplot(melt.table[is.na(merge.table$Super_population),],

    aes(x = Sample, y = Admixture, fill = Population)) +

       geom_bar(stat = "identity") +

       ggtitle("Admixture population proportions") +

       scale_fill_brewer(palette = "Set1") +

       theme(panel.grid = element_blank(),

       panel.background = element_blank(),

       axis.line = element_line(),

       axis.text.x = element_blank(),axis.ticks.x = element_blank()) +

       scale_y_continuous(expand = c(0,0)) +

       scale_x_discrete(expand = c(0,0))

png("admixture_unknowns.png",width = 12,height = 3,units = "in",res = 600)

P

dev.off()
```

9.4.5 Burden testing scripts

Burden testing - Association_tests.sh [BASH]

```
#!/bin/bash

if [[ ! -d ${OUTPUT}${PROJECT} ]]; then

        mkdir ${OUTPUT}${PROJECT}

fi


if [[ "$MODE" != "no_prep" ]]; then

        cp tests/* ${OUTPUT}${PROJECT}/

        cp ${VCF} ${OUTPUT}${PROJECT}/input_file.vcf

        mv assoc_log.txt ${OUTPUT}${PROJECT}/

        cd ${OUTPUT}${PROJECT}/

        VCF="input_file"


## Further vcf filtering removing sites with >10% missing particularly

        vcftools --vcf ${VCF}.vcf --hwe 0.05 --non-ref-ac-any 1 --minGQ ${MINGQ} \

                       --minDP ${MINDP} --max-missing ${MISS} --minQ ${MINQ} \

                       --recode --out ${VCF}

        mv ${VCF}.recode.vcf ${VCF}.filt.vcf


## Spliting multiallelics

        java -Xmx30g -jar ${GATK} \

               -T LeftAlignAndTrimVariants \

               -R /data/Resources/References/${REFERENCE}/${REFERENCE}.fa \

               --variant ${VCF}.filt.vcf \

               -o ${VCF}.filt.bi.vcf \

               --splitMultiallelics


## Generate list of chr files for

        sed -n '/#CHROM/,$p' ${VCF}.filt.bi.vcf | cut -f1 | sort -u | \

                grep -v '#CHROM' > chr_list

        cat chr_list | xargs -n1 -P${CORES} -I {} mkdir temp_{}

        cat chr_list | xargs -n1 -P${CORES} -I {} vcftools --vcf ${VCF}.filt.bi.vcf \

                                                     --chr {} --recode --recode-INFO-all
\

                                                     --out temp_{}/${VCF}.splt.{}
        cat chr_list | xargs -n1 -P${CORES} \
                -I {} ${ANNO}table_annovar.pl temp_{}/${VCF}.splt.{}.recode.vcf \
                ${ANNO}humandb/ -vcfinput -buildver hg38 -out temp_{}/${VCF}_{} \
                -remove -protocol refGene,exac03,dbnsfp30a -operation g,f,f -nastring .

        cat chr_list | xargs -n1 -P${CORES} \
                -I {} mv temp_{}/${VCF}_{}.hg38_multianno.vcf
${VCF}_{}.hg38_multianno.vcf
        rm -r temp_*
        sed '/#CHROM/,$d' ${VCF}.filt.bi.vcf > header

        for i in `cat chr_list`; do
                cat header ${VCF}_${i}.hg38_multianno.vcf > \
                              ${VCF}_${i}.hg38_multianno.header.vcf
        done

        ls *.header.vcf > vcf_list

        bcftools concat -o ${VCF}.FINAL.vcf -Ov -f vcf_list

        rm *_multianno*.vcf

## Remove header
        sed -i -n '/#CHROM/,$p' ${VCF}.FINAL.vcf
else
        ## Run vcf processing script
        mv assoc_log.txt ${OUTPUT}${PROJECT}/
        cd ${OUTPUT}${PROJECT}/
        VCF="input_file"
fi

Rscript vcf_prep.R ${VCF}.FINAL.vcf ${PED} ${CORES} ${AF_ref} ${AF_all} \
${AF_case} ${AF_cont} ${CONSEQS}


Rscript SKAT_test.R
```

Burden testing – vcf_prep.R [R]

```
args = commandArgs(trailingOnly=TRUE)
library(stringr)
library(stringi)
library(tidyr)
library(dplyr)
library(data.table)
library(parallel)
options(scipen=999)

## Load list of excluded samples
samples_rm <- c()
CONSEQS <- c("nonframeshift_deletion","nonframeshift_insertion",
       "frameshift_deletion","stopgain","frameshift_insertion",
       "splicing","nonsynonymous_SNV","synonymous_SNV","stoploss")
CONSEQS <- CONSEQS[CONSEQS %in% as.character(unlist(strsplit(args[8],",")))]

## Load column header from vcf file
col_headers <- fread(args[1],nrows = 1,header = F,sep="\t")
col_headers <- gsub(pattern = "#",replacement = "",col_headers)

## Load vcf data and append to column headers
vcf_file <- fread(input = args[1],skip = 1,stringsAsFactors = F,
         header = F,,sep="\t")
names(vcf_file) <- col_headers
vcf_file <- as.data.frame(vcf_file)

## Load case/control T/F data - Sort them into the same order as vcf
samples <- read.table(args[2])
samples <- samples[match(names(vcf_file[10:ncol(vcf_file)]),samples$V1),]
samples <- samples[!samples$V1 %in% samples_rm,]
af_unaf <- as.logical(samples[,2])

## Converting genotypes
out <- mclapply(vcf_file[10:ncol(vcf_file)],mc.preschedule = T,mc.cores = 2,
function(x){
 x <- stri_replace_all_regex(x,pattern = "^0/0.*",replacement = 0)
 x <- stri_replace_all_regex(x,pattern = "^0/1.*",replacement = 1)
 x <- stri_replace_all_regex(x,pattern = "^1/1.*",replacement = 2)
 x <- stri_replace_all_regex(x,pattern = "^\\./\\..*",replacement = -9)
})
vcf_file[10:ncol(vcf_file)] <- do.call(cbind.data.frame, out)

## Coerce all genotype columns as.numeric
vcf_file[,10:ncol(vcf_file)]<-as.data.frame(sapply(vcf_file[,10:ncol(vcf_file)],
          function(f) as.numeric(as.character(f))),stringsAsFactors=F)

## Adding internal AFs
cases <- as.character(samples$V1[samples$V2 == TRUE])
controls <- as.character(samples$V1[samples$V2 == FALSE])

intAF <- data.frame(intAF_cases=as.numeric(seq_len(nrow(vcf_file))),
          intAF_controls=as.numeric(seq_len(nrow(vcf_file))),
          intAF_set=as.numeric(seq_len(nrow(vcf_file))))

intAF$intAF_cases <- signif(apply(vcf_file[,
           which(names(vcf_file) %in% cases)],
           1,function(x) sum(x != 0) / length(cases)),digits = 2)
intAF$intAF_controls <- signif(apply(vcf_file[,
           which(names(vcf_file) %in% controls)],
           1,function(x) sum(x != 0) / length(controls)),digits = 2)
intAF$intAF_set <- signif(apply(vcf_file[,
           which(names(vcf_file) %in% c(cases,controls))],
           1,function(x) sum(x != 0) / length(c(cases,controls))),
           digits = 2)

vcf_file <- cbind(intAF,vcf_file)
## Retrieving annotation information on Allele freq, region function, and mutation
consequence
info_split <- as.data.frame(
 str_split(string =
 gsub(".*Func\\.refGene=(.*?);.*Gene\\.refGene=(.*?);
 .*ExonicFunc\\.refGene=(.*?);.*ExAC_ALL=(.*?);.*",
             replacement = "\\1#\\2#\\3#\\4",
              x = vcf_file$INFO),
       pattern = "#",
       simplify = T),
 stringsAsFactors = F)

## Naming annoation information - replacing uncoded
names(info_split) <- c("FUNC","GENE","CONSEQ","AF")
info_split$FUNC <- gsub(pattern = "\\\\x3b",replacement = ";",info_split$FUNC)
info_split$GENE <- gsub(pattern = "\\\\x3b",replacement = ";",info_split$GENE)
info_split$AF[info_split$AF == "."] <- 0
info_split$AF <- as.numeric(info_split$AF)

## bind new columns to vcf data
vcf_file <- cbind(info_split,vcf_file)

## Adding chr:pos ids to rsID column and replacing "." missing value
vcf_file$ID[vcf_file$ID == "."] <- paste(vcf_file$CHROM[vcf_file$ID == "."],
                  vcf_file$POS[vcf_file$ID == "."],sep = ":")
calcID <- paste(vcf_file$ID,vcf_file$REF,vcf_file$ALT,sep = "_")
vcf_file <- cbind(calcID,vcf_file)

## Add splicing anntation to CONSEQ field
vcf_file$CONSEQ[vcf_file$FUNC == "splicing" |
               vcf_file$FUNC == "exonic;splicing"] <- "splicing"

## PCA analysis
vcf_file_PCA <- vcf_file[vcf_file$AF > 0.05,18:ncol(vcf_file)]
vcf_file_PCA_t <- as.data.frame(t(vcf_file_PCA))
vcf_file_PCA_t <- vcf_file_PCA_t[,which(apply(vcf_file_PCA_t,2,var)!=0)]

PCA.out <- prcomp(vcf_file_PCA_t,center = T, scale. = T)
PCAs <- as.data.frame(PCA.out$x[,1:5])
rm(vcf_file_PCA,vcf_file_PCA_t,PCA.out)

colours <- ifelse(af_unaf == T,"blue","grey")
colours[which(abs(PCAs$PC1) > sd(PCAs$PC1)*3 &
      abs(PCAs$PC2) > sd(PCAs$PC2)*3)] <- "red"
```

```
colours[which(abs(PCAs$PC2) > sd(PCAs$PC2)*3 &
      abs(PCAs$PC3) > sd(PCAs$PC3)*3)] <- "red"

png(filename = "association_test_PCA.png",width = 16,
  height = 8,units = "in",res = 600)
layout(matrix(c(1,2), 1, 2, byrow = TRUE))
plot(abs(PCAs$PC1),abs(PCAs$PC2),col=colours,xlab = "PC1",
  ylab = "PC2",
  main = "Association tests - PC1 ~ PC2",sub = "Red = Excluded")
abline(v=sd(PCAs$PC1)*3, col="red")
abline(h=sd(PCAs$PC2)*3, col="red")

plot(abs(PCAs$PC2),abs(PCAs$PC3),col=colours,xlab = "PC2",
  ylab = "PC3",
  main = "Association tests - PC2 ~ PC3",sub = "Red = Excluded")
abline(v=sd(PCAs$PC2)*3, col="red")
abline(h=sd(PCAs$PC3)*3, col="red")
dev.off()

PCA_excluded <- unique(c(rownames(
    PCAs[abs(PCAs$PC1) > sd(PCAs$PC1)*3 & abs(PCAs$PC2) > sd(PCAs$PC2)*3,]),
    rownames(
    PCAs[abs(PCAs$PC2) > sd(PCAs$PC2)*3 & abs(PCAs$PC3) > sd(PCAs$PC3)*3,]))
    )

writeLines(PCA_excluded,sep = "\n",con = "PCA_excluded.samples")
## Adjust Samples and data to remove samples
PCAs <- PCAs[!rownames(PCAs) %in% PCA_excluded,]
samples <- samples[!samples$V1 %in% PCA_excluded,]

af_unaf <- as.logical(samples[,2])

vcf_file <- vcf_file[!colnames(vcf_file) %in% PCA_excluded]

## Filtering vcf data on various traits - Rarity, Function, Consequence
vcf_file <- vcf_file[vcf_file$CONSEQ %in% CONSEQS,]
vcf_file <- vcf_file[vcf_file$AF < args[3],] # 0.005
vcf_file <- vcf_file[vcf_file$intAF_set < args[4],] # 0.05

vcf_file <- vcf_file[vcf_file$intAF_cases < args[5],] # 0.2

vcf_file <- vcf_file[vcf_file$intAF_controls < args[6],] #0.2


save(vcf_file,PCAs,samples,af_unaf,file="association.RData")
```

Burden testing – skat_test.R [R]

```
## Script for SKAT-O implementation

rm(list=ls())

library(stringr)

library(stringi)

library(tidyr)

library(dplyr)

library(data.table)

library(parallel)

library(SKAT)


## Load data

load("association.RData")

## Set missing to 9

vcf_file[vcf_file == -9] <- 9


## Split by gene

split_region <- split(vcf_file,as.factor(vcf_file$GENE))


## Weights

allele_Freq <- vcf_file$AF

weights <- Get_Logistic_Weights_MAF(MAF = allele_Freq)


## Setting binary phenotype

binary <- af_unaf

binary[binary == T] <- 1

binary[binary == F] <- 0


## Generating matrix_list

gene_matrix_list <- mapply(function(x, i){
 mat <- as.data.frame(x)
 if(nrow(mat) > 1){
 col.n <- colnames(mat[c(18:ncol(mat))])
 row.n <- as.character(mat[,1])
 mat <- as.matrix(t(mat[c(18:ncol(mat))]))
 rownames(mat) <- col.n
 colnames(mat) <- row.n
 return(mat)
 }
}, split_region, names(split_region),SIMPLIFY = F)

## SKAT null model
obj <- SKAT_Null_Model(binary ~ PCAs$PC1, out_type="D")
## Performing binary SKAT
out <- mapply(function(x, i){
 tryCatchAdv({
 cat(paste("[ASSOCIATION TESTS][SKAT] Testing ",i," \n",sep = ""))
 SKATBinary(as.matrix(x), obj, method = "SKAT", kernel = "linear.weighted")
 })
}, gene_matrix_list, names(gene_matrix_list),SIMPLIFY = F)

skat_results <- do.call(rbind,mapply(function(x, i){
  if(length(x$value) == 1){
   data.frame(gene=i,pvalue=NA,warning=x$status,description=x$message$message)
  } else {
  unique(data.frame(gene=i,pvalue=x$value$p.value,warning=x$status,
      description=ifelse(!is.na(x$message),x$message$message,NA)))
  }
}, out, names(out),SIMPLIFY = F))

skat_results <- skat_results[order(skat_results$pvalue),]
skat_results$q.value <- p.adjust(skat_results$pvalue,"fdr")

write.table(skat_results,"skat_output.results",
      quote=F,row.names=F,col.names=T,sep="\t")
png(filename = "SKAT_QQ_PC1_MAFw.png",
   width = 8,
   height = 8,
   units = "in",res = 600)
QQPlot_Adj(
Pval = as.numeric(unlist(
    lapply(out,function(x) if(length(x$value) > 1 ){x$value$p.value}))),
MAP = as.numeric(unlist(
    lapply(out,function(x) if(length(x$value) > 1 ){x$value$MAP}))))
dev.off()
```

9.4.6 Burden testing results

SKAT-O Burden association testing results (p < 0.01)

Gene	p value	q value (FDR corrected)
FBLIM1	2.55E-06	0.03563319
SNX30	1.08E-05	0.054276049
CTSV	1.17E-05	0.054276049
SLPI	4.89E-05	0.170566669
PNRC2	0.000134573	0.264815975
FAM151B	0.000156261	0.264815975
OR5K1	0.000173994	0.264815975
SLC23A2	0.000188126	0.264815975
PRAP1	0.000203361	0.264815975
SLC19A2	0.000242856	0.264815975
GPR65	0.000247932	0.264815975
TBX19	0.000267781	0.264815975
DPRX	0.000271117	0.264815975
LILRB3	0.000292	0.264815975
GFAP	0.00034382	0.264815975
GSK3B	0.00038061	0.264815975
OR10P1	0.000399109	0.264815975
SMPD4	0.000402619	0.264815975
SC5D	0.000412803	0.264815975
FBXW4	0.000412876	0.264815975
PACS1	0.000426772	0.264815975
COX6A1	0.000433019	0.264815975
TONSL	0.000436333	0.264815975
ZNF346	0.000458236	0.266521319
PRG3	0.000518547	0.289535762
KCNJ8	0.000654497	0.349503469
DMRTC2	0.000701635	0.349503469
LAMTOR5	0.000728328	0.349503469
CORO1C	0.000735446	0.349503469
NGDN	0.000751136	0.349503469
PRSS22	0.000979471	0.413986965
TMED3	0.001010605	0.413986965
SLC6A11	0.001012629	0.413986965
KCNK7	0.001104079	0.413986965
ZNF250	0.001152795	0.413986965
CCL4,CCL4L1,CCL4L2	0.001154802	0.413986965
SLC8B1	0.001170377	0.413986965
TIGD3	0.001238785	0.413986965
SH3RF2	0.001254344	0.413986965
HMGB4	0.001261796	0.413986965
ZFP57	0.001263514	0.413986965
LFNG	0.001275334	0.413986965
RP1L1	0.001323406	0.413986965
FNDC5	0.001330022	0.413986965
OR13C4	0.001334581	0.413986965
VPS33A	0.001388261	0.420908624
PTGR1	0.001429968	0.420908624
TBX15	0.001447354	0.420908624
PSMD8	0.001497021	0.424130617
KCNN2	0.001519201	0.424130617
KSR1	0.001570575	0.428019911
TM9SF4	0.00166613	0.428019911
ZNF714	0.00173174	0.428019911
DET1	0.001735973	0.428019911

Gene	p value	q value (FDR corrected)
ZNF416	0.001737172	0.428019911
CALHM2	0.001738639	0.428019911
XPNPEP1	0.00180327	0.428019911
PANK1	0.001834203	0.428019911
CLCA4	0.001867313	0.428019911
CHRAC1	0.001882703	0.428019911
DUSP6	0.001898997	0.428019911
CD1E	0.001922296	0.428019911
HCFC2	0.001931747	0.428019911
KRTAP4-7	0.001991673	0.434402518
SERPINB6	0.002032936	0.436580907
CST8	0.002468087	0.522000314
DMPK	0.002524601	0.525983717
IFT88	0.002583276	0.530293297
HIPK2	0.002741558	0.540888182
HBP1	0.002774881	0.540888182
GABRA3	0.002779539	0.540888182
UBN1	0.002843189	0.540888182
TEAD1	0.002881216	0.540888182
PLEKHO1	0.002904529	0.540888182
ZNF705A	0.002906126	0.540888182
PKDREJ	0.002966456	0.544852105
MRPL40	0.003009531	0.545585057
KPTN	0.003255227	0.5750819
HIF1A	0.003286868	0.5750819
NUDT16	0.003322268	0.5750819
MEDAG	0.00337031	0.5750819
LRRC74B	0.003418878	0.5750819
KBTBD4	0.003419428	0.5750819
LYSMD4	0.003488999	0.579796832
CTTN	0.003531331	0.579927579
RRP15	0.003663402	0.580204652
VAV2	0.003726035	0.580204652
ITCH	0.00377388	0.580204652
OR4F4	0.003802435	0.580204652
FAAH	0.003879128	0.580204652
PKNOX2	0.003890677	0.580204652
PHF20L1	0.003900951	0.580204652
C1QTNF7	0.003969547	0.580204652
GIMAP7	0.003998001	0.580204652
ACMSD	0.004026266	0.580204652
OIT3	0.004037775	0.580204652
MRPL39	0.004119993	0.580204652
CLEC17A	0.004121411	0.580204652
KRTAP5-8	0.004220275	0.580204652
C17orf78	0.004270211	0.580204652
PREP	0.004306123	0.580204652
PPM1A	0.004327817	0.580204652
SLC22A15	0.004388291	0.580204652
HOXC10	0.004395015	0.580204652
C4orf27	0.004403175	0.580204652
LGALS12	0.004405881	0.580204652
SLC5A1	0.004775543	0.618382577
SPEG	0.004802565	0.618382577
FYTTD1	0.004828691	0.618382577
AMDHD1	0.004920644	0.621823193
MS4A2	0.004982337	0.621823193
CPA2	0.004989197	0.621823193
CA14	0.005035638	0.622057282

Gene	p value	q value (FDR corrected)
C10orf12	0.005226798	0.633847033
ADGRD1	0.005236317	0.633847033
AKR1C4	0.005269664	0.633847033
TAOK3	0.005319086	0.633847033
ZNF430	0.005409051	0.633847033
KIF5C	0.005501874	0.633847033
GPD1L	0.005573342	0.633847033
REEP6	0.005585432	0.633847033
SH2B2	0.005632483	0.633847033
ST6GAL1	0.005812554	0.633847033
B3GALT2	0.005854457	0.633847033
SPAG16	0.005854845	0.633847033
MYH1	0.005855493	0.633847033
SEC22C	0.005857836	0.633847033
PDE12	0.005923886	0.633847033
FGD5	0.005942027	0.633847033
ENTPD4	0.005963749	0.633847033
RPUSD2	0.005966535	0.633847033
SCGN	0.005993825	0.633847033
ASB18	0.00607613	0.637719549
TGFBI	0.006237223	0.646677384
LRIT1	0.006254133	0.646677384
ZFP42	0.006335164	0.647966604
DMTF1	0.00635944	0.647966604
DAPK2	0.006461977	0.65364307
ARMC7	0.006550323	0.657812621
A1CF	0.006613826	0.659445725
NAV3	0.006892369	0.682344512
CDCA3	0.007109488	0.698882698
ADCY7	0.007281647	0.710800775
DDX54	0.00742003	0.715038593
RBM15	0.007427509	0.715038593
SAMD7	0.007565645	0.720872629
C5orf60	0.007591395	0.720872629
TMA16	0.007668263	0.723251946
STT3B	0.007736165	0.724759272
BROX	0.00785703	0.72911864
GOLIM4	0.007887163	0.72911864
PADI1	0.008077093	0.733139724
TRMT2A	0.008090709	0.733139724
SLC36A4	0.008095321	0.733139724
OR2AG1	0.008142547	0.733139724
ADAMTS2	0.00825169	0.733139724
MYL2	0.008371296	0.733139724
CXCL1	0.008418193	0.733139724
EPHB4	0.008434813	0.733139724
APITD1,APITD1-CORT	0.008535441	0.733139724
FCRL2	0.008538744	0.733139724
LCN12	0.008551669	0.733139724
CWC27	0.008560912	0.733139724
MAEL	0.008794906	0.747131388
CHPF	0.00883134	0.747131388
VSIG10L	0.009300606	0.764899502
AXIN1	0.009328601	0.764899502
FPR3	0.009450124	0.764899502
ZNF202	0.009477217	0.764899502
SGPP2	0.009572906	0.764899502
SLC35F1	0.009585344	0.764899502
GAN	0.009703024	0.764899502

Gene	p value	q value (FDR corrected)
WLS	0.009774578	0.764899502
KCNB1	0.009842355	0.764899502
LIPF	0.009844052	0.764899502
PIGA	0.009867894	0.764899502
OR1S2	0.009888138	0.764899502
CHCHD2	0.009898729	0.764899502
CNN1	0.009907776	0.764899502
ENAH	0.009977957	0.764899502

9.5 Chapter 6 RCC-associated translocations

9.5.1 Copy number and structural variant calling scripts

Copy number calling – CANVAS.sh [BASH]

Canvas CNV Caller (version 1.38.0.1598) was used to call copy number variation from WGS BAM files. Reference genomes and required supporting files were downloaded from http://canvas-cnv-public.s3.amazonaws.com/ for GRCh38. The following command was used to generate copy number alterations;

```
#!/bin/bash


for SAMPLE in `cat /home/pss41/translocs_rcc/canvas_samples.list`; do
        mkdir ${OUTPUT}${SAMPLE}_canvas
        cd ${OUTPUT}${SAMPLE}_canvas
##decoy VCF files
        echo –e “${DECOY_VCF_HEADER" > ploidy.vcf
dotnet ${CANVAS} SmallPedigree-WGS -b ${INPUT}${SAMPLE}${SUFFIX} \
                        --population-b-allele-vcf ${CANVAS_RESOURCES}${BUILD}/dbsnp.vcf \
                        -o ${OUTPUT}${SAMPLE}_canvas \
                -g ${CANVAS_RESOURCES}${BUILD}/Sequence/WholeGenomeFasta/ \
                        -r ${CANVAS_RESOURCES}${BUILD}/Sequence/WholeGenomeFasta/genome.fa
\
                        -f ${CANVAS_RESOURCES}${BUILD}/filter13.bed \
                        --ploidy-vcf ploidy.vcf
        tabix CNV.vcf.gz
        bcftools view -f "PASS" -o ${SAMPLE}_canvas.vcf -Ov CNV.vcf.gz


sed -n '/#CHROM/,$p' ${SAMPLE}_canvas.vcf | grep -v '#CHROM' | \
        sed 's%\(\S\+\)[10]%\3\t\1|\2|\3|\4|\5|\6|\7|\8|\9%g' | \
        sed –r 's%Canvas:GAIN:%%g' | sed –r 's%Canvas:LOSS:%%g' | \
        sed –r 's%Canvas:REF:%%g' | \
        sed 's%\(\S\+\):\(\S\+\)-\(\S\+\)\t\(\S\+\)%\1\t\2\t\3\t\4%g' >
${SAMPLE}_canvas.bed
bedtools intersect -wa -wb -a ${SAMPLE}_canvas.bed -b ${BED} >
${SAMPLE}_annotated_canvas.bed
done
```

Structural variant calling – MANTA.sh [BASH]

Manta Structural variant caller (version 1.3.1) was used to identify candidate chromosomal break points matching cytogenetic banding and assess if structural variants had impacted on known RCC predisposition genes (VHL, MET, FH, SDHB, SDHD, SDHC, BAP1, CDKN2B). The following command was used to generate SV calls using Manta;

```
#!/bin/bash


configManta.py --bam=${SAMPLE}.bam \
        --referenceFasta=${REFERENCE}.fa \
        --runDir=${OUTPUT_FOLDER}


${OUTPUT_FOLDER}/runWorkflow.py -m local -j 8
```

9.5.2 IGV visualisations of translocation break point

t(2;17)(q21;q11.2)

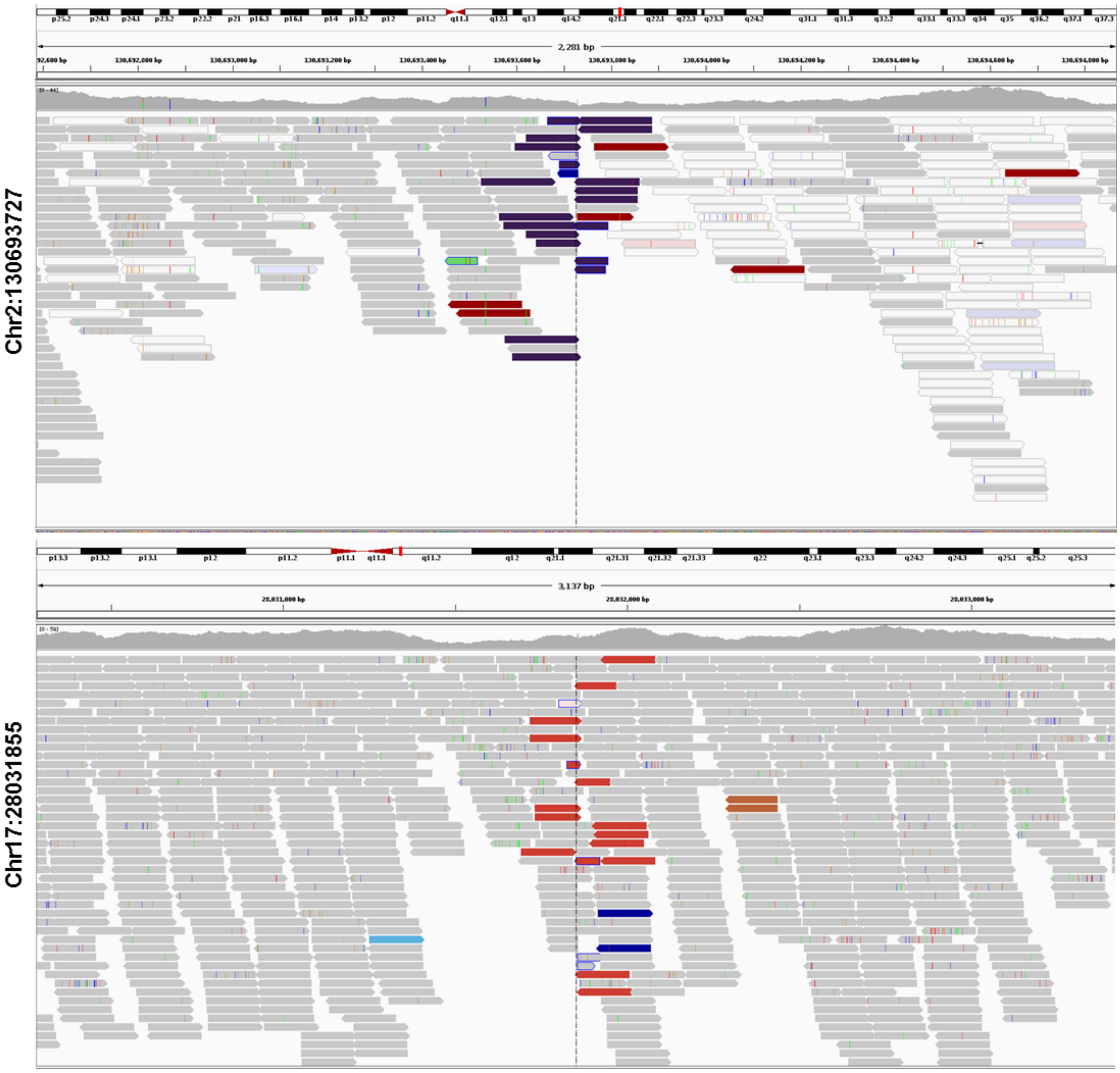
Chr2:130693727
p25.2 p24.3 p24.1 p23.2 p22.2 p21 p16.3 p16.1 p14 p13.2 p12 p11.2 q11.1 q12.1 q13 q14.2 q21.1 q22.1 q22.3 q23.3 q24.2 q31.1 q31.3 q32.2 q33.1 q33.3 q34 q35 q36.2 q37.1 q37.3
2,281 bp
92,600 bp
130,692,800 bp
130,693,000 bp
130,693,200 bp
130,693,400 bp
130,693,600 bp
130,693,800 bp
130,694,000 bp
130,694,200 bp
130,694,400 bp
130,694,600 bp
130,694,800 bp
[0 - 44]
Chr17:28031855
p13.3 p13.2 p13.1 p12 p11.2 p11.1 q11.1 q11.2 q12 q21.1 q21.31 q21.32 q21.33 q22 q23.1 q23.3 q24.2 q24.3 q25.1 q25.2 q25.3
3,137 bp
28,031,000 bp
28,032,000 bp
28,033,000 bp
[0 - 54]

t(3;6)(p14.2;p12)

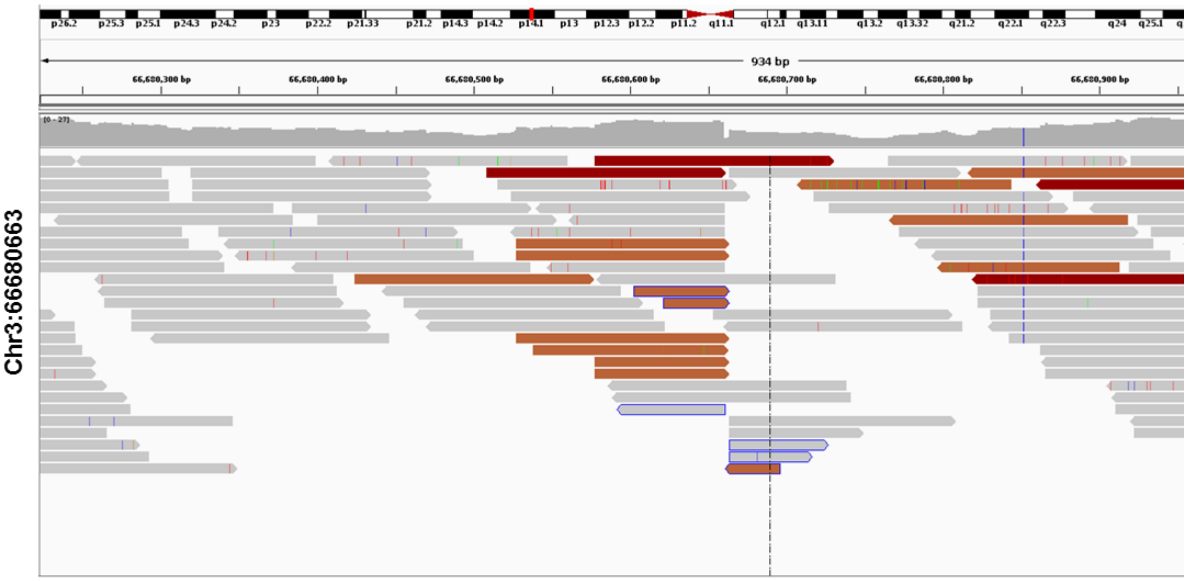
Chr3:66680663
p26.2 p25.3 p25.1 p24.3 p24.2 p23 p22.2 p21.33 p21.2 p14.3 p14.2 p14.1 p13 p12.3 p12.2 p11.2 q11.1 q12.1 q13.11 q13.2 q13.32 q21.2 q22.1 q22.3 q24 q25.1 q
934 bp
66,680,300 bp
66,680,400 bp
66,680,500 bp
66,680,600 bp
66,680,700 bp
66,680,800 bp
66,680,900 bp
[0 - 27]

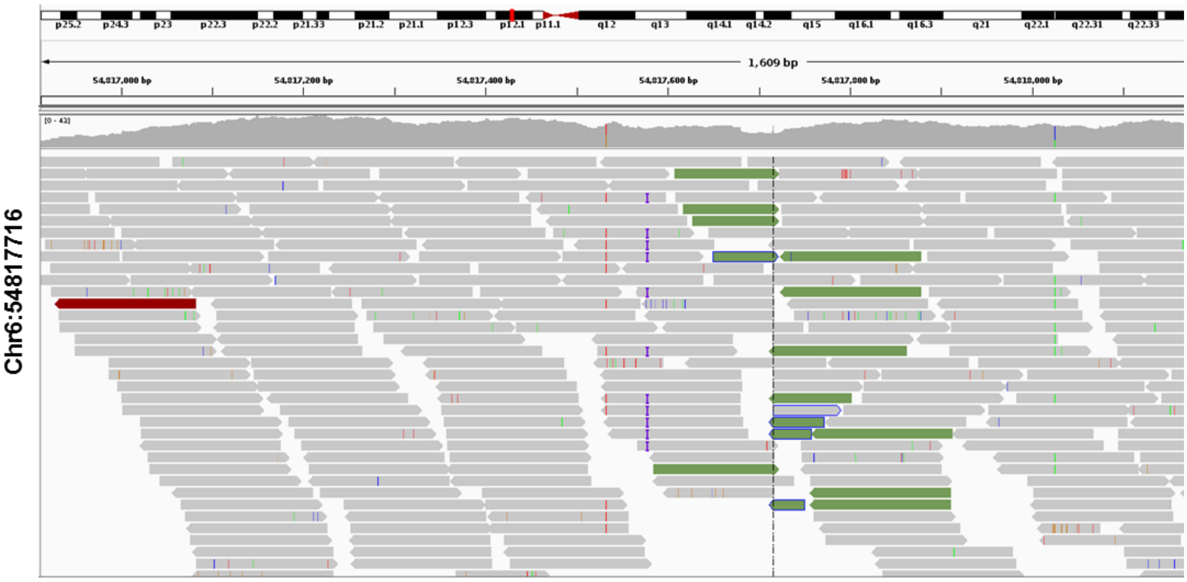
Chr6:54817716
p25.2 p24.3 p23 p22.3 p22.2 p21.33 p21.2 p21.1 p12.3 p12.1 p11.1 q12 q13 q14.1 q14.2 q15 q16.1 q16.3 q21 q22.1 q22.31 q22.33
1,609 bp
54,817,000 bp
54,817,200 bp
54,817,400 bp
54,817,600 bp
54,817,800 bp
54,818,000 bp
[0 - 43]

inv(3)(p21.1q12)

Chr3:59964935

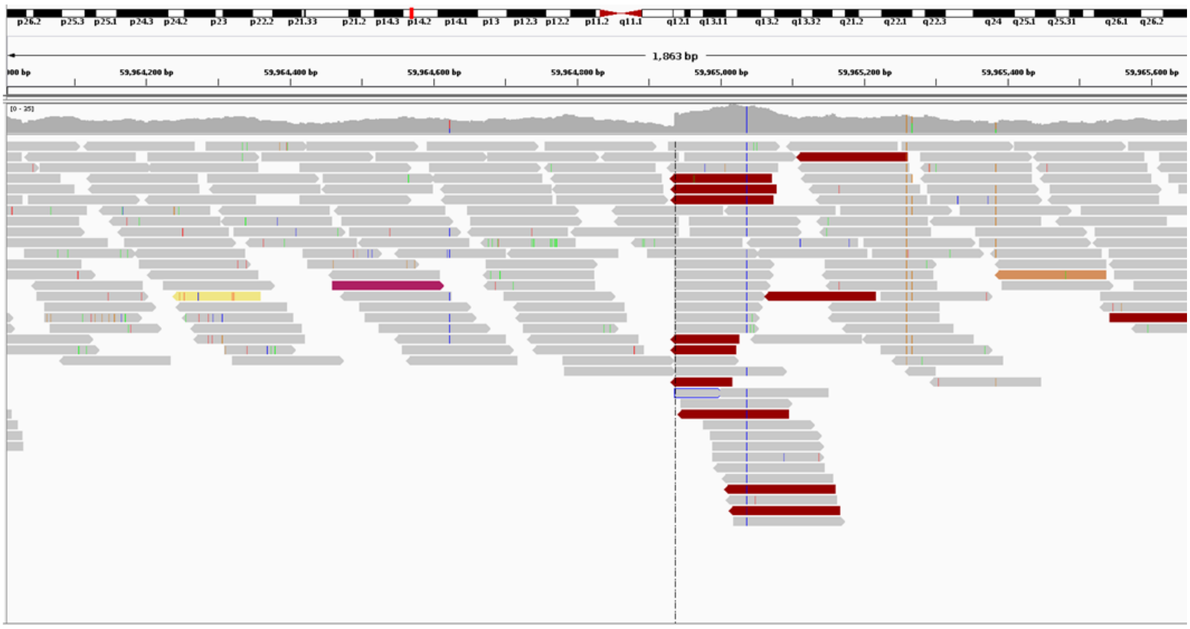

Chr3:98667603

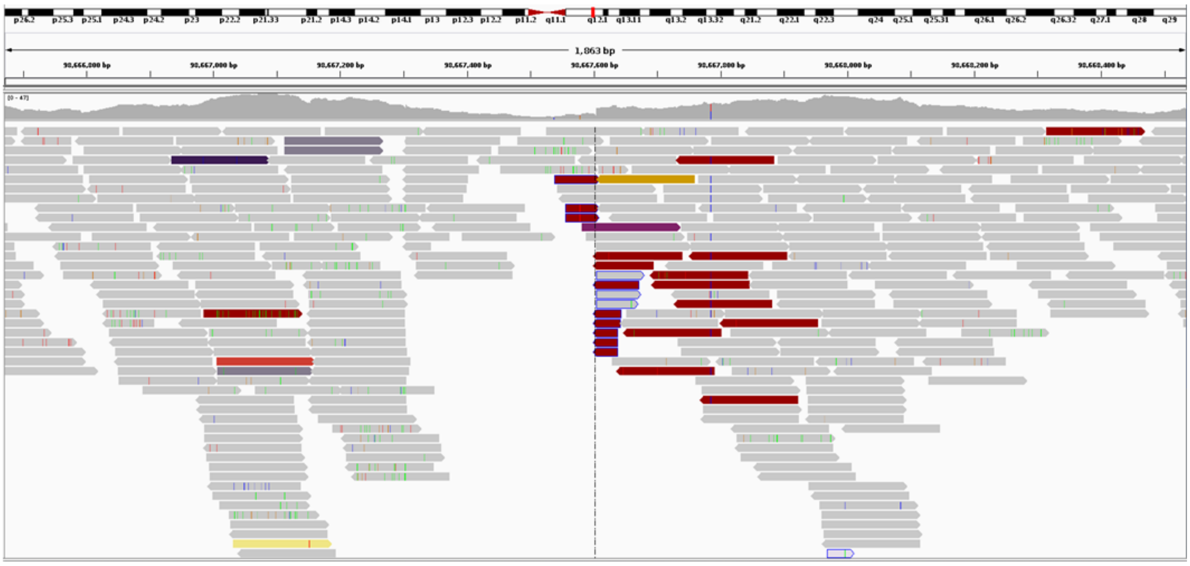

t(3;14)(q13.3;q22)

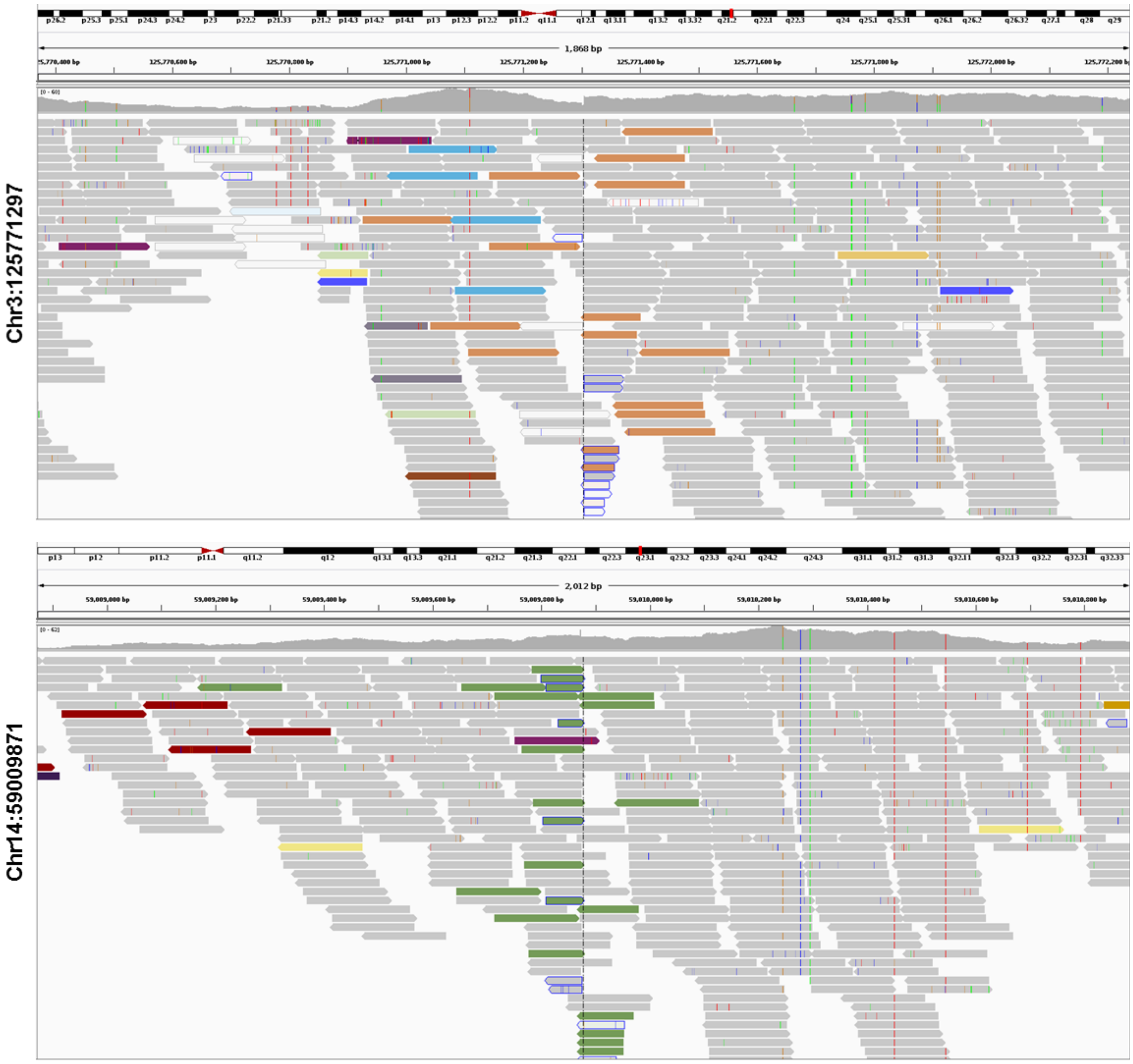

t(10;17)(q11.22;p12)

Chr10:43731495

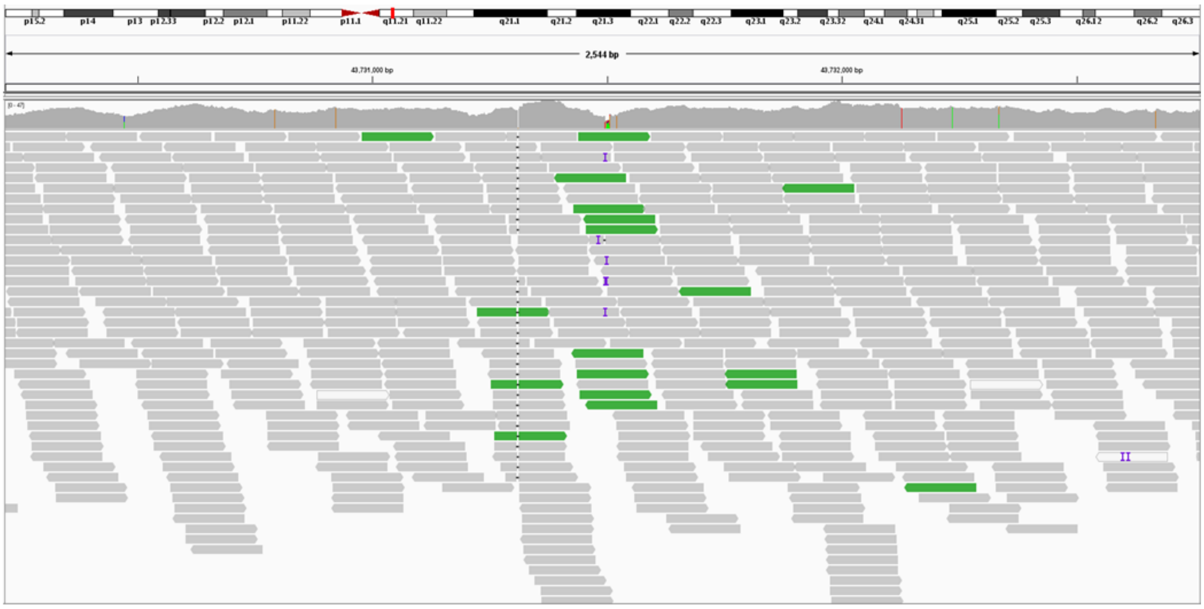

Chr17:17121525

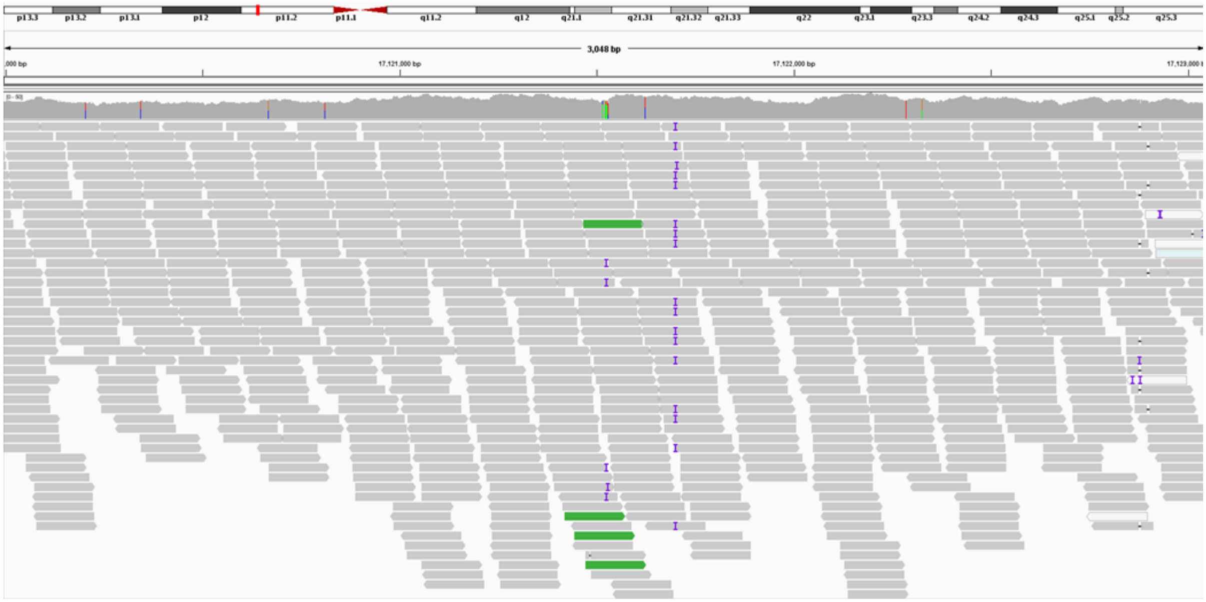

9.5.3 Sanger sequencing of translocation break points

Translocation break point primers

Translocation	**Pair one (5’ to 3’)**		**Pair two (5’ to 3’)**	
	Left	**Right**	**Left**	**Right**
t(2;17)(q21;q11.2)	TTCTGGCAGCGGGTCCA	CAAAAGGGCAGCAATGAACCA	TTCAATGATGTCATACTAGCAGCTT	GTGGACTTCAGGGAGATGCG
t(3;6)(p14.2;p12)	TCACCTGAAGTCTCTTCTTTCTT	CTCCAGGAAGTGATACATGGAA	GTCCTGTTTCCCTAGTCCTGC	AGGGAGGCAAGAAGGAAGTG
inv(3)(p21.1q12)	Failed to generate PCR products – 3 independent primer sets and nested primers			
t(3;14)(q13.3;q22)	CCCCAACAAACCCCACAACA	TGGACTCTGTATTCTGTTCCGT	GAGCTGAGATCATGCCATTGT	CTGAGTGGAGTCTGTATTTCCCA
t(10;17)(q11.22;p12)	GGCCACAATACTATGTCTCACC	ATACATGCGCACACAAGGTC	GGGACAGTGGAGAACGCAT	AAATTAGCTGGGCATGGTGG

Translocation Sanger sequencing traces

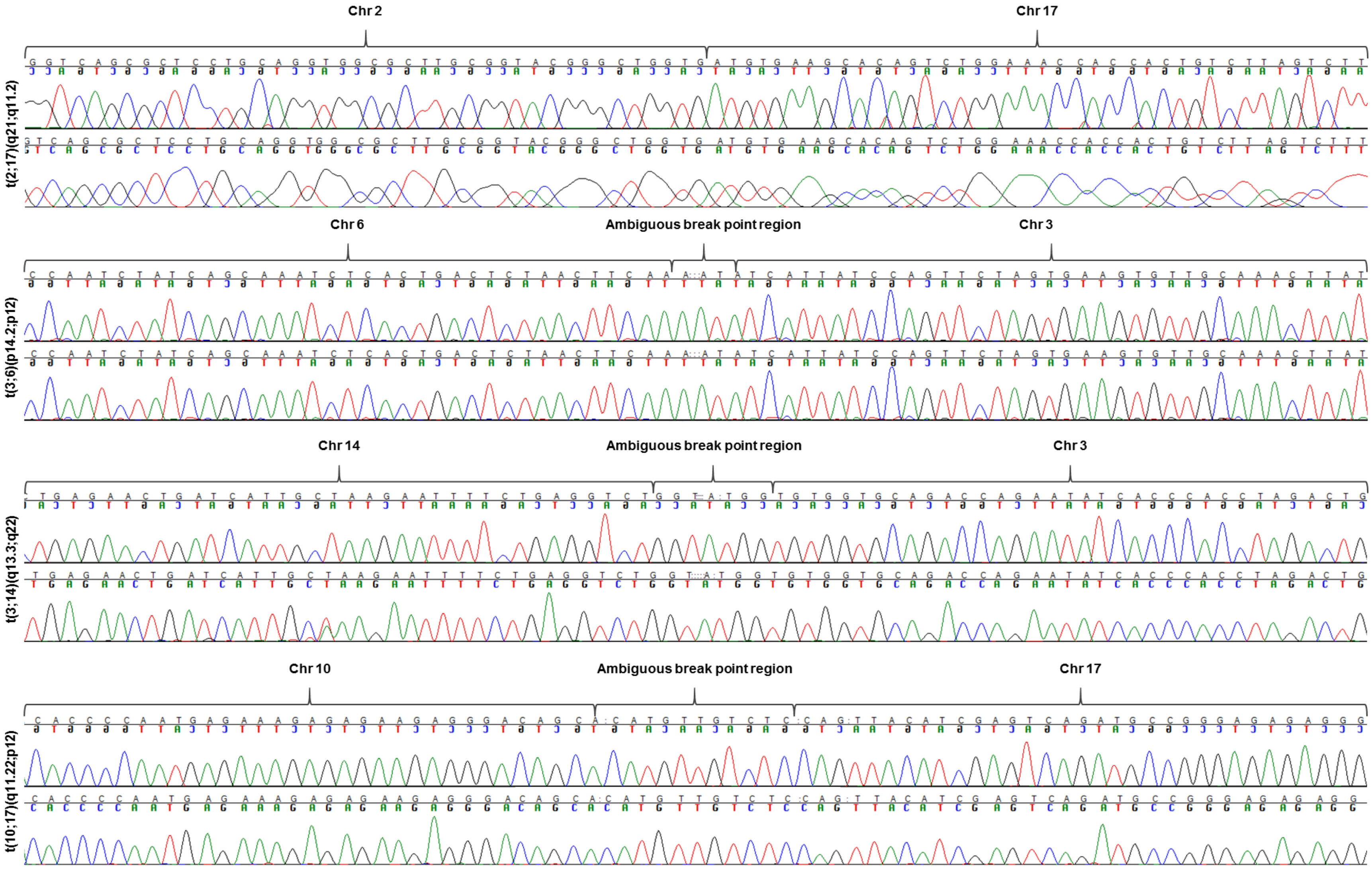

9.5.4 Translocation Manta structural variant calls

Case	ChrA	START A	END A	Chr B	START B	END B	QUAL	BND PAIR COUNT	PAIR COUNT	CIPOS	HOM LEN	HOM SEQ	JUNCTION QUAL	BND DEPTH	MATE BND DEPTH
t(2;17) (q21;q11.2)	chr2	130693727	130693729	chr17	28031855	28031856	491	N/a	N/a	0,1	1	A	N/a	19	37
	chr17	28031855	28031857	chr2	130693727	130693728	491	N/a	N/a	0,1	1	T	N/a	37	19
t(3;6(p14.2;p12)	chr3	66680663	66680664	chr6	54817716	54817717	837	N/a	N/a	N/a	N/a	N/a	227	21	30
	chr6	54817716	54817717	chr3	66680663	66680664	837	N/a	N/a	N/a	N/a	N/a	227	30	21
t(3;14) (q13.3;q22)	chr3	125771297	125771301	chr14	59009871	59009872	999	N/a	N/a	0,3	3	ATG	333	40	50
	chr14	59009871	59009875	chr3	125771297	125771298	999	N/a	N/a	0,3	3	TGT	333	50	40
t(10;17) (q11.22;p12)	chr10	43236058	43236059	chr17	17218216	17218217	1602	16	16	N/a	N/a	N/a	914	39	59
	chr17	17218216	17218217	chr10	43236058	43236059	1602	16	16	N/a	N/a	N/a	914	59	39
	chr10	43236047	43236050	chr17	17218213	17218214	1602	22	22	0,2	2	TG	637	39	58
	chr17	17218211	17218214	chr10	43236049	43236050	1602	22	22	0,2	2	CA	637	58	39

Case	CHR A	START A	END A	CHR B	START B	END B	QUAL	END	SVLEN	FORMAT
inv(3) (p21.1q12)	chr3	59964935	59964936	chr3	98667603	98667604	602	98667604	38702668	